THE UNIVERSITY
of EDINBURGH

Geochemical Characteristics of Unconventional Gas Resources in the U.K. and the Applications for Gas Tracing

Rory McKavney

Thesis submitted for the degree of Doctor of Philosophy

School of Geosciences

University of Edinburgh

2018

Declaration

I declare that all work in this thesis, unless otherwise referenced, is entirely my own. None of this work has been submitted for any degree or professional qualification other than that specified on the title page.

Signed: ……..

Date: ……../……../……..

Abstract

Unconventional gas extraction has caused controversy due to induced seismicity, inadequate disposal of waste by-products, and alleged incidents of shallow groundwater contamination. Determining the origin of shallow gases is problematic because methane and other hydrocarbons have numerous sources that may have overlapping geochemical characteristics, and few baseline measurements were taken prior to drilling. Additionally, hydrocarbons can be fundamentally altered by physico-chemical and microbial processes which can mask the original geochemical signatures.

This project develops the understanding of natural tracers in UK unconventional gas resources and reports the results of major gas composition, stable carbon and hydrogen isotopes, radiocarbon content of methane, and novel noble gas (He, Ne, Ar, Kr, Xe) measurements from unconventional gas sites across the UK. Characterising different gas sources reveals processes within unconventional gas reservoirs, develops a baseline for future work, and allows the development of a geochemical 'fingerprint' which allows more accurate and precise determination of the different sources of methane.

The Coal Bed Methane (CBM) field at Airth, Central Scotland, is characterised by a methane-dominated thermogenic gas based on $\delta^{13}C_{CH4}$ and δD_{CH4} data and elevated ethane and propane contents. Gases show high helium concentrations (1105 ppm – 2984 ppm) with a $^{3}He/^{4}He$ isotopic ratio (0.18 R_a) which is uniform across the field, indicating a small (<4%) but resolvable mantle helium contribution not previously observed onshore in the UK. Also observed are elevated concentrations of excess $^{40}Ar^*$ ($^{40}Ar/^{36}Ar$ = 371 – 1031), and enrichments of $^{20}Ne/^{36}Ar$ relative to the ratios normally expected in air saturated water which cannot be explained by simple solubility fractionation or mass-fractionation.

A model is outlined where increasing dewatering of the wells as the field is developed for commercial extraction results in lower overall noble gas concentrations, a decrease in the air-derived inventory, and an increase in crustal and mantle components. This is hypothesised to occur via the progressive degassing and removal of dissolved air-derived components from formation waters from the more permeable cleat and fracture networks surrounding wellbores, leaving the remaining gases with a greater contribution from crustal-rich components sourced from within the coal matrix.

Abandoned mine gases from Nottinghamshire and South Yorkshire coal mines showed variable methane concentrations (39 – 75%), with the remaining volume being mainly composed of a mixture of nitrogen and carbon dioxide. Correlation of N_2 and ^{36}Ar concentrations in some samples showed ingress of atmospheric air as a result of the suction applied to the mine to facilitate gas production, which was subsequently depleted of oxygen in the mine environment. Carbon dioxide was sourced in lower volumes from coal oxidation, variably mixed with higher concentrations formed from the chemical dissolution of carbonates in the acidic mine environment. Coal gases were characterised by a narrow range of $\delta^{13}C_{CH4}$ and δD_{CH4} values of a primarily thermogenic origin, thermogenic levels of ethane and propane, and high levels of purely radiogenic helium (350 - 1506 ppm at 0.006 – 0.039 R_a).

The stable isotope $\delta^{13}C_{CH4}$ and δD_{CH4} measurements for unconventional gases typically overlapped those of other coal gases, North Sea gases, and landfill gas, which demonstrates this commonly used tool can be an ambiguous for gas source determination. Elevated levels of helium were found to be ubiquitous in all unconventional gases, and up to 3 orders of magnitude above the concentration found in air (5.24 ppm), which shows helium is an excellent tracer for unconventional gases.

Lay Summary

Natural gas for home and industry is extracted from well bores that penetrate deep into the Earth to reach trapped gas accumulations. The gas is stored in rocks such as sandstone that have open pore spaces between the sand grains, allowing the gas to flow freely through the rock into the well. New resources of 'unconventional' gas have been found, where gas is trapped in tiny pores in rocks such as shales, or adsorbed onto coal surfaces, and is less free to flow through the rock. These types of gas often require special techniques to make the gas flow, which might include "hydraulic fracturing", also known as "fracking". In America, hundreds of thousands of well bores have been drilled for this unconventional oil and gas. Some people worry that the fracking or the well bores might be causing methane natural gas to rise up through the rocks and contaminate groundwater near the surface.

Methane gas in groundwater can come from lots of places, such as coal seams, swamps, or rotting rubbish dumps. The gas in water might be naturally occurring in an area, and not a result of human activity. However, simply measuring the amount of gas in water is not a good way to tell where it came from, so sometimes there can be problems in finding out why it is there, how to stop it, and if anyone is to blame.

This project takes samples of these deep unconventional gases in the UK, and measures a chemical 'fingerprint'. This fingerprint relies on the chemistry of the hydrocarbon gases, as well as from noble gases such as helium and neon, which exist in tiny amounts alongside the deep gases. These fingerprints could be used later on to see if they match any gas found in groundwater, and allow us to confirm if the gas has leaked from deep down or came from somewhere else.

Samples were taken from Coal Bed Methane (CBM) well bores in Central Scotland, from abandoned mines near Yorkshire in England, and from two wells drilled into shale. These were found to be rich in helium. Because helium is so light, once it is in the atmosphere it escapes into space, and so the atmosphere has a very low concentration. The high helium concentrations in deep gases compared with the low concentrations in the air mean that even very small amounts of deep gas can be traced at the surface.

The chemistry of the carbon and hydrogen contained within the methane was found to be in two narrow ranges for the Scottish and the English coal gases, which is useful for characterising and distinguishing between the gases.

Measuring the chemistry of the gases helps us to learn more about how unconventional gas formed, how it is stored, and how long it was been there.

Acknowledgements

This thesis is dedicated to my parents and family for their support and patience, for which I am deeply indebted. I'm glad I can now ascribe a sense of fulfilment to the end of both a rewarding and occasionally gruelling experience.

Firstly, I would like to thank my primary supervisor Dr. Stuart Gilfillan for his guidance throughout the project. Thank you also to Dr. Domokos Györe and Prof. Fin Stuart for their immersive introduction to noble gas analysis, supervision and troubleshooting when analysing samples, and relieving me from the distraction of having windows in the lab. Terry Donnelly and Dr. Pauline Gulliver at SUERC are thanked for their sampling advice and support with stable isotope and radiocarbon analyses.

Permission to take samples was kindly granted by Cuadrilla Resources Ltd., DART Energy Ltd. (now part of the INEOS group), Ground Gas Solutions Ltd. and Alkane Energy Ltd. I am also grateful for the funding provided by NERC and SEPA that made this project possible, and brought me to live in the beautiful city of Edinburgh. The team at Speck and Burke are thanked for going above and beyond to help me with the very basics of gas chromatography, when I couldn't resolve the charts from my elbow and almost lost the PLOT.

So many people made the experience wonderful and unforgettable, and I hugely appreciate the help many of you have given me. Thanks to everyone for helping me move, mull over ideas, being great friends, proofreading, organising geology trips (*a.k.a.* 'holidays'), sharing meals, and generally talking rubbish with me!

Here's a massive shout-out to Dr. Matt Holloway, with whom from the first week I enjoyed gallons of shared interests, amongst other cultural pursuits. Long may it continue. A wholehearted thank you goes out to Dr. Emma Turner, Dr. Rūta Karolytė, Rachel Bartlett, Dom Cummings, Shauna Colgan, Ellen Mears, Kelsey Austin for their love, support, and great memories throughout the years.

Interim accommodation woes were hugely aided by Dr.'s Gillian McCay, Tom Russon, Amelia Bain, and Sarah Shelley. I am immensely grateful to Dr. Chris and Steph Haggarty-Weir, who so kindly invited me into their home *for the entire Fringe Festival* in the final push.

The Geoscience Crew made tackling endless spreadsheets Excelent, so special mentions go out to Maddie Berg, Pádraig Ó Conbhuí, Rachel Kilgallon, Mr Chrystiann,

The Cyprus Trip staff, John Leslie, Alice Macente, Johannes 'Jonas' Miocic, John Preston, Nicola 'Tricky' Rigonat, Hugh Tennent, Axel, Gus, Kit C, Morag, Rami E, Rebecca W, Romesh P, the Poker Gang, Warwick W, the lovely people at SUERC for making me feel welcome, and the people and institutions of Edinburgh. To my former flatmates Amos, Bridget, Caterina, Daisy, Hannah, Piera, Sara, and Todd, I offer my commiserations, some cheese toasties, and the latest developments in homebrew. Thanks.

I would lastly like to thank my examiners Dr. Chris McDermott and Prof. Jon Gluyas for making the viva experience both fulfilling and enjoyable.

Table of Contents

List of Terms and Abbreviations

ANG = Atmospheric Noble Gases, gases assumed to be originally derived from the atmosphere.

ASW = Air Saturated Water, a term used to describe the inventory of atmospheric noble gases in equilibrium with fresh water.

δ = 'delta notation' used for reporting isotopic ratios, *e.g.*

$$\delta^{13}C = \left[\frac{(^{13}C/^{12}C)_{sample})}{(^{13}C/^{12}C)_{standard})} - 1\right] \times 1000$$

$\delta^{13}C_{CH4}$ = carbon isotopic ratio (see above equation) of methane, expressed as '‰– per mille'

VPDB = Vienna Pee Dee Belemnite, a reference calibration standard for $\delta^{13}C$ analyses. VSMOW= Vienna Standard Mean Ocean Water, a reference calibration standard for δD analyses.

δD_{CH4} = hydrogen isotopic ratio of methane, per mille - ‰

C_1 = methane

C_2 = ethane

C_3 = propane

C_{2+} = ethane and higher hydrocarbons

Firedamp = Gases emanated from coal seams, typically during the mine process, primarily methane.

Blackdamp = Oxygen deficient air found in mine workings.

CBM = Coal Bed Methane

CSG = Coal Seam Gas (term typically used in Australia), synonymous with CBM.

AMM = Abandoned Mine Methane, methane from abandoned mine workings.

R_o = Vitrinite reflectance; a measure of incident light reflected off the maceral vitrinite under oil, measured in percent. Vitrinite is a coaly maceral derived from vascular plants, and is present in sedimentary rocks and is one of the primary components of coal. The reflectance changes with heat, and is a commonly used and referenced indicator of thermal maturity. Reported R_o % are usually a mean value from multiple vitrinite particles in a rock (AAPG, 2015).

GC = Gas Chromatography, a tool used to separate and analyse volatile components of a sample such as gases.

Ma = Millions of years ago

Ga = Billions of years ago

mD = millidarcy, a unit of permeability.

pMC = percent modern carbon, for radiocarbon analysis interpretation.

$^{40}Ar^*$ or $^{21}Ne^*$ = the asterisks notation refers to 'excess' of the isotope in question above the air-ratio.

AAPG (2015) *Vitrinite Reflectance*, *AAPG Wiki*. Available at: http://wiki.aapg.org/Vitrinite_reflectance (Accessed: 3 February 2015).

1 Introduction

Widespread unconventional gas production as a result of horizontal drilling and hydraulic fracturing technologies have greatly increased the global hydrocarbon reserves over the past decade. However, this development has not been without controversy, in part due to high-profile cases of alleged methane contamination of groundwater , (*e.g.* Osborn *et al.*, 2011; Saba and Orzechowski, 2011), and induced seismic events due to drilling, production, and water disposal practices (Schultz, 2013; Clarke *et al.*, 2014) Methane can be an explosive hazard when handled incorrectly (Gooddy and Darling, 2005), and is a greenhouse gas ×86 times more potent than CO_2 over a 20-year period (IPCC, 2013). Therefore, to prevent and mitigate potential methane emissions, it is important to know how and when methane was formed and its method of migration.

Initial investigations attributed the presence of methane in groundwaters in Pennsylvania, USA, to the practice of unconventional gas extraction (Osborn *et al.*, 2011; Warner *et al.*, 2012). However, the presence of methane does not imply anthropogenic pollution. Methane is found naturally in many groundwaters and natural seeps (Selley, 1992; Judd *et al.*, 2002; Molofsky *et al.*, 2011) and was common in Pennsylvania where Osborn et al. (2011) found alleged pollution before any hydraulic fracturing operations occurred (Harrison, 1985; Révész *et al.*, 2010; Davies, 2011; Molofsky *et al.*, 2013). Within the UK, methane is naturally present in many groundwaters, occasionally in potentially explosive concentrations (Gooddy and Darling, 2005).

In the United States a lack of baseline groundwater chemistry and gas concentration measurements collected prior to drilling has made the determination of pollution more difficult. This controversy has been exacerbated by the use of methane concentration and C and H isotope determination to resolve CH_4 origins in groundwater, which are not definitive tracers of CH_4 origin due to overlapping geochemical ranges and the difficulty of resolving CH_4 from mixed sources.

More conclusive results can be obtained by comparing measured concentrations and stable isotope values to a baseline developed prior to the onset of drilling activity. Changes from the baseline can be tracked and the composition of the gas can be compared with the composition of possible sources of contamination. The need for a baseline has been recognised by many (Davies, 2011; Mair *et al.*, 2012; Jackson *et al.*,

2013; Dusseault *et al.*, 2014). Unfortunately for many areas including the majority of the USA, pre-drilling baselines are unavailable.

The British Geological Survey (BGS) has previously undertaken baseline methane samples – in response to the Loscoe (Williams and Aitkenhead, 1991) and Abbeystead (HSE, 1985) methane gas explosions in the 1980's (Hitchman *et al.*, 1989). They have extended their baseline monitoring program over areas where shale gas prospecting is likely to occur, and included comprehensive data from the Environment Agency (EA). This study will add to a larger UK effort by the Scottish Environmental Protection Agency (SEPA), BGS, and the EA (Gooddy and Darling, 2005; Bell *et al.*, 2016, 2017) to characterise water quality data to form a baseline prior to any extensive drilling activity occurring.

This chapter introduces the concepts behind unconventional gas, some of the problems encountered with the process in North America, and a brief overview of geochemistry and relevant data.

1.1 Unconventional Gas

1.1.1 Unconventional Gas Definition

In the oil and gas industry, sources of oil and natural gas are typically categorised as conventional or unconventional. All hydrocarbons form via the decomposition of organic materials such as kerogens and hydrocarbons found within source rocks, however 'conventional' hydrocarbons have typically migrated from their source rocks before becoming geologically trapped in a porous and permeable reservoir rock. This type of deposit can be produced at economic flow rates without special stimulation treatments. The locating and exploiting of this type of resource using traditional techniques has been the mainstay of the oil and gas industry for decades. Unconventional hydrocarbons have a somewhat arbitrary definition, in that they do not fit the 'conventional' checklist. The difference typically lies primarily on geology; unconventional gas is produced from any source which does not fit this Source → Migration → Trap system (see Figure 1-1)

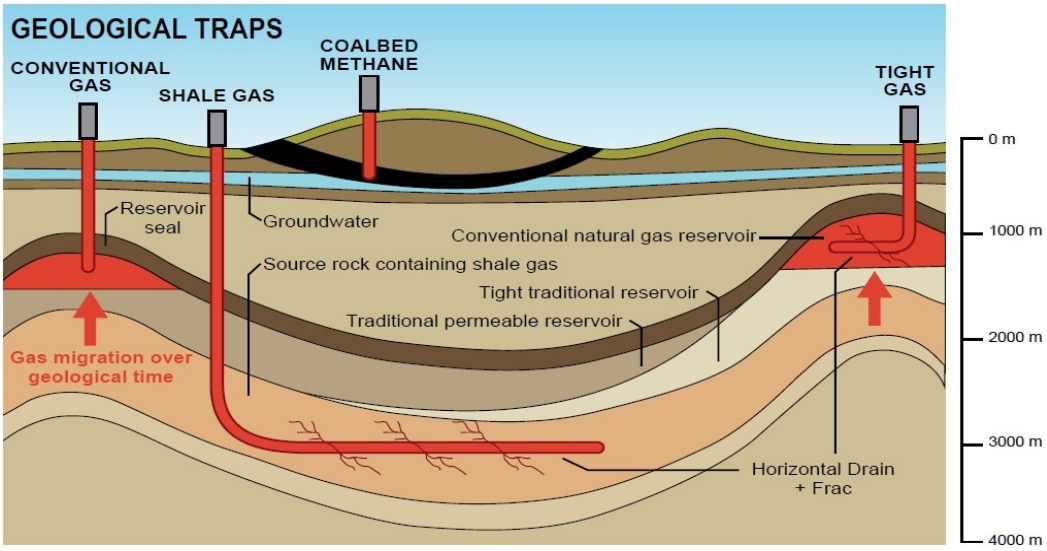

Figure 1-1 – Schematic of gas types and methods of emplacement. Image reproduced from Australian Dept. Mines and Petroleum http://www.dmp.wa.gov.au/onshoregas

Unconventional petroleum types include:

- Shale Gas/Oil - where the target reservoir formation shale is also the source rock.
- Coal Bed Methane/Coal Seam Gas - where gas is adsorbed onto the surface of coals in fractures and cleats, which can desorb when water is removed from the pore space.
- Tight Gas/Oil – often included in 'unconventional' hydrocarbons, is typified by absolute permeabilities below 0.1 millidarcy (onshore USA), requiring stimulation to produce economically.
- Any other novel gas source such as Coal Mine Methane (CMM), Abandoned Mine Methane (AMM), methane clathrates, anaerobic digestion, underground coal gasification, coal gas and synthetic oil shale gases and liquids derived from retorting shale (pyrolysis).

1.1.2 Economics

In the USA, unprecedented development of shale gas and shale oil reserves has entirely altered the US energy market, with shale gas production seeing an increase from 2% (0.01 trillion cubic meters, tcm) of natural gas in 2000, to 23% (0.14 tcm) in 2010, with projections set to nearly triple by 2035 (Kuuskraa *et al.*, 2013).

There has been a huge expansion of shale gas development within the USA; Pennsylvania alone went from 8 wells in 2005 to over 7000 as of 2014 (Brantley *et al.*,

2014). The production of domestic oil has exceeded imports for the first time in 18 years (BBC, 2013), and the US has become a net exporter of refined oil products for the first time in 60 years (Chojna *et al.*, 2013).

Natural gas also carries with it lower sulphur, particulate, NO_2, and mercury emissions than coal (Cathles III *et al.*, 2012), and has been controversially touted as a lower-carbon bridge fuel on the path to a sustainable energy future (Jenner and Lamadrid, 2013).

The economic success of the American story has led to many other countries looking to develop their unconventional natural gas reserves.

1.1.3 Hydraulic Fracturing and Horizontal Drilling

Improvements to horizontal drilling and hydraulic fracturing ("fracking"/"fraccing") technologies in recent decades have helped lift the technological and economic barriers to the large-scale exploitation of unconventional hydrocarbon reserves (Kargbo *et al.*, 2010; Kerr, 2010). Hydraulic fracturing is a situation that occurs where fluids in a rock exceed the principle normal stress and tensile strength of the rock, inducing fractures (Hubbert and Willis, 1957). This phenomenon occurs naturally due to fluid overpressure (*e.g.* Cosgrove, 1995; Hurst et al., 2011), but is commonly induced to 'stimulate' low-permeability reservoirs such as tight-gas, shales and some coal beds, to allow the commercially viable production of hydrocarbons (Holditch, 2006; Jackson *et al.*, 2013).

During the process, a fluid such as H_2O, N_2, CO_2 or Liquified Petroleum Gas (LPG) is pumped down a wellbore at high pressures to create fractures or expand and connect existing fractures (Engelder and Lash, 2008). A proppant material is pumped down with the fluid to hold the fractures open when the pressure is reduced (Hubbert and Willis, 1957; Simonson *et al.*, 1978; Davies *et al.*, 2012).

The process was developed by Stanolind Oil and Gas Corporation in 1947 using 'napalm' gels, and the water-based variant was developed by Halliburton Oilwell Cementing Company in 1953, and has seen extensive use worldwide (Montgomery and Smith, 2010). The 'shale gas revolution' arguably started when hydraulic fracturing was combined with advances in horizontal drilling in the Barnet Shale Formation, Texas, in 1991 which allowed the exploitation of shale gas (Kharak *et al.*, 2013).

During the development of a modern shale gas well typical of the Marcellus Shale in Pennsylvania, wells are drilled vertically with cores often being taken around the target

shale. A horizontal 'lateral' section up to 3.5 km long is then drilled away from the vertical well at depth, following the thin shale horizons and vastly increasing the volume of shale to which the well is connected. The wellbore within the target formation is perforated from the inside, and is hydraulically fractured over multiple stages with 'slick water' (Kharak *et al.*, 2013). Huge volumes of water (~10,000 -50,000 m3/well), chemical additives (see Barati and Liang, 2014 for more detail) and hundreds of tonnes of proppant (usually sand) are pumped down the wellbore, producing fracture networks of up to 9.2 million m^2 surface area (Myers, 2012). Following the hydraulic fracturing, the pressure is reduced and a mixture of fracturing fluid, formation brines and dissolved and free gases are produced at the surface for several days to weeks, before the well flows gas with only minor produced water. 0 – 75% of the injected fluid is recovered as flowback, but typically less than half (Broomfield and Donovan, 2012; Engelder *et al.*, 2014). The residual treatment fluid is sequestered by the shale via capillary and osmotic forces (Engelder, 2012; Engelder *et al.*, 2014)

1.2 Geochemistry of Hydrocarbons

The geochemical analysis of gaseous hydrocarbons mainly focusses on the molecular composition of the gases, and the isotopic ratios of the carbon and hydrogen stable isotopes of individual components. There is also an increasing attention to the analysis of trace components within these gases (such as the noble gases).

1.2.1 Carbon and Hydrogen Stable Isotopes

The analysis of carbon and hydrogen isotopes is a commonly used tool when investigating hydrocarbons as they are composed entirely of carbon and hydrogen atoms, and can display characteristic isotopic ranges which can be used to determine the generation mechanism (Schoell, 1980; Whiticar, 1994, 1996; Golding *et al.*, 2013). Carbon contains 2 stable isotopes, ^{12}C and ^{13}C. The ratio of the two isotopes normalized to a standard is known as $\delta^{13}C$:

$$\delta^{13}C = \left[\frac{(^{13}C/^{12}C)_{sample})}{(^{13}C/^{12}C)_{standard})} - 1 \right] \times 1000$$

The most commonly used standard is the Vienna Pee Dee Belemnite (VPDB) (Coplen, 1995). More positive $\delta^{13}C$ values represent isotopically heavier ^{13}C-rich samples, and more negative values represent isotopically lighter ^{13}C-poor samples. $\delta^{13}C$

can be a useful diagnostic feature of a carbon source, especially when combined with stable hydrogen isotopes (δD) (Whiticar, 1994).

The formation of natural gas in the subsurface is a by-product of the decomposition of organic matter to low molecular weight hydrocarbons, which can be split into two regimes; thermogenic methane produced by abiotic reactions at elevated temperatures and pressures usually >1km depth, and biogenic methane, produced by anaerobic microbial processes such as methanogenesis (Schoell, 1980; Whiticar, 1994; Golding *et al.*, 2013). Methane and light hydrocarbons can also be produced in small quantities abiotically through processes such as serpentinization (Hosgormez *et al.*, 2008; Potter *et al.*, 2013)

Thermogenic methane can generally be distinguished from biogenic methane via higher $\delta^{13}C_{CH4}$ (typically greater than -50‰), typically higher $\delta^{2}H$ values where $\delta^{13}C_{CH4}$ ranges overlap microbial ranges, and greater concentrations of 'wet' gases (*i.e.* associated higher order hydrocarbons in the C_2 - ethane through to C_5 – pentane range). Biogenic methane generally has lower $\delta^{13}C$ and δD_{CH4} values and low concentrations of associated gases ('dry'). CBM and shale gases can be of thermogenic, biogenic, or mixed origin. Additionally, thermogenic gas can be altered by microbial processes such as anaerobic methane oxidation which enriches the residual methane in heavier isotopes (Whiticar, 1999; Kinnaman *et al.*, 2007). Thermogenic gas geochemistry and isotopic signature is also affected by source rock, kerogen type and thermal maturity (Schoell, 1980; Whiticar, 1994; Rooney *et al.*, 1995; Golding *et al.*, 2013). Biogenic gas can form anywhere where organic matter and suitable conditions for microbial growth exist (Meslé *et al.*, 2013). The biogenic gas geochemistry and isotopic signature is affected by a myriad of factors including, but not limited to, source rock, substrate type and availability, water availability, nutrient levels, temperature, methanogenic pathway, etc. (Whiticar, 1999; Strąpoć *et al.*, 2011).

1.2.2 Radiocarbon

Carbon has 2 stable isotopes: ^{12}C and ^{13}C, and one radioactive isotope: ^{14}C. Carbon-14 (^{14}C) is formed in the upper atmosphere by neutron bombardment of nitrogen due to the presence of cosmic rays via the following reaction:

$$^{14}_{7}N + {}^{1}_{0}n \rightarrow {}^{14}_{6}C + {}^{1}_{1}p$$

^{14}C decays back to ^{14}N with a half-life of 5730 years. In the atmosphere, the ^{14}C reacts with O_2 to form CO_2, which is fixed into the biosphere via photosynthetic

reactions within organisms such as plants and algae. When these organisms are alive, the ^{14}C:^{12}C ratio remains constant relative to the atmosphere, where the rate of formation of ^{14}C is assumed to be constant. After death, without atmospheric replenishment the ratio of ^{14}C:^{12}C in the organic matter drops as ^{14}C decays to ^{14}N. Thus the age of a sample can be determined by comparing the amount of ^{14}C left in a sample to the initial amount of ^{14}C (Libby, 1946; Arnold and Libby, 1949), simplified via the following equation:

$$t = \frac{1}{\lambda} \ln\left[\frac{Ao}{At}\right]$$

Where t = time, λ = half-life of ^{14}C, A_0 = initial radioactivity of ^{14}C and A_t = radioactivity of ^{14}C at time t.

This technique allows dating of a sample to around 60,000 years, after which there is insufficient ^{14}C in a sample to resolve, and is said to be 'radiocarbon dead'.

There are many limitations to this technique when applied to archaeological dating of specific objects, where precise dates are important *e.g.* such as isotopic fractionation variations between C3 and C4 plant types, calibration to tree-rings or other datasets, skewing due to thermonuclear generation of ^{14}C, and the Suess effect where anthropogenic emissions of CO_2 from radiocarbon-dead fossil fuels skew current atmospheric ratios (Tans *et al.*, 1979). However, in the context of geochemical tracing of methane, any inaccuracies of dating are merely academic insoforth that the technique can show that the source of a gas is either ancient (*i.e.* >~60 ka and so radiocarbon-dead) or more recent. This technique was used successfully in the Loscoe landfill explosion in 1989, where ^{14}C-dating was used to determine that the source of stray gas was migrating from a nearby landfill, and was not from underlying coal measures (Williams and Aitkenhead, 1991).

While ^{14}C can aid in the determination of microbial gas formed from 'recently' formed sources (<60 ka) such as landfill, certain 'geologically young' surficial deposits that have biogenic methane potential *e.g.* glacial till, peat, swamps, etc. can be much older than this and hence radiocarbon-dead (Martini *et al.*, 1998) .

Obtaining accurate ages of gas would be very problematic due to the complex biological coupling of carbon-based gases. As subsurface gases are formed from the degradation of organic matter, it is the radiocarbon content of this organic matter which is imparted to the gas. This can have an affect the radiocarbon ages of ecosystems in close proximity to ancient carbon sources; in soils above a CBM seep,

methanotrophic microbes have used the methane as a substrate oxidising it to carbon dioxide leading to a situation where up to 91% of carbon assimilated into soils was derived from CBM (Mills et al., 2013 and references therein), and thus would not have yielded an accurate radiocarbon date, despite being modern soil.

1.2.3 Noble Gases

The noble gases (helium, neon, argon, krypton, xenon, radon) occupy IUPAC group 18 of the periodic table and possess a full shell of outer valence electrons, rendering them chemically inert at typical temperatures and pressures (Ozima and Podosek, 2001; Ballentine *et al.*, 2002). Noble gas studies typically disregard radon which is a radionuclide. The unreactive nature of noble gases means they are unaffected by chemical processes, but their isotopic and relative abundances can be affected by physical processes, which makes them ideal tracers in the natural environment (Ballentine *et al.*, 1991, 2002; Castro *et al.*, 1998; Ozima and Podosek, 2001; Ballentine and Sherwood Lollar, 2002; Burnard, 2013).

On Earth, noble gases largely originate from two sources; 'primitive' gases trapped during the accretion of the planet, and gases generated via radioactive activity. Over time the noble gases have partitioned, resulting in 3 distinct sources of gases with different elemental abundances and isotopic compositions (see Figure 1-2) (Ballentine *et al.*, 2002):

- The atmosphere - where outgassed noble gases reside (excluding helium, which is lost to space).
- The crust - where radiogenic noble gases are generated from the decay of U, Th and K, and nucleogenesis.
- The mantle - which contains primordial noble gases trapped during the formation of the earth.

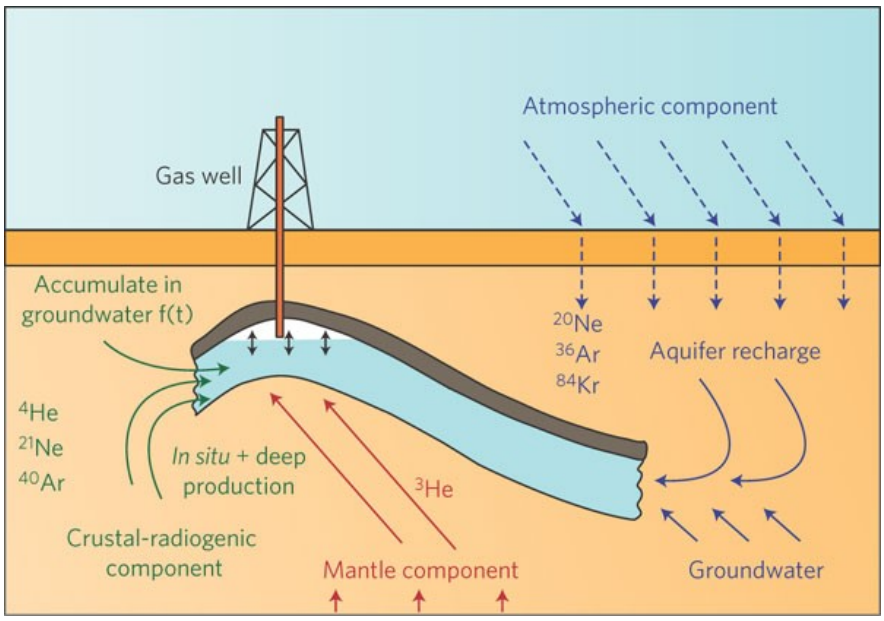

Figure 1-2 – Schematic of the three unique sources of noble gases (reproduced from Chapter 8 of Burnard, 2013)

Noble gases in the atmosphere exist in trace quantities (except ^{40}Ar) and their isotopic and elemental abundances are well constrained (Porcelli *et al.*, 2002). Many atmospheric noble gas components were originally derived from radiogenic or nucleogenic processes and have outgassed and accumulated in the atmosphere over geological time. ^{20}Ne, ^{36}Ar, ^{84}Kr, and ^{132}Xe are regarded as atmospheric noble gases, as in the subsurface they are primarily sourced from the atmosphere and have little relative radiogenic or mantle component (Ozima and Podosek, 2001).

Atmospheric noble gases are introduced into the subsurface via rainwater infiltration. The solubility of noble gases in water is dependent on atomic mass following the pattern Xe>Kr>Ar>Ne>He, and is affected by temperature, salinity, and partial pressure (which is proportional to altitude) (Crovetto *et al.*, 1982; Ozima and Podosek, 2001). These solubility differences cause the elemental noble gas ratios in water to be distinctly and predictably fractionated from the original atmospheric ratios, and the composition of noble gases in recharge water is commonly referred to as Air Saturated Water (ASW).

In natural water samples, sometimes an enrichment in the lighter noble gases above the experimentally determined solubility constants is observed. This is termed 'excess-air', and hypothesised to be an artefact of the trapping of gas bubbles in porous media during wetting in the recharge zone, the area in which water enters an aquifer (Kipfer *et al.*, 2002; Stute and Schlosser, 2013).

Atmospheric helium concentrations are low (5.24 ppm) (Mamyrin *et al.*, 1970; Lupton and Evans, 2013) partly because helium is lost to space. Atmospheric helium is composed of outgassed mantle ^{3}He, cosmic ^{3}He, and radiogenic crustal ^{4}He at the ratio $^{3}He/^{4}He = 1.39\times10^{-6}$, which is often used as a reference with which other helium ratios are compared *i.e.* R_a; where the atmosphere = 1 (Ozima and Podosek, 2001).

In the crust, noble gases are generated by radiogenic and nucleogenic processes. ^{4}He is produced by alpha decay of radioactive elements, which in the crust are primarily ^{235}U, ^{238}U, ^{232}Th, and the various daughter isotopes of each decay chain (Ozima and Podosek, 2001). Smaller concentrations of ^{3}He are also produced from thermal neutron capture of ^{6}Li, but predicted average crustal production rates are low (Ballentine and Burnard, 2002). Typical $^{3}He/^{4}He$ crustal ratios are 0.02 Ra – 0.10 Ra (Ballentine and Burnard, 2002). The especially low concentration of helium in the atmosphere facilitates the resolution of the small concentrations found in subsurface samples, making helium analysis a powerful tool to trace deep gas migration (Mackintosh and Ballentine, 2012).

$^{40}Ar^*$ forms from the radiogenic decay of ^{40}K, the asterisk notation refers to 'excess' or radiogenic ^{40}Ar, which raises the $^{40}Ar/^{36}Ar$ above the atmospheric ratio. ^{21}Ne is primarily sourced from the atmosphere, however nucleogenic $^{21}Ne^*$ and $^{22}Ne^*$ are also produced by the reactions $^{18}O(\alpha,n)^{21}Ne$ and $^{19}F(\alpha,n)^{22}Na(\beta)^{22}Ne$. The production of crustal noble gases is related to radioelement and (for nucleogenic) target element abundances and proximities (Ballentine and Burnard, 2002). Release of these elements from minerals is related to temperature (Ozima and Podosek, 2001; Ballentine and Burnard, 2002), and crustal noble gases are largely age-accumulative. Therefore, different areas of the crust will exhibit varying crustal contributions to fluids in response to these parameters. The mantle is enriched in primordial ^{3}He and $^{40}Ar^*$ (Ozima and Podosek, 2001).

Noble gases have been used successfully in tracing gas from CO_2 reservoir systems (Gilfillan *et al.*, 2008, 2011; Gilfillan and Haszeldine, 2011; Giustini *et al.*, 2013), and are finding application in conjunction with stable isotopes in determining the origin of methane gas from a cold seep (Tomonaga, 2013), and tracing crustal fluids (Mackintosh and Ballentine, 2012).

The scarcity of noble gases makes their isotopic ratios sensitive to the addition of radiogenic isotopes (Yokochi *et al.*, 2012) which could be particularly useful in tracing fluids that have been in contact with or derived from shales, which are known to be high in Naturally Occurring Radioactive Minerals (NORMS).

The biggest potential for noble gas analyses focusses on the inert nature of the gases. Carbon and hydrogen stable isotopes are strongly coupled to the biosphere and geosphere. The isotopic ratios of gases are affected by source material, mineralogy, microbial alteration and oxidation, substrate availability, thermal maturity and seasonal variability, *etc.* (Golding *et al.*, 2013). Moreover, stable isotopes are not definitive tracers of methane origin due to overlapping geochemical ranges of sources, and the difficulty of resolving mixed sources. Noble gas analysis provides a complimentary method alongside carbon and hydrogen stable isotopes that is independent of these factors, and acts as another reference point. For example, Hunt *et al.*, (2012) utilised ^{4}He and ^{21}Ne isotopes normalised to ^{40}Ar alongside standard geochemical techniques to distinguish between two different subsurface gas types (Upper Devonian shale gas and Lower Ordovician migrated gas) in the Appalachian Basin where there is a complex history of gas mixing.

Noble gas analysis can also be used to investigate physical processes occurring in a reservoir such as the interactions of hydrocarbon gases and oils with groundwaters, and constrain groundwater residence times (Bosch and Mazor, 1988; Zhou *et al.*, 2005; Zhou and Ballentine, 2006; Hunt *et al.*, 2012; Yokochi *et al.*, 2012).

1.3 Overview of Project Resources

Funding for 3.5 years was provided by NERC (National Environment Research Centre) with a CASE partnership with SEPA (Scottish Environmental Protection Agency). Additional funds for various costs including equipment, fieldwork, travel etc. were provided by the Scottish government. Permission for gas sampling of 'deep' gases and water monitoring wells was kindly granted by DART Energy (later, INEOS), Cuadrilla Resources Ltd., Ground Gas Solutions Ltd., Alkane Energy Ltd., and the owner of Leadburn House.

1.4 Thesis Outline

This project aims to improve the geochemical understanding of natural tracers in unconventional gas systems, using a suite of analytical methods (involving stable isotopes, noble gases and radiocarbon analysis), and use this to develop a methodology to fingerprint gases from various sources. This should allow us to better identify and constrain the presence, extent, and the potential migration mechanisms of any fugitive

gas (*e.g.* Darrah *et al.*, 2014). Another practical application of the research is further understanding the geochemical signatures of unconventional gas systems, as noble gases can reveal information about the state of gas storage, emplacement, gas/water ratios, the effects of field development, and help to determine if fingerprints are unique to fields or hydrocarbon type (*e.g.* shale vs. coal vs. conventional).

In addition to the introduction to unconventional gas and hydrocarbon geochemistry, this thesis is composed of six additional chapters. Chapter 2 outlines the sampling methodology and analytical techniques used in the study. Chapter 3 outlines the Airth Coal Bed Methane field at Airth, Central Scotland, reports the geochemistry of seven well gases, and describes a model where continuing field development changes the noble gas signature of the produced gases. Chapter 4 explains the processes behind Abandoned Mine Methane sites in Yorkshire and Nottinghamshire, and reports the geochemistry with predictions for future gas evolution. Chapter 5 reports and briefly characterises various unconventional hydrocarbons sites and natural seepages in the UK. In Chapter 6, the work is briefly summarised and with respect to tracing potential, describes a workflow methodology for determining the source of a gas. Chapter 7 is the appendix containing supplementary data.

1.5 Bibliography

Arnold, J. R. and Libby, W. F. (1949) 'Age Determinations by Radiocarbon Content : Checks with SampIes of Known Age', *Science*, 110(2869), pp. 678–680. doi:10.1126/science.110.2869.678.

Ballentine, C. J., O'Nions, R. K., Oxburgh, E. R., Horvath, F. and Deak, J. (1991) 'Rare gas constraints on hydrocarbon accumulation, crustal degassing and groundwater flow in the Pannonian Basin', *Earth and Planetary Science Letters*, 105(1–3), pp. 229–246. doi:10.1016/0012-821X(91)90133-3.

Ballentine, C. J., Burgess, R. and Marty, B. (2002) 'Tracing Fluid Origin, Transport and Interaction in the Crust', *Reviews in Mineralogy and Geochemistry*, 47(1), pp. 539–614. doi:10.2138/rmg.2002.47.13.

Ballentine, C. J. and Burnard, P. G. (2002) 'Production, Release and Transport of Noble Gases in the Continental Crust', *Reviews in Mineralogy and Geochemistry*, 47(1), pp. 481–538. doi:10.2138/rmg.2002.47.12.

Ballentine, C. J. and Sherwood Lollar, B. (2002) 'Regional groundwater focusing of nitrogen and noble gases into the Hugoton-Panhandle giant gas field, USA', *Geochimica et Cosmochimica Acta*, 66(14), pp. 2483–2497. doi:10.1016/S0016-7037(02)00850-5.

Barati, R. and Liang, J.-T. (2014) 'A review of fracturing fluid systems used for hydraulic fracturing of oil and gas wells', *Journal of Applied Polymer Science*, 131(16). doi:10.1002/app.40735.

BBC (2013) 'US oil output beats imports for first time in 18 years', *BBC News online*, 13 November. Available at: http://www.bbc.co.uk/news/business-24935364.

Bell, R. A., Darling, W. G., Manamsa, K. and Ó Dochartaigh, B. E. (2016) *The Baseline Concentrations of Methane in Great British Groundwater - the National Methane Baseline Survey*, *British Geological Survey Open Report OR/15/071*. Nottingham, U.K.: British Geological Survey. Available at: http://nora.nerc.ac.uk/id/eprint/514557/1/National Methane Baseline Survey OR15071.pdf.

Bell, R. A., Darling, W. G., Ward, R. S., Basava-Reddi, L., Halwa, L., Manamsa, K. and Ó Dochartaigh, B. E. (2017) 'A baseline survey of dissolved methane in aquifers of Great Britain', *Science of The Total Environment*, 601–602, pp. 1803–1813. doi:10.1016/j.scitotenv.2017.05.191.

Bosch, A. and Mazor, E. (1988) 'Natural gas association with water and oil as depicted by atmospheric noble gases: case studies from the southeastern Mediterranean Coastal Plain', *Earth and Planetary Science Letters*, 87(3), pp. 338–346. doi:10.1016/0012-821X(88)90021-0.

Brantley, S. L., Yoxtheimer, D., Arjmand, S., Grieve, P., Vidic, R., Pollak, J., Llewellyn, G. T., Abad, J. and Simon, C. (2014) 'Water Resource Impacts during Unconventional Shale Gas Development: the Pennsylvania Experience', *International Journal of Coal Geology*. Elsevier B.V., (2014). doi:10.1016/j.coal.2013.12.017.

Broomfield, M. and Donovan, B. (2012) *Monitoring and Control of Fugitive Methane from Unconventional Gas Operations*. Bristol, U.K.: Environment Agency.

Burnard, P. (2013) *The Noble Gases as Geochemical Tracers*. Edited by P. Burnard. Berlin, Heidelberg: Springer Berlin Heidelberg. doi:10.1007/978-3-642-28836-4 ISBN: 978-3-642-28835-7.

Castro, M. C., Jambon, A., de Marsily, G. and Schlosser, P. (1998) 'Noble gases as natural tracers of water circulation in the Paris Basin: 1. Measurements and discussion of their origin and mechanisms of vertical transport in the basin', *Water Resources Research*, 34(10), p. 2443. doi:10.1029/98WR01956.

Cathles III, L., Brown, L., Taam, M. and Hunter, A. (2012) 'A commentary on "The greenhouse-gas footprint of natural gas in shale formations" by R.W. Howarth, R. Santoro, and Anthony Ingraffea', *Climatic Change*. Springer Netherlands, 113(2), pp. 525–535. doi:10.1007/s10584-011-0333-0.

Chojna, J., Losoncz, M. and Suni, P. (2013) 'Shale Energy Shapes Global Energy Markets', *National Institute Economic Review*, 226(1), pp. F40–F45. doi:10.1177/002795011322600115.

Clarke, H., Eisner, L., Styles, P. and Turner, P. (2014) 'Felt seismicity associated with shale gas hydraulic fracturing: The first documented example in Europe', *Geophysical Research Letters*, 41(23), pp. 8308–8314. doi:10.1002/2014GL062047.

Coplen, T. B. (1995) 'Reporting of stable hydrogen, carbon, and oxygen isotopic abundances', *Geothermics*, 24(5–6), pp. 707–712. doi:10.1016/0375-6505(95)00024-0.

Cosgrove, J. W. (1995) 'The expression of hydraulic fracturing in rocks and sediments', *Geological Society, London, Special Publications*, 92(1), pp. 187–196. doi:10.1144/GSL.SP.1995.092.01.10.

Crovetto, R., Fernández-Prini, R. and Japas, M. L. (1982) 'Solubilities of inert gases and methane in H2O and in D2O in the temperature range of 300 to 600 K', *The Journal of Chemical Physics*, 76(2), pp. 1077–1086. doi:10.1063/1.443074.

Darrah, T. H., Vengosh, a., Jackson, R. B., Warner, N. R. and Poreda, R. J. (2014) 'Noble gases identify the mechanisms of fugitive gas contamination in drinking-water wells overlying the Marcellus and Barnett Shales', *Proceedings of the National Academy of Sciences*, 111(39), pp. 14076–14081. doi:10.1073/pnas.1322107111.

Davies, R. J. (2011) 'Methane contamination of drinking water caused by hydraulic fracturing remains unproven', *Proceedings of the National Academy of Sciences*. National Acad Sciences, 108(43), pp. E871–E871. doi:10.1073/pnas.1113299108.

Davies, R. J., Mathias, S. A., Moss, J., Hustoft, S. and Newport, L. (2012) 'Hydraulic fractures: How far can they go?', *Marine and Petroleum Geology*. Elsevier Ltd, 37(1), pp. 1–6. doi:10.1016/j.marpetgeo.2012.04.001.

Dusseault, M. B., Jackson, R. E. and MacDonald, D. (2014) *Towards a Road Map for Mitigating the Rates and Occurrences of Long-Term Wellbore Leakage*. University of Waterloo/Geofirma. Available at: http://www.geofirma.com/Links/Wellbore_Leakage_Study compressed.pdf.

Engelder, T. (2012) 'Capillary tension and imbibition sequester frack fluid in Marcellus gas shale', *Proceedings of the National Academy of Sciences*, 109(52), pp. E3625–E3625. doi:10.1073/pnas.1216133110.

Engelder, T., Cathles, L. M. and Bryndzia, L. T. (2014) 'The fate of residual treatment water in gas shale', *Journal of Unconventional Oil and Gas Resources*. Elsevier Ltd, 7(0), pp. 33–48. doi:10.1016/j.juogr.2014.03.002.

Engelder, T. and Lash, G. (2008) 'Marcellus Shale Play's Vast Resource Potential Creating Stir in Appalachia', *The American Oil and Gas Reporter*. Available at: http://ithacalibrary.com/sp/assets/users/_rgilmour/EngelderLash08OGRept.pdf (Accessed: 4 June 2014).

Gilfillan, S. and Haszeldine, S. (2011) *Report on Noble Gas, Carbon Stable Isotopes and HCO3 Measurements from the Kerr Quarter and Surrounding Area, Goodwater, Saskatchewan*. IPAC CO2 Research Incorporated. Available at: https://www.geos.ed.ac.uk/homes/sgilfil1/Kerrreport.pdf.

Gilfillan, S. M. V., Ballentine, C. J., Holland, G., Blagburn, D., Lollar, B. S., Stevens, S., Schoell, M. and Cassidy, M. (2008) 'The noble gas geochemistry of natural CO2 gas reservoirs from the Colorado Plateau and Rocky Mountain provinces, USA', *Geochimica et Cosmochimica Acta*, 72(4), pp. 1174–1198. doi:10.1016/j.gca.2007.10.009.

Gilfillan, S. M. V., Wilkinson, M., Haszeldine, R. S., Shipton, Z. K., Nelson, S. T. and Poreda, R. J. (2011) 'He and Ne as tracers of natural CO2 migration up a fault from a deep reservoir', *International Journal of Greenhouse Gas Control*, 5(6), pp. 1507–1516. doi:10.1016/j.ijggc.2011.08.008.

Giustini, F., Blessing, M., Brilli, M., Lombardi, S., Voltattorni, N. and Widory, D. (2013) 'Determining the origin of carbon dioxide and methane in the gaseous emissions of the San Vittorino plain (Central Italy) by means of stable isotopes and noble gas analysis', *Applied Geochemistry*. Elsevier Ltd, 34(0),

pp. 90–101. doi:10.1016/j.apgeochem.2013.02.015.
Golding, S. D., Boreham, C. J. and Esterle, J. S. (2013) 'Stable isotope geochemistry of coal bed and shale gas and related production waters: A review', *International Journal of Coal Geology*, 120, pp. 24–40. doi:10.1016/j.coal.2013.09.001.
Gooddy, D. C. and Darling, W. G. (2005) 'The potential for methane emissions from groundwaters of the UK', *Science of The Total Environment*, 339(1–3), pp. 117–126. doi:10.1016/j.scitotenv.2004.07.019.
Harrison, S. S. (1985) 'Contamination of Aquifers by Overpressuring the Annulus of Oil and Gas Wells', *Ground Water*. Blackwell Publishing Ltd, 23(3), pp. 317–324. doi:10.1111/j.1745-6584.1985.tb00775.x.
Hitchman, S. P., Darling, W. G. and Williams, G. M. (1989) *STABLE ISOTOPE RATIOS IN METHANE CONTAINING GASES IN THE UNITED KINGDOM*, *Technical Report WE/89/30*. Nottingham: British Geological Survey.
Holditch, S. (2006) 'Tight Gas Sands', *Journal of Petroleum Technology*, 58(6). doi:10.2118/103356-MS.
Hosgormez, H., Etiope, G. and Yalcin, M. N. (2008) 'New evidence for a mixed inorganic and organic origin of the Olympic Chimaera fire (Turkey): a large onshore seepage of abiogenic gas', *Geofluids*, 8(4), pp. 263–273. doi:10.1111/j.1468-8123.2008.00226.x.
HSE (1985) *The Abbeystead Explosion - A report of the investigation by the Health and Safety Executive into the explosion on 23 May 1984 at the valve house of the Lune/Wyre Water Transfer Scheme at Abbeystead*. Health and Safety Executive.
Hubbert, M. K. and Willis, D. G. (1957) 'Mechanics of Hydraulic Fracturing', *Transactions of Society of Petroleum Engineers of AIME*, 210, pp. 153–168.
Hunt, A. G., Darrah, T. H. and Poreda, R. J. (2012) 'Determining the source and genetic fingerprint of natural gases using noble gas geochemistry: A northern Appalachian Basin case study', *AAPG Bulletin*, 96(10), pp. 1785–1811. doi:10.1306/03161211093.
Hurst, A., Scott, A. and Vigorito, M. (2011) 'Physical characteristics of sand injectites', *Earth-Science Reviews*. Elsevier B.V., 106(3–4), pp. 215–246. doi:10.1016/j.earscirev.2011.02.004.
IPCC (2013) *Climate Change 2013: The Physical Science Basis. Contribution of Working Group I to the Fifth Assessment Report of the Intergovernmental Panel on Climate Change*. Edited by T. F. Stocker et al. Cambridge, U.K., and New York, U.S.A.: Cambridge University Press. ISBN: 978-1-107-66182-0.
Jackson, R. E., Gorody, A. W., Mayer, B., Roy, J. W., Ryan, M. C. and Van Stempvoort, D. R. (2013) 'Groundwater Protection and Unconventional Gas Extraction: The Critical Need for Field-Based Hydrogeological Research', *Groundwater*, 51(4), pp. 488–510. doi:10.1111/gwat.12074.
Jenner, S. and Lamadrid, A. J. (2013) 'Shale gas vs. coal: Policy implications from environmental impact comparisons of shale gas, conventional gas, and coal on air, water, and land in the United States', *Energy Policy*. Elsevier, 53, pp. 442–453. doi:10.1016/j.enpol.2012.11.010.
Judd, A., Sim, R., Kingston, P. and McNally, J. (2002) 'Gas seepage on an intertidal site: Torry Bay, Firth of Forth, Scotland', *Continental Shelf Research*, 22(16), pp. 2317–2331. doi:10.1016/S0278-4343(02)00058-4.
Kargbo, D. M., Wilhelm, R. G. and Campbell, D. J. (2010) 'Natural gas plays in the Marcellus Shale: challenges and potential opportunities.', *Environmental science & technology*, 44(15), pp. 5679–84. doi:10.1021/es903811p.
Kerr, R. A. (2010) 'Natural Gas From Shale Bursts Onto the Scene', *Science*, 328(5986), p. 1624. doi:10.1126/science.328.5986.1624.
Kharak, Y. K., Thordsen, J. J., Conaway, C. H. and Thomas, R. B. (2013) 'The Energy-Water Nexus: Potential Groundwater-Quality Degradation Associated with Production of Shale Gas', *Procedia Earth and Planetary Science*, 7, pp. 417–422. doi:10.1016/j.proeps.2013.03.132.
Kinnaman, F. S., Valentine, D. L. and Tyler, S. C. (2007) 'Carbon and hydrogen isotope fractionation associated with the aerobic microbial oxidation of methane, ethane, propane and butane', *Geochimica et Cosmochimica Acta*, 71(2), pp. 271–283. doi:10.1016/j.gca.2006.09.007.
Kipfer, R., Aeschbach-Gertig, W., Peeters, F. and Stute, M. (2002) 'Noble Gases in Lakes and Groundwaters', in Porcelli, D., Ballentine, C. J., and Wieler, R. (eds) *Noble Gases in Geochemistry and Cosmochemistry*. Washington, D.C.: Mineralogical Society of America and the Geochemical Society, pp. 615–700. doi:10.1017/S0026461X00011713.
Kuuskraa, V., Stevens, S. and Moodhe, K. (2013) *Technically Recoverable Shale Oil and Shale Gas Resources: An Assessment of 137 Shale Formations in 41 Countries Outside the United States*. Washington, D.C.: U.S. Department of Energy.
Libby, W. (1946) 'Atmospheric Helium Three and Radiocarbon from Cosmic Radiation', *Physical Review*, 69(11–12), pp. 671–672. doi:10.1103/PhysRev.69.671.2.
Lupton, J. and Evans, L. (2013) 'Changes in the atmospheric helium isotope ratio over the past 40 years', *Geophysical Research Letters*, 40(23), pp. 6271–6275. doi:10.1002/2013GL057681.
Mackintosh, S. J. and Ballentine, C. J. (2012) 'Using 3He/4He isotope ratios to identify the source of deep reservoir contributions to shallow fluids and soil gas', *Chemical Geology*. Elsevier B.V., 304–305(0), pp. 142–150. doi:10.1016/j.chemgeo.2012.02.006.

Mair, R., Bickle, M., Goodman, D. and Koppelman, B. (2012) *Shale gas extraction in the UK: a review of hydraulic fracturing*. The Royal Society and The Royal Academy of Engineering. Available at: http://eprints.gla.ac.uk/69554/1/PY-Shale-gas-2012-06-28-.pdf.

Mamyrin, B. W., Annufriev, G., Kamenskiy, G. S. and Tolstikhin, I. L. (1970) 'Determination of the isotopic composition of atmospheric helium', *Geochem. Int.*, 7, pp. 498–505.

Martini, A. M., Walter, L. M., Budai, J. M., Ku, T. C. W., Kaiser, C. J. and Schoell, M. (1998) 'Genetic and temporal relations between formation waters and biogenic methane: Upper Devonian Antrim Shale, Michigan Basin, USA', *Geochimica et Cosmochimica Acta*, 62(10), pp. 1699–1720. doi:10.1016/S0016-7037(98)00090-8.

Meslé, M., Dromart, G. and Oger, P. (2013) 'Microbial methanogenesis in subsurface oil and coal', *Research in Microbiology*, 164(9), pp. 959–972. doi:10.1016/j.resmic.2013.07.004.

Mills, C. T., Slater, G. F., Dias, R. F., Carr, S. A., Reddy, C. M., Schmidt, R. and Mandernack, K. W. (2013) 'The relative contribution of methanotrophs to microbial communities and carbon cycling in soil overlying a coal-bed methane seep', *FEMS Microbiology Ecology*, 84(3), pp. 474–494. doi:10.1111/1574-6941.12079.

Molofsky, L. J., Connor, J. A., Farhat, S. K., Wylie, A. S. and Wagner, T. (2011) 'Methane in Pennsylvania water wells unrelated to Marcellus shale fracturing', *Oil & Gas journal*. Pennwell, 109(19), pp. 54–93. Available at: https://www.researchgate.net/publication/279578853_Methane_in_Pennsylvania_water_wells_unrelated_to_Marcellus_Shale_fracturing (Accessed: 11 December 2013).

Molofsky, L. J., Connor, J. A., Wylie, A. S., Wagner, T. and Farhat, S. K. (2013) 'Evaluation of Methane Sources in Groundwater in Northeastern Pennsylvania', *Groundwater*. Blackwell Publishing Ltd, 51(3), pp. 333–349. doi:10.1111/gwat.12056.

Montgomery, C. T. and Smith, M. B. (2010) 'Hydraulic Fracturing: History of an Enduring Technology', *Journal of Petroleum Technology*, 62(12), pp. 26–40. doi:10.2118/1210-0026-JPT.

Myers, T. (2012) 'Potential Contaminant Pathways from Hydraulically Fractured Shale to Aquifers', *Groundwater*, 50(6), pp. 872–882. doi:10.1111/j.1745-6584.2012.00933.x.

Osborn, S. G., Vengosh, A., Warner, N. R. and Jackson, R. B. (2011) 'Methane contamination of drinking water accompanying gas-well drilling and hydraulic fracturing', *Proceedings of the National Academy of Sciences*, 108(20), pp. 8172–8176. doi:10.1073/pnas.1100682108.

Ozima, M. and Podosek, F. A. (2001) *Noble Gas Geochemistry*. 2nd edn. Cambridge: Cambridge University Press. doi:10.1017/CBO9780511545986 ISBN: 9780511545986.

Porcelli, D., Ballentine, C. J. and Wieler, R. (2002) 'An Overview of Noble Gas Geochemistry and Cosmochemistry', *Reviews in Mineralogy and Geochemistry*, 47(1), pp. 1–19. doi:10.2138/rmg.2002.47.1.

Potter, J., Salvi, S. and Longstaffe, F. J. (2013) 'Abiogenic hydrocarbon isotopic signatures in granitic rocks: Identifying pathways of formation', *Lithos*. Elsevier B.V., 182–183(0), pp. 114–124. doi:10.1016/j.lithos.2013.10.001.

Révész, K. M., Breen, K. J., Baldassare, A. J. and Burruss, R. C. (2010) 'Carbon and hydrogen isotopic evidence for the origin of combustible gases in water-supply wells in north-central Pennsylvania', *Applied Geochemistry*. Elsevier Ltd, 25(12), pp. 1845–1859. doi:10.1016/j.apgeochem.2010.09.011.

Rooney, M. A., Claypool, G. E. and Moses Chung, H. (1995) 'Modeling thermogenic gas generation using carbon isotope ratios of natural gas hydrocarbons', *Chemical Geology*, 126(3–4), pp. 219–232. doi:10.1016/0009-2541(95)00119-0.

Saba, T. and Orzechowski, M. (2011) 'Lack of data to support a relationship between methane contamination of drinking water wells and hydraulic fracturing', *Proceedings of the National Academy of Sciences*, 108(37), p. E663. doi:10.1073/pnas.1108435108.

Schoell, M. (1980) 'The hydrogen and carbon isotopic composition of methane from natural gases of various origins', *Geochimica et Cosmochimica Acta*, 44(5), pp. 649–661. doi:10.1016/0016-7037(80)90155-6.

Schultz, C. (2013) 'Marcellus Shale fracking waste caused earthquakes in Ohio', *Eos, Transactions American Geophysical Union*, 94(33), pp. 296–296. doi:10.1002/2013EO330008.

Selley, R. C. (1992) 'Petroleum seepages and impregnations in Great Britain', *Marine and Petroleum Geology*, 9(3), pp. 226–244. doi:10.1016/0264-8172(92)90072-M.

Simonson, E. R., Abou-Sayed, A. S. and Clifton, R. J. (1978) 'Containment of Massive Hydraulic Fractures', *Society of Petroleum Engineers Journal*, 18(1). doi:10.2118/6089-PA.

Strąpoć, D., Mastalerz, M., Dawson, K., Macalady, J., Callaghan, A. V., Wawrik, B., Turich, C. and Ashby, M. (2011) 'Biogeochemistry of Microbial Coal-Bed Methane', *Annual Review of Earth and Planetary Sciences*. Annual Reviews, 39(1), pp. 617–656. doi:10.1146/annurev-earth-040610-133343.

Stute, M. and Schlosser, P. (2013) 'Principles and Applications of the Noble Gas Paleothermometer', in *Climate Change in Continental Isotopic Records, Volume 78*. American Geophysical Union, pp. 89–100. doi:10.1029/GM078p0089.

Tans, P. P., M., D. J. A. F. and Mook, W. G. (1979) 'Natural atmospheric 14C variation and the Suess effect',

Nature, 280(5725), pp. 826–828. doi:10.1038/280826a0.
Tomonaga, Y. (2013) 'Using noble gases in the pore water of ocean sediments to characterize CH4 seepage off the coast of New Zealand', in *EGU General Assembly*, pp. 7–8. Available at: http://meetingorganizer.copernicus.org/EGU2013/EGU2013-2878.pdf (Accessed: 28 November 2013).
Warner, N. R., Jackson, R. B., Darrah, T. H., Osborn, S. G., Down, A., Zhao, K., White, A. and Vengosh, A. (2012) 'Geochemical evidence for possible natural migration of Marcellus Formation brine to shallow aquifers in Pennsylvania', *Proceedings of the National Academy of Sciences*, 109(30), pp. 11961–11966. doi:10.1073/pnas.1121181109.
Whiticar, M. J. (1994) 'Correlation of natural gases with their sources', in *The Petroleum System - from Source to Trap*. AAPG Special Edition, pp. 261–283.
Whiticar, M. J. (1996) 'Stable isotope geochemistry of coals, humic kerogens and related natural gases', *International Journal of Coal Geology*, 32(1–4), pp. 191–215. doi:10.1016/S0166-5162(96)00042-0.
Whiticar, M. J. (1999) 'Carbon and hydrogen isotope systematics of bacterial formation and oxidation of methane', *Chemical Geology*, 161(1–3), pp. 291–314. doi:10.1016/S0009-2541(99)00092-3.
Williams, G. M. and Aitkenhead, N. (1991) 'Lessons from Loscoe: the uncontrolled migration of landfill gas', *Quarterly Journal of Engineering Geology and Hydrogeology*, 24(2), pp. 191–207. doi:10.1144/GSL.QJEG.1991.024.02.03.
Yokochi, R., Sturchio, N. C. and Purtschert, R. (2012) 'Determination of crustal fluid residence times using nucleogenic 39Ar', *Geochimica et Cosmochimica Acta*. Elsevier Ltd, 88(0), pp. 19–26. doi:10.1016/j.gca.2012.04.034.
Zhou, Z., Ballentine, C. J., Kipfer, R., Schoell, M. and Thibodeaux, S. (2005) 'Noble gas tracing of groundwater/coalbed methane interaction in the San Juan Basin, USA', *Geochimica et Cosmochimica Acta*, 69(23), pp. 5413–5428. doi:10.1016/j.gca.2005.06.027.
Zhou, Z. and Ballentine, C. J. (2006) '4He dating of groundwater associated with hydrocarbon reservoirs', *Chemical Geology*, 226(3–4), pp. 309–327. doi:10.1016/j.chemgeo.2005.09.030.

2 Methodology

2.1 Introduction

The bulk gas composition, stable carbon and hydrogen isotopes of methane, radiocarbon of methane, and noble gases, were required to be analysed from both gaseous and liquid samples. This required a significant amount of specific equipment and handling to correctly capture, transport, and process samples into forms suitable for inlet into the numerous pieces of analytical equipment. "Off-the-shelf" equipment was not available for gas transfers or radiocarbon sample collection, and had to be designed and constructed by the author to specific requirements, which are detailed below.

This chapter provides a brief overview of the methodology of sample capture, storage, processing, and analysis for each of the analytical methods. Several problems with the sample collection, sample storage, and analytical methods were noted, and suggestions made to improve outcomes in future work.

2.2 Field Sample Collection

Gas samples for the Airth Field (Chapter 3) were collected by Dr. S Gilfillan (University of Edinburgh). Dr. D Györe (SUERC) collected the Mine Gas samples (Chapter 4). The author collected all remaining gas samples (Chapter 5). All water samples were collected by the author (Chapter 5).

2.2.1 Gases

Samples were collected in 3/8th inch (9.525 mm) outer diameter L-type (wall thickness = 0.040"/1.016 mm), soft-annealed, internally cleaned and polished refrigeration grade copper tubing. A clamp system was used to seal both ends (see Figure 2-1). The jaws of the clamps are set to compress the ends of the tube to a thickness of 0.7 mm to ensure a gas-tight cold welded seal between the copper surfaces (Kennedy *et al.*, 1985; Kulongoski and Hilton, 2002).

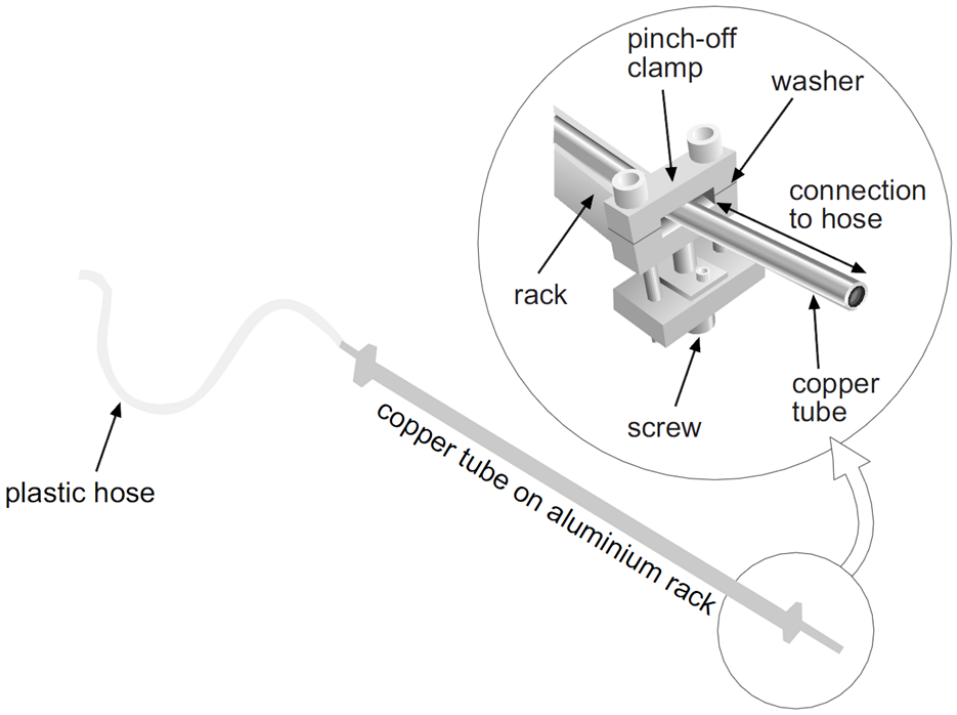

Figure 2-1 – Diagram of sample collection tubing and clamp assembly. Figure reproduced from Becker (2005).

Samples were collected from the wellheads/vents by attaching a stainless steel high-pressure regulator to a sampling port on the wellhead, or onto the sampling port for vents, with flexible high-pressure plastic tubing connecting the regulator to the copper tube and clamp. High-pressure plastic tubing was connected to the outflow to prevent turbulent back-mixing of air. For well gases, the regulator pressure was set to 1 bar gauge (2 bar absolute) and flowed for several minutes to purge air from the sampling system. For seep gases, the outflow end was submerged in water to prevent air contamination and sample gases were allowed to bubble through for >5 minutes. The tubes were then clamped shut at the outflow side before sealing the inflow side.

2.2.2 Waters

Due to the relatively large volumes of methane required for radiocarbon analysis compared to stable isotope analysis, standard equipment for collecting water samples could not be used. The water sample collection method was designed by the author, modified from elements of standard methane collection methods (*e.g.* Isotech Labs procedure developed by Anthony Gorody (Isotech Labs, 2014), US-EPA method RSKSOP-175 (Hudson, 2004), Kampbell and Vandegrift, (1998), and advice from Dr. Pauline Gulliver (Scottish Universities Education Research Council; East Kilbride)). The

procedure mainly differs from the above in that non-standard equipment and larger (2l) sample volumes are collected. A review of commonly used sampling procedures for volatile gases can be found in Molofsky *et al.,* (2016) and appears to validate the method chosen.

To ensure sufficient methane volumes for radiocarbon, samples for stable isotopes/radiocarbon were collected in 2l borosilicate glass bottles. These required custom rubber stoppers to be fabricated by the author, featuring two 6mm stainless steel tubes attached to gas-tight coupling connectors with Tygon® tubing.

Water was collected by attaching a battery driven impeller pump to the outflow side of the sampling container and then drawing water through with a siphon to prime the pump (Figure 2-2). When collecting waters for dissolved gas analysis it is imperative to not allow degassing of water during sampling, as methane and noble gases are highly volatile and will escape from the water phase giving erroneous results.

After sampling, the Tygon® tubing was clamped to minimise isotopic fractionation by diffusion through the plastic, and stored inverted to ensure any gas generated would not escape.

Noble gas samples were collected in copper tubes as described previously for gas samples.

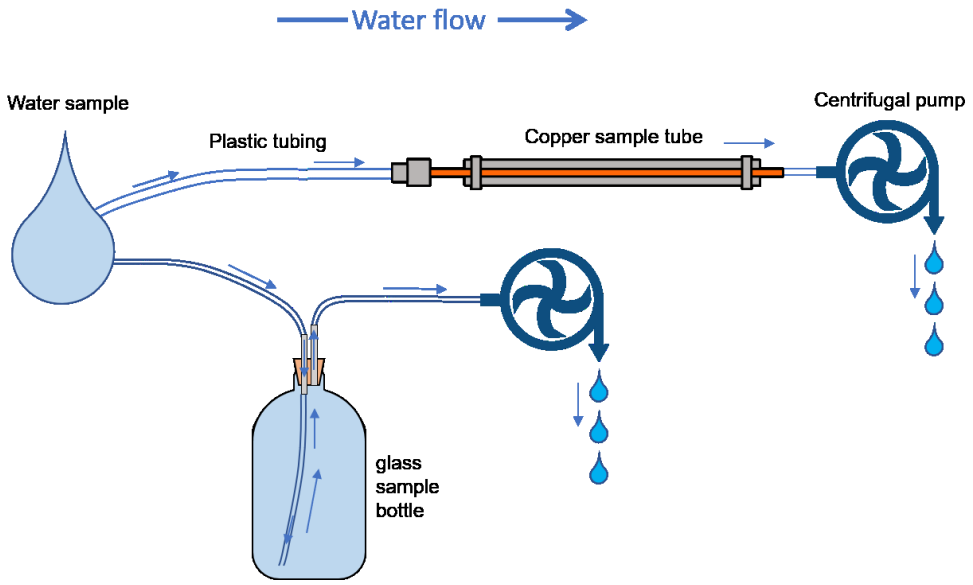

Figure 2-2 – Schematic of sample collection procedures in copper tubes (for noble gas analysis) and glass bottles (for radiocarbon and stable isotope analysis).

The pump placement ensured that the fast-moving impeller blades did not degas the sample on the inflow side. For noble gases, water was flowed through the copper tubes for several minutes before sealing the outflow end and then the inlet end. For radiocarbon/stable isotopes, the glass bottle was filled and several bottle volumes were pumped through before sealing the outlet and inlet valves. Water was collected from a wellhead with flow reducers attached for the artesian well at Balcombe, flushing several volumes through the sample bottle. All glass bottles were stored in cool boxes and kept refrigerated, and analysed within 1 week as per standard practice (Kampbell and Vandegrift, 1998; Hudson, 2004).

Sampling of St. Catherine's well waters. Copper tubing and battery-driven pump on the outflow side can be observed.

2.3 Sample Preparation

2.3.1 Gas Extraction Line

As gas samples were captured in sealed copper tubes, it was necessary for the author to construct a custom gas extraction line to allow the splitting of a gas sample, so that it could be analysed with several machines in different laboratories. The extraction line allowed the transfer of gas from the copper sampling tubes to a silicone septum for bulk gas analysis by gas chromatography at Edinburgh University, and then transfer the remaining sample into a gas bag for stable isotope and radiocarbon analyses at SUERC.

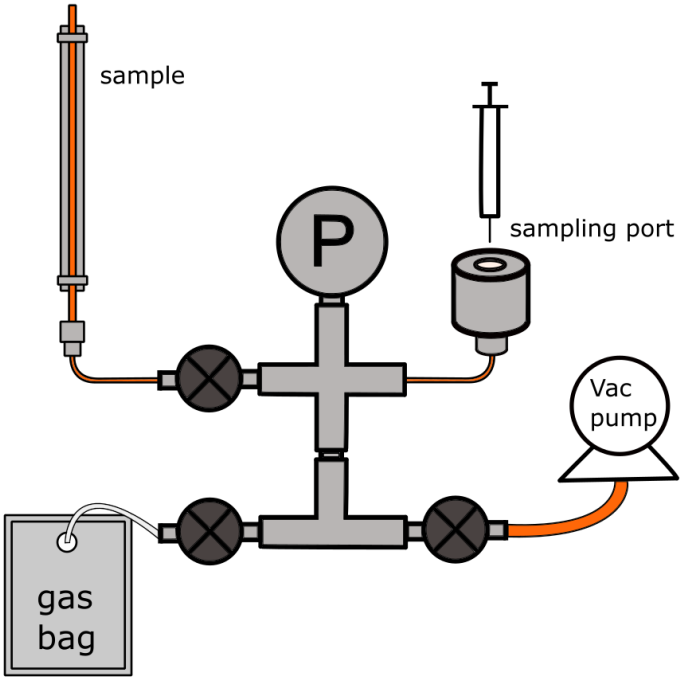

Figure 2-3 – Schematic of gas extraction line

The extraction line was comprised of a mix of all-metal Swagelok® tube fittings, 1/8" BSPP fittings, and 1/8" diameter copper tubing to minimise internal volume. At one end a 3/8" ferrule adaptor is used for attaching copper sample tubes, attached to a 4-way tee for attaching a digital vacuum pressure gauge, a needle valve for isolating the vacuum pump, and another tee. Connected to that tee was a sampling port constructed from Swagelok® Ultratorr adaptor fitted with a 7 mm silicone rubber septum, and a valve for isolating connection to a gas bag. An oil-free rotary vacuum pump was used to reduce the pressure in the vacuum line to ~0.001 atm, before isolating the vacuum pump and gas bag, then opening the cold-weld seal on the copper tube to release gas into the initial section of the line. Aliquots of gas for GC analysis were then manually taken with a gas syringe from the septum and injected into the inlet of the GC. Once complete, the remaining sample was diluted with 300 ml high-purity helium through the septum in order to transfer it to a gas bag (previously helium flushed and then evacuated). Samples were then transported in gas bags to SUERC (East Kilbride) for stable isotope and radiocarbon analysis.

2.3.2 Water degassing

Degassing water was performed by the author for methane radiocarbon samples dissolved in water. This involved replacing a volume (200 cc) of water within the 2 litre sample bottle with the equivalent volume of inert gas via the sampling ports built into

the custom rubber stopper using two syringes. The bottle is then vigorously shaken to promote degassing of methane. The methane enriched gas headspace is then transferred into a gas bag by re-introducing the water.

2.4 Bulk Gases

Bulk gases were analysed by Gas Chromatography (GC). Gas Chromatography was determined to be the most accurate and reliable method for major gas analysis, and this equipment and its related consumables was assembled, purchased, upgraded, set up, programmed, and calibrated over several months by the author. The GC used was a Perkin-Elmer AutoSystem XL, which was fitted with a 30 m, 0.53 mm internal diameter Sigma-Aldrich Carboxen-1010 Porous Layer Open Tubing (PLOT) column. This activated-carbon lined capillary column was chosen over more typical zeolite-based packed columns (e.g. Molsieve-5A) for several reasons. The lower helium carrier flow rates, ability to resolve O_2(+Ar) from N_2 whilst maintaining practical run-times, propane resolution, and smaller sample volume requirements relative to packed columns (necessary due to small sample volumes available in the copper tubes and subsequent analyses) were the main reasons. Further to these, the chosen column offered greater water and H_2S tolerance for the carbon-based stationary phase for environmental samples, and fewer phase-conditioning and bake-outs required.

The machine was modified to route the outlet from the Thermal Conductivity Detector (TCD) to the Flame Ionisation Detector (FID) allowing the operation of both detectors in series, and a second flow control valve retrofitted to allow more precise carrier gas flow adjustments which are necessary for PLOT columns. Additionally, the author installed and tested new gas lines and a regulator for hydrogen, synthetic air, and helium utilising pre-cleaned 1/8” copper tubing, as well as a replacement computer system and monitor.

A GC program was developed for the analysis over hundreds of iterations by the author, eventually settling on a temperature of 40°C for 7 minutes to allow low-temperature resolution between O_2(+Ar) and N_2, then 30°C/min temperature ramp up to 240°C for heavier components. High purity helium carrier gas was used at 30 ml/min with no flow ramping. Separate programs were required to resolve higher CO_2 concentrations in some samples, incorporating higher detector attenuation for CO_2 so that it could be detected without saturating the signal. 7-point calibration curves for methane, ethane, propane, nitrogen, carbon monoxide and acetylene were produced

from the averages of multiple (n≥10) runs at each concentration to account for manual injection error, using custom calibration standards manufactured by CalGaz Ltd. (UK) (see Figure 2-4 and Figure 2-5).

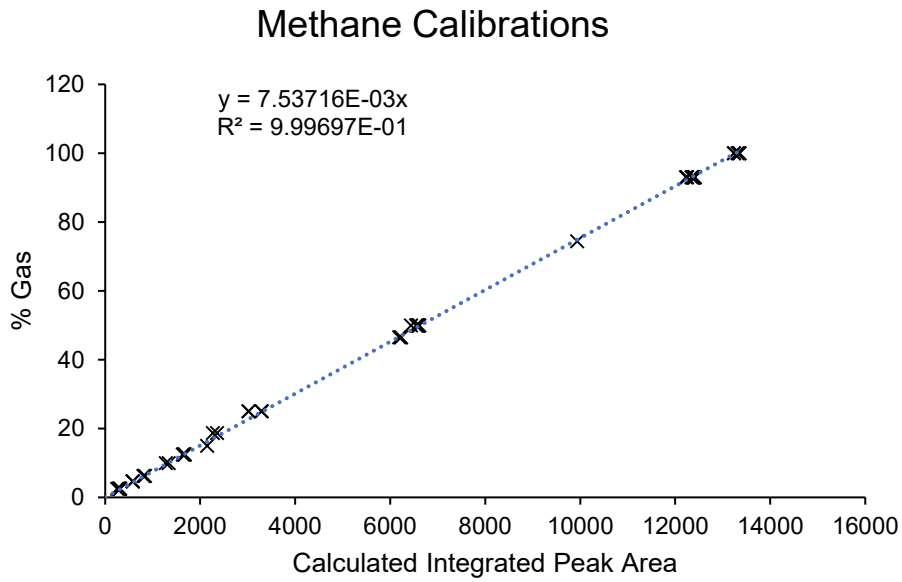

Figure 2-4 – Example of a methane calibration curve with linear response.

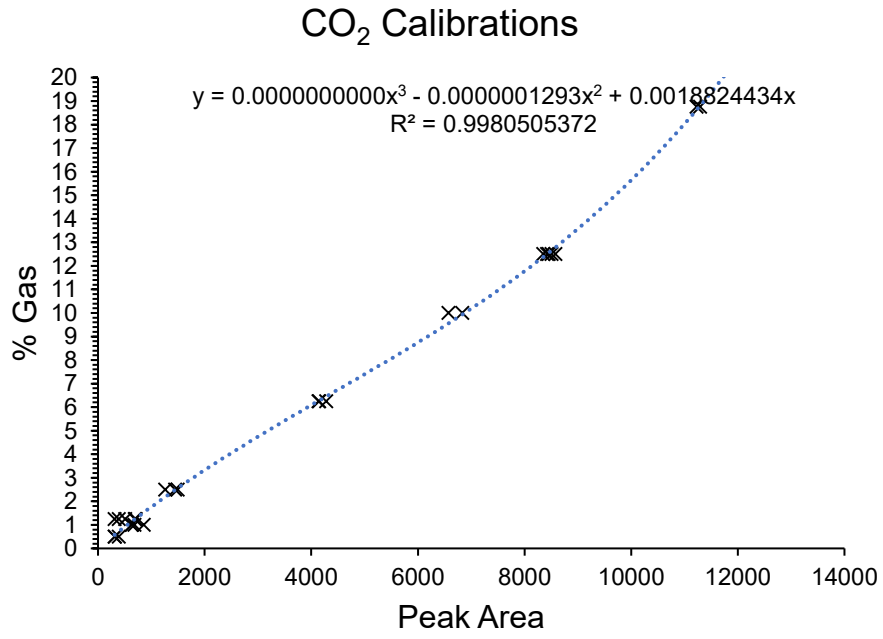

Figure 2-5 – Example of a CO_2 calibration curve with an almost linear response, for samples up to 20% CO_2.

A second calibration curve was also generated for the higher-CO_2 GC program. The FID response was found to be linear, while the TCD response varied with the range in concentrations for CO_2 and N_2. H_2 determination was attempted, however there is not a significant difference in the thermal conductivity between H_2 and He for detection via TCD (Thompson, 1977) and the Carboxen-1010 column is likely to have little resolution between He (carrier) and H_2 (analyte). Such analyses are usually performed with Ar or Ar-blended carrier gas due to non-linear effects with helium such as obtaining both negative and positive peak shapes depending on H_2 concentration (Couwper and DeRose, 1983), so this was deemed beyond the scope of the project.

Aliquots of sample gas (200 µl) were transferred from the gas extraction line in gas syringes and manually injected into the GC, before starting the programmed run cycle and data logger. O_2, N_2, acetylene, CO, and CO_2 were detected via TCD, whilst all other carbon-based species were detected by FID. Raw data was digitised by a PeakSimple USB data logger, and displayed on a computer using PeakSimple software. A series of GC programs utilising different sensor ranges were created to facilitate measurements of varying concentrations, as the TCD detector is not linear over 0-100% concentration ranges. Sample measurements were integrated and referenced to the set of calibration curves to determine absolute concentrations. Measurements were performed in triplicate, and the mean measurements are reported to mitigate errors arising from manual syringe injection. Errors are calculated using the standard error of multiple calibration measurements. Calibration runs were performed before every sample to ensure consistent operation of the GC.

Manual sample injection requires gas to be at (or above) atmospheric pressure so that samples can be referenced to identical volumes of calibration gas, as well as preventing air-ingress into gas syringes from samples that are below atmospheric pressure. In some cases this was not possible as some samples were at, or near, atmospheric pressure. For this reason, data are reported as ratios rather than absolute concentrations to remove the effects of potential air contamination, as hydrocarbons and CO_2 are not found in the atmosphere in significant concentrations.

2.5 Carbon and Hydrogen Stable Isotopes

After bulk gas determination by GC, the remaining gas in the copper tube connected to the extraction line was diluted with high-purity helium and transferred to a flexfoil gas bag. Dilution was necessary to increase the gas pressure partially above atmospheric so

the remaining gas could be transferred into a foil gas bag for analysis at SUERC. Aliquots of sample gas (diluted with helium) were transferred manually from foil gas bags by gas syringe to the combustion line at SUERC, East Kilbride. CO_2 was separated from hydrocarbons using a liquid nitrogen cooled isopentane trap (-160°C) following a method modified after Kusakabe, (2005). Samples were mixed with pure O_2 and combusted over a CuO catalyst at 900°C into CO_2 and water, which were collected cryogenically in a liquid nitrogen cooled cold finger. A pressure gradient drawing gases through the furnace was maintained by the cold finger trapping combustion products. After combustion, the cold finger was isolated and heated to ~-78°C with a dry-ice/acetone slush bath to retain water and vaporise CO_2, which was collected separately in a liquid nitrogen cooled cold finger. CO_2 combustion gas pressures were measured to ensure sufficient quantities were present for analysis, but not exceeding limits that significantly degrade catalysts for hydrogen isotope determination (typically 1 cm^3 STP pure methane).

Figure 2-6 - Gas combustion line at SUERC, East Kilbride, for stable isotope analysis.

The combusted CO_2 was analysed on a VG SIRA II dual-inlet IRMS, calibrated to internal standards (Dunbar *et al.*, 2016), and figures reported relative to VPDB (Coplen, 1995) via the equation:

$$\delta^{13}C = \left[\frac{(^{13}C/^{12}C)_{sample})}{(^{13}C/^{12}C)_{standard})} - 1 \right] \times 1000$$

$\delta^{13}C$ measurements were reported to a 1σ uncertainty of 0.1‰. The cold finger containing H_2O was connected to a manifold then heated to vapour, before being reduced to H_2 over a nickel catalyst at 800°C. H_2 was analysed in a separate Delta Optima Plus dual-inlet IRMS, calibrated to internal standards (Donnelly *et al.*, 2001), and figures reported relative to VSMOW (Gonfiantini, 1984) via the equation:

$$\delta D = \left[\frac{(^{2}H/^{1}H)_{sample})}{(^{2}H/^{1}H)_{standard})} - 1 \right] \times 1000$$

2.6 Radiocarbon

For radiocarbon analysis, the author transferred gaseous samples from the Cu tubes into gas bags in Edinburgh using the aforementioned gas extraction line with helium dilution. Water-based samples were degassed by the author and transferred into gas bags. All samples were transported to SUERC radiocarbon facility, East Kilbride, within a short time frame to prevent isotopic fractionation through the rubber gas bag septa.

The team at SUERC then scrubbed CO_2 from the samples with soda lime, with the CO_2 concentrations measured with an IR CO_2 monitor. The hydrocarbons were combusted in excess O_2 over a platinum catalyst at 950°C to CO_2, which was subsequently cryogenically collected. An aliquot was graphitised via zinc/iron reduction for introduction into SUERC's Accelerator Mass Spectrometer (AMS) (Dr. Pauline Gulliver, *pers comms*). Results are reported in terms of percent modern carbon (pMC), where 100 pMC is defined as the ^{14}C in the atmosphere prior to anthropogenic disturbance from thermonuclear bomb testing from 1950 (Coleman *et al.*, 1995; Hua *et al.*, 2013). A further aliquot of CO_2 was used for stable carbon isotope analysis on a VG SIRA 11 IRMS, with results reported relative to the Pee Dee Belemnite (PDB) standard. A detailed methodology of the ^{14}C Accelerator Mass Spectrometry (AMS) analysis procedures at SUERC can be found in Dunbar *et al.* (2016)

2.7 Noble Gas Analysis

Noble gases and bulk gas compositions in water samples were analysed by the University of Ohio. Noble gases in gaseous samples were analysed by the author at Scottish Universities Environmental Research Centre (SUERC) in East Kilbride, Central Scotland, with the assistance and supervision of Prof. F Stuart, Dr. D Györe, and Dr. Marta Zurakowska. Sample tubes were connected via an all-metal Swagelok 3/8" tube fitting to an all-metal ultra-high vacuum (UHV pressure = $< 10^{-7}$ mbar) gas preparation line. Atmospheric air was then pumped from the blank end of the copper tube using a Pfeiffer Vacuum HiPace 80 dual-stage turbo-molecular pump, reducing pressure down to $< 5x10^{-7}$ Torr. The samples were then expanded to the UHV line by crimping open the cold weld formed by the clamp, and the pressure within a known volume was measured with a MKS 615-A Baratron capacitance manometer to an uncertainty of ±0.5% (1σ). The active non-noble-gas components were then removed via exposure to a VG Scienta ST22 titanium sublimation pump at 900°C. The pressure in the line was monitored until it stabilised, indicating that all of the active gas component had been removed. Following this procedure the remaining gas was exposed to a SAES GP50 ZrAl getter at 250°C for 20 minutes. The purified gas was then expanded into a stainless steel 0.5 litre reservoir. Aliquots of gas (~1 cm^3) were taken from the reservoir and further purified with four GP50 ZrAl getters for analysis. Heating tape is attached to the line to keep the temperature >35°C to prevent condensing of Kr and Xe.

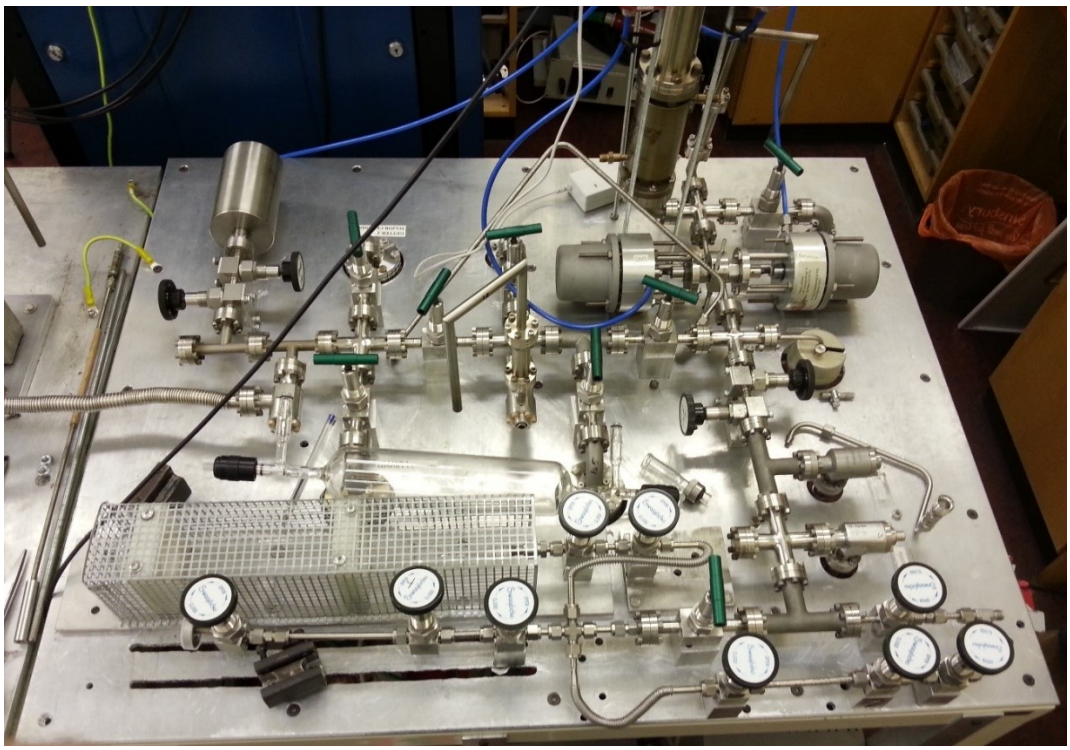

Figure 2-7 – Gas preparation line for noble gases at SUERC, East Kilbride.

All noble gases were analysed on a dual collector magnetic sector mass spectrometer (MAP 215-50) in static mode. ^{4}He, ^{36}Ar, ^{38}Ar, and ^{40}Ar were measured with a Faraday detector (10^{11} amplification), and ^{3}He, ^{20}Ne, ^{21}Ne, ^{22}Ne, ^{84}Kr, and ^{132}Xe were measured with an electron multiplier (pulse count, 2.5 kV). Measurements were calibrated against the HESJ international standard for helium (Matsuda *et al.*, 2002), and air for neon, argon, krypton and xenon.

Corrections were made for blanks which were analysed weekly. ^{3}He was resolved from HD^{+} by the mass spectrometer. Isobaric interferences that cannot be resolved (e.g. $^{40}Ar^{2+}$ results in mass/charge = 20; i.e. identical to ^{20}Ne requires a resolving power greater than the MS can provide) were corrected for by observing $40^{+}/40^{2+}$ and $44^{+}/44^{2+}$ ratios vs. H_2^{+} concentrations. Neon analysis also measured 40^{+}, $44^{+}/44^{2+}$, and H_2^{+}, which allowed corrections to be performed. $^{1}H_2{}^{19}F^{+}$ and $^{1}H_2{}^{18}O+$ (affecting ^{20}Ne) and $^{63}Cu^{3+}$ (affecting ^{21}Ne) were found to be negligible (Györe, 2015). Reproducibility was typically ±0.5% (1σ) (Györe *et al.*, 2015).

Helium analysis typically involved 1-5 aliquots of sample gas. Ar, Kr & Xe were trapped on a charcoal cold finger with liquid nitrogen (-173°C). Neon was removed for some samples by trapping on charcoal at -243°C before inletting helium into the mass spectrometer for analysis. Neon analysis involved multiple aliquots of gas; Ar, Kr, and

Xe were trapped on a charcoal cold-finger at (-173°C), neon was subsequently trapped on charcoal with a cryogenic pump at -243°C for 20 minutes, before the helium was pumped. Neon was released at -173°C for 15 minutes before expanding into the mass spectrometer. Duplicates were run for all neon measurements at Airth, but were not duplicated for samples in AMM which displayed air-like values. Argon analysis was performed by trapping Ar, Kr, and Xe on the charcoal cold-finger (-173°C), pumping the helium and neon, before releasing the argon at room temperature and expanding to the mass spectrometer. Krypton and xenon analyses were prepared as per argon, except that krypton was partially released in an acetone-dry ice slush trap (-78°C) for 15 minutes before being released to the mass spectrometer, and a second analysis was performed for xenon after releasing it with boiling water for 15 minutes.

Due to the low relative abundance of ^{3}He in sample gases, it was sometimes necessary to introduce large ^{4}He volumes into the mass spectrometer to ensure sufficient ^{3}He concentrations for reliable determination. To assess any unintended 'bleed' of ^{4}He into the ^{3}He multiplier detector mass range when large ^{4}He volumes are used, a zircon crystal was crushed in a furnace at 1500°C to release purely radiogenic ^{4}He, and the $^{3}He/^{4}He$ ratio was measured. No ^{3}He above the baseline was detected, indicating that no bleed had occurred.

2.8 Discussion

2.8.1 Sample Collection

The copper sampling tubes physically contain enough gas to perform all of the separate analytical techniques when the samples have high methane concentrations. However, noble gas analysis requires splitting the copper tubes in half, and for samples lower in methane concentration there can be insufficient methane remaining for repeat bulk gas or stable isotopes analyses, or radiocarbon analysis. This is ultimately reflected in this study by the lack of stable isotope data for some samples, and limited radiocarbon data.

The three separate locations for bulk gas, stable isotope, and radiocarbon analytical equipment required the samples to be first removed from the copper tubes, and transferred into gas bags for transporting and taking aliquots via gas syringe. This involved additional labour and materials to achieve, and was not without caveats. A custom vacuum line was built for this purpose, however the resulting volume change

when the gas in the tubes was expanded into the vacuum line meant that some samples in the vacuum line were under-pressured with respect to the atmosphere. A greater vacuum then formed when subsequent gas aliquots were removed for bulk gas analysis by GC. As a result, air ingress occurred when the gas needle was removed from the sampling septum, diluting the samples and giving non-representative absolute concentrations. This was a particular problem for Abandoned Mine Methane (AMM) samples which could only be collected at low pressures.

2.8.2 Stable Carbon and Hydrogen Isotopes

$\delta^{13}C_{CH4}$ and δD_{CH4} are reported in the text, however due to the analytical method the values are a combined methane-ethane value. It is frequent in the literature to report the $\delta^{13}C_{CH4}$ values of gases without specific details of laboratory conditions. This may be somewhat misleading, as the ethane content is difficult to separate from methane depending on the method used. For this work, CO_2 and methane were cryogenically separated at isopentane slush temperatures (-180°C), which would have removed propane and higher hydrocarbons from the analysed methane. However, ethane has a high enough partial pressure at these temperatures to be carried over with the methane (Slobod, 1951; IGT, 1955), and thus the measured values are not strictly $\delta^{13}C_{CH4}$ or δD_{CH4} values, but a more bulk combined methane-ethane value.

Even though methane is almost always the dominant gas in hydrocarbon resources, non-methane carbon-bearing species (e.g. CO_2, ethane, propane) in the gases need only to be present in small quantities to alter the carbon and hydrogen stable isotope ratios if they are not effectively separated before analysing. Simple binary mixing calculations between methane (of an assumed end member: $\delta^{13}C_{CH4}$ = -60‰) and ethane (of an assumed end member $\delta^{13}C_{C2H6}$ = -25‰) show that only 0.7% ethane is required to affect the bulk $\delta^{13}C_{Chydrocarbons}$ outside of the analytical error of the measurements (0.5‰). A 5% ethane contribution (of the previous end-members) would result in a bulk $\delta^{13}C_{hydrocarbons}$ of 56.6‰. In coals, the $\delta^{13}C_{C2H6}$ of thermogenically generated ethane is typically 6‰ heavier than the corresponding co-generated methane $\delta^{13}C_{CH4}$, but ~11‰ for type I/II kerogens (Stahl, 1977; Berner, 1989; Whiticar, 1996; Bao *et al.*, 2014).

Relative to the assumed differences in $\delta^{13}C_{CH4}$ between purely biogenic (>-60‰) and purely thermogenic coal-derived (>32‰) gases (Stahl, 1977; Berner, 1989; Whiticar, 1996; Golding *et al.*, 2013), the addition of heavier ethane isotopes can be

disregarded as a significant effect when the values are used for determining gas genetic sources from isotope values. However this could be an issue with mixed biogenic-thermogenic systems, systems with high ethane contents, or in studies where higher resolution is required such as using small isotopic differences to differentiate between different thermogenic sources (e.g. Baldassare *et al.,* 2014).

The use of a zeolite sorbent for scrubbing C_2+ contents before combustion was tested (Triebe *et al.*, 1996; Al-Baghli and Loughlin, 2005; Magnowski, 2014), but after determination of actual C_2+ contents in the gases it was not deemed necessary as the gases have low enough C_2+ content to not affect the isotopic ratios significantly. Supplementary discussion with relevant data is included in the subsequent chapters.

Addition of isotopically heavier ethane also affects radiocarbon measurements of methane, however because the use of radiocarbon in these circumstances is limited in its useful applications (outside of merely identifying the presence of modern carbon), it can be disregarded. Microbial ethanogenesis is rare and not expected in coal seams or other deep subsurface environments (Oremland *et al.*, 1988; Formolo, 2010), so all ethane is assumed to be thermogenic and thus radiocarbon dead.

2.8.3 Gas Chromatography

The bulk gas data in this study are reported as ratios of species instead of absolute concentrations. This is because of the aforementioned issue with atmospheric contamination of the gas syringe. Reporting ratios of gases remove the effects of atmospheric contamination, as there is negligible methane, ethane, propane and carbon dioxide in the atmosphere relative to the samples. The reported ratios are the average over a minimum of 3 repeat analyses and showed good reproducibility. Absolute concentrations (where given) were determined from the first run of a sample, and can be accurate to within errors of ± 5%.

Setting up the TCD on the GC to quantitatively analyse N_2 proved problematic due to the concentrations expected (0 - 80+%) and the unsuitability of the Thermal Conductivity Detector (TCD) with the small sample volumes associated with PLOT capillary columns. The GC used was built *circa* 1990; while the physics and principles behind gas chromatography have not changed, better results could be obtained with more modern equipment. This is partly due to the difficulties encountered when retrofitting the older GC with the necessary equipment (PLOT column, additional micro-flow gas regulator, dual-detector analysis), and also because advancements in

the field (e.g. automatic split-sampling, automated sample injection) help mitigate inherent human error in sample handling and calibrations.

A more modern GC equipped with a split sampling inlet would allow the reduction of non-linear effects with TCD detectors, and eliminate the need for separate GC programs and linked calibration data. More modern micro-TCD technology designed for operation with PLOT columns would also allow accurate quantitative determination.

2.8.4 Suggested Method Improvements

2.8.4.1 Sampling

For future sampling work, samples should be collected in both copper tubes and directly into foil gas bags. This would provide long-term storage for noble gas samples, and avoid the issues encountered when transferring samples from copper tubes into gas bags, as well as providing sufficient sample for all analytical techniques. It should be noted that the 'shelf-life' of methane in bags before isotopic fractionation occurs is less than a month (Eby *et al.,* 2015, T. Donnelly, *pers comms*). If longer time spans between sampling and analysis are required, samples should be collected in copper tubes at higher pressures where possible so that the pressure of the sample gas in the extraction line is above atmospheric to eliminate air ingress during GC measurements, and there would be sufficient gas for subsequent analyses.

For water sampling, creating a siphon in the field was difficult especially when the body of water was significantly below the level at which access could be gained. A diaphragm pump could allow the submerging of the pump and the pumping of water up a hydraulic gradient without degassing due to it's lack of impeller blades. Or at the very least would at least help generate a siphon over short vertical distances as diaphragm pumps, unlike most impeller pumps for water, can also displace gases.

Water sample collection is also possible directly into foil-lined gas bags (Eby *et al.*, 2015). Degassing samples in the field is also possible if larger gas volumes are required and quantitative gas concentration data is not necessary (e.g. radiocarbon analyses), and may be preferable as gas samples have a longer shelf life than water samples.

2.8.4.2 Noble Gas Storage Clamp Design

The clamp system utilised for sample collection (see Figure 2-1) was observed to have leaked helium out of selected Airth samples over a 300 day period, but not to have caused an obvious ingress of atmospheric neon or argon into the tube, suggesting that

the leakage was on a small scale and only affecting helium (see Appendix). The large volumes of helium present in samples (both ^{3}He and ^{4}He) relative to the atmosphere meant that no change in helium isotopic ratios was observed from atmospheric ingress of either ^{3}He or ^{4}He. The leakage rates are hard to quantify, as they are specific to each tube (which can only be analysed once). The leakage could also have been related to the splitting of tubes into 2 sections in the lab which is required for noble gas analysis.

The mechanism of gas storage relies on a 'cold weld', formed when copper is compressed between the clamp jaws. Annealed (soft) and internally polished tubing for the refrigeration industry is used to help attain a good seal, but the internal surfaces are likely to have impurities such as lubrication from the tubing drawing process or oxides in older tubing which will hinder the formation of a cold weld. Nonetheless a perfect cold weld would impractical, as the purpose of this seal is that it can easily be undone. The simplest solution to this problem is to minimise the time between sample collection and analysis, however there are many practical reasons why this is not always possible.

One simple amendment to the clamp system could be to increase the jaw-width of the clamps in subsequent clamp designs, so the mating surfaces are thicker and thus less gas permeable. However, this could make opening the tubes difficult, and would in effect only reduce (but not eliminate) gas loss. The author suggests a better solution for gas storage by using two sealing jaw clamps at each end, where the gap between the inner and outer jaws should be wide enough so that the tube remains circular in the centre. The open end of the tube outside the outer jaws could then be soldered shut with a simple hand-held butane torch and rosin-core electronics solder to give a permanent gas-tight seal. To prepare the tube for analysis, a pipe cutter would be used to remove the outer soldered clamp and the tube can then be attached to the gas line. In this manner the inner clamp need only be gas tight for minutes rather than months, and existing clamps could be modified to accommodate a second set of jaws. Storage of half-tubes for later analysis could be attained by just soldering this clamp end shut, allowing the other end of the tube (with two clamps) to be opened at a later date in the same manner. Commercially available solutions may also be explored e.g. cold weld forming tools to crimp internal sections of tube after sample collection (e.g. Kulongoski and Hilton, 2002). Other solutions could include using a higher grade of cleaned copper (e.g. acid treated oxygen-free copper) more amenable to forming cold welds, however the cost of this tubing is an order of magnitude more expensive than commercial refrigeration tubing.

2.8.4.3 Analytical Methods

Some commercial laboratories combine Gas Chromatography with automated online combustion systems and Isotope Resolution Mass Spectrometry (GC-IRMS). GC physically separates methane and ethane whilst determining the bulk gas composition. This allows the determination of the $\delta^{13}C$ and δD of methane, ethane, higher hydrocarbons, and the $\delta^{13}C_{CO2}$ of carbon dioxide in the same analysis, requiring less time and smaller sample volumes.

2.9 Bibliography

Al-Baghli, N. A. and Loughlin, K. F. (2005) 'Adsorption of Methane, Ethane, and Ethylene on Titanosilicate ETS-10 Zeolite', *Journal of Chemical & Engineering Data*. American Chemical Society, 50(3), pp. 843–848. doi:10.1021/je0496793.

Baldassare, F. J., McCaffrey, M. A. and Harper, J. A. (2014) 'A geochemical context for stray gas investigations in the northern Appalachian Basin: Implications of analyses of natural gases from Neogene-through Devonian-age strata', *AAPG Bulletin*, 98(2), pp. 341–372. doi:10.1306/06111312178.

Bao, Y., Wei, C., Wang, C., Wang, G. and Li, Q. (2014) 'Geochemical characteristics and generation process of mixed biogenic and thermogenic coalbed methane in luling coalfield, China', *Energy and Fuels*. American Chemical Society, 28(7), pp. 4392–4401. doi:10.1021/ef500599s.

Becker, J. A. (2005) *Quantification of Himalayan metamorphic CO_2 fluxes : impact on global carbon budgets*. University of Cambridge. Available at: http://ethos.bl.uk/OrderDetails.do?uin=uk.bl.ethos.596512.

Berner, U. (1989) *Entwicklung und Anwendung empirischer Modelle für die Kohlenstoffisotopenvariationen in Mischungen thermogener Erdgase*. T.U. Clausthal.

Coleman, D. D., Liu, C., Hackley, K. C. and Pelphrey, S. R. (1995) 'Isotopic Identification of Landfill Methane', 2.

Coplen, T. B. (1995) 'Reporting of stable hydrogen, carbon, and oxygen isotopic abundances', *Geothermics*, 24(5–6), pp. 707–712. doi:10.1016/0375-6505(95)00024-0.

Couwper, C. J. and DeRose, A. J. (1983) *The Analysis of Gases by Chromatography*. II. Pergamon.

Donnelly, T., Waldron, S., Tait, A., Dougans, J. and Bearhop, S. (2001) 'Hydrogen isotope analysis of natural abundance and deuterium-enriched waters by reduction over chromium on-line to a dynamic dual inlet isotope-ratio mass spectrometer', *Rapid Communications in Mass Spectrometry*. John Wiley & Sons, Ltd., 15(15), pp. 1297–1303. doi:10.1002/rcm.361.

Dunbar, E., Cook, G. T., Naysmith, P., Tripney, B. G. and Xu, S. (2016) 'AMS 14C Dating at the Scottish Universities Environmental Research Centre (SUERC) Radiocarbon Dating Laboratory', *Radiocarbon*. New York, USA, 58(01), pp. 9–23. doi:10.1017/RDC.2015.2.

Eby, P., Gibson, J. J. and Yi, Y. (2015) 'Suitability of selected free-gas and dissolved-gas sampling containers for carbon isotopic analysis', *Rapid Communications in Mass Spectrometry*, 29(13), pp. 1215–1226. doi:10.1002/rcm.7213.

Formolo, M. (2010) 'The Microbial Production of Methane and Other Volatile Hydrocarbons', in Timmis, K. N. (ed.) *Handbook of Hydrocarbon and Lipid Microbiology*. Berlin, Heidelberg: Springer Berlin Heidelberg, pp. 113–126. doi:10.1007/978-3-540-77587-4_6.

Golding, S. D., Boreham, C. J. and Esterle, J. S. (2013) 'Stable isotope geochemistry of coal bed and shale gas and related production waters: A review', *International Journal of Coal Geology*, 120, pp. 24–40. doi:10.1016/j.coal.2013.09.001.

Gonfiantini, R. (1984) *Advisory Group Meeting on Stable Isotope Reference Samples for Geochemical and Hydrological Investigations*, *Report to the Director General - IAEA - Vienna 19-21st September 1983*. Available at: http://www-naweb.iaea.org/naalihl/docs/pub/iaea-1984-gonfiantini_agmeeting-stableisotoperm.pdf.

Györe, D. (2015) *Noble gases as tracers of injected CO2 in the Cranfield enhanced oil recovery field*. University of Glasgow.

Györe, D., Stuart, F. M., Gilfillan, S. M. V and Waldron, S. (2015) 'Tracing injected CO2 in the Cranfield enhanced oil recovery field (MS, USA) using He, Ne and Ar isotopes', *International Journal of Greenhouse Gas Control*. Elsevier Ltd, 42, pp. 554–561. doi:10.1016/j.ijggc.2015.09.009.

Györe, D., McKavney, R., Gilfillan, S. M. V. and Stuart, F. M. (2018) 'Fingerprinting coal-derived gases from

the UK', *Chemical Geology*, 480, pp. 75–85. doi:10.1016/j.chemgeo.2017.09.016.
Hua, Q., Barbetti, M. and Rakowski, A. Z. (2013) 'Atmospheric Radiocarbon for the Period 1950–2010', *Radiocarbon*, 55(04), pp. 2059–2072. doi:10.2458/azu_js_rc.v55i2.16177.
Hudson, F. (2004) *RSKSOP-175 - Sample preparation and calculations for dissolved gas analysis in water samples using a GC headspace equilibration technique*. Available at: https://archive.epa.gov/region1/info/testmethods/web/pdf/rsksop175v2.pdf.
IGT (1955) *INSTITUTE OF GAS TECHNOLOGY PHYSICAL-CHEMICAL PROPERTIES OF ETHANE-NITROGEN MIXTURES*, *Institute of Gas Technology Bulletin 26*. Chicago: INSTITUTE OF GAS TECHNOLOGY.
Isotech Labs (2014) *Collection of Ground Water Samples from Domestic and Municipal Water Wells for Dissolved Gas Analysis Using Gas Bottles*. Champaign, IL: Weatherford Laboratories. Available at: http://www.isotechlabs.com/customersupport/samplingprocedures/DGbottle.pdf.
Kampbell, D. H. and Vandegrift, S. A. (1998) 'Analysis of Dissolved Methane, Ethane, and Ethylene in Ground Water by a Standard Gas Chromatographic Technique', *Journal of Chromatographic Science*, 36(5), pp. 253–256. doi:10.1093/chromsci/36.5.253.
Kennedy, B. M., Lynch, M. A., Reynolds, J. H. and Smith, S. P. (1985) 'Intensive sampling of noble gases in fluids at Yellowstone: I. Early overview of the data; regional patterns', *Geochimica et Cosmochimica Acta*, 49(5), pp. 1251–1261. doi:10.1016/0016-7037(85)90014-6.
Kulongoski, J. T. and Hilton, D. R. (2002) 'A quadrupole-based mass spectrometric system for the determination of noble gas abundances in fluids', *Geochemistry, Geophysics, Geosystems*, 3(6), pp. 1–10. doi:10.1029/2001GC000267.
Kusakabe, M. (2005) 'A closed pentane trap for separation of SO2 from CO2 for precise δ18O and δ34S measurements', *GEOCHEMICAL JOURNAL*, 39(3), pp. 285–287. doi:10.2343/geochemj.39.285.
Magnowski, N. B. K. (2014) *Adsorptive separation of C2H6 and H2S from CH4*. University of Alberta. doi:10.7939/R3M90293V.
Matsuda, J., Matsumoto, T., Sumino, H., Nagao, K., Yamamoto, J., Miura, Y., Kaneoka, I., Takahata, N. and Sano, Y. (2002) 'The 3He/4He ratio of new internal He Standard of Japan (HESJ)', *Geochemical Journal*, 36(2), pp. 191–195. doi:10.2343/geochemj.36.191.
Molofsky, L. J., Richardson, S. D., Gorody, A. W., Baldassare, F., Black, J. A., Mchugh, T. E. and Connor, J. A. (2016) 'Effect of Different Sampling Methodologies Groundwater Samples', 54(5), pp. 669–680. doi:10.1111/gwat.12415.
Oremland, R. S., Whiticar, M. J., Strohmaier, F. E. and Kiene, R. P. (1988) 'Bacterial ethane formation from reduced, ethylated sulfur compounds in anoxic sediments', *Geochimica et Cosmochimica Acta*, 52(7), pp. 1895–1904. doi:10.1016/0016-7037(88)90013-0.
Slobod, R. L. (1951) 'Low Temperature Separation of Ethane from Methane and Air', *Analytical Chemistry*, 23(2), pp. 361–363. doi:10.1021/ac60050a037.
Stahl, W. J. (1977) 'Carbon and nitrogen isotopes in hydrocarbon research and exploration', *Chemical Geology*, 20, pp. 121–149. doi:10.1016/0009-2541(77)90041-9.
Thompson, B. (1977) *Fundamentals of Gas Analysis by Gas Chromatography*. Varian.
Triebe, R. W., Tezel, F. H. and Khulbe, K. C. (1996) 'Adsorption of methane, ethane and ethylene on molecular sieve zeolites', *Gas Separation & Purification*, 10(1), pp. 81–84. doi:10.1016/0950-4214(95)00016-X.
Whiticar, M. J. (1996) 'Stable isotope geochemistry of coals, humic kerogens and related natural gases', *International Journal of Coal Geology*, 32(1–4), pp. 191–215. doi:10.1016/S0166-5162(96)00042-0.

3 Noble Gas and Stable Isotope Tracing of Groundwater-Coalbed Methane Interaction and Migration in the Airth CBM Field, Scotland

3.1 Introduction

The Coal Bed Methane (CBM) field at Airth, in the Midland Valley of Central Scotland, is one of only two schemes to target CBM in the UK, and the only unconventional gas development in Scotland.

Despite a current moratorium on "fracking" onshore in Scotland, increased interest in CBM and shale gas resources has seen various Petroleum Exploration and Development Licences (PEDLs) recently change hands in the region. Exploration and development of unconventional gas could occur in a region that has a legacy of previous oil and gas exploration, industry, coal mining, and natural hydrocarbon seeps. The geochemistry of these potential sources of gas is poorly understood and limited baseline data are available, which could present a problem in the event of identifying the source of any unintended gas contamination of the surface and subsurface environment

In this chapter the concepts behind CBM production are explained, and the geological setting and technical development of the Airth Field is outlined. The bulk gas geochemistry, carbon and hydrogen stable isotopes of methane, radiocarbon of methane, and noble gas isotopes are analysed and reported with reference to coal geology and geochemistry, and regional and local contexts such as well development history. The processes by which the noble gas tracers in gases are affected by

interactions with water and the history of field development are investigated, and predictions for the future evolution of gas geochemistry in the field are proposed.

Improving the geochemical understanding of natural tracers in CBM gas systems should allow us to better identify and constrain the presence, abundance, and the potential migration mechanisms of any fugitive gas.

3.1.1 CBM concept

Coal Bed Methane (CBM), also known as Coal Seam Gas (CSG), is the name given to a suite of gases derived from coal formations in which methane is the dominant component (Moore, 2012). Firedamp, a historic term for methane-rich coal gases encountered by coal miners, has long been a safety hazard during coal mining. Efforts to improve safety by draining firedamp from gassy seams ahead of longwall mining via vertical and horizontal boreholes led to the development of commercial sales of CBM in the early 1970's (Flores, 1998). CBM in many areas is now exploited purely for its commercial value with no intent to mine the coal, and allows exploitation of coal gas in seams that are uneconomical to mine. Coal seams represent both the source rock and the reservoir of a CBM resource (Thomas, 2013).

3.1.2 Gas Generation in Coal

Methane in coals is generated via two mechanisms. Thermogenic gas is produced by devolitisation of coals as a result of coalification, with the amount of gas generated being a function of increasing coal rank. Onset of gas production occurs at 0.5-0.6 % vitrinite reflectance (a proxy for thermal maturity, see List of Abbreviations) and is a function of time, heat and pressure in the basin (Clayton, 1998; Moore, 2012). Coals may generate more gas than they are physically able to store, especially at higher ranks (medium-volatile bituminous and above) with the excess being expulsed (Rice, 1993), which is generally the case for coals in the United Kingdom (CEC, 1988; Creedy, 1988)

Biogenic gas can be produced at any point in the generation of peats and coals via complex biological systems, with the final result being methane production by methanogenic archaea utilising carbon as the terminal electron-acceptor. The carbon is liberated from more complex organic matter via a chain of metabolic reactions performed by a symbiotic consortia of anaerobic bacteria and methanogens; a comprehensive review of these species and reactions in coal and oil systems can be found in Meslé *et al.,* (2013). Biogenic gas production typically produces lower seam

gas content than thermogenic production (Creedy, 1991). Hence, CBM reservoirs can be classified as thermogenic, biogenic, or mixed systems.

3.1.3 Coal Structure and Gas Storage in Coal

Coal contains natural fractures or 'cleats', which are large open pore spaces and are the major permeability pathways in a seam and the dominant means of macroscale flow in CBM production (Thomas, 2013). Coals also exhibit complex microporosity; 1 cm^3 of coal can contain up to 3 m^2 surface area, which allows a large volume of gas to be adsorbed onto coal surfaces (Radlinski *et al.,* 2004).

The nature of porosity in coals is a complicated subject. Conceptually, porosity is simply the volume percentage of void spaces between the solid components in a rock. Practically however, coal porosity is the percentage volume that can be occupied by a fluid, which varies depending on the fluid (or fluids) occupying the void space (Levine, 1993; Rodrigues and Lemos de Sousa, 2002).

Investigations into porosity, pore-size distribution, and surface area are carried out using two key principles, namely some form of fluid penetration, or an electromagnetic scanning technique (Zhao *et al.,* 2014; Okolo *et al.,* 2015). Fluid penetration techniques involve measuring the properties of a fluid introduced to coal samples. Common techniques in coals include Mercury Intrusion Porosimetry (MIP), helium pycnometry, and Low Pressure Adsorption (LPA) using CO_2 or N_2. The resolution of fluid penetration techniques is limited to the atomic radius of the penetrating fluid *e.g.* mercury used in MIP is unable to penetrate smaller micropores (Zhao *et al.,* 2014; Okolo *et al.,* 2015). These techniques also cannot measure porosity or pore size distribution within closed pores, or where the pore-throat size is smaller than the fluid's atomic radius (Radlinski *et al.,* 2004; Liu *et al.,* 2012; Okolo *et al.,* 2015). This may not be a disadvantage in some cases, as 'effective' porosity for a given gas (such as CH_4 or CO_2) can be a more useful parameter than true porosity.

Electromagnetic techniques for investigating the nature of porosity include Scanning Electron Microscope (SEM), Transmission Electron Microscopy (TEM), optical microscopy, Synchrotron small Angle X-ray Scattering (SAXS), Small-Angle Neutron Scattering (SANS), Nuclear Magnetic Resonance (NMR) and X-ray micro computed tomography (Micro-CT) (Zhao *et al.,* 2014). These techniques have a range of effective length scales, with SACS/SANS being capable of resolving the smallest pore sizes. Electromagnetic techniques allow the measurement of pore-size in closed pores where

fluids are unable to infiltrate (Rodrigues and Lemos de Sousa, 2002; Zhao *et al.,* 2014; Okolo *et al.,* 2015).

Coal surface area can calculated from gas/mercury adsorption isotherm data (*e.g.* Brunauer–Emmett–Teller (BET), Langmuir, or and Barrett–Joyner–Halenda (BJH) models), though these can underestimate surface area in micropores (Wang *et al.,* 2014). Surface area can also be calculated from SAXS data. Any one technique used in isolation cannot give a full understanding of the porosity or pore size distribution in coal. Readers are directed to Okolo *et al.,* (2015) for method comparisons and background literature.

Gas is stored in coal seams in three states (Moore, 2012) (see Figure 3-1):

1 – Free gas in cleats and macropores, or dissolved in formation water, depending on water saturation.

2 – Absorbed into coal components, *e.g.* kerogens

3 – Adsorbed onto and into coal surfaces and micropores

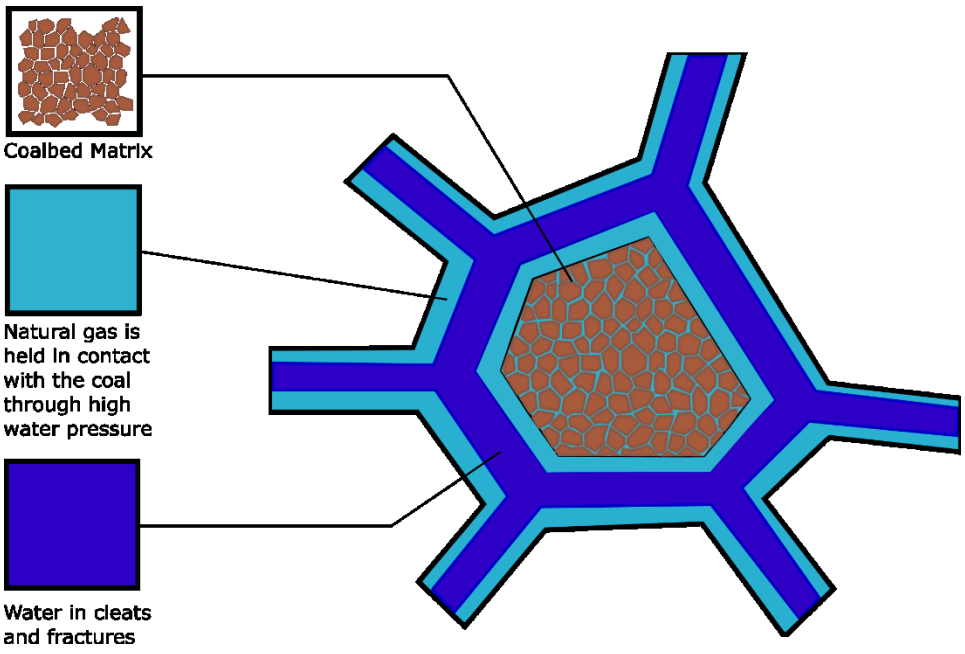

Figure 3-1 – Cartoon schematic of gas storage in coals showing a series of fractures in the coal (not to scale) and main storage type of adsorpsion in fractures and microfractures. In the absence of water, the pressure from free-gas holds methane in its adsorped state.

The specifics of methane storage in coals is the subject of ongoing research, but the majority of methane in coals is adsorbed in micropores (Moore, 2012, and references therein). At low coal ranks, macro and microporosity dominate. As rank increases, there is a shift from the dominance of macroporosity towards mesoporosity and

microporosity (Levine, 1993; Radlinski *et al.,* 2004). At the highest ranks microporosity is the dominant form of porosity (Gan *et al.,* 1972; Rodrigues and Lemos de Sousa, 2002).

Gas content is a function of pore-structure and pore-size distribution (itself a function of rank and organic matter composition) (Levine, 1993; Crosdale *et al.,* 1998; Radlinski *et al.,* 2004). While higher rank coals are thought to typically give higher gas storage capacity, internal surface area of low-volatile bituminous coals have been measured as having the highest internal surface area and hence are the most favourable coals for gas contents (Zhao *et al.,* 2014).

Due to the property of adsorption on vast internal surface areas, coals can store much greater volumes of methane in an adsorbed state in the coal vs. as a free phase within the pores. The ability of a coal to store gas is heavily dependent on internal surface area and water content preventing adsorption on internal sites (Moore, 2012).

Gas content of coal seams is usually described by Langmuir isotherms, for a particular temperature the quantity of methane q adsorbed at pressure P can be represented mathematically (Langmuir, 1918):

$$q = \frac{AbP}{(1 + bP)}$$

Equation 1 – Langmuir equation. A+b = Langmuir constants. P = pressure, q = maximum stored gas content.

Increasing pressure enables a higher adsorbed gas content, while increasing temperature lowers the gas storage potential. Any gas produced in the coal that exceeds the storage capacity is expelled from the coal (Rice, 1993; Moore, 2012). Coals in the UK are commonly undersaturated with methane relative to their P-T conditions. This is a result of uplift and erosion leading to a confining pressure decrease, degassing of methane from coals, and then subsequent reburial which in the UK leads to gas seam pressures being approximately a fifth of hydrostatic pressure (Creedy, 1991; Jones *et al.,* 2004). In the US, coal seam gas pressures are typically hydrostatic (Creedy, 1991; Rice, 1993).

3.1.4 Permeability in coal

The primary system of permeability in coals is the cleat/fracture system, the formation of which is dependent on local stresses. In UK Carboniferous coals these are generally

the result of deformation caused by Variscan stress fields. Permeability generally decreases with depth (Rippon *et al.,* 2006; Moore, 2012).

Coal is a reasonably elastic material, and initial pressure drop due to dewatering can cause cleats to restrict due to compaction as formation pressure is reduced, causing permeability to drop (Gray, 1987; Yi *et al.,* 2009). Conversely, reduction of the adsorped gas content in coals during production changes the structure of micropores, and can cause the coal matrix to shrink, thus increasing permeability (Moore, 2012).

Movement of gas within the coal matrix (towards the cleat system) is modelled as following Fick's law of diffusion (Moore, 2012).

3.1.5 Production of CBM

CBM is usually produced by pumping formation water from the coal seams in order to reduce the pressure which holds the methane in solution and adsorbed to coals, causing the coal to degas methane (see Equation 1). This occurs initially within saturated water and at the cleat interface, which creates a concentration gradient across the coal matrix causing gas to diffuse to the cleats via Fick's law (Moore, 2012).

Unlike a conventional porous gas reservoir where a buoyant gas phase of migrated gas sits in the pore space, only a small gas phase (if any at all) exists initially in most CBM reservoirs. The dewatering/pumping process creates a gas phase at depth, through lowering the pressure, which allows gas to degas from both the coals and the formation water.

The pressure reduction caused by dewatering occurs as a gradient, with areas proximal to the wellbore showing the biggest pressure drop, and therefore experiencing the most degassing. Thus, the storage and release of gases in coals occurs over a wide range of length-scales, and will be both spatially and temporally variable, related to the pressure gradient exerted by the degree of dewatering over the various length scales, and over time as the pressure front advances (see Figure 3-2).

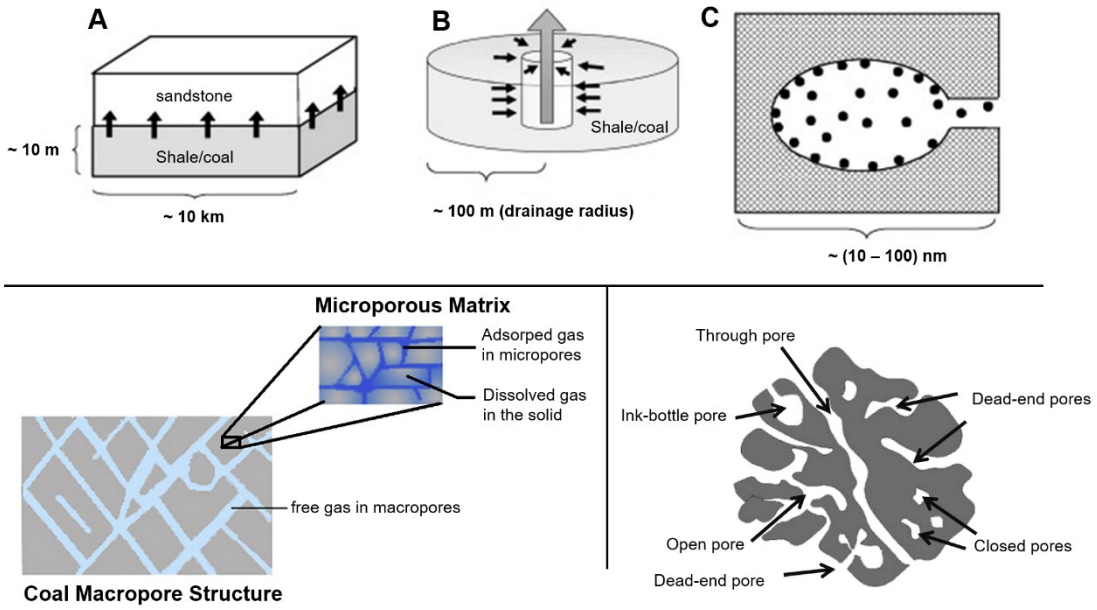

Figure 3-2 – Schematic diagram of coal scales on gas storage potential. Upper panel: schematic cartoon highlighting the ranges of scale of gas transfer from coals; a) basinal scale transfer b) macroscale transfer of gas to the well bore c) microscale desorpsion of gas from coal matrix and surfaces into pore spaces (modified after Xia and Tang, 2012). Lower left panel: schematic cartoon of the ranges of macropore and micropore matrices typical of coal (from Yi et al. 2009). Lower right panel: cartoon schematic showing the variety and accessibility of pore spaces within coal micropore structures (from Tang et al., (2016)).

Figure 3-3 shows a typical production curve for water and gas from a CBM well. The three stages of typical CBM production are as follows:

1 – Dewatering stage – Large volumes of gas and water are produced as formation water is pumped from the well to lower the bottom-hole-pressure.

2 – Stable production stage – after the initial reduction of formation water and consequent pressure drop, this stage encompasses peak gas production with low quantities of produced water.

3 – Decline stage – The formation is mostly dewatered and gas production is declining due to depletion of the reservoir. Production will cease when the operator decides it is no longer economic to continue.

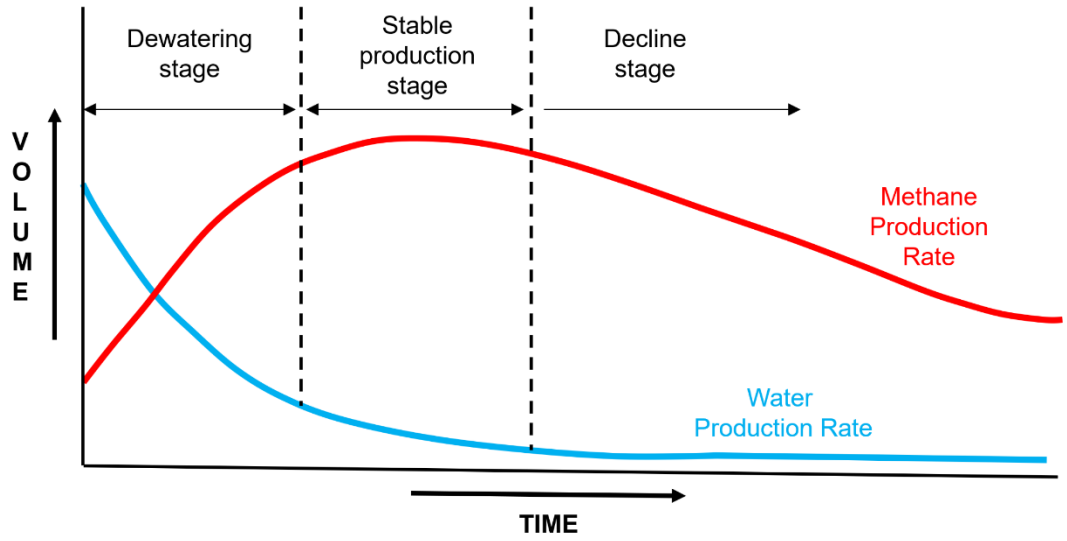

Figure 3-3 – Generalised CBM production curve for gas and water, showing increasing methane volume with increasing water removal (water production) during dewatering, a stable gas production timespan, and eventual decline as gas reserves are exhausted. Reproduced after Nuccio (2000).

3.2 Geological Background of Airth CBM Field

3.2.1 The Midland Valley

The Midland Valley is a NE-SW trending terrane, bounded to the North by the Highland Boundary Fault separating the Grampian Highlands terrane, and to the South by the Southern Upland Fault separating the Southern Uplands terrane. Structurally, the Midland Valley is an ancient graben, where the two major faults represent the boundaries to the downthrown Midland Valley, which consists principally at the surface of Carboniferous and Devonian strata.

At the base of the Midland Valley sits a high grade metamorphic Precambrian basement which Cameron and Stephenson (1985) inferred to be ~25km thick based on seismic discontinuities and xenoliths found in Carboniferous and Permian volcanics (see Figure 3-4), and is located 7-9 km below the sedimentary succession in the Eastern Midland Valley

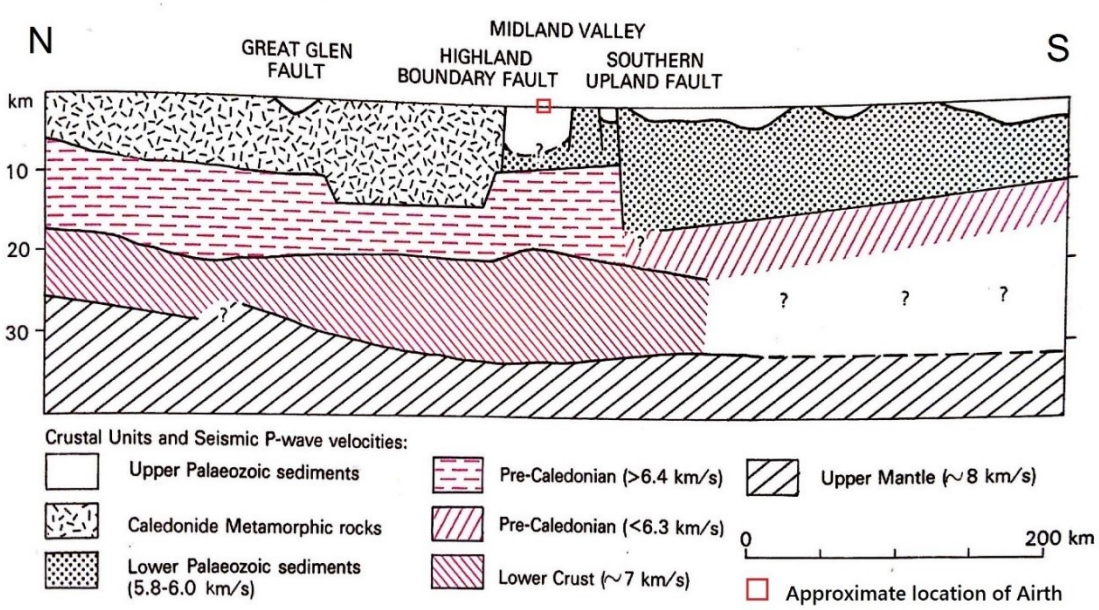

Figure 3-4 – N-S seismic profile cross section of Northern Britain, with the Midland Valley in the centre. Modified after Cameron and Stephenson, (1985).

The Precambrian basement is hypothesised to consist of an upper quartzo-feldspathic foliated acidic gneissic layer, and a lower gabbroic/dioritic layer, though the boundaries and actual compositions are poorly constrained. The Precambrian basement is overlain by Paleozoic sediments; Ordovician conglomerates and marine Silurian sediments are known to be present from inliers bounding and close to the Southern Upland Fault. Following a transition to semi-arid fluvial conditions in the Lower Devonian, thick beds of sandstones and conglomerates derived from the Caledonian Orogeny, Southern Uplands and further afield (Bluck, 2000) interspersed with lavas, were deposited mainly unconformably onto earlier units. A period of uplift and erosion followed, resulting in an unconformity in the Middle Devonian, followed by further Upper Devonian deposition of sandstones and siltstones onto a peneplaned surface to the East, with thicker coarser units to the West (Cameron and Stephenson, 1985).

During the Carboniferous, continued northwards continental drift of the British Isles brought a transition to an equatorial paleolattitude and the deposition of huge volumes of sands and muds, with tropical swamps forming in deltas, and cyclical marine incursions (Cameron and Stephenson, 1985). Cyclical deposition resulted from marine regression, forming marine limestones and mudstones, to sandstones, seatearths, then coals, before marine transgression resulted in rapid re-flooding and subsequent repetition of the sequence. Lateral differences in sediment thicknesses and

facies variations were partly controlled by differential subsidence from recurrent movement of pre-existing fractures (Cameron and Stephenson, 1985). The extant structures of Clackmannan, Midlothian and Leven synclines (and related Balmule, Burntisland and D'Arcy-Cousland anticlines) were syn-depositional and were formed before the end of the Carboniferous (Rippon *et al.,* 1996; Underhill *et al.,* 2008).

The Late Carboniferous era saw the completion of the supercontinent Pangaea. The uplift removed the paralic swamp environments conducive to coal formation, and the carbon sink they represented. This led to atmospheric warming which continued throughout the Permian and Triassic. NW Europe began the transition from tropical swamps to an arid continental climate. In the Midland Valley this led to Permian deposits of aeolian sands, and basaltic lavas (Cameron and Stephenson, 1985).

A series of Late Carboniferous to Early Permian dykes crosscut the area and they are not deformed, suggesting that subsequent tectonic activity had little deformation expression in the Eastern Midland Valley (Cameron and Stephenson, 1985). No sedimentary rocks younger than this are preserved in the MVS, but sedimentary cover is thought to have been >1km with uplift and erosion commencing with the onset of the opening of the N. Atlantic (Vincent *et al.,* 2010).

Tertiary dykes associated with the Mull and Arran volcanic centres are known in the W and SE of the Midland Valley, and Tertiary igneous rocks are known to have been emplaced up the Ochil Fault (Cameron and Stephenson, 1985).

3.2.2 Airth Field

The Airth Field is located ~3 km west of the Kincardine Bridge (Figure 3-5), within PEDL133, a licence area of 330 km^2. CBM has been produced from the field for gas flowrate testing for resource appraisal, but the field has not been extensively produced to date.

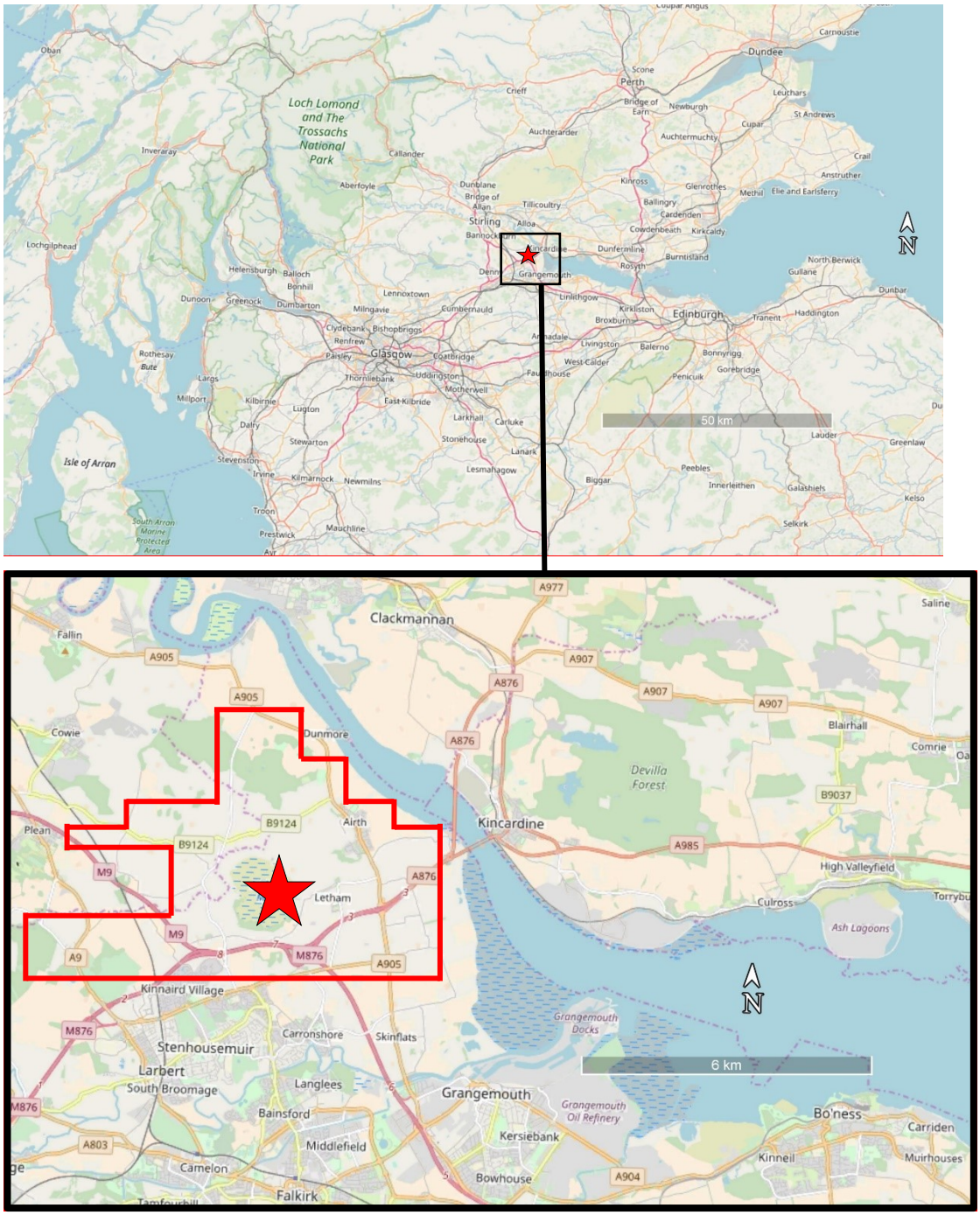

Figure 3-5 – Location maps of the Airth Field in Scotland. Upper: Overview map of Airth Field in relation to Greater Scotland. Lower: Airth Field location and boundary (red), after Envoi, (2013). Imagery from http://www.openstreetmap.org

The Airth Field lies on the western limb of the Clackmannan Syncline, also known as the Central Coalfield Syncline (see W-E cross-section, Figure 3-6). This is a NNE-SSW trending structure with asymmetric limbs dipping ~30° on the eastern limb and ~5-10° on the western limb, which plunges gently to the North where it is bounded by the

Ochil fault (see N-S cross-section, Figure 3-6). The Clackmannan syncline is part of a series of syn-sedimentary structures hypothesised to have formed in the Visean (Hooper, 2003), with related synclinal structures to the East (Midlothian and Leven synclines).

The Airth Field targets coals in the Limestone Coal Formation (formerly the Limestone Coal Group, now part of the Clackmannan Group (BGS)), defined at the base by the Top Hosie Limestone and at the top by the base of the Index Limestone, and are Pendleian (Lower Namurian) in age. The coals dip to the East, ~5-10° towards the syncline axis.

The field straddles BGS maps 39E (Alloa) and 31E (Falkirk). The general syncline structure can be seen in the general E-W cross section reproduced from BGS sheet map 39E (see Figure 3-6).

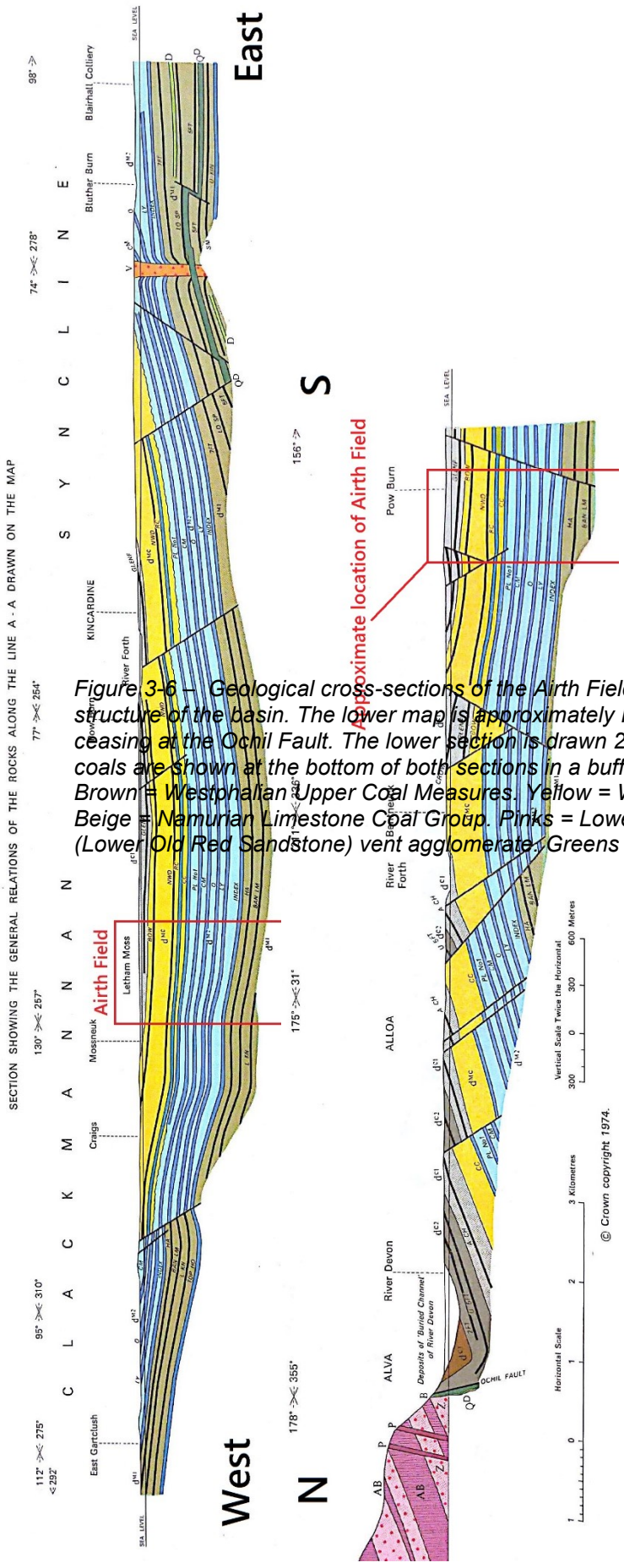

Figure 3-6 – Geological cross-sections of the Airth Field area.The upper section is approximately E-structure of the basin. The lower map is approximately N-S and shows a series of normal faulted blo ceasing at the Ochil Fault. The lower section is drawn 2km east of the Airth Field so the field location coals are shown at the bottom of both sections in a buff colour (e.g. Bannockburn LM). Reproduced f Brown = Westphalian Upper Coal Measures. Yellow = Westphalian-Namurian Passage Group. Blues Beige = Namurian Limestone Coal Group. Pinks = Lower Old Red Sandstone aged intrusive and extr (Lower Old Red Sandstone) vent agglomerate. Greens = Permo-Carboniferous intrusive igneous (Q^P

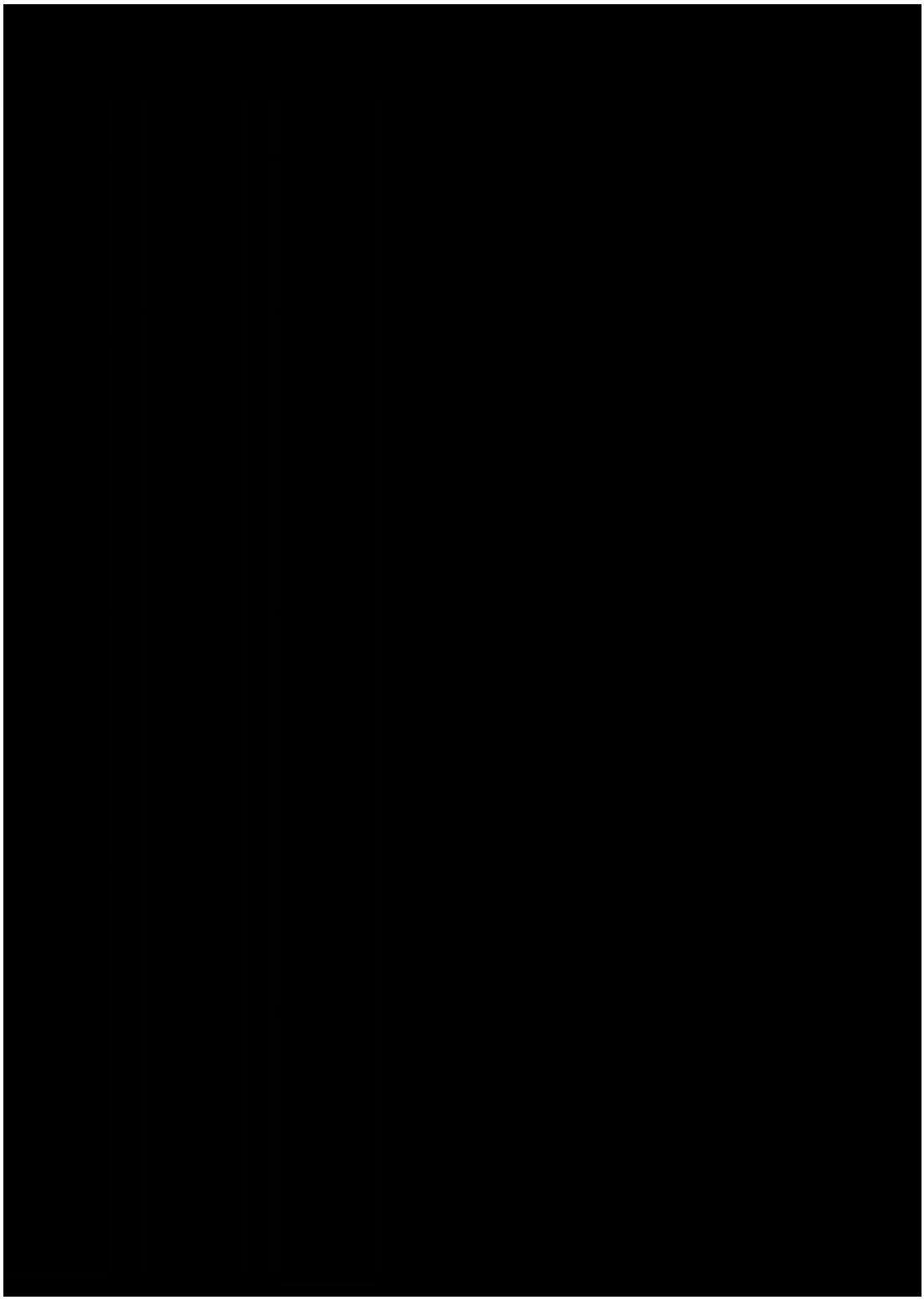

Figure 3-7 – Generalised geology of the Airth Field. Stratigraphic column, and well log of target coals from the Airth-1 well. Data compiled after Cameron and Stephenson, (1985); Composite Energy Ltd., (2006); Sinayuc et al., (2011); Wells et al., (2014), BGS maps 39E (Alloa) and 31E (Falkirk),and BGS well-log records for Airth-1.

3.2.2.1 Units

The Airth-1 well targets the Limestone Coal Formation (LCF) (formerly the Limestone Coal Group), which at Airth-1 comprises of 14 coals, each 1-4.5 ft (0.3-1.3 m) thick with 43 ft (13.1 m) total coal seam thickness, interbedded with sandstones. Airth-6 recorded 33 ft (10 m) of total coal in this section. The coals are reported to have a combined average thickness of 4.92 m, be classified as 'medium volatile bituminous' in rank, and contain 9 – 13 m^3/tonne methane (Envoi, 2013).

The lateral bores drilled more recently at Airth target four major seams from deepest to shallowest: Greenyards (a.k.a. Lower 20"), Upper Bannockburn Main (Upper Bannockburn Steam), Lower Bannockburn Main (Lower Bannockburn Steam), and Knott, which locally range between 3-6 ft (0.9-1.8 m) thickness. The generalised geology and selected well log are shown in Figure 3-7.

3.2.2.2 Permeability of Airth Coals

The permeability of Airth coals were measured by DART Energy to be 0.5 mD to 25 mD after hydraulic fracturing at Airth-1 (Bacon, 1995). The 4 target coals are reported by DART Energy Ltd. to have a permeability of around 0.5 mD (Envoi, 2013).
Sinayuc *et al.,* (2011) produced a numerical model to investigate methane production and CO_2 storage potential based on production history matching from proprietary data from 4 produced wells. They noted a higher permeability consistent with higher structural relief of coals around the Airth-10 well. Lower permeabilities surround this area, particularly in the SW.

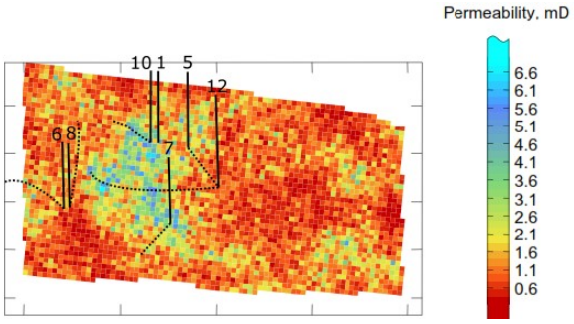

Figure 3-8 - Visualisation of a permeability computer simulations for the Airth field, modified from Sinayuc et al., (2011). Approximate locations of well bores denoted by black solid line (vertical location) and black dotted line (lateral section). The permeability across the field varies, but is highest around the developed area, most likely related to structural highs.

Structurally, in the Clackmannan Syncline the main face cleat is thought to run E-W, mirroring the series of normal faulting and is affected by carbonate mineralisation (Rippon *et al.,* 2006). For this study the absolute values of permeability are less important than the relative distribution of permeability around the different wells.

3.2.2.3 Thermal Maturity and Uplift History

The nearby Inch-of-Ferryton-1 well shows vitrinite reflectance measurements in the Limestone Coal Formation to be 0.87% – 0.9% R_o above 835 m, which is mature for oil and gas generation, and 1.45% – 1.7% R_o below 835 m, mature for wet gas and methane generation (Monaghan, 2014). This is in line with the designation of the coals at Airth being 'Medium volatile bituminous' reported by DART Energy Ltd (Envoi, 2013) (which corresponds to ~1.1% - 1.5% R_o (Moore, 2012)).

Maximum burial (and hence maximum thermal maturity) of the LCF in the Kincardine Basin may have been reached in the Late Carboniferous (Marshall *et al.*, 1994), before Variscan-related uplift caused erosion of Late Carboniferous to Early Permian sediments. The region was subsequently buried in the early Permian, with maximum burial depths also possibly being reached in the Early Cenozoic (Underhill *et al.*, 2008; Vincent *et al.*, 2010), prior to the uplift of the region resulting from the North Atlantic Igneous Province which commenced 61 Ma (Mackay *et al.*, 2005).

Regionally, the maturity of the lower Limestone Coal Formation (LCF), Lower Limestone and upper West Lothian Oil-Shale formations towards the central and eastern area of the Midland Valley are affected by the Carboniferous tholeiitic Midland Valley Sill (Berrow *et al.,* 2014; Monaghan, 2014). In the Clackmannan syncline, it dips towards the syncline axis on both limbs and variably intrudes the lower LCF and Lower Limestone formations, stepping between them. LCF coals in the Manor Powis and

Polmaise collieries are known to be anthracitised or replaced by the intrusion, and notable increases in vitrinite reflection are known in LCF strata in bores near the Airth Field (*e.g.* Inch-of-Ferryton-1) (Monaghan, 2014). The Midland Valley Sill was not encountered in the Airth-6 borehole drilled down to the Black Metals Group, and is therefore assumed to underlie the target units in the Lower Limestone group (Berrow *et al.,* 2014).

3.2.2.4 History of Coal Extraction Surrounding the Airth Field

The extensive dewatering of coal mines and coal exploration boreholes will influence the pressures, gas content of seams, and local groundwater flow, so assessing the coal extraction history of the area is essential. The Limestone Coal Formation (LCF) has been worked heavily to the west, and the target coal seams at Airth bear the names of the towns or collieries from where coals were originally mined (*e.g.* Bannockburn seams). At Airth, plans were made to mine the Bannockburn Main seam for the Scottish steel industry in the 1950's. Two shaft collars were built south of the Kincardine Bridge, but the shafts were never sunk.

Shallow opencast coal mines are known in the area (Coal Authority records) but are unlikely to have affected the >800m seams. The nearest deep workings were ~3 km away at the Longannet complex, targeting the Upper Hirst seam which lies ~300 m (~1000 ft) higher in the sequence than the stratigraphically highest target coal (Greenyards). This is also ~125 m (400 ft) up-dip, despite normal faulting by the NNW-SSE Kincardine Ferry fault, downthrowing to the East. Mining took place under the Firth of Forth towards Kincardine Bridge and could have extended over the Airth field area, but work ceased in 2002 due to a flooding accident. From this it can be reasonably concluded that the target coals at Airth are unworked, and have not been significantly physically or hydrologically disturbed by nearby mining and pumping operations.

However, the surrounding area has been heavily bored for coal exploration since the early 1800's., At least four recorded bores are known to exceed 800m depth (Airth Estate No.1 (967 m), Mossneuk (1081 m), South of Letham Bore No.1 (1094 m), Rosehill No.1 Diamond Bore (814 m)), and more are known to be present but details are not publicly available. These would breach the Index Limestone overlying the Limestone Coal Formation (LCF) target units, as well as some of the underlying LCG coal measures. These boreholes are unlikely to have significantly disturbed the target coals and the gases they contain, especially as gas release pressures in the UK are typically 1/5th hydrostatic pressure (Creedy, 1991) thus requiring a substantial drop in

water pressures at formation depth to de-gas. However, these could be a potential hazard as a flow conduit for fugitive gas to the surface or shallow aquifers. Furthermore, the methods of drilling, casing, and abandonment are not well documented, so they could in theory connect any gas-bearing unit higher up in sequence to the surface or subsurface aquifers.

3.2.2.5 Field Development History

The technical development of well drilling technology has influenced the design of successive wells drilled at the Airth field, as well as the UK as a whole. The changing architectures represent an evolution of construction over 20 years designed to meet the requirements of the local geology, as typical construction methods common in the USA and Australia were not suited to the thinner and less permeable coals which are typical of the UK Carboniferous Coal Measures.

It is important to understand well architecture, as the design influences which seams are targeted, the extent to which they are drilled, and therefore the zone of influence the wellbore exhibits on the coals and groundwaters contacted. It is also important to know the general pumping history of the wells, as this affects the history of gas generation and subsequently the gas/water ratios and geochemistry. Well architecture is explained in Figure 3-9. DART Energy Ltd. estimates that the dewatered horizontal 'zone of influence' around the dewatered seams is circa 250 m (Smythe, 2013).

Information for these wells has been compiled from Sinayuc *et al.,* (2011), Thwaites and James, (2014), BGS well-log records submitted to the BGS from the respective drilling companies, and field notes taken by Dr. S. Gilfillan on 21st August 2013. Brief numerical details are given in Table 1 before a longer description in subsequent text. Only the wells for which there are samples are described in detail.

Well	Well architecture	Spud date	Total well length inc. laterals (m)	Wellhead pressure when samples (kPa/psi)	Dewatering status
Airth-1	Vertical	9/8/1993	1074	6495/942	Multiple stages
Airth-2	Vertical	18/1/1996	1110	-	N/A
Airth-3	Vertical	24/5/1997	1196	-	N/A
Airth-4	Vertical	14/9/1997	1268	-	N/A
Airth-5	Down-dip multilateral	18/12/2004	4063	130/18.8	Never pumped
Airth-6	Vertical, N/A	15/10/2005	1062	276/40	Never pumped
Airth-7	Multilateral	4/8/2006	Vertical - 1214	-	N/A
Airth-8	Up-dip multilateral	21/10/2008	3355	350/51	2008, 2009
Airth-9	Multilateral	13/7/2007	Vertical - 1551	-	N/A
Airth-10	Up-dip multilateral	13/10/2007	3867	4300/624	Prior to 2008
Airth-11	Multilateral	14/12/2007	Vertical - 1616	-	N/A
Airth-12	Surface to in-seam	11/9/2011	6271	5900/856	Jan-March 2013
Airth-13	Vertical	12/1/2013	957	-	N/A
Airth-14	Multilateral	12/2/2013	N/A	-	N/A

Table 1 – Brief summary of Airth well architecture and total well length including laterals. Information compiled from BGS wellbore records and Thwaites and James, (2014). Public records are missing for Airth-6, which was drilled and cored and subsequently had one or more laterals drilled from it.

Airth-1 – The first well drilled by Coalbed Methane Ltd. (owned by Hillfarm Coal Ltd.). Positioned into a major fault block based on British Coal core samples and seismic images. Primary targets were coals below the Index Limestone, with secondary targets being Upper Coal seams just below Calmy Limestone. Airth-1 was "fracture stimulated" in 9 treatments, targeting all potentially productive coals (14 in total, 1-4.5 ft each, and 43 ft total seam thickness) and sandstones. 3 more vertical wells (#2,#3,#4) were drilled 1994-1997 and completed similarly to Airth-1. Pumping at Airth-1 began in 1994, producing water at 260 bpd initially before declining to 30 bpd in 1995 (Bacon, 1995), while gas production started at 60 mcfd declining to 35 mcfd in 1995 (DECC, 2013). This gas could have originated from adjacent sandstones or dissolved in formation water (DECC, 2013)

The Airth-12 multilateral well was drilled in 2012 and intersected Airth-1 underground in 2012. Dewatering at Airth-1 continued again in Jan 2013 and ended March 2013 in order to dewater Airth-12.

Airth-5 – drilled by Composite Energy after buying out CBM Ltd.'s interest in the PEDL. Utilised new surface-to-inseam directional drilling to drill a "toe intersection" type borehole, with two laterals heading ~SE to intersect Airth-3. Never pumped.

Airth-6 – Vertical well, drilled by Composite Energy. Never pumped, just a small volume of gas present in the annulus. Wellhead pressure: 276 kPa (40 psi), which dropped 221 kPa (32 psi) after sampling. Laterals wells subsequently drilled.

Airth-8 – Up-dip horizontal, drilled by Composite Energy. 4 laterals but with poor "hole-in-coal" percentages.

Airth-10 - Up-dip horizontal, drilled by Composite Energy, 4 laterals. Pumped prior to 2008, producing >200,000 scf/day (19822 m^3/day)

Airth-12 – First "heel-intersection" type – drilled by Dart Energy, intersecting Airth-1 as the vertical well with associated pumping equipment. Pumping commenced January 2013 via the Airth-1 borehole from January 2013 to March 2013. Produced commercially viable flows of gas at 700,000 scf/d during 2013.

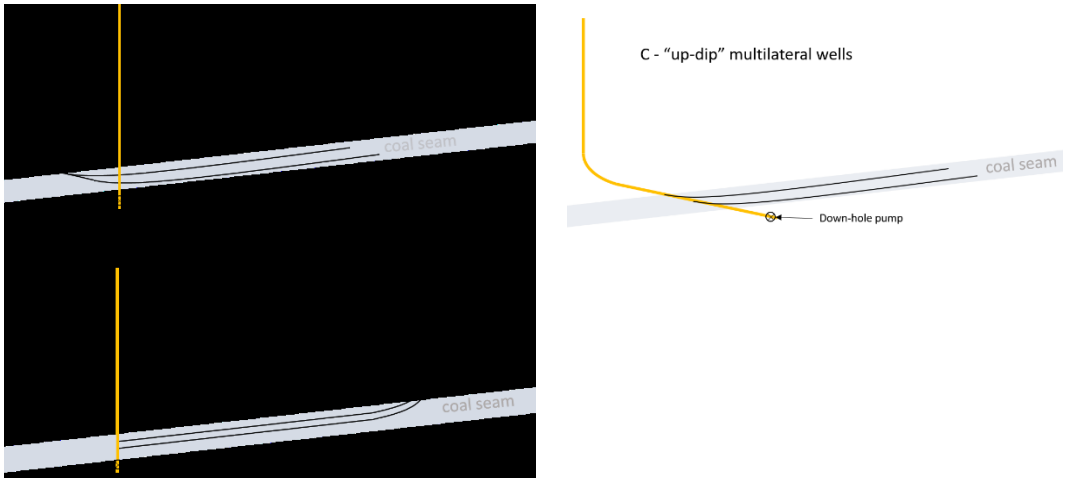

Figure 3-9 – Schematic of well architecture. A – "heel intersection": laterals are drilled from surface to in-seam up-dip, to intersect a vertical well which houses pumping apparatus, e.g. Airth-1 (vertical), Airth-12 (multilaterals). B – "toe intersection" – laterals are drilled surface to in-seam down-dip, to intersect a vertical well at the base or 'toe'.e.g. Airth-3 (vertical) and Airth-5 (laterals). C – up-dip multilateral wells drilled off a motherbore e.g. Airth-8.

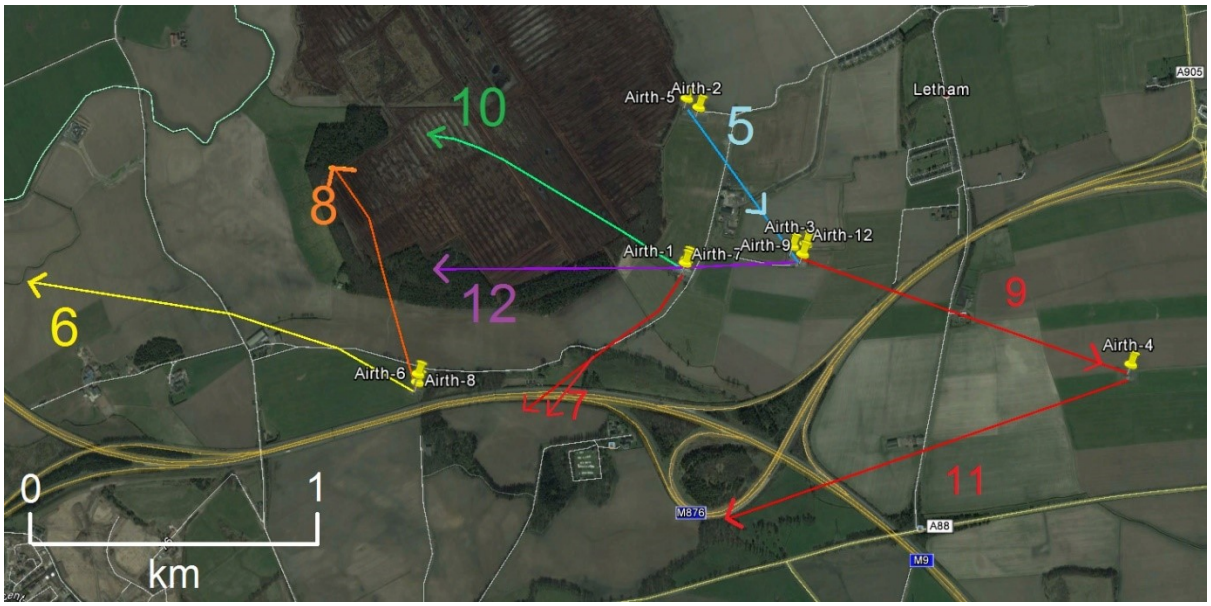

Figure 3-10 – Approximate surface locations of multilateral wellbores at the Airth site. Arrows show direction of drilling to indicate surface location of the well. Yellow pins depict location of surface well pads.

3.3 Results

Noble gases for the Airth field were collected in copper tubes from Airth-1, Airth-5, Airth-6, Airth-8, Airth-10, and Airth-12 in August 2013. A further sample was collected from Airth-1 in August 2014.

3.3.1 Bulk Geochemistry

Bulk gas composition was determined by gas chromatography (GC), see Methodology (this volume) for details. The dominant gas in all measured samples was, unsurprisingly, methane. Trace quantities of ethane and propane were found and the ratios are presented in Table 2. CO_2 and N_2 contents were above the limit of detection (LOD) but below the limit of quantitation (LOQ ~ <0.5%) for all samples. No traces of ethylene, acetylene, oxygen, or carbon monoxide were detected. All measured gas species broadly fit within the range of other measured UK coal gas samples desorbed from exploration borehole cores (Creedy, 1988, 1991).

	C_1/C_2	d	C_1/C_3	d	$C_1/(C_2+C_3)$	d	C_1/CO_2
Airth-1 (2014)	104.9	0.17	2135	9.4	100.0	0.33	NA
Airth-1 (2013)	79.2	0.13	1366	6.0	74.9	0.24	NA
Airth-6	81.6	0.13	924	4.1	74.9	0.24	NA
Airth-10	129.8	0.21	1841	8.1	121.3	0.39	NA

Table 2 – Table of measured gas ratios for gases from the Airth field.

The gases are considered 'dry', with C_2+C_3 components of ~1-2%, however these levels are significantly wetter than biogenically derived gas (where typically $C_1/(C_2+C_3)$ = >1000), and indicate a thermogenic source with little to no mixing with biogenically derived gas (Rice, 1993; Strąpoć *et al.,* 2008).

3.3.2 Stable Carbon and Hydrogen Isotopes

Gases from Airth were analysed for carbon and hydrogen isotopes, and plot firmly in the thermogenic regime (See Table 3, Figure 3-11, and Figure 3-12).

Sample Name	$\delta^{13}C_{CH4}$	δD_{H2O}
Airth-1 (2014)	-39.5 ± 0.5	-163 ± 3
Airth-1 (2013)	-40.2 ± 0.5	-220 ± 3
Airth-6 *	-43.5 ± 0.1	
Airth-8	-41.8 ± 0.1	-188 ± 3
Airth-10	-40.4 ± 0.1	-193 ± 3

Table 3 – Table of stable carbon and hydrogen isotopes of methane from Airth field samples.
** - result from SUERC radiocarbon lab (analysis number: SUERC-70393).*

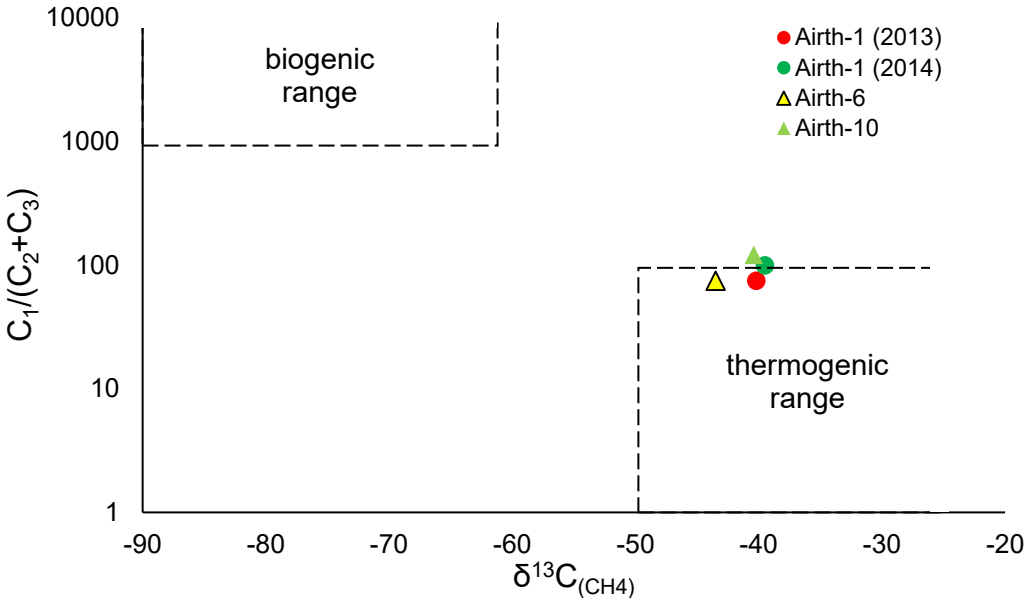

Figure 3-11 - Plot of $C_1/(C_2+C_3)$ vs. $\delta^{13}C_{CH4}$. Airth coal bed gases plot in the thermogenic range both isotopically and compositionally (compositional ranges after Bernard et al., 1978).

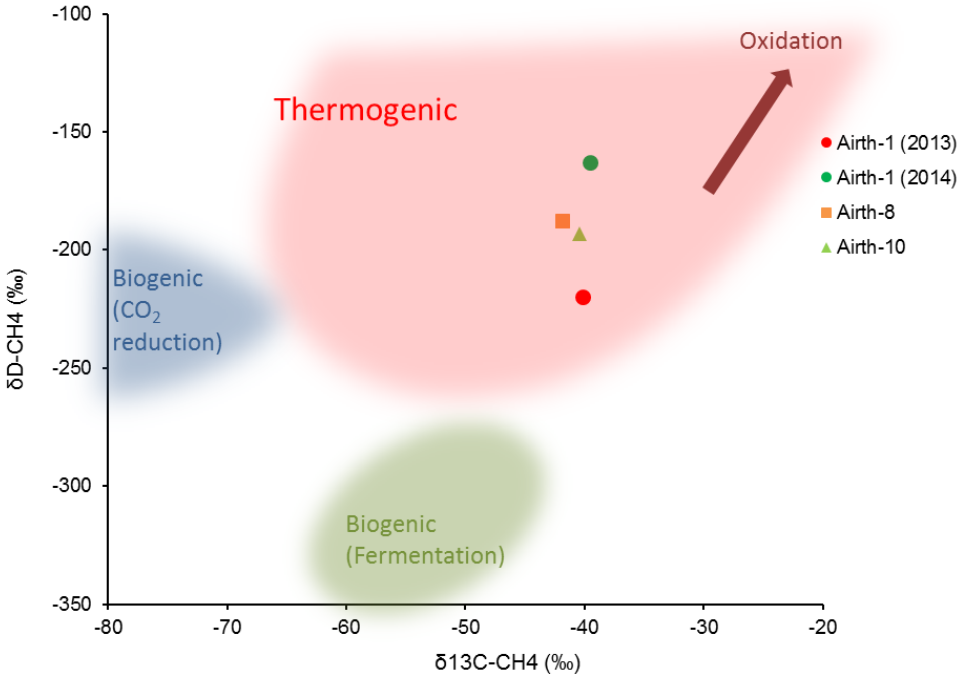

Figure 3-12 – Plot of δD_{CH4} vs $\delta^{13}C_{CH4}$ after Schoell, (1980). Airth gases plot in the thermogenic regime, indicating no microbial contribution to the methane.

3.3.3 Radiocarbon

Airth-6 well gas was submitted for radiocarbon analysis, performed at SUERC (analysis number: SUERC-70393). The ^{14}C content was found to be indistinguishable from background *i.e.* "radiocarbon dead".

3.3.4 Noble gases

The noble gas concentrations and isotopic ratios are given in Table 4.

3.3.5 Air Saturated Water (ASW)

Air Saturated Water (ASW) is the mechanism by which most atmosphere-derived noble gases are assumed to enter subsurface systems. The solubility of noble gases in water is dependent on atomic mass following the pattern Xe>Kr>Ar>Ne>He. These solubility differences result in noble gas ratios in water being distinctly fractionated from the air ratios. ASW ratios are calculated for the Airth Field assuming recharge of fresh (meteoric) water and current surface recharge temperature and altitude (8.6 °C, climate-data.org, 12 m above mean sea level) using Henry's constants from Crovetto *et al.,* (1982) with no excess air component.

3.3.5.1 Helium

^{4}He concentrations range from 1105±48 ppm in Airth-10 to 2984±145 ppm for Airth-5 (see Figure 3-13). These are 211 to 569 times greater than the air value of 5.24 ppm (Mamyrin *et al.,* 1970), and 24000 to 65000 times greater than the concentration that would be expected in ASW.

The $^{4}He/^{20}Ne$ ratios range from 12931±674 at the unpumped Airth-5 to 28255±1357 at Airth-1 (2013), a few months after extensive flow-testing had ceased. These ratios are several orders of magnitude larger than the air or ASW $^{4}He/^{20}Ne$ ratios of 0.381 and 0.261 respectively, indicating negligible atmospheric input and minimal interaction with groundwater (see Figure 3-14).

Multiple samples of Airth-1 (2014) were collected and analysed over a 300 day period, and were found to have experienced helium loss in storage. No obvious ingress of neon was reported. Nonetheless up to 2 years elapsed from the sample collection to the analysis, so the reported helium concentrations can be regarded as minima (see Sample Collection and Storage Issues Affecting Noble Gas Abundances)

Concentration data

Well	^{4}He ($x10^{-4}$)		^{20}Ne ($x10^{-8}$)		^{40}Ar ($x10^{-5}$)		^{84}Kr ($x10^{-9}$)		^{132}Xe ($x10^{-11}$)	
Airth-1 (2013)	1.18	(0.05)	4.159	(0.090)	9.023	(0.172)	2.01	(0.08)	9.55	(0.50)
Airth-1 (2014)	1.29	(0.06)	5.141	(0.111)	7.190	(0.137)	2.24	(0.09)	11.28	(0.67)
Airth-5	2.98	(0.14)	35.370	(0.766)	29.594	(0.563)	21.91	(0.91)	83.30	(4.36)
Airth-6	2.13	(0.10)	9.728	(0.211)	14.870	(0.283)	2.92	(0.12)	9.53	(0.50)
Airth-8	2.00	(0.09)	8.934	(0.194)	14.904	(0.283)	2.45	(0.10)	13.01	(0.68)
Airth-10	1.11	(0.05)	4.931	(0.107)	9.234	(0.176)	3.73	(0.15)	14.92	(0.77)
Airth-12	2.44	(0.12)	18.456	(0.400)	24.388	(0.464)	4.93	(0.20)	25.15	(1.33)

Units: cm^3 STP/cm^3 - (Standard T (0°C) and P (0.101 Mpa) after Ozima and Podosek (2002))
1σ uncertainty shown in parentheses

Isotopic ratios

Well	$^{3}He/^{4}He$ (R/R_a)		$^{20}Ne/^{22}Ne$	$^{21}Ne/^{22}Ne$	$^{40}Ar/^{36}Ar$	$^{38}Ar/^{36}Ar$
Airth-1 (2013)	0.178 (4)		10.04 (4)	0.0439 (6)	1015 (6)	0.191 (2)
Airth-1 (2014)	0.179 (3)		9.96 (4)	0.0400 (6)	879 (5)	0.187 (3)
Airth-5	0.184 (7)		9.86 (4)	0.0330 (4)	371 (4)	0.192 (2)
Airth-6	0.172 (4)		9.82 (4)	0.0415 (5)	779 (5)	0.191 (1)
Airth-8	0.174 (2)		9.69 (5)	0.0393 (6)	844 (5)	0.189 (2)
Airth-10	0.182 (3)		9.71 (5)	0.0438 (8)	1032 (6)	0.189 (2)
Airth-12	0.187 (6)		9.91 (5)	0.0360 (5)	631 (4)	0.190 (2)

Table 4 - Table of noble gas concentrations and noble gas

$^{3}He/^{4}He$ ratios are normalised to the air ratio (Mamyrin *et al.,* 1970) and corrected for atmospheric contributions after (Craig *et al.,* 1978), represented by R_a (relative to atmospheric ratio) to allow direct comparison with other datasets. The air corrected values do not differ from the measured ratios within 3 significant figures due to the minimal atmospheric/ASW component. The mean $^{3}He/^{4}He$ ratio of 0.18 R_a is well below the atmospheric ratio (defined as 1), but also above the expected crustal range of 0.02-0.1 R_a (Ballentine and Burnard, 2002). The $^{3}He/^{4}He$ across the field is strikingly uniform at 0.18 R_a within error, regardless of the ^{4}He concentrations.

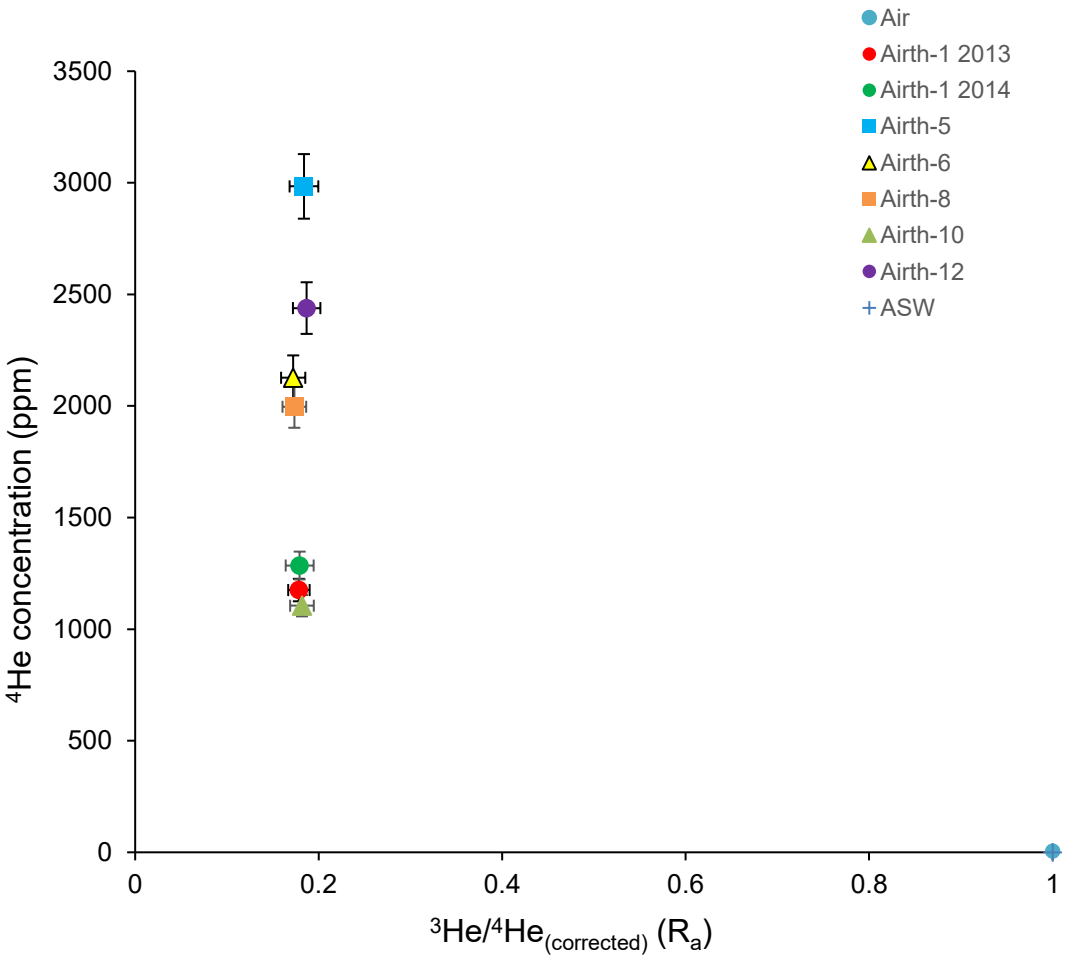

Figure 3-13 – Plot showing air-corrected $^{3}He/^{4}He$ (relative to atmosphere (R_a)) vs. measured ^{4}He concentrations in the Airth field.

3.3.5.2 Neon

^{20}Ne concentrations range from 0.042±0.0009 ppm at Airth-1 (2014) to 0.354±0.008 ppm at the unpumped Airth-5. Airth-5 and Airth-12 show neon

concentrations ×2 and ×1.05 greater than the ASW value of 0.176 ppm (see Figure 3-14).

The dominant control on $^{4}He/^{20}Ne$ ratios is the concentration of ^{20}Ne and its effect on lowering the ratio. Figure 3-14 shows the effects of mixing deep gases (with high $^{4}He/^{20}Ne$ ratios) with ASW/air, where they gain neon and the $^{4}He/^{20}Ne$ ratios are reduced.

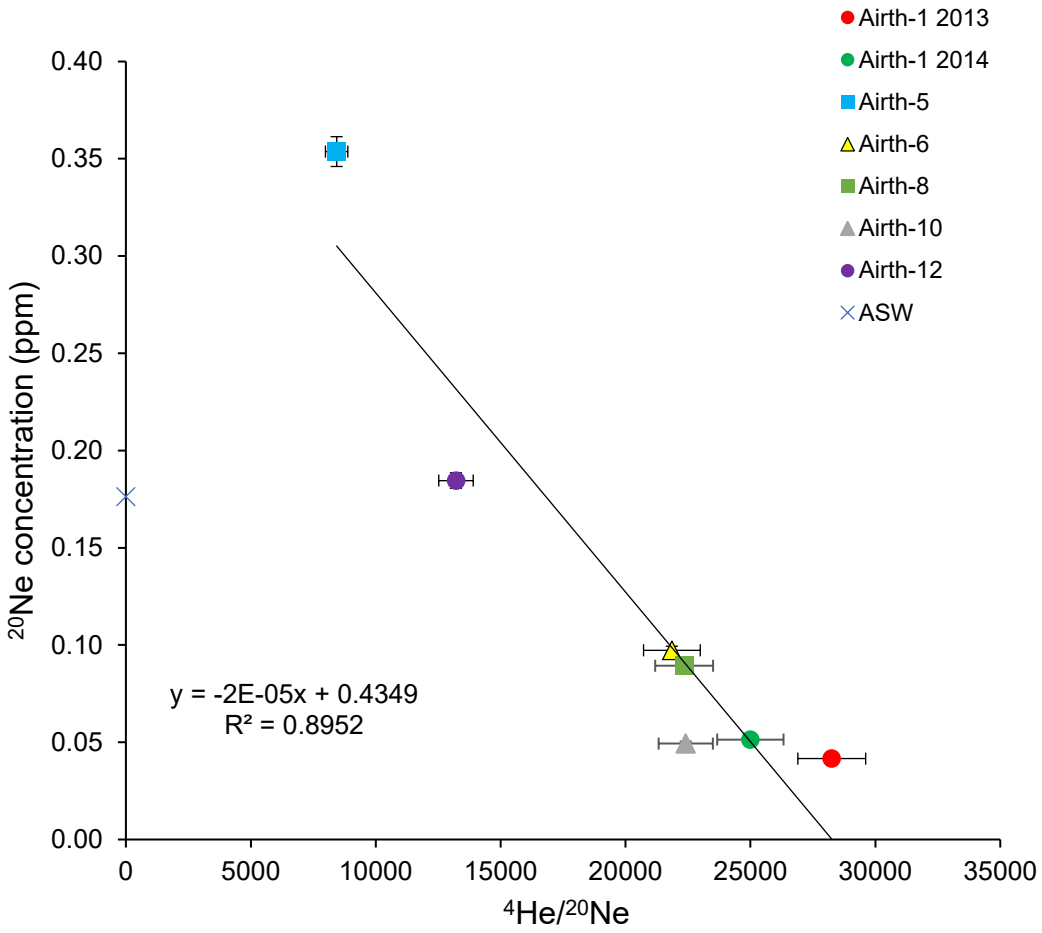

Figure 3-14 –- Graph of $^{4}He/^{20}Ne$ ratios vs. ^{20}Ne concentration. The ASW value can be seen on the left hand-side at 20Ne = 0.176 ppm. Note that higher ^{20}Ne concentrations generally equate to lower $^{4}He/^{20}Ne$ ratios. The intercept of line of best fit passes through ~0.43; a composition between ASW and air.

The isotopes of neon can reveal useful information about samples. In the subsurface, neon has three unique sources (atmosphere, mantle, crust) with defined isotope ratios (Ballentine and Burnard, 2002). This can be represented on a $^{21}Ne/^{22}Ne$. *vs.* $^{20}Ne/^{22}Ne$ isotope graph, with measured samples falling in between the three end-members defining the vertices of a triangle (Figure 3-15). $^{20}Ne/^{22}Ne$ ratios range from

10.04±0.09 at Airth-1 (2014) to 9.67±0.11 at Airth-8. The $^{21}Ne/^{22}Ne$ ratios range from 0.033±0.001 at Airth-5, to 0.0439±0.001 at Airth-1 (2013). This is attributed mainly to different amounts of atmosphere-derived input into each sample, masking contributions from more crustal and mantle signatures (more detail in the discussion).

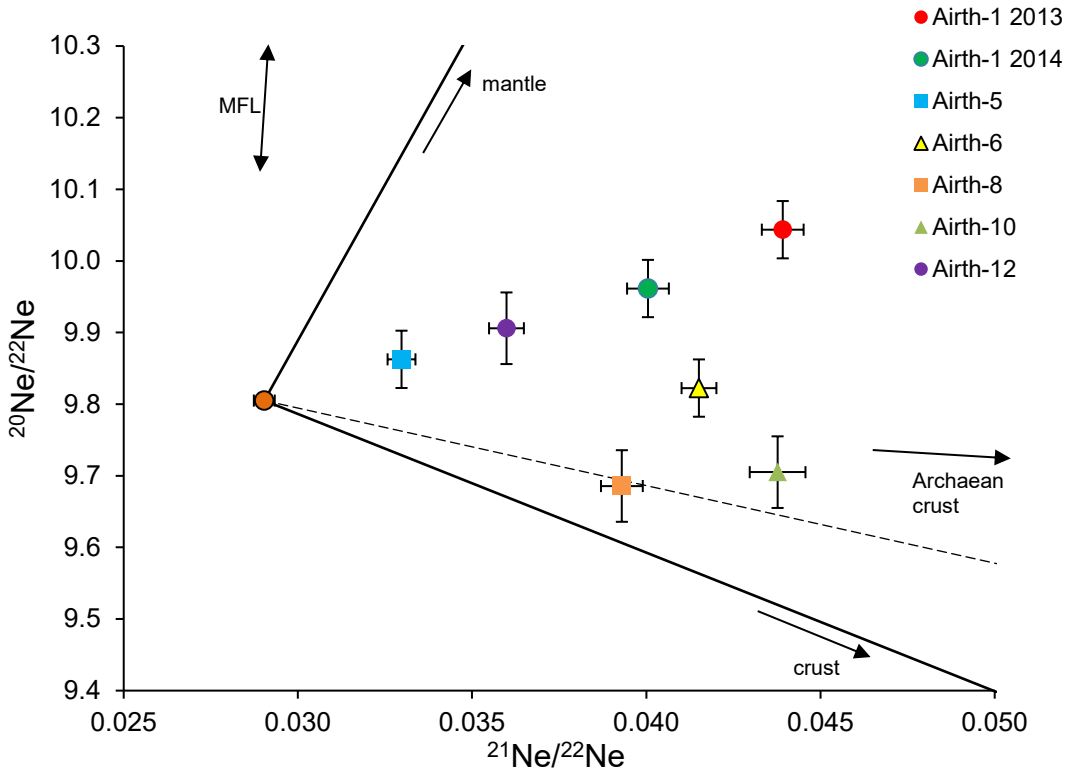

Figure 3-15 – Neon 3-isotope plot for Airth data. The orange circle represents the air end-member, the mixing line between air and the crustal end member is to the lower right, and the air-mantle mixing line follows to the upper-right. The central sub-horizontal line (long-dashes) represents an alternative Archaean crust end-member of Lippmann-Pipke et al., (2011). The mass fractionation line (MFL) is near-vertical (dotted line).

In the subsurface, the predominant source of neon is derived from the atmosphere, introduced via the dissolution of noble gases in water which is subsquently buried (ASW). This is evident in Figure 3-15, showing that all the deep gas samples are sited close to the atmopsheric air end-member compared with either the crustal or mantle end-members. The samples with greater concentrations of ^{20}Ne display neon ratios closer to atmospheric (see Figure 3-16), attributed to an increasing addition of ASW derived neon. This greater ASW component dilutes the lower concentrations of a more crustal/mantle component.

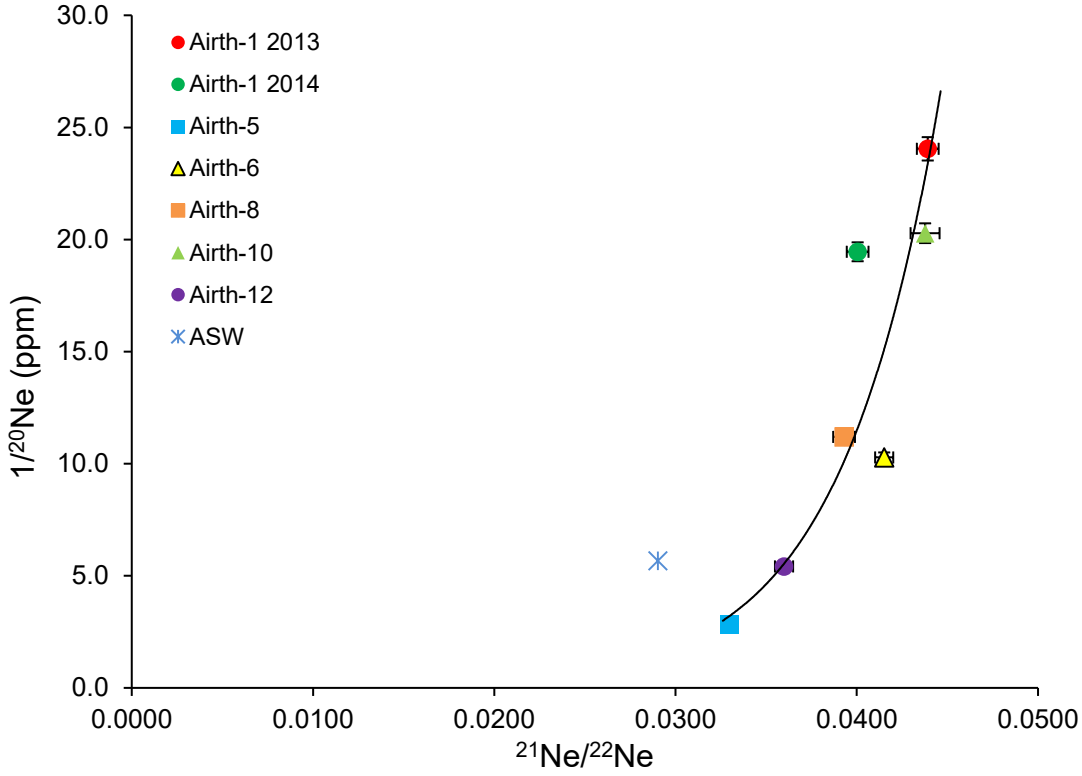

Figure 3-16 – Graph of 1/^{20}Ne vs. ^{21}Ne/^{22}Ne. A general trend exists between the addition of an atmospheric component (^{20}Ne - mainly derived from the atmosphere) and the dilution of the more crustal ratios (i.e. higher ^{21}Ne/^{22}Ne).

3.3.5.3 Argon

^{40}Ar is sourced from three reservoirs: the atmosphere, the crust and the mantle (Ballentine and Burnard, 2002). ^{36}Ar can be considered solely derived from the atmosphere and is thus a groundwater/air proxy. ^{40}Ar is prevalent in the atmosphere but is also produced in the crust by the decay of ^{40}K, and can also be introduced from magmatic fluids (Ballentine and Burnard, 2002). ^{40}Ar in excess of ASW derived ^{40}Ar is known as 'excess' argon, labelled ^{40}Ar*, and can be resolved from the ASW component via the equations of Ozima and Podosek (2002).

Airth ^{40}Ar concentrations range from 71.9±1.4 ppm to 296±5.6 ppm, these are lower than the ASW value of 347 ppm, and orders of magnitude below the air value of 9430 ppm ^{40}Ar. ^{36}Ar concentrations range from 0.082±0.002 ppm to 0.80±0.018 ppm, which are 8% to 68% of the ASW value of 1.17 ppm (see Figure 3-17), and again orders of magnitude below the air value of 31.3 ppm ^{36}Ar. ^{40}Ar concentrations increase with ^{36}Ar concentrations, but the relationship is non-linear. The ^{40}Ar* as a percentage of total

^{40}Ar ranges from 19.6% to 71% but generally are >50% of the measured ^{40}Ar, the proportion increasing as a function of decreasing total ^{36}Ar (see Figure 3-17).

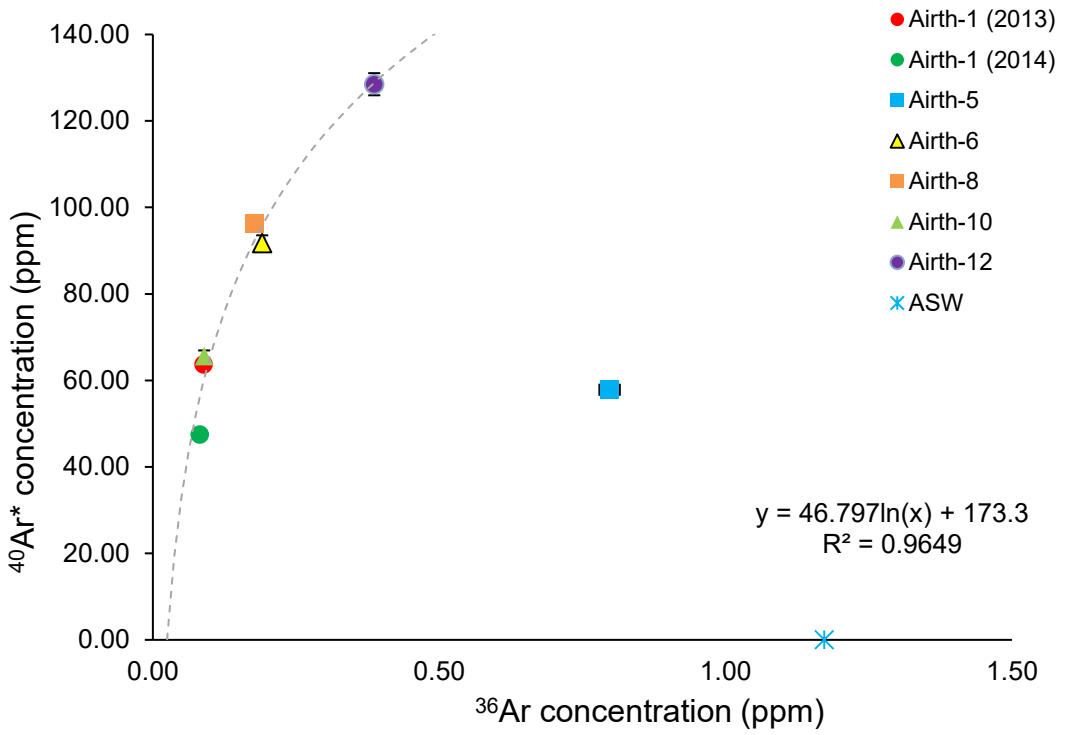

Figure 3-17 – Plot of ^{40}Ar vs ^{36}Ar for Airth gases. ASW has no excess ^{40}Ar* component. ^{40}Ar* concentrations increase with increasing ^{36}Ar concentration, the gradient of the line being proportional to ^{40}Ar/^{36}Ar, with Airth-1 (2013) and Airth-10 showing the highest ^{40}Ar/^{36}Ar and the greatest relative ^{40}Ar*/^{36}Ar. Airth-5 represents a mix between a ^{40}Ar*-rich end-member and ASW. Reported errors may be smaller than symbols.*

^{40}Ar/^{36}Ar ratios range from 371±4 at the unpumped Aith-5 well, to 1032±6 at the pumped Airth-10 well. These are all well above the ASW value of 296 and air value of 298.6, due to addition of 'excess' ^{40}Ar* from radiogenic ^{40}Ar production and potential mantle ^{40}Ar addition. The ^{40}Ar/^{36}Ar ratio decreases as a function of total argon concentration, being lowered by the relative increase in atmosphere-derived ^{36}Ar, apparently masking the more crustal-mantle ratios (see Figure 3-18).

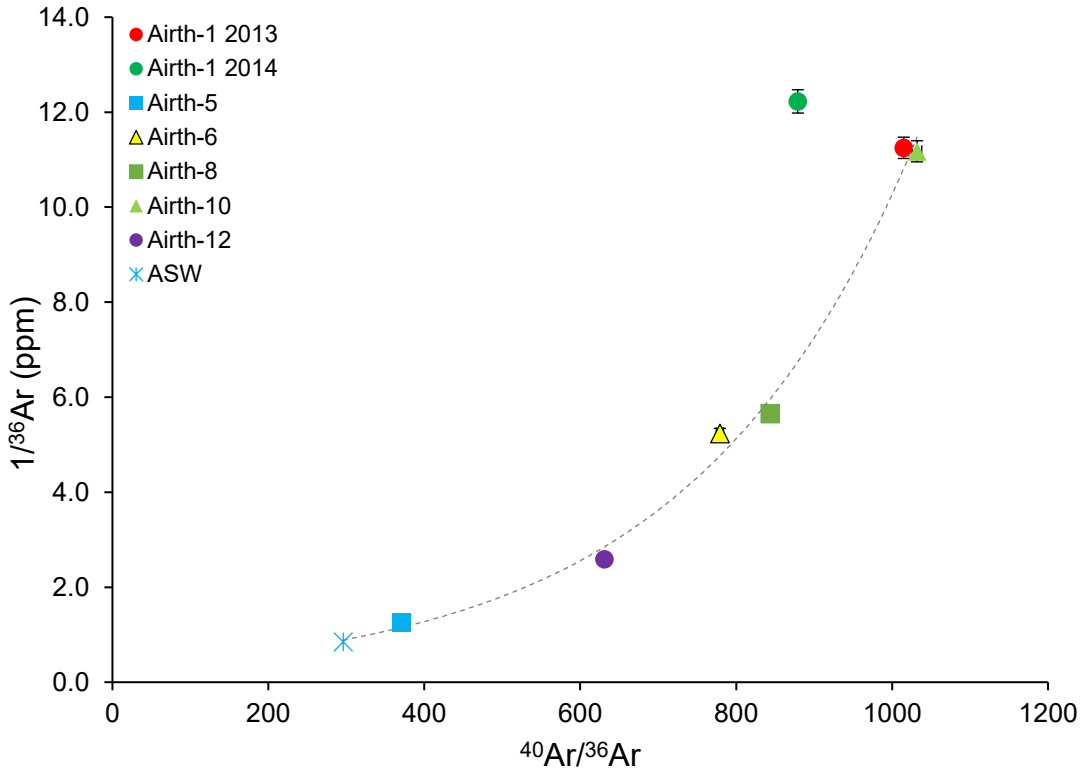

Figure 3-18 – Plot of $1/^{36}Ar$ vs. $^{40}Ar/^{36}Ar$. The $^{40}Ar/^{36}Ar$ ratio as the crustal+mantle component is diluted with increasing ASW-derived argon.

The principle of atmosphere-derived noble gases masking or diluting a more crustal/mantle signature is also seen in the $^{4}He/^{20}Ne$ system, where the increase in predominantly atmosphere derived ^{20}Ne (and hence a reduction in the $^{4}He/^{20}Ne$ ratio) correlates with a decrease in the $^{40}Ar/^{36}Ar$ ratios (see Figure 3-19), again a higher $^{4}He/^{20}Ne$ ratio generally correlating with lower total noble gas concentrations. The coherent fractionation between the $^{4}He/^{20}Ne$ and $^{40}Ar/^{36}Ar$ shows that the crustal/mantle ^{4}He and $^{40}Ar^{*}$ are derived from the same source and were well mixed prior to degassing.

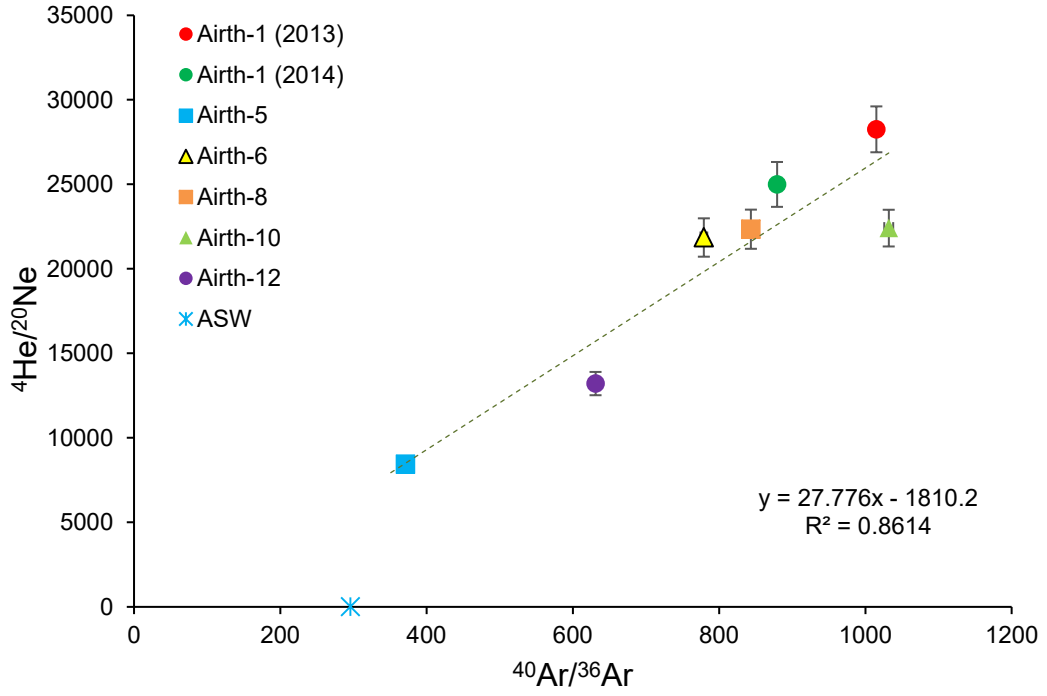

Figure 3-19 – Plot of $^{4}He/^{20}Ne$ vs. $^{40}Ar/^{36}Ar$. With the exception of Airth-10, there is clear coherent fractionation between the $^{4}He/^{20}Ne$ ratio and $^{40}Ar/^{36}Ar$ ratio.

Figure 3-20 shows a plot of ^{36}Ar *vs.* ^{20}Ne; ^{36}Ar is unambiguously derived from the atmosphere, while ^{20}Ne is primarily derived from the atmosphere with a small mantle input (see Table 6). Note that samples plot coherently towards the air value implying that both components were well mixed in the system prior to pumping, and appear primarily air-derived with Airth-5 and Airth-12 showing small ASW contributions shown by an elevated ^{36}Ar value relative to the air ratio (dotted black line). From this we can see a lower $^{20}Ne/^{36}Ar$ value generally corresponds with a higher ASW content.

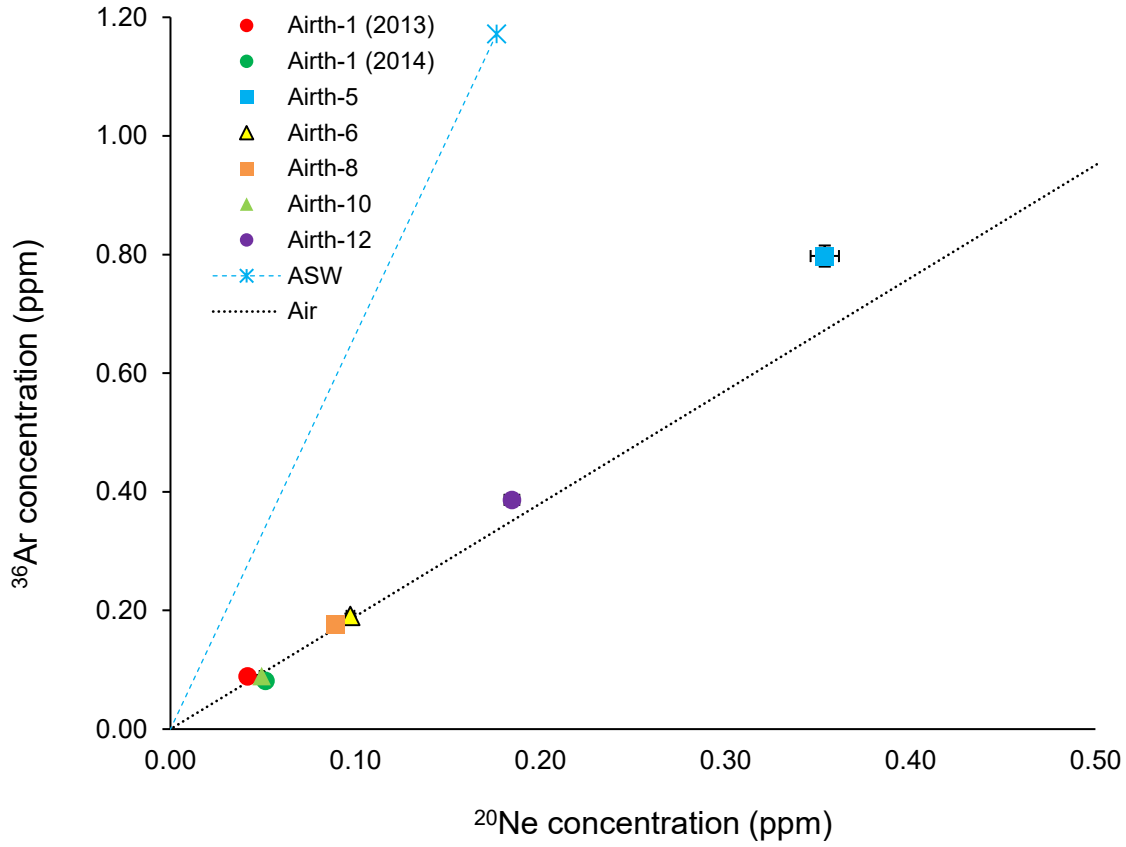

Figure 3-20 – Plot of ^{36}Ar vs. ^{20}Ne. Note that the ratio of the primarily atmosphere-derived ^{36}Ar and ^{20}Ne isotopes follow the air-line (dotted black) rather than the ASW value (blue dash).

3.3.5.4 Krypton & Xenon

^{84}Kr concentrations range from 0.0010±0.00004 ppm at Airth-1 (2013) to 0.0219±0.00091 ppm at Airth-5. These range from 2% to 48% of the predicted ASW concentration of 0.046 ppm, and 0.15% to 3.3% of the air concentration of 0.65 ppm. ^{132}Xe isotopes show a similar pattern, with concentrations ranging from 4.8×10^{-5} $\pm2.5\times10^{-6}$ ppm at Airth-1 (2013) to 8.33×10^{-4} $\pm4.36\times10^{-5}$ ppm at Airth-5. These range from 1.6% to 25% of the predicted ASW concentration of 3.04×10^{-3} ppm, and 0.21% to 3.6% of the air concentration of 2.3×10^{-2} ppm. All samples show lower concentrations of both ^{36}Ar and ^{132}Xe than ASW, and much lower than air (Figure 3-21). The same pattern is repeated in the krypton system. The ratios of ^{132}Xe to ^{36}Ar are at or nearer to the air value, rather than the ASW water value that would be expected. ^{84}Kr *vs.* ^{36}Ar shows a similar pattern.

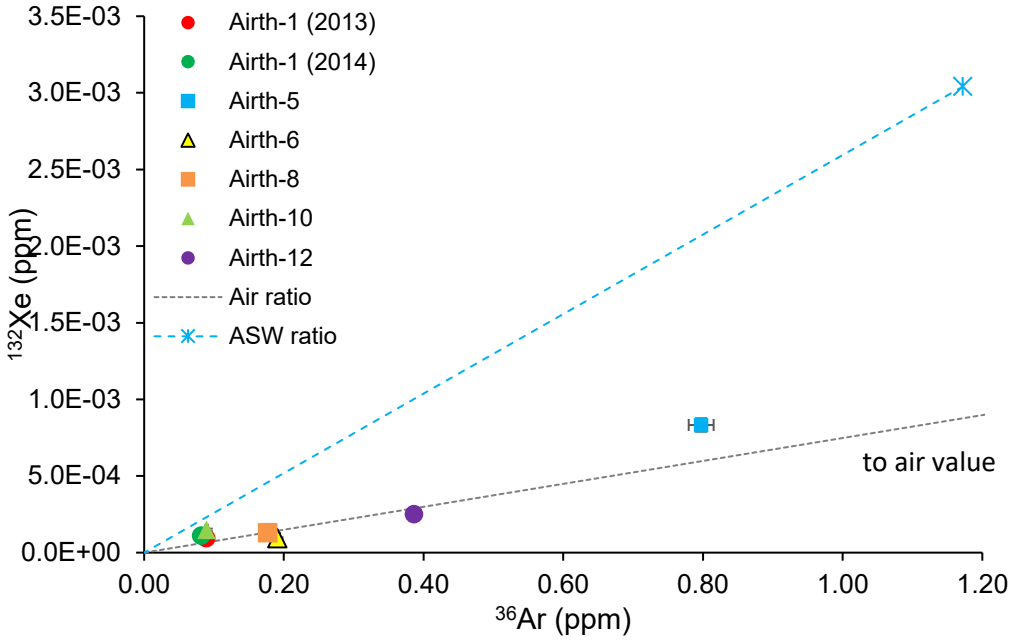

Figure 3-21 – Plot of 132Xe vs. ^{36}Ar. The dotted black line plots to the air value, while the blue line plots along ASW.

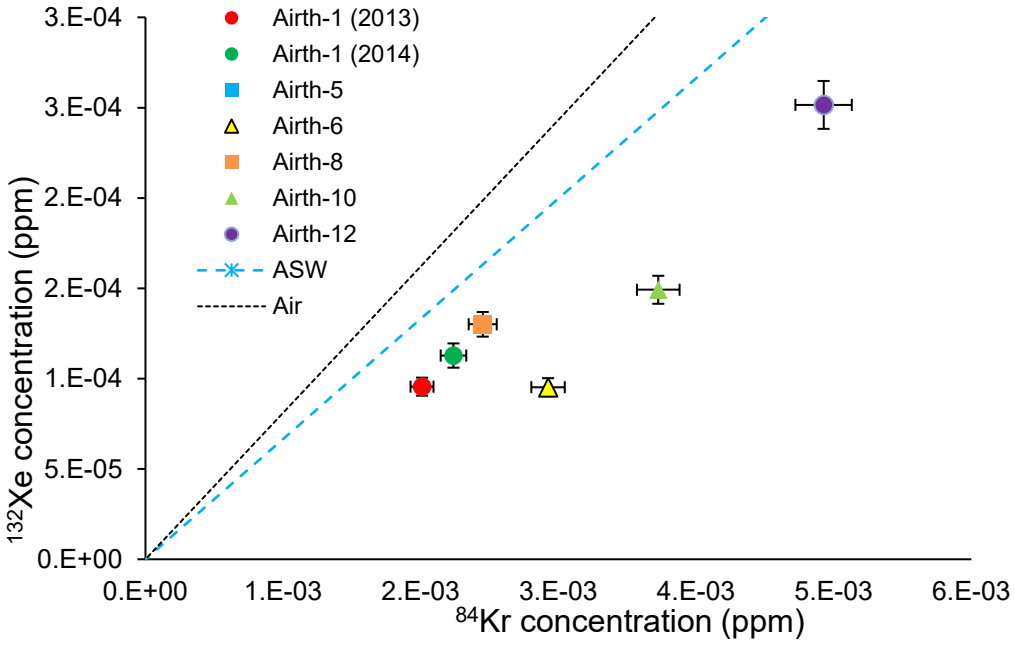

Figure 3-22 – Plot of ^{132}Xe concentrations vs. ^{84}Kr concentrations. The dashed blue line extends to the predicted ASW value (off chart). The dashed grey line extends to the air value (off chart). Airth-5 sits within error of the air ratio.

The concentrations of ^{132}Xe *vs*. ^{84}Kr show a mixture between air and ASW (Figure 3-22), with the exception of Airth-6 that shows a relative depletion in ^{132}Xe.

3.4 Discussion

3.4.1 Bulk Geochemistry

Airth gases displayed detectable, but unquantifiable levels of nitrogen (<0.1%), which is lower than the typical range in UK coals of 2-8% (Creedy, 1991, 1988), with an average of 0.47 m^3/tonne (Creedy and Pritchard, 1983). Nitrogen is formed as part of coalification and diagenetic processes, derived from buried organic matter (Rightmire *et al.*, 1984; Baxby *et al.*, 1994; Krooss *et al.*, 1995) and so is expected in coal seams.

The low nitrogen content is indicative of negligible ASW-derived nitrogen input to the gas, but also shows negligible input from coalification or magmatic sources (Gold and Held, 1987; Sano *et al.*, 1993; Krooss *et al.*, 1995). Nitrogen is preferentially desorbed over methane from coals due to its smaller molecular size and affinity with coal beds (Clayton, 1998; Creedy and Pritchard, 1983; Thomas, 2013), so it is possible that part of the original nitrogen content has been lost over geological time.

CO_2 contents in Airth gases correlate with the low end of the UK average of 0.2-6% (Creedy, 1991, 1988). This broadly correlates with the observation that more mature coals do not retain coalification CO_2, and deeper seams exhibit lower CO_2 contents (Creedy and Pritchard, 1983). The lack of CO_2 does not point to significant microbial activity in the coalbeds, and no other indicators of microbial activity were detected (ethylene, acetylene, oxygen, or carbon monoxide). The quantity of higher hydrocarbons is low compared with published previous UK coal gases (see Figure 3-23). Coals with greater concentrations of heavier hydrocarbons are often associated with oil-bearing strata (Creedy, 1991), which are known in this area below the LCF and are a prospective target for shale oil. There is no direct evidence for interaction with oil-bearing strata within the Airth field, but hydrocarbon shows were found in the LCF in the nearby Inch-of-Ferryton well (Monaghan, 2014). The methane and higher hydrocarbons are most probably the result of coalification, as similar components have been observed in other UK coal derived gases (Creedy, 1988).

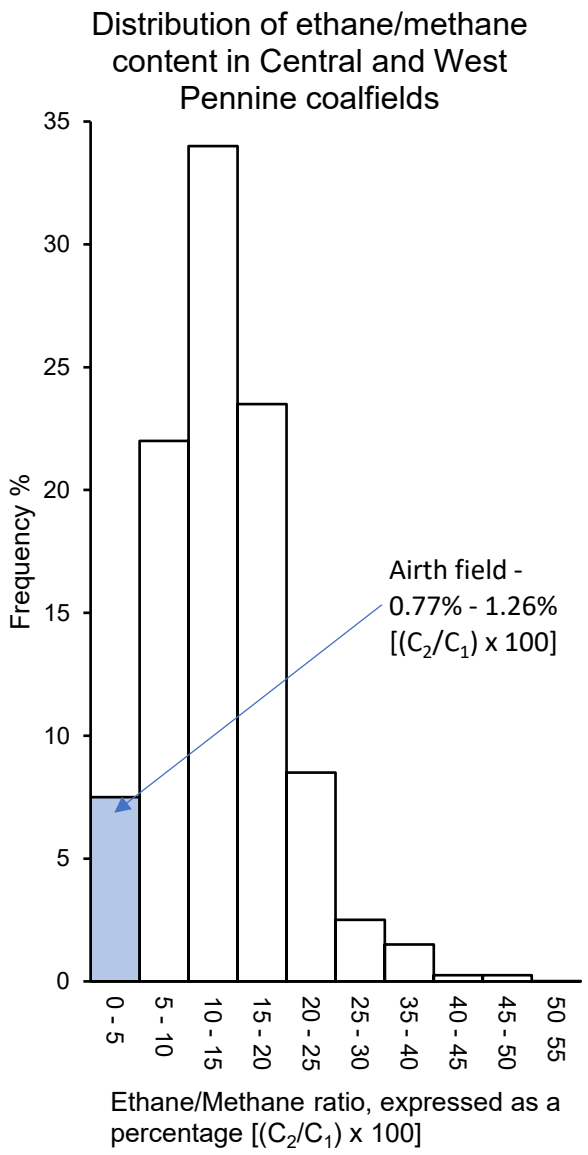

Figure 3-23 – Distribution of ethane/methane contents from measured gases in the Central and West Pennine coalfields. Reproduced after CEC (1988).

The ratios of C_1/C_2 and $C_1/(C_2+C_3)$ vary, and are controlled by the small concentrations (<2%) of ethane and higher hydrocarbons present in the gas. The C_{2+} concentrations in coal derived gases are known to vary throughout other coalfields by several percent and may be related to paleotopography (CEC, 1988), so these data with minor differences (0.77% – 1.26% difference in C_2/C_1) are indicative of a fairly low and narrow range of ethane contents, and can be considered to be within natural variance.

Airth-1 showed an increase in the C_1/C_2 (30%) and C_1/C_3 (50%) ratios between 2013 and 2014; with a greater relative concentration of methane present after being shut-in. Typically, coal gases can become both compositionally and isotopically heavier over time as the residual gas desorbing from coals is enriched in heavier components as the reservoir is depleted (Creedy, 1991; Rice, 1993). This was not observed in this case; a possible cause could be that the evolution towards compositionally and isotopically heavier gases would be observed in producing fields which are losing a component of their stored gas. Airth-1 (and all other wells) were not being produced during this period. The cessation of gas production reduces the pressure gradient in the coal seams, affecting the desorption of heavier C_{2+} components

from the coal which are bound more strongly and desorb less readily than methane (Creedy, 1991).

3.4.2 Carbon and Hydrogen Stable Isotopes

The gases at Airth are unambiguously thermogenic (Figure 3-12), and no input of isotopically lighter microbial methane is inferred. Thermogenic gas in coals is produced by devolitisation as a result of the coalification process, and gas generation and storage capacity in coals increases with increasing thermal maturity (Moore *et al*., 2012). As thermal maturity cannot be reversed, the gases present in the coals probably coincide with the period of maximum thermal maturity. In the Kincardine Basin this should coincide with the period of maximum burial which occurred either in the late Carboniferous (Marshall *et al.*, 1994), or the Early Cenozoic (Underhill *et al.*, 2008; Vincent *et al.*, 2010), so the methane within the coals can be considered to date from at least the early Cenozoic, prior to the uplift of the region resulting from the North Atlantic Igneous Province which commenced 61 Ma (Mackay *et al.*, 2005). Due to the low permeability of coals and interbedded sandstone units in the region, and the target zone's proximity to the deepest part of the basin, it is improbable that any significant methane recharge into the coals could have occurred from other horizons to change the isotopic composition. No significant input of oil is inferred due to the dry nature of the gases generated.

Airth gases occupy a narrow range of $\delta^{13}C_{CH4}$ values from -39.5‰ to 43.5‰. Overall the stable isotopes overlap with previous measurements of UK coal gases and North Sea gases (Hitchman *et al.*, 1989). The range in $\delta^{13}C_{CH4}$ values is much smaller than in the range of reported δD_{CH4} values, it is unknown if this is an effect of fractionation between samples or an artefact of the δD_{CH4} analysis technique (*e.g.* memory effect of residual H_2O during reduction to H_2 in subsequent analyses).

A "Bernard" plot (Figure 3-11) shows the gases based on the boundary ($C_1/(C_2+C_3) = 50$) of the thermogenic field. Coal gases are typically dry compared with 'typical' gases generated from type I/II kerogens (Whiticar, 1994; Golding *et al.,* 2013), and some authors prefer to use 100 as the thermogenic boundary for $C_1/(C_2+C_3)$ when referring to coalbed gases (Golding *et al.,* 2013), therefore the gases can be considered entirely thermogenically generated.

Rice (1993) observed that CBM wells can produce increasingly isotopically heavy and wetter gases over time of production, related to the 'chromatographic' effects of

desorpsion, as coals preferentially retain heavier components. Airth-1 shows a negligible increase in $\delta^{13}C_{CH4}$ (-40.2‰ to -39.5‰), and a δD_{CH4} decrease from -163‰ to -220‰ from 2013 to 2014. The Airth field has seen very little gas extraction and dewatering, with some wells having never been dewatered. These untouched wells are hypothesised to show a hydrocarbon isotopic and compositional assemblage in equilibrium with the coals and groundwater, and represent the very initial stages of a CBM development. Importantly however, the molecular and isotopic compositions of the gases are not fixed spatially or temporally in a field due to desorpsion effects, and this has significant implications for defining a fixed geochemical 'fingerprint' for CBM fields, *i.e.* a narrow range of geochemical bounds that can be used to define a gas source. If the field were ever to be put on production, the gases could be expected to become isotopically and molecularly different, which may obfuscate the interpretation of migrated gas.

3.4.3 Radiocarbon

The radiocarbon-dead sample confirms no resolvable modern carbon input to the coal gases, to be expected from 'ancient' (>65,000 year) gas, or sourced solely from ancient material with no input of modern carbon in to the system, and is concordant with the thermogenic origin of the well gases. Starch and cellulose derived polymers (PureBore™, derived partly from potato starch) were used in the drilling process and these contain modern carbon, but no modern carbon input was resolved in the well gas.

3.4.4 Noble Gases

The copper tubes containing samples were observed to leak small volumes of helium in the period of time between sampling and storage. This was not determined to have affected the isotopic ratios of gases, or any other noble gas species (*e.g.* from atmospheric ingress). A full documentation of this effect and discussion is presented in the Appendix (this volume).

3.4.4.1 Air Saturated Water

As noted previously (see Air Saturated Water (ASW)), ASW is assumed to represent the mechanism by which most atmosphere-derived noble gases enter the subsurface. The input variables for calculating ASW in this study are the altitude and average surface temperature of the modern Airth site into fresh water (*i.e.* rain), as these would be

reasonable assuming meteoric recharge to the Airth field. However, it is clear from analysis of produced waters from Airth (SEPA, 2014) that this is not a valid assumption, as the waters are highly saline (of the approximate chemical composition of seawater, but around ~1/3 as saline), and high in dissolved heavy metals suggesting that they have been present at depth for a long period of time as immobile formation water, and thus are unlikely to have been recently recharged by meteoric water. Any ancient meteoric recharge likely equilibrated with the atmosphere in conditions that might not be relevant to modern conditions. Furthermore, the site's current and ancient proximity to the ocean mean that Air-Saturated-Seawater recharge (or a sea-meteoric water mix) cannot be discounted. For this reason, the exact values of ASW and any inferences with regards to precise mixing ratios need to be used with caution. Nonetheless the noble gas inventory as a result of the accumulation of salinity in sedimentary brines or from seawater is predictable (Zaikowski and Spangler, 1990), and the ranges expected ($^{20}Ne/^{36}Ar$ = 0.14-0.20) are relatively small in relation to the variation in the field for the purposes of this study.

3.4.4.2 Helium

The $^{3}He/^{4}He$ ratio across the field is uniform at 0.18 R_a within error, regardless of the ^{4}He concentrations. The wells target different coal seams over geographically diverse areas, and local variations might be expected in ^{4}He due to natural variations in U-Th series element distributions across coals and shale horizons (*e.g.* Black Metals Group). This indicates that the helium inventory has been well mixed laterally as well as vertically between seams. This potentially implies a non-coal source for the majority of helium contained in the samples.

Györe *et al.,* (2018) calculated the ^{4}He production in Airth coals to be 48.7 to 156.8 cm^3 STP/tonne (after Vermeesch, (2008)), corresponding to 19.6 ppmv at a methane concentration of 8 m^3/tonne (Bacon, 1995), which is a small fraction of the observed ^{4}He concentrations. It was concluded that the *in situ* ^{4}He generation in coals cannot account for the concentrations observed.

The ^{4}He concentrations are an order of magnitude higher than the previously published dataset for CBM (Zhou *et al.,* 2005), as well as other datasets published in the UK region (Ballentine *et al.,* 1996). The higher ^{4}He concentrations (and high $^{4}He/^{20}Ne$ ratios) draw parallels with the 'under-pressured' region of Zhou *et al.,* (2005) which saw less groundwater recharge than the more productive 'over-pressured' area. This is

concordant with the low permeability of the coal seams compared to US analogues (Creedy, 1991). ^{4}He concentration in a gas phase in the subsurface is dependent on the gas/water ratio, the concentration of ^{4}He dissolved in the formation water, and any diluting gas phase such as methane added to the resultant gas phase. The amount of noble gas dilution is a function of the dewatering process, as more methane can degas from coal with greater dewatering and resultant pressure drop.

Due to the low solubility of helium in water and its low atmospheric abundance (*i.e.* ASW) and the predominantly radiogenic signature of $^{3}He/^{4}He_{(Ra)}$, it is obvious that the majority of helium in the system is crustal derived ^{4}He produced from the U and Th decay series, with a large proportion coming from an *ex situ* source. However, because the ^{3}He concentrations are higher than would be expected from a purely crustal system, a small mantle contribution is inferred.

Based on $^{4}He/^{20}Ne$ ratio of ASW and assuming complete degassing of helium and neon into a gas phase, the ^{4}He and ^{3}He contributions from ASW can be calculated from the ^{20}Ne concentrations in the samples to be a maximum of 0.003% and 0.017% of the total ^{4}He and ^{3}He inventories, respectively (for the Airth-5 sample, other samples show smaller ASW derived contributions). This negligible input via ASW is expected considering the high $^{4}He/^{20}Ne$ ratios, but demonstrates that an external contribution of a ^{3}He-rich component to the field is necessary to explain the elevated $^{3}He/^{4}He$ ratio of 0.18 R_a.

3.4.4.3 Assessing the Mantle Contribution:

3.4.4.3.1 Mantle Helium

The majority of the ^{3}He is hypothesised to be of mantle origin with a negligible ASW component, but ^{3}He has numerous other sources. ^{3}He addition could also arise from thermal neutron capture by ^{6}Li, however predicted average crustal production rates are very low (Ballentine and Burnard, 2002), and no obvious lithium enrichment is expected, or has been reported in the region. Due to the depth of the formation, cosmogenic ^{3}He input can be ruled out, along with ^{3}He input from tritium decay in recent waters due to the low permeability of the coals, and high dissolved heavy metal content implying a long formation water residence time. Outgassing 'fossil' ^{3}He stored in fluid inclusions from previous magmatic events is regarded as insignificant in the overall He budget (Ballentine and Burnard, 2002).

Assuming a non-ASW source, the mantle input to the helium inventory can then be calculated from Equation 2 by subtracting $[^{4}He]_{crust}$ from $[^{4}He]_{total}$, assuming an absence

of air-derived helium, and expressing it as a percentage of the total [^{4}He] (see Equation 3)

$$[^4He]_{crust} = \frac{[He]_{total} \times [(\frac{^3He}{^4He})_{mantle} - (\frac{^3He}{^4He})_{sample:\,air\,corrected}]}{[(\frac{^3He}{^4He})_{mantle} - (\frac{^3He}{^4He})_{crust}]}$$

Equation 2 – Equation for calculating the crustal ^{4}He contribution to measurements.

$$\%\,[He]_{mantle} = \frac{[^4He]_{total} - [^4He]_{crust}}{[^4He]_{total}}$$

Equation 3 – Equation for calculating the mantle contribution to the ^{4}He inventory.

The selection of ^{3}He/^{4}He mantle end-member is important for this calculation; it is unreasonable to select a MORB ^{3}He/^{4}He ratio for the mantle end-member due to the geological setting, and there is a range of appropriate Sub Continental Lithospheric Mantle (SCLM) end-members calculated from mantle xenoliths in the literature (Ballentine *et al.,* 2002). Kirstein *et al.,* (2004) measured Permo-Carboniferous mantle xenoliths from the Midland Valley and measured low (~1 R_a) values attributed to ^{4}He ingrowth and alteration, but found ~6 R_a in mantle xenoliths from NW Scotland which fits well with other published SCLM values (Dunai and Baur, 1995; Gautheron and Moreira, 2002, and references therein). However a smaller contribution from a high-R_a (>15 R_a) source is also possible, as such volcanism in the Tertiary related to the Iceland Plume is known to have affected NW Scotland (Stuart *et al.,* 2000). A range of calculated mantle contributions to the helium inventory for the Airth field with different end-members is given in Table 5:

^{3}He /^{4}He mantle end-member	Range calculated mantle ^{4}He contribution
8 R_a MORB	2.71 – 2.95 %
6 R_a SCLM (^{3}He/^{4}He = 8.54×10^{-6})*	2.71 – 3.34 %
4.7 R_a SCLM (^{3}He/^{4}He = 6.53×10^{-6})	3.54 – 3.86 %
5.4 R_a 'Mean' SCLM (^{3}He/^{4}He = 7.53×10^{-6})	3.07 – 3.34 %
15 R_a 'Plume'	1.11 – 1.21 %
50 R_a Early Proto-Iceland plume**	0.34 – 0.36 %

*Table 5 - Table of calculated mantle helium contributions to measured gases * Guatheron and Moreira (2012). **Stuart et al., (2000).*

Regardless of the assumptions made with the $^{3}He/^{4}He$ mantle end-member, the mantle contribution remains a small yet resolvable component to the crustally-dominated ^{4}He inventory, and is the first recorded example in UK onshore gases (Oxburgh *et al.,* 1986). The total helium contents in Airth are considerable at over 1000 ppm, so despite the relatively small proportion of non-crustal ^{4}He addition, the mantle component is significant, (*e.g.* assuming a MORB mantle input, non-crustal derived ^{4}He ranges from 18.7 ppm to 66.0 ppm, of which the majority is mantle derived, assuming negligible ASW helium input).

As the region is underlain by Paleozoic basement, which is at least 400 Ma (Badenszki *et al.,* 2015) (though older Grenvillian 1090 – 1020 Ma ages are historically preferred (Cameron and Stephenson, 1985), the $^{3}He/^{4}He$ ratios would be expected to be very close to the crustal production ratio (~0.01 R_a). In general higher $^{3}He/^{4}He$ ratios are found in regions of relatively recent (<50 Ma) tectonic activity (Polyak and Tolstikhin, 1985), which has been notably absent in the MVS in at least the last 50 Ma (Cameron and Stephenson, 1985).

The majority of ^{20}Ne in the subsurface originates from the atmosphere and introduced via ASW, so higher ^{20}Ne concentrations indicate a greater relative degree of groundwater input to the gas. Increasing ^{20}Ne concentrations correlate with increasing ^{4}He concentrations showing that the ^{4}He is also expectedly sourced from the groundwater. This relationship has been seen previously in numerous crustal fluids systems *e.g.* (Sherwood Lollar *et al.,* 1997; Ballentine and Sherwood Lollar, 2002; Gilfillan *et al.,* 2008; Györe *et al.,* 2015). Despite helium and neon having similar solubilities, the relationship between the two in Airth gases in not linear (Figure 3-24), and ^{20}Ne concentration is the dominant control on the $^{4}He/^{20}Ne$ ratio.

An external mantle helium contribution from depth must by definition have passed through intermediate strata, so the total helium budget in gas samples must be comprised of both *in situ* generated helium as well as externally derived mantle and basement sources. Mantle input to the Airth system is apparent from the elevated $^{3}He/^{4}He$ ratio compared with the expected crustal component of <0.1 R_a, and minimal atmospheric input. This mantle input can be investigated further using the three isotopes of neon.

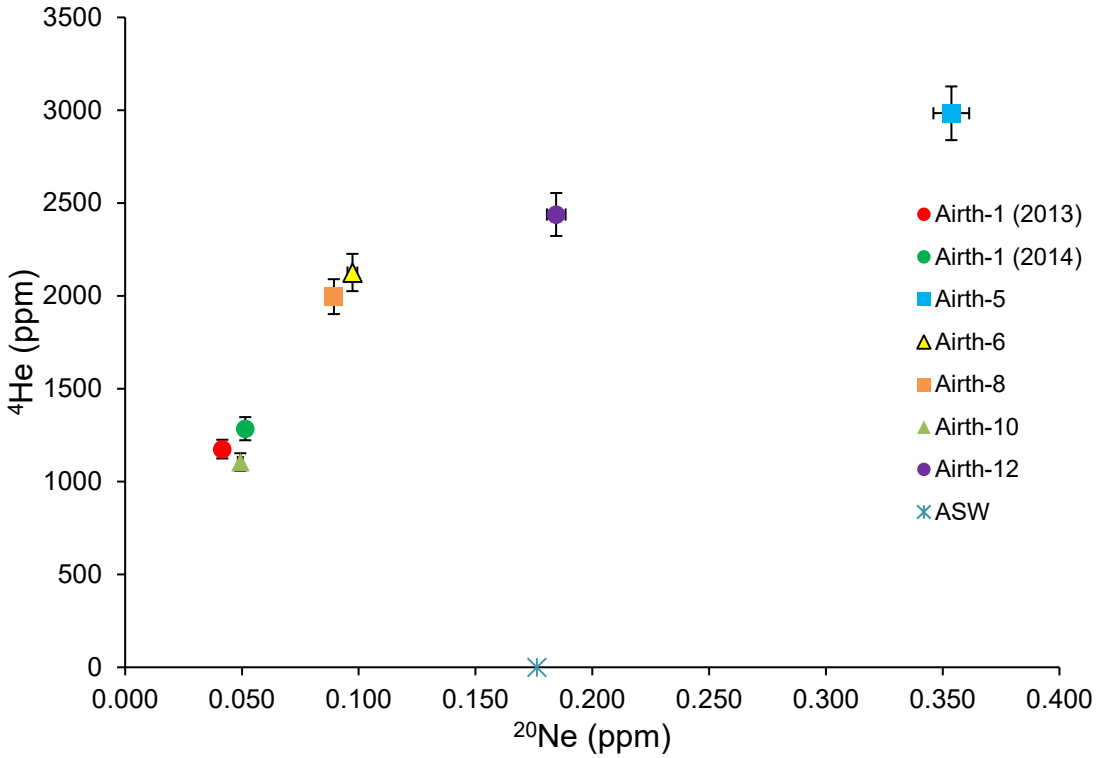

Figure 3-24 – Graph of ^{4}He vs. ^{20}Ne for Airth gases.

3.4.4.3.2 Mantle Neon

Constraining mantle neon contributions is an important step toward identifiying mantle input, as helium data alone may not be sufficient. In the subsurface, there are 3 primary sources of neon: atmospheric, mantle, and crustal, which are resolveable due to their unique isotopic ratios (Ballentine and O'Nions, 1992; Ballentine *et al.,* 1996; Ozima and Podosek, 2001). The mantle end-member is rich in primordial ^{20}Ne, the crust is dominated by ^{21}Ne and ^{22}Ne primarily from the reactions $^{18}O(\alpha,n)^{21}Ne$ and $^{19}F(\alpha,n)^{22}Na(\beta)^{22}Ne$ (Yatsevich and Honda, 1997; Ballentine and Burnard, 2002), and the atmospheric end-member is well constrained (Ozima and Podosek, 2001). These end-members can be represented as the vertices of a triangle within a $^{20}Ne/^{22}Ne$ *vs.* $^{21}Ne/^{22}Ne$ plot. Samples found on the Earth will plot within these bounds, and the relative contributions from each end-member can be determined.

On a plot of $^{20}Ne/^{22}Ne$ *vs.* $^{21}Ne/^{22}Ne$, none of the deep gas samples fall within error of the air-crust mixing line (see Figure 3-25), which suggests either a small mantle addition or mass-dependent-fractionation.

The air-crust mixing line is defined by the well constrained air value and the crustal end-member, which is less reliably constrained. For reference, the crustal end-

member for fluorine-depleted Archaean crust is also shown on the sub-horizontal line (Lippmann-Pipke *et al.,* 2011). Fluorine-depleted crust will produce less nucleogenic ^{22}Ne, producing an extreme crustal end-member which has an inherently higher $^{20}Ne/^{22}Ne$ ratio. This is not realistic for the Airth field, but is provided as further confirmation that many of the the $^{20}Ne/^{22}Ne$ ratios are in excess of even the most extreme crustal ratios, implying a mantle contribution.

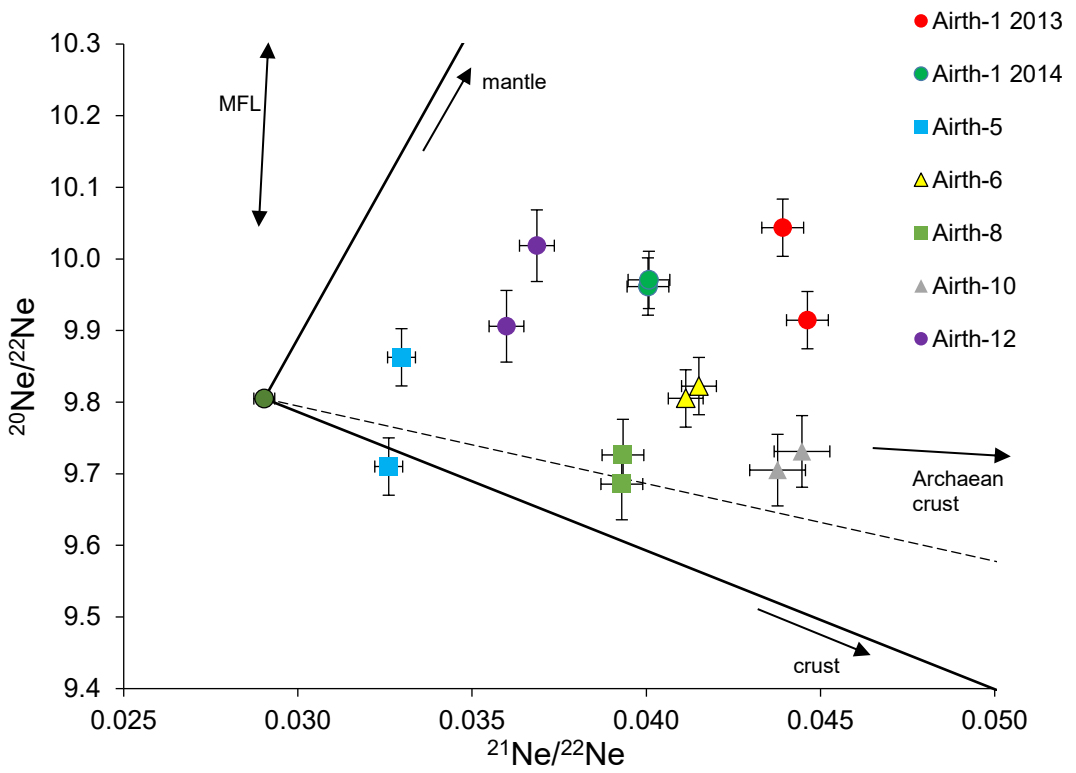

Figure 3-25 - Neon 3-isotope plot with Airth samples and duplicate runs. The air value is represented by the orange circle. The crustal end-member lies to the lower right (off chart), with the mixing line with air between the two. The mantle end-member lies to the upper right (off chart), with air-mantle mixing line shown. The alternative Archaean crust end-member-air mixing line is denoted by the long-dashed line. The Mass-Fractionation line is shown to the upper left. All samples were run in duplicate to ensure reproducibility. The final data used in the text was selected based on the quality of the raw data.

It is important to assess the possibility of mass-fractionation as this can severely affect the interpretation of neon isotope data, especially in the resolving of mantle components. The effects of mass fractionation have a greater effect on the $^{20}Ne/^{22}Ne$ ratio than the $^{21}Ne/^{22}Ne$ ratio due to the relative mass difference between the isotopes in each ratio. The mass difference between different isotopes of an element can result in kinetic isotopic fractionation effects due to the increased velocity/energy/diffusivity

of lighter isotopes. Mass-fractionation trends can be an observed property of a sample, or can be introduced during the analytical procedures.

Duplicate samples from Airth-1 were previously run (see Appendices 7.1), and these showed neon isotopes within error of those reported in this text. This, combined with the internal consistency of these data (see Figure 3-25) suggest machine-induced mass-fractionation is not a factor here, as the degree of mass fractionation would be unlikely to be constant over the sample sites, a year between sampling, duplicate sample runs, and the several weeks analysis time required for this dataset.

Figure 3-26 shows a plot of $^{20}Ne/^{22}Ne$ *vs.* $^{38}Ar/^{36}Ar$ and the mass-fractionation line derived from the air ratio (based on square roots of the isotopic mass-differences). If mass-fractionation is present in the samples in the neon system, it would be reasonable to expect fractionation in the $^{38}Ar/^{36}Ar$ ratio, as seen in Zhou *et al.,* (2005) from intensive gas production. The 3 values which lie in error of the MF line also lie within error of the air value. 4 of the values do not fit on the MF line and there is no clear trend, but they all possess an elevated $^{20}Ne/^{22}Ne$ ratio above the air-crust mixing line, which suggests that the elevated $^{20}Ne/^{22}Ne$ ratios in these samples causing deviation from the air-ratio are caused by a small mantle ^{20}Ne addition.

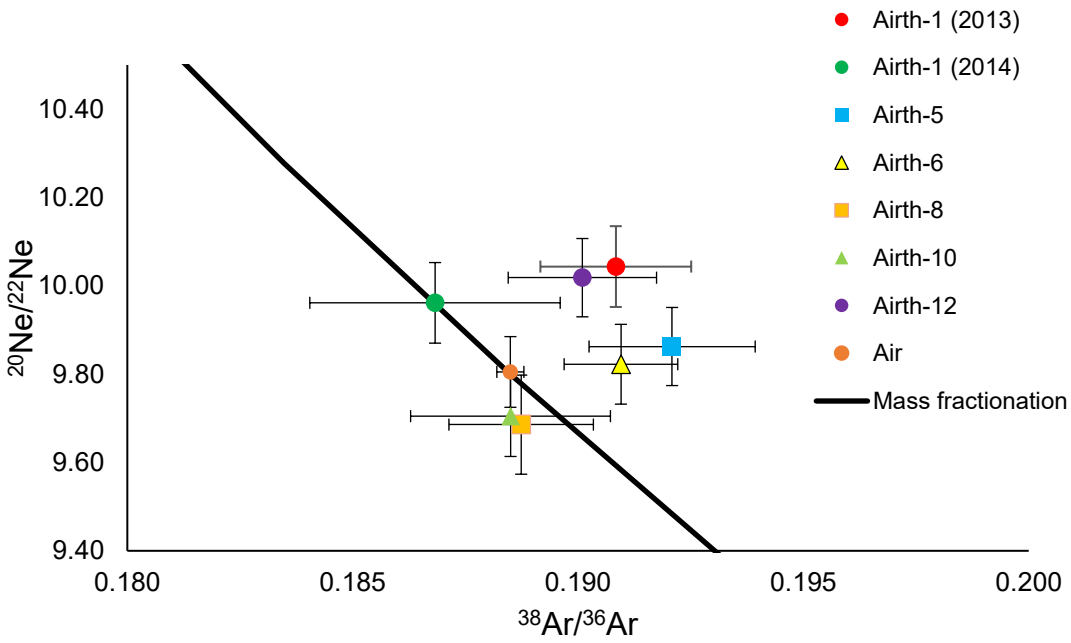

Figure 3-26 – Plot of $^{20}Ne/22Ne$ vs. $^{36}Ar/^{36}Ar$. The mass-fractionation line from the air ratio is shown with the black line. In the absence of mass-fractionation or mantle addition, the $^{38}Ar/^{36}Ar$ points should plot within error of air.

$^{38}Ar/^{36}Ar$ measurements are troublesome as they are analysed in the same analytical sequence as $^{40}Ar/^{36}Ar$, and performed on the same Faraday detector. Natural abundances of ^{38}Ar are very low compared to ^{40}Ar, especially for samples where there is excess ^{40}Ar, so achieving satisfactory ^{38}Ar measurements in a sample without introducing excessive ^{40}Ar into the mass spectrometer leads to less reliable determinations of $^{38}Ar/^{36}Ar$. There may also be detector linearity effects which would not be apparent in the calculated errors. Nevertheless, although minor MF cannot be conclusively ruled out, the degree to which these values deviate from the air value, and the variations being mainly accounted for by mantle ^{20}Ne addition, impies that mass-dependent fractionation at Airth is insignificant.

Mass fractionation is also be explored in Figure 3-27; in principle a mass fractionation trend should be more pronounced in the $^{20}Ne/^{36}Ar$ system due to the greater difference in isotopic masses than the $^{20}Ne/^{22}Ne$ system, but no obvious trend can be seen.

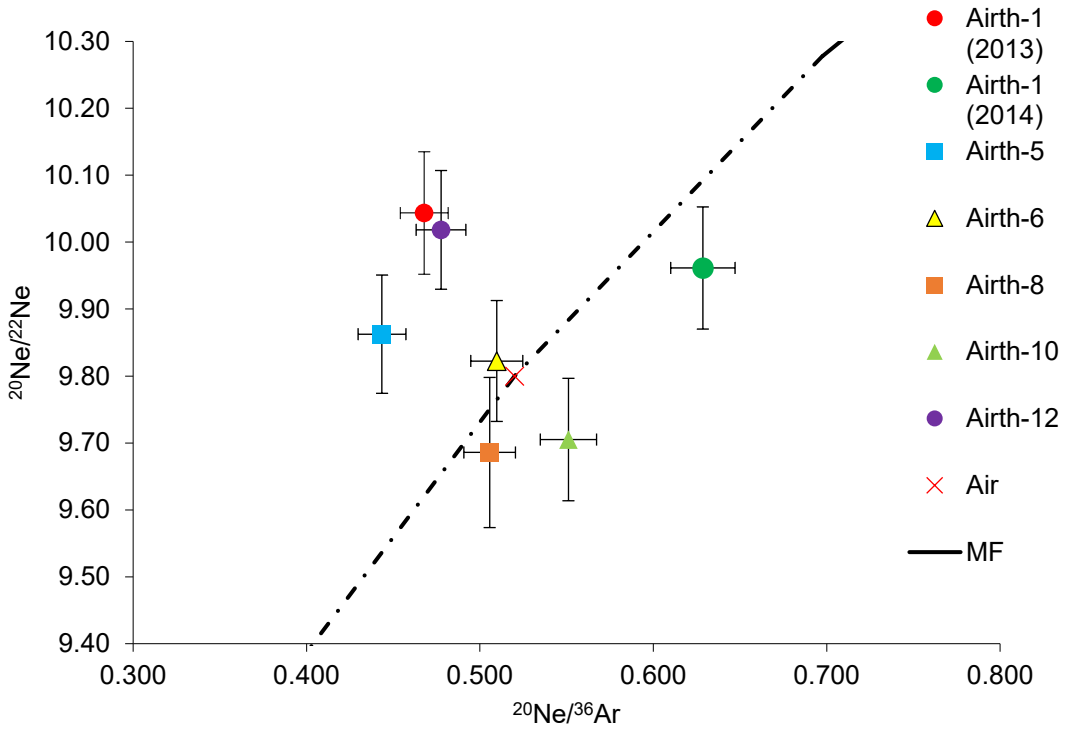

Figure 3-27 – Plot of $^{20}Ne/^{22}Ne$ vs. $^{20}Ne/^{36}Ar$. The mass fractionation trend from air is shown as a dashed line. No clear mass-fractionation trend is visible in the data.

It can be concluded that a definite small mantle contribution can be inferred by the enrichments in air-corrected $^{3}He/^{4}He$, commensurate enrichments in $^{20}Ne/^{22}Ne$ ratios confirmed by duplicate measurements, and the absence of obvious mass-fractionation which could be affecting the neon system.

On the neon 3-isotope plot, Airth-1 (2013), Airth-1 (2014), and Airth-5 all fit onto a mixing line between a hypothetical end-member and air (dashed arrow, Figure 3-28) Airth-1 (2013) has the lowest helium and neon concentrations and the highest $^{4}He/^{20}Ne$ ratio. $^{4}He/^{20}Ne$ ratios decrease for samples following the mixing line towards the air value, interpreted as an increase in ASW-derived ^{20}Ne. Airth-12 also lies on the same mixing line, but a duplicate measurement with lower analytical error is shown for reference. Nevertheless an average of the two measurements would also fit this trend within error. This could be expected as Airth-12 is physically connected at depth to the Airth-1 wellbore, with pumping equipment attached to Airth-1 being used to dewater Airth-12. Neon isotope values for the study were picked from the more reliable of two duplicate measurements that showed the least analytical error (often the second measurement after fine-tuning gas volumes let into the mass spectrometer). The Airth-5 well is not physically connected to this same system and has never been pumped. Hence the correlation with the mixing trend could imply a geographical/geological control on neon dynamics, however Airth-10 is geographically close to this area but shows a different mantle contribution.

Airth-6 and Airth-8 both sit on the same well pad, Airth-6 has never been pumped, and Airth-8 is a multi-lateral well that has been pumped. Despite the proximity of the wells and the possibility that dewatering Airth-8 may have affected the adjacent Airth-6, there does not appear to be a connection in the neon system, even via mass-fractionation. Interestingly the two wells are remarkably similar in noble gas concentrations and isotopic ratios in almost every other plot. Airth-10 is known to intersect an area with higher permeability, interpreted to be a result of greater fracture development due to higher structural relief, and therefore assumed to be more permeable across all targeted horizons.

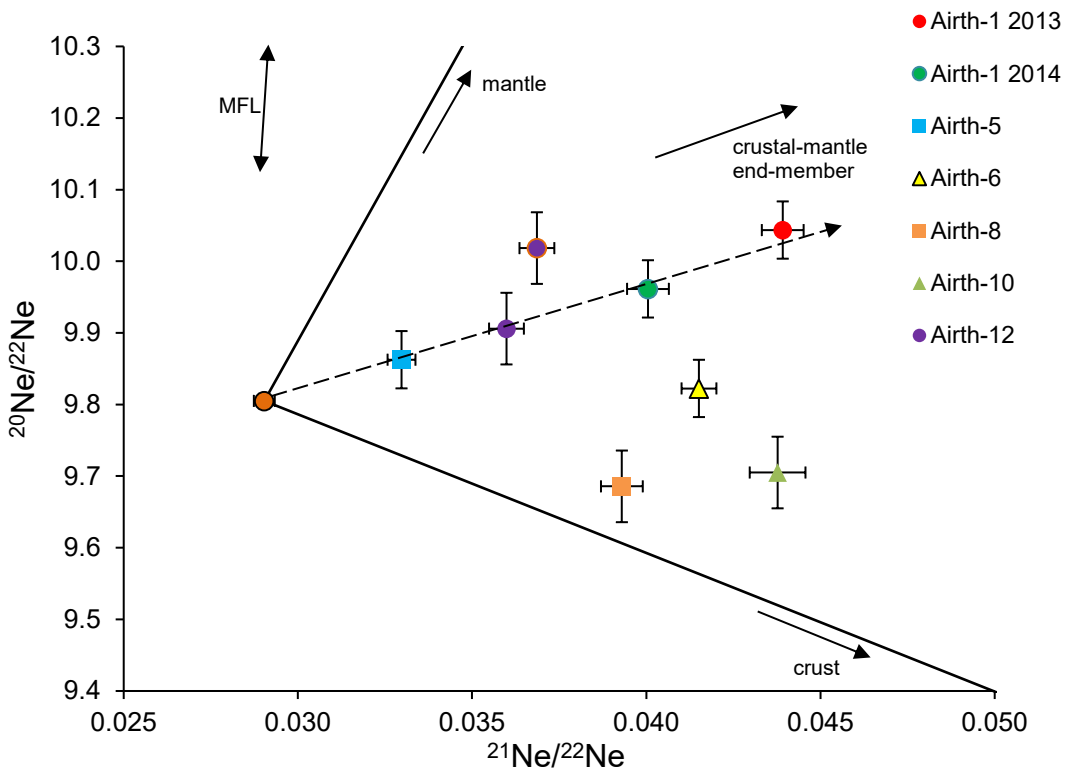

Figure 3-28 - Neon three-isotope plot, and mixing line between air and a hypothetical crustal-mantle end-member composition (dashed line). Four samples lie in the mixing line, but the other three show lower mantle contributions, suggesting a geographic control on mantle input.

The samples show deviation from the air-ratios both via addition of crustal nucleogenic neon (elevated $^{21}Ne/^{22}Ne$) as well as via potential mantle ^{20}Ne input (elevated $^{20}Ne/^{22}Ne$). It is possible to ascribe a percentage from each source to a measured gas on a neon 3-isotope plot via the weighted average of a sample between the three end-member vertices.

Table 6 shows the component breakdown, which expectedly shows a predominantly atmospheric-derived component in all samples of >80%. Airth-5 shows the highest atmospheric-derived component and also has the highest neon concentration, and Airth-1 (2013) shows the highest mantle input and the lowest neon concentration. Resolving the different neon isotopes allows the assessment of the three sources to each individual isotope. Mantle-derived [^{20}Ne] comprises 3.9% to 20.7% of the total [^{20}Ne] inventory, with a greater mantle contribution generally associated with a lower overall [^{20}Ne] concentration. This is attributed to a smaller contribution from atmospheric ^{20}Ne input.

Well	Air	Mantle	Crust	^{20}Ne concentration (ppm)	Percentage of ^{20}Ne derived from mantle
Airth-1 (2013)	81.2%	16.6%	2.21%	0.042 ±0.001	20.7%
Airth-1 (2014)	86.6%	11.7%	1.67%	0.051 ±0.001	14.7%
Airth-5	95.2%	4.24%	0.60%	0.354 ±0.008	5.4%
Airth-6	89.3%	8.52%	2.23%	0.097 ±0.002	10.8%
Airth-8	94.9%	3.03%	2.11%	0.089 ±0.002	3.9%
Airth-10	90.6%	6.47%	2.89%	0.049 ±0.001	8.3%
Airth-12	87.7%	11.4%	0.98%	0.189 ±0.004	9.4%

Table 6 –Neon isotope data from Airth and component breakdown, based on weighted averages of the proximity to each end member.

The source of mantle-derived noble gases is an enigma considering the lack of recent volcanic activity in the Midland Valley. Possible sources for mantle input then point to magmatic underplating in the Tertiary (Stuart *et al.,* 2000), or a more general Sub-Continental Lithospheric Mantle input entering via deep-seated faults such as the E-W trending Ochil Fault, of which the maximum vertical throw of ~4km lies only 12 km to the North (Rippon *et al.,* 1996). Furthermore, the Ochil Fault and related splay faults are known to host uraniferous bitumens migrated from deeply buried down-thrown Carboniferous rocks, mobilised by the heat from igneous intrusions (Gallagher *et al.,* 1971; Robinson *et al.,* 1989), and host various metal ore deposits; this demonstrates the mobility of fluids from depth migrating up the fault. The Ochil fault is understood to have remained active throughout geological time and is responsible for recent minor seismic activity (Rippon *et al.,* 1996), so is a plausible conduit for the input of deeper mantle fluids.

3.4.4.4 Atmospheric Noble Gases (ANG)

In attempting to define a geochemical 'fingerprint' of a field, it is important to ascertain whether the observed noble gas inventories are endemic to the system, a result of production processes, or the relationships between the two. The air-derived inventory of subsurface systems is assumed to be emplaced via the medium of groundwater (Ballentine and Burnard, 2002), and thus most systems have an air-derived inventory compatible with Air Saturated Water (ASW) that has been variably affected by solubility fractionation of ASW with an oil phase, gas phase, or combined oil/gas phases *e.g.* Bosch and Mazor (1988).

In contrast with conventional systems, in CBM reservoirs only a small gas phase (if any at all) exists initially, the gas phase being generated during the CBM production process. The gas does not have a diverse migration history, and is hypothesised to

contain only noble gases derived from the vicinity of the wellbores from formation waters or coals at the time of production. The noble gas inventory of gases produced from a system which was previously saturated in water should be expected to follow abundances based on simple solubility modelling from that water, often assumed to be ASW. In theory, only three processes affect the balance of noble gases in the subsurface: diffusion, adsorption, and mass balance between phases (Prinzhofer, 2013) and these are investigated to ascertain the source and resultant compositions of ANG's in the Airth field.

Noble gases are variably soluble in different mediums (*e.g.* water, gas, oil). The primary source of ANG's in subsurface systems is the atmosphere via the medium of water, be it air saturated water from groundwater infiltration, or air saturated seawater. When ASW equilibrates with a gas phase at depth (assumed to have no initial noble gas component), two end-member scenarios are visualised (Bosch and Mazor, 1988):

As Gas/Water → infinity, *i.e.* fully stripped water, the gas phase will take on the noble gas inventory of the initial water, *i.e.* ASW.

As Gas/Water → zero, the noble gases will equilibrate in the gas phase related to their solubility in the gas phase. The maximum fractionation possible corresponds to the equilibration of gas with water (at Gas/Water → 0) at recharge solubility conditions, and parallels the air value for gas/water equilibration.

Enrichments or depletions of ANG's can be expressed as ratios relative to ^{36}Ar (*e.g.* $i/^{36}Ar$), and then these ratios normalised to the corresponding air ratio to give a fractionation factor F:

$$F = [(i/^{36}Ar)_{sample} / (i/^{36}Ar)_{air}]$$

Fractionation factors are shown for the Airth samples in Table 7. They can be presented graphically along with the Fractionation Factors for air and ASW in Figure 3-29. This plot references the ANG ratios relative to the ratios found in air, in ASW, and oil, based on calculated solubilities. This allows a graphical representation of where the samples fall in relation to solubility-based distribution patterns with gas-water or gas-oil interactions.

	$(^{20}Ne/^{36}Ar)_{sample}/(^{20}Ne/^{36}Ar)_{Air}$	$(^{36}Ar/^{36}Ar)_{sample}/(^{36}Ar/^{36}Ar)_{Air}$	$(^{84}Kr/^{36}Ar)_{sample}/(^{84}Kr/^{36}Ar)_{Air}$	$(^{132}Xe/^{36}Ar)_{sample}/(^{132}Xe/^{36}Ar)_{Air}$
Airth-1 (2013)	0.89	1.00	1.09	1.44
Airth-1 (2014)	1.20	1.00	1.32	1.84
Airth-5	0.84	1.00	1.32	1.40
Airth-6	0.97	1.00	0.74	0.67
Airth-8	0.96	1.00	0.67	0.98
Airth-10	1.05	1.00	2.00	2.23
Airth-12	0.91	1.00	0.61	0.87

Table 7 - Table of fractionation factors (F) relative to the air-ratio for Airth gases.

The air ratio is represented by the horizontal line (F=1).

The ASW line is shown in dashed blue, and shows the relative enrichments of $^{84}Kr/^{36}Ar$ and $^{132}Xe/^{36}Ar$ compared to the air value, and a relative depletion in $^{20}Ne/^{36}Ar$ relative to air. This is because the solubility of noble gases in water is dependent on atomic mass following the pattern Xe>Kr>Ar>Ne>He. The end-member scenario of Gas/Water → infinity (*i.e.* fully degassed ASW) is represented by the ASW line on the plot, showing the maximum fractionation from the air value possible for single-step solubility-controlled Gas/Water equilibration. The other end-member scenario of Gas/Water → 0 is represented by the air value (horizontal line), showing the minimum fractionation away from the air value. All possible scenarios of single-step Gas/Water equilibration will fit between the two end members, and will fall between the air line and ASW line on the diagram.

Bosch and Mazor (1988) extended the solubility fractionation plot to include equilibration between water, gas, and oil phases. Oil/Water and Gas/Oil maximum solubility fractionation lines are also calculated for two crude oils of different densities using the solubility data from (Kharaka and Specht, 1988) and Airth field conditions. The diagram shows lines representing extreme examples of possible solubility fractionation for oil interacting with an ASW water phase (labelled O/W); note how the oil interaction can result in more significant depletions of $^{20}Ne/^{36}Ar$ and more significant enrichments in $^{84}Kr/^{36}Ar$ and $^{132}Xe/^{36}Ar$ due to the different solubilities of noble gases in an oil phase *vs.* gas phase.

Gas equilibrated with an oil-phase which has been previously equilibrated with ASW is also calculated (labelled G/O); note how this process can cause extreme fractionation *or* enrichment in noble gas ratios, and also encompasses the entire range of previous situations.

These are plotted on a solubility fractionation diagram after Bosch and Mazor, (1988) in Figure 3-29 in order to investigate any field-wide patterns in solubility fractionation of ANG's to determine the role of groundwater in the system, and the mechanism of partitioning ANG's into produced gases.

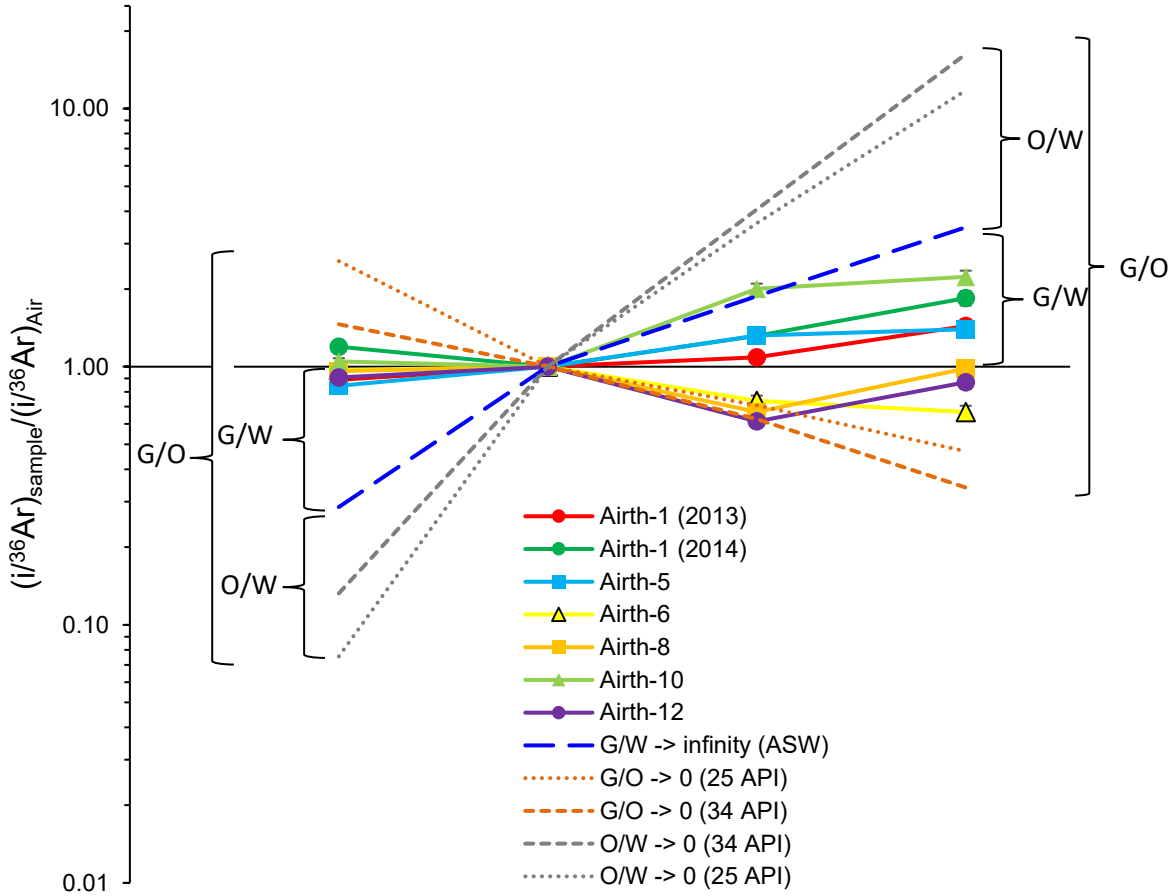

Figure 3-29 – Plot of $i/^{36}Ar$ (sample) normalised to the $i/^{36}Ar$ air-ratio, after Bosch and Mazor (1988). The x-axis line represents the air-ratios (and consequently the hypothetical non-solubility controlled gas/water ratio → 0), while the gas-water maximum solubility fractionation line (gas/water → ∞) calculated for the Airth field is represented by the dashed blue line (ASW). Thus a system where gas equilibrates with water would be expected to fit between the ASW and air lines (labelled G/W field). Oil/Water and Gas/Oil maximum fractionation lines are also calculated for 2 crude oils of different densities using the solubility data from Kharaka and Specht (1988) and Airth field subsurface conditions, representing extreme examples of possible solubility fractionation (labelled O/W). Gas equilibrated with an oil-phase which has been previously equilibrated with ASW is also calculated (labelled G/O).

Almost all $^{84}Kr/^{36}Ar$ and $^{132}Xe/^{36}Ar$ in samples are lower than ASW values; Airth-1 (2013), Airth-1 (2014), Airth-5, and Airth-10 (within error) sit between the ASW and air lines in Figure 3-29, in the domain of a gas-water system, however only

Airth-1 (2013) and Airth-5 show $^{20}Ne/^{36}Ar$ isotopic fractionation which are concordant with a water-gas model. Airth-6, Airth-8, and Airth-12 exhibit depletions in both ^{84}Kr and ^{132}Xe which are below even the air value (=1), which is unexpected for gas in equilibrium with ASW which would typically show enrichments due to the higher solubility of heavier noble gases initially in a water phase. The maximum fractionation of ^{84}Kr and ^{132}Xe was 2.00 and 2.23 respectively (Airth-10). This is (within error) of the maximum fractionation expected from ASW, which shows there are no enrichments of $^{84}Kr/^{36}Ar$ or $^{132}Xe/^{36}Ar$. This is also somewhat unexpected in a hydrocarbon field, as enrichments in $^{84}Kr/^{36}Ar$ and $^{132}Xe/^{36}Ar$ are common in hydrocarbons and sedimentary rocks, *e.g.* Torgersen and Kennedy, (1999) and Zhou *et al.,* (2005) found considerable enrichments of krypton (F=58, F=31) and xenon (F=576, F=146), believed to be fossil air-derived sedimentary gases adsorbed onto coal macerals, shales or sediments.

Smaller relative enrichments of heavy noble gases are expected in oil-related systems due to respective noble gas solubilities in oil (Bosch and Mazor, 1988, and references therein), as heavier noble gases are more soluble in oil than lighter noble gases (*e.g.* (Ballentine *et al.,* 2002; Kharaka and Specht, 1988), thus gas-equilibration between water that has been stripped of heavy noble gases could account for F-Kr and F-Xe depletions similar to those values which fit below the horizontal air-line in Figure 3-29. However, no associated enrichment of neon is found for these samples, and overall noble gas concentrations are too high to be a result of previously degassed water.

A Gas/Water equilibration model for ANG's was expected in the CBM field, where waters are progressively degassed by the dewatering process. However, it can be seen that only two samples (Airth-1 2013, Airth-5) have relative ANG fractionation patterns concordant with a gas-water system. Overall, there is no coherent fractionation pattern over the field, with no significant enrichments or depletions of ANG's from the air value which point towards a specific simple mechanism *e.g.* equilibration of ASW with either an oil or gas phase. Furthermore, solubility controlled fractionation should ideally be "monotonous" on the plot, *i.e.* a mostly-straight line should be drawn across the F-values for each sample, as solubilities are almost directly correlated with mass (Bosch and Mazor, 1988). This generally suggests that the principle of single step fluid equilibration with ASW does not apply across the Airth field.

The $^{20}Ne/^{36}Ar$ ratios are challenging to explain; as they range from 0.444 - 0.629 and are far in excess of typical ASW (~0.150) and are closer to, or exceed, the air value

(0.526) (see Figure 3-20). Solubility fractionation between ASW and a gas phase typically enriches the gas phase with lighter noble gases compared to the residual water phase due to the lower solubility of lighter noble gases in water. To produce air-like $^{20}Ne/^{36}Ar$ ratios (0.52) in a gas phase from typical ASW $^{20}Ne/^{36}Ar$ (0.15) would require a fractionation factor from ASW of 3.6. However, when solubilities are calculated for the temperature, pressure and salinity of the Airth field, a maximum fractionation of F_{asw}=~2.4 is achieved for a single-step equilibration process (see Figure 3-30). Introducing a maximum realistic excess air into the equations (35%, Kipfer, (2002)) or using a maximum ASW $^{20}Ne/^{36}Ar$ value (*e.g.* seawater, 35% excess air, ~0.2) also cannot achieve $^{20}Ne/^{36}Ar$ ratios as high as those in the Airth field.

Mantle-derived ^{20}Ne comprises 3.9% - 20.7% of the total ^{20}Ne, but in most samples it is <11% (excepting Airth-1 (2013) and Airth-1 (2014)), and so cannot account for significant enrichment of the initial groundwater $^{20}Ne/^{36}Ar$ ratio. This presents a problem in determining the source of ANG's in the Airth field which is investigated further.

In Figure 3-30 numerous elemental fractionation patterns from ASW are calculated for the ANG components in the Airth field to investigate what, if any, possible mechanisms can account for the extreme fractionation of $^{20}Ne/^{36}Ar$ and observed heavy noble gas ratios in the Airth field from an assumed ASW end-member. Models tested include:

- Closed-system Gas/Water fractionation ("batch" type), where ASW components fractionate into the gas phase based on their solubilities related to the Gas/Water ratio (solid black line)
- Open-system Gas/Water fractionation (Rayleigh type), where components in the gas phase are equilibrated with water and continually removed from the system (light blue line)
- The degassing of water partially stripped by Rayleigh fractionation (dark blue line)

These models are solubility-controlled based on Airth subsurface conditions. Henry's constants, fugacity coefficients, and activity coefficients for reservoir conditions (temperature, pressure, salinity) were calculated from the empirical equations of Crovetto *et al.,* (1982) and methodology of Ballentine and Burnard, (2002) to plot the fractionation curves. The calculated maximum fractionation (when Gas/Water → 0, where the fractionation lines converge) results in $^{20}Ne/^{36}Ar$ of ~0.4. The resultant $^{84}Kr/^{36}Ar$ is also not depleted enough to account for most of the samples even at

Gas/Water = 0. These models clearly cannot account for the ANG's measured in Airth gas samples. Degassed water has very low concentrations of noble gases, which is not concordant with several samples at the Airth field. It also does not produce low enough $^{84}Kr/^{36}Ar$ and $^{132}Xe/^{36}Ar$ for several samples. Further models tested were:

- Oil equilibration – an oil phase could account for strong depletions in $^{84}Kr/^{36}Ar$ and $^{132}Xe/^{36}Ar$, and enrichments in $^{20}Ne/^{36}Ar$ (red dashed line). In the case of minimal degassing, a gas phase generated from oils equilibrated with ASW would have significant depletions in $^{84}Kr/^{36}Ar$ and $^{132}Xe/^{36}Ar$ (Bosch and Mazor, 1988).
- Mass-dependent fractionation – this may be applicable to gases diffusing through solids or pore spaces.
- The degassing of water previously fractionated by mass-dependent fractionation.

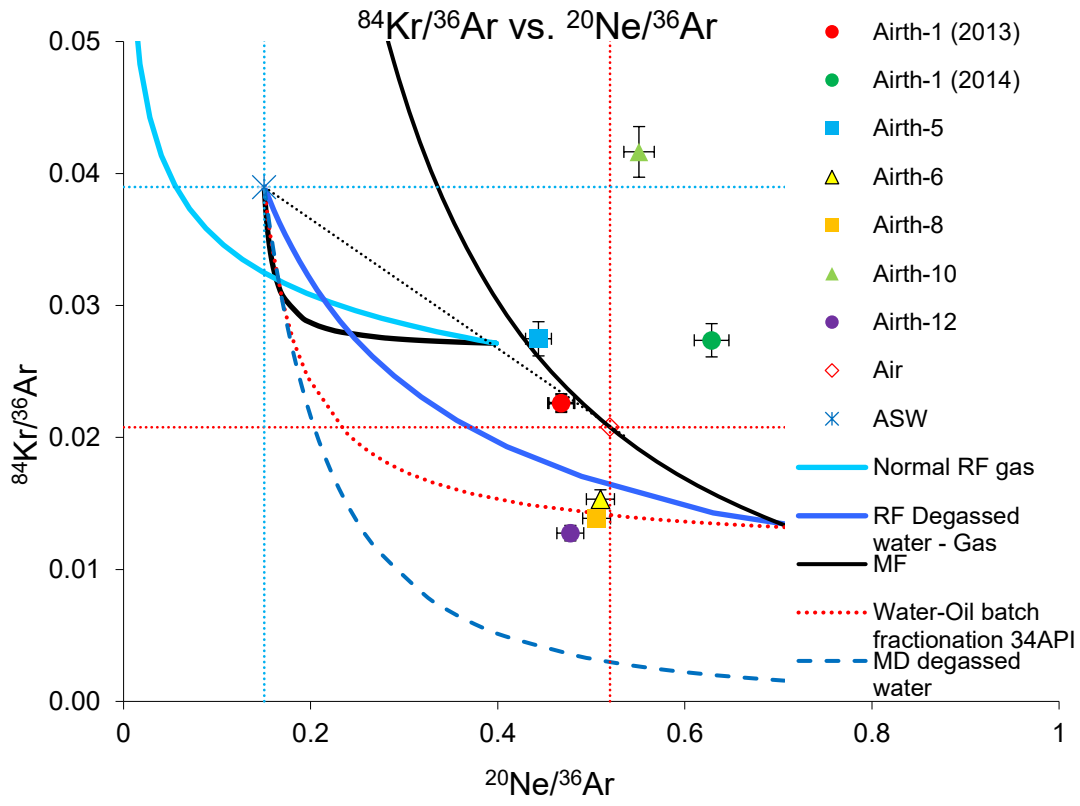

Figure 3-30 – Plot of $^{84}Kr/^{36}Ar$ vs. $^{20}Ne/^{36}Ar$. The air-ratio is depicted by the red star. Airth ratios generally plot closer to the air ratio than ASW. ASW is depicted by the blue star, and plots to the upper-left. The adjoining fractionation lines (batch mixing and Rayleigh fractionation with a water-gas phase in black and blue, with maximum fractionation (gas/water → 0)) show that processes acting on groundwater cannot produce air-like $^{20}Ne/^{36}Ar$ ratios. Rayleigh fractionation with water-oil phase (dashed red) can produce the $^{20}Ne/^{36}Ar$ ratios but not the $^{84}Kr/^{36}Ar$ ratios. Black and blue dotted lines represent mass-fractionation from the Air and ASW compositions respectively.

The xenon system ($^{132}Xe/^{36}Ar$ *vs.* $^{20}Ne/^{36}Ar$, not shown) shows a very similar distribution of samples to the krypton system, showing coherent behaviour between Kr and Xe. Airth-12, Airth-8 and Airth-6 pose a particular problem as they show air-like $^{20}Ne/^{36}Ar$ ratios, yet $^{84}Kr/^{36}Ar$ ratios are depleted even relative to air (see Figure 3-30)

It can be seen that no single-step equilibrium process can account for the range of ANG ratios found in the Airth field, but that values tend to cluster around the air-value of $^{20}Ne/^{36}Ar$ rather than the ASW value, with both enrichments and depletions of $^{84}Kr/^{36}Ar$ (and $^{132}Xe/^{36}Ar$). This suggests multiple processes may be at work.

As well as the isotopic ratios, gas-water equilibration cannot explain the observed concentrations in the noble gases. Initially, as Gas/Water → 0, a gas phase would be most enriched in lighter components, and the gas phase noble gas concentrations the highest. Subsequent depletion of the water phase results in a decrease in gas phase

$^{20}Ne/^{36}Ar$ and lower noble gas concentrations. At Airth this is not the case. Similar to Battani *et al.,* (2000) we see a trend where higher $^{20}Ne/^{36}Ar$ ratios are observed with lower overall concentrations of noble gases, and greater relative crustally derived components. In a plot of $1/^{36}Ar$ *vs.* $^{20}Ne/^{36}Ar$ (Figure 3-31) the gases across the field show a coherent trend where the $^{20}Ne/^{36}Ar$ ratios are controlled by the ^{36}Ar concentration. A general mixing trend can be seen between an end-member with higher noble gas concentrations and lower $^{20}Ne/^{36}Ar$, and an end-member with lower noble gas concentrations and a more enriched $^{20}Ne/^{36}Ar$ ratio. This cannot be a process of pure gas-water equilibration, as enrichments in $^{20}Ne/^{36}Ar$ would be accompanied by commensurate increases in the ^{20}Ne and ^{36}Ar inventories (Battani *et al.,* 2000; Bosch and Mazor, 1988), and the opposite is observed.

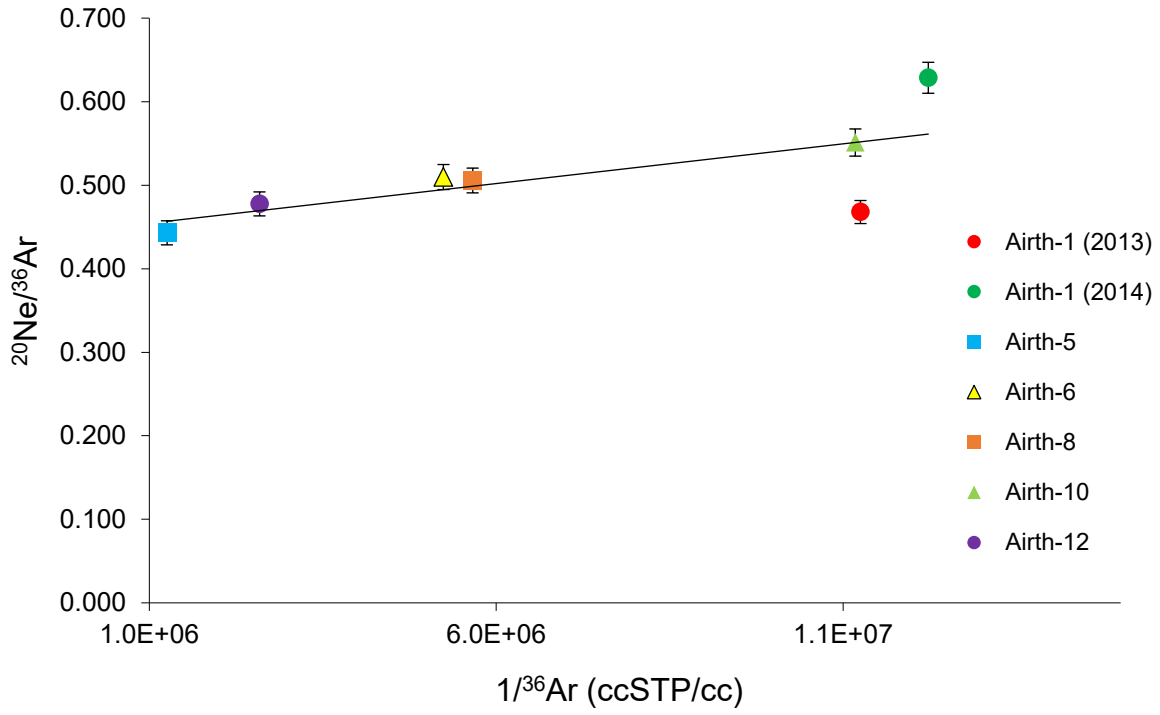

Figure 3-31 – $^{20}Ne/^{36}Ar$ vs $1/^{36}Ar$. A mixing trend (black line) between a noble gas-rich ^{20}Ne enriched endmember (relative to ASW), and a noble gas-poor, elementally fractionated end-member. $^{20}Ne/^{36}Ar$ at $[^{36}Ar] = 0$ is extrapolated be ~0.45. In typical gas/water equilibration, $^{20}Ne/^{36}Ar$ would decrease with increasing gas concentration.

$^{20}Ne/^{36}Ar$ ratios increase and become increasingly air-like as noble gas concentrations decrease, and could be explained by inferring an atmospheric-air source (not derived from ASW), which is being diluted with ASW which masks the air-like end-member. This pattern would provide a closer fit to the $^{84}Kr/^{36}Ar$ and $^{132}Xe/^{36}Ar$ ratios,

as they closer to the air value than that of the ASW value, especially at lower concentrations (Figure 3-21).

Firstly, it should be reiterated that atmospheric contamination of samples is very unlikely as the $^{4}He/^{20}Ne$ are very high compared with either the air or ASW values. Furthermore, the lowest $^{4}He/^{20}Ne$ ratios (which would be associated with the greatest air contamination) contain the highest ^{4}He concentrations, which would not be expected from air ingress into samples, or infinitesimal exchange from the sample container to the atmosphere from long term storage.

Air-like $^{132}Xe/^{36}Ar$ and $^{84}Kr/^{36}Ar$ ratios are also seen in Figure 3-30 where they appear to fractionate coherently from the air-value rather than from ASW, although with some $^{132}Xe/^{36}Ar$ enrichment relative to $^{84}Kr/^{36}Ar$, probably related to some ASW input. Airth-6, Airth-8 and Airth-12 show depletions relative to the air-value, which could indicate retention of heavier noble gases within the coals. Air-like sedimentary heavy noble gases (Kr, Xe) are known from Torgersen and Kennedy, (1999) and Zhou *et al.,* (2005), and are believed to be fossil air-derived gases adsorbed onto coal macerals or shales. Both studies found considerable enrichments of krypton (x58, x31) and xenon (x576, x146) relative to their ratios in air normalised to ^{36}Ar. However, enrichments at Airth never exceed F=2 for Kr and F=2.2 for ^{132}Xe, so there are no significant enrichments of $^{84}Kr/^{36}Ar$ or $^{132}Xe/^{36}Ar$ as found in some hydrocarbon systems, which include the only other CBM dataset (Zhou *et al.,* 2005).

Enrichments of ^{20}Ne are known in sediments (Podosek *et al.,* 1980; Hiyagon and Kennedy, 1992; Pinti *et al.,* 1999), and (Kennedy *et al.,* 1990) and (Battani *et al.,* 2000) found enrichments in ^{20}Ne in hydrocarbon gases, attributed either to water previously fractionated by an oil-phase, or a ^{20}Ne-enriched phase trapped within reservoir sediments.

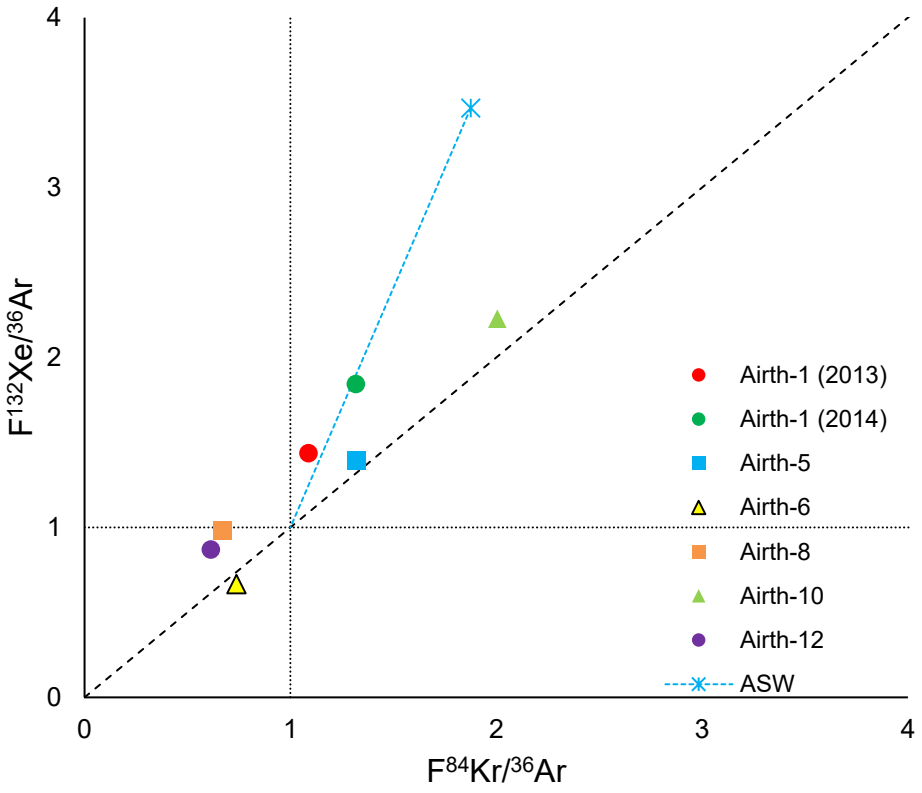

Figure 3-32 – Plot of fractionation factors (F) of $^{132}Xe/^{36}Ar$ relative to the air ratio, vs. $^{84}Kr/^{36}Ar$ relative to the air ratio. A clear trend of fractionation along the air-line (black dashed) can be seen for the heavy noble gases, rather than a pattern fractionating along the ASW line (dashed blue line).

The ANG inventories appear air-like with decreasing concentrations of all noble gas species, but with commensurate enrichments in radiogenic, nucleogenic and some mantle components (see Crustal Noble Gases). The $^{20}Ne/^{36}Ar$ are enriched in ^{20}Ne approaching, or exceeding, the air ratio of 0.52. The $^{84}Kr/^{36}Ar$ and $^{132}Xe/^{36}Ar$ follow a fractionation pattern from the air ratio, but are seemingly unconnected to the $^{20}Ne/^{36}Ar$ ratios via any fractionation trend or standard single-step solubility model. A possible explanation is an air-like initial composition where the heavier noble gases remain partially adsorped onto coal/kerogen surfaces or trapped in porespaces, possibly controlled by a non steady-state diffusion-based process combined with labyrinths/restrictions as described by Torgersen *et al.,* (2004) and investigated experimentally by Sathaye *et al.,* (2016). Interestingly, Airth-1 and Airth-12 are physically connected at depth with Airth-1 hosting the pumping equipment; the two samples taken contemporaneously after pumping operations show similar $^{20}Ne/^{36}Ar$

ratios, but different heavy noble gas ratios. This could suggest a diffusive, non-steady state or otherwise temporal control on the addition of heavier noble gases into the produced gas phase.

Airth-5 has never been pumped, and this shows that a high $^{20}Ne/^{36}Ar$ is inherent to the field. $^{20}Ne/^{36}Ar$ at [^{36}Ar] = 0 is extrapolated be ~0.45 (Figure 3-31), suggesting that the $^{20}Ne/^{36}Ar$ are either a result of a mix between a ^{20}Ne enriched water (such as a ^{20}Ne enriched ASW), and a lower concentration of an even higher $^{20}Ne/^{36}Ar$ endmember (possibly air-like), or a fractionation away from an initial formation water that was enriched in ^{20}Ne prior to gas production.

A potential source of air-like patterns could be fossil air, or an air-enriched component – trapped within the low-permeability coal matrix, either in the free phase as immiscible bubbles in the formation, or trapped and dissolved into the fossil groundwater in non-connected porespace. In this case a good correlation between $^{20}Ne/^{36}Ar$ and $^{40}Ar^*/^{36}Ar$ (or other crustal ratios) would be expected if both a residual 'trapped air' and *in situ* generated $^{40}Ar^*$ are held within the same reservoir, being released from the degrading coal due to matrix shrinkage as methane desorbs. This is investigated further by scrutinising the crustal and mantle noble gases.

3.4.4.5 Crustal Noble Gases

Assessing the crustal contributions to gases allow insights into gas and water residence times, as they are typically age accumulative. Correlating the crustal component with the atmospherically derived component can constrain the nature of gas storage and gas interactions. Crustal noble gases in this study refer to:

- radiogenic $^{40}Ar^*$, produced from the decay of ^{40}K. It is important to note however that the mantle is also a source of $^{40}Ar^*$.
- nucleogenic $^{21}Ne^*$ and $^{22}Ne^*$, produced by the reactions $^{18}O(\alpha,n)^{21}Ne$ and $^{19}F(\alpha,n)^{22}Na(\beta)^{22}Ne$.
- ^{4}He produced from the uranium and thorium decay chains.

The majority of ^{4}He (> 96.14%) in the Airth field is generated from the decay series of U and Th within minerals, and most likely predominantly derived from *ex situ* sources other than the coals. Coals have a low detrital mineral component, and thus cannot be a significant source of U & Th bearing minerals to generate helium. So, *in situ* generated ^{4}He is more likely produced in surrounding lithologies such as shales and sandstones. The small but resolvable mantle component is proof that gases have

migrated into the field from significant depth, and probably accumulated additional ^{4}He from underlying strata such as the metamorphic basement underlying the Midland Valley, and intermediate units. The consistent $^{3}He/^{4}He_{(Ra)}$ ratios show helium is homogenously distributed across the field, which is not common in most classic noble gas studies. This is probably related to the high diffusivity of helium and the long residence time in the field. The main source of the helium in the system is from the formation water, which readily degasses with the onset of pressure reduction from the dewatering process. As well as the water, there is probably a smaller contribution residing in the coals which will degas more slowly than connected water volumes, as it will experience a smaller pressure drop than formation water.

The helium concentrations vary, despite their apparent homogeneity. There is a tendency for wells that have been dewatered to a greater extent to have lower concentrations of all noble gases. This is partly attributed to differing gas/water interactions, with wells contacting and degassing variable volumes of water. Furthermore, gas production both removes and progressively depletes the noble gas inventory, and increases the dilution with desorbed coal bed methane which further reduces noble gas concentrations. The decrease in noble gas concentrations is accompanied by greater relative proportions of crustal components (^{4}He, $^{21}Ne^{*}_{(crust)}$ and $^{40}Ar^{*}$) in the gas relative to the ANG component (*e.g.* Figure 3-19, Figure 3-33, Figure 3-34).

The relationship between $^{4}He/^{36}Ar$ and $^{40}Ar/^{36}Ar$ can be used as a measure of the mixing between crustal components and atmosphere-derived components. Figure 3-33 shows that the crustal+mantle ^{4}He and $^{40}Ar^{*}$ generally fractionate coherently with ^{36}Ar. When crustal ^{4}He and $^{21}Ne^{*}_{(crust)}$ are normalised to ^{36}Ar (Figure 3-34), a very similar distribution of data points and trend can be seen. $^{21}Ne^{*}/^{36}Ar$ and $^{40}Ar/^{36}Ar$ also display the same pattern (not shown). This shows that all the crustal components (^{4}He, $^{21}Ne^{*}$, $^{40}Ar^{*}$) are sourced from the same location, and are mixed prior to degassing.

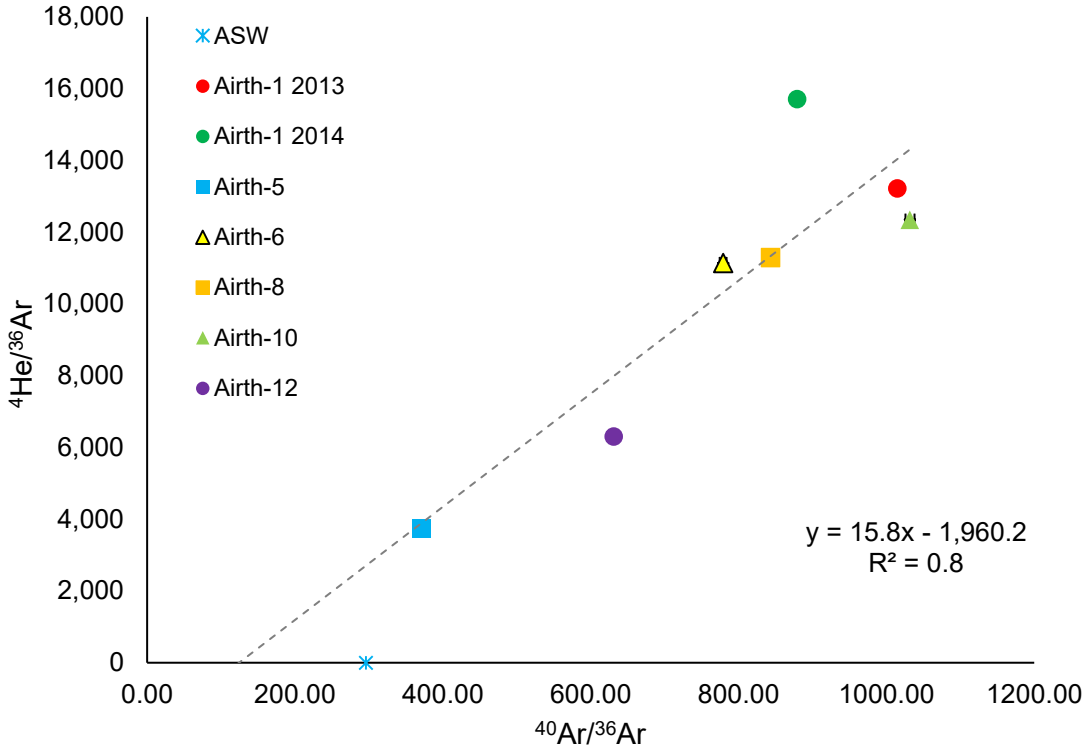

Figure 3-33 – Graph of $^{4}He/^{36}Ar$ vs. $^{40}Ar/^{36}Ar$ showing good correlation, showing that ^{4}He and ^{40}Ar are sourced from the same location and are premixed before degassing of coals. Errors are smaller than symbols. The gradient of the line of regression shown is 15.8 ($R^2 = 0.78$).

The resolution between crustal and mantle components within the excess argon ($^{40}Ar^*$) is usually investigated by noting the correlations with $^{3}He/^{4}He_{(Ra)}$ (Ballentine *et al.,* 1991), as ^{3}He is also sourced from the mantle. At Airth, the $^{40}Ar^*$ concentrations vary significantly but the $^{3}He/^{4}He$ is practically constant, thus it is impossible to decouple $^{40}Ar^*_{(crust)}$ from $^{40}Ar^*_{(mantle)}$. Nonetheless, the coherent fractionation observed in samples shows that the crustal and mantle components are well mixed.

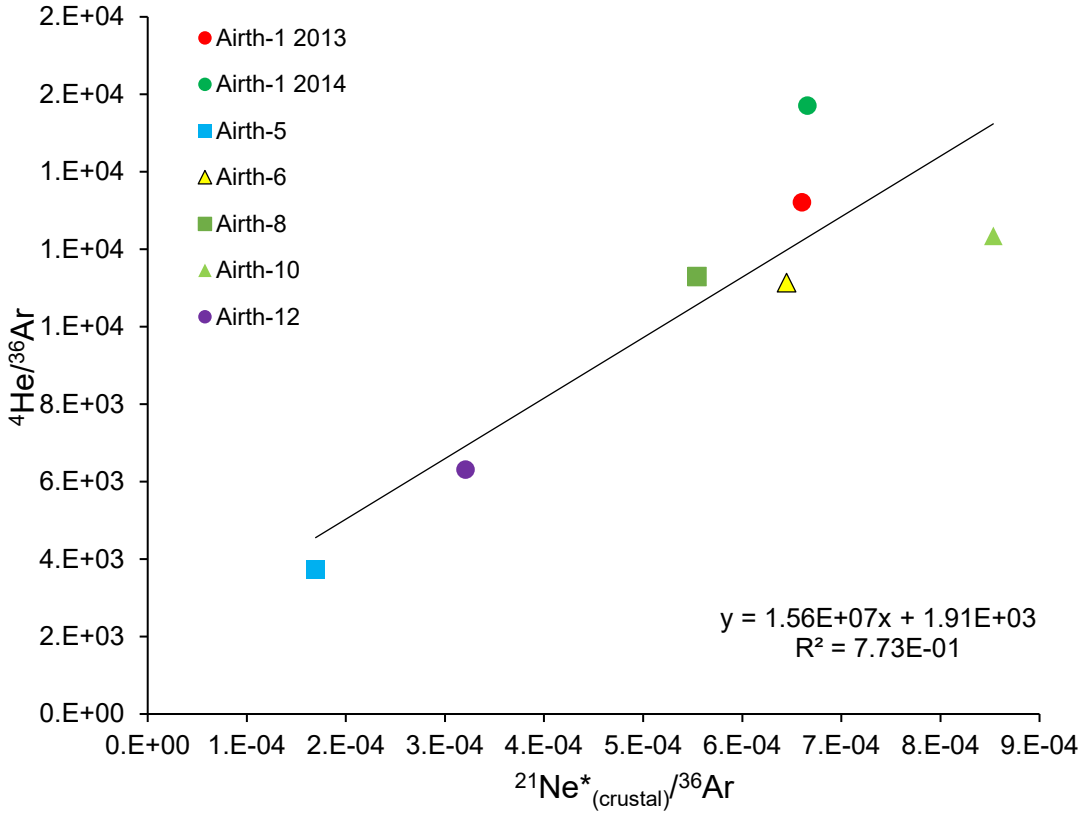

Figure 3-34 – Plot of $^{4}He/^{36}Ar$ vs. $^{21}Ne^{*}_{(crust)}/^{36}Ar$. There is a degree of correlation between the ^{4}He and $^{21}Ne^{*}_{(crust)}$ when normalised to ^{36}Ar. The long-dashed line represents the correlation line for all samples.

If the water were the only reservoir of noble gases in the subsurface then degassing would simply strip the dissolved gases, and the produced gases would show similar isotopic ratios with the concentrations variably diluted with desorbing methane. In the Airth field, the relative increase in crustal noble gas components is intimately linked with an absolute decrease in the ANG components. This requires a reservoir for noble gases outside of the formation water, which is considered to be the coals themselves. Trapped gases, particularly heavier species, are known in coals (Zhou *et al.,* 2005). The increase in crustal ratios is hypothesised to be caused by the preferential removal of ANG components, allowing a more crustal signature to be resolved, *i.e.* the removal of a 'diluting' ASW phase. Comparing the crustal components to the ANG components will help to resolve the mechanisms of gas storage.

There is reasonable correlation between the atmospheric components $^{20}Ne/^{36}Ar$ with crustal noble gas ratios such as $^{4}He/^{36}Ar$, $^{21}Ne^{*}_{(crust)}/^{36}Ar$, $^{21}Ne/^{22}Ne$, and $^{40}Ar/^{36}Ar$ (see Figure 3-35), though Airth-1 (2013) and Airth-1 (2014) are often outliers. All of these correlations in both elemental and isotopic ratios demonstrate increasing crustal

component with increasing $^{20}Ne/^{36}Ar$, which itself increases with decreasing concentration of all noble gas species (*e.g.* see Figure 3-31). The importance of this is two-fold; the increase in isotopic ratios cannot be solubility based, as isotopes of the same element have effectively identical solubility (such as ^{40}Ar and ^{36}Ar, and ^{21}Ne and ^{22}Ne), and it cannot be related to mass-fractionation as the heavier $^{40}Ar^*$ *increases* relative to ^{36}Ar, while the lighter ^{21}Ne *increases* relative to ^{22}Ne. The correlations are also linear. These trends can only be a result of mixing between a crustal-rich end-member and a less crustal-rich end-member. These are hypothesised to reside within the coals, and the formation water respectively.

The second point of significance is the resolution of ANG ratios, where extrapolating trends in ratios with crustal additions back to their atmospheric end-members results in elevated $^{20}Ne/^{36}Ar$ ratios. Extrapolating an end-member $^{20}Ne/^{36}Ar$ ratio from the air $^{40}Ar/^{36}Ar$ value results in a value of ~0.43 (Figure 3-35 – plot D), which is similar to the end-member of ~0.45 derived from the purely atmospheric neon-argon system (Figure 3-31), and ~0.4 from the $^{21}Ne/^{22}Ne$ *vs.* $^{20}Ne/^{36}Ar$ plot (Figure 3-35 – plot C).

Again, this is indicative of a $^{20}Ne/^{36}Ar$ enriched 'air-like' end-member residing in coals, and a less enriched end-member contained in the formation water with a $^{20}Ne/^{36}Ar$ of around ~0.4. There is however, no correlation with crustally derived components and $^{84}Kr/^{36}Ar$ or $^{132}Xe/^{36}Ar$. The crustal end-member also correlates reasonably well with the mantle neon component, despite the different contribution of mantle sources to different wells (Figure 3-36), showing that the mantle component also resides in the coals.

Zhou et al. (2005) found that the crustal components ($^{4}He/^{40}Ar^*$) from CBM fractionated coherently with ANG components ($^{20}Ne/^{36}Ar$) derived from ASW following a predicted open-system Rayleigh fractionation pattern as gases were removed from wells during production, showing the ANG and radiogenic components were well mixed in groundwater prior to gas production. In Airth, there is a trend in increasing crustal component with decreasing overall noble gas concentrations, but apparently following a mixing trend between two end-members. This is probably a result of the field having never been put on production outside of gas flow testing, representing the very initial stages of CBM development.

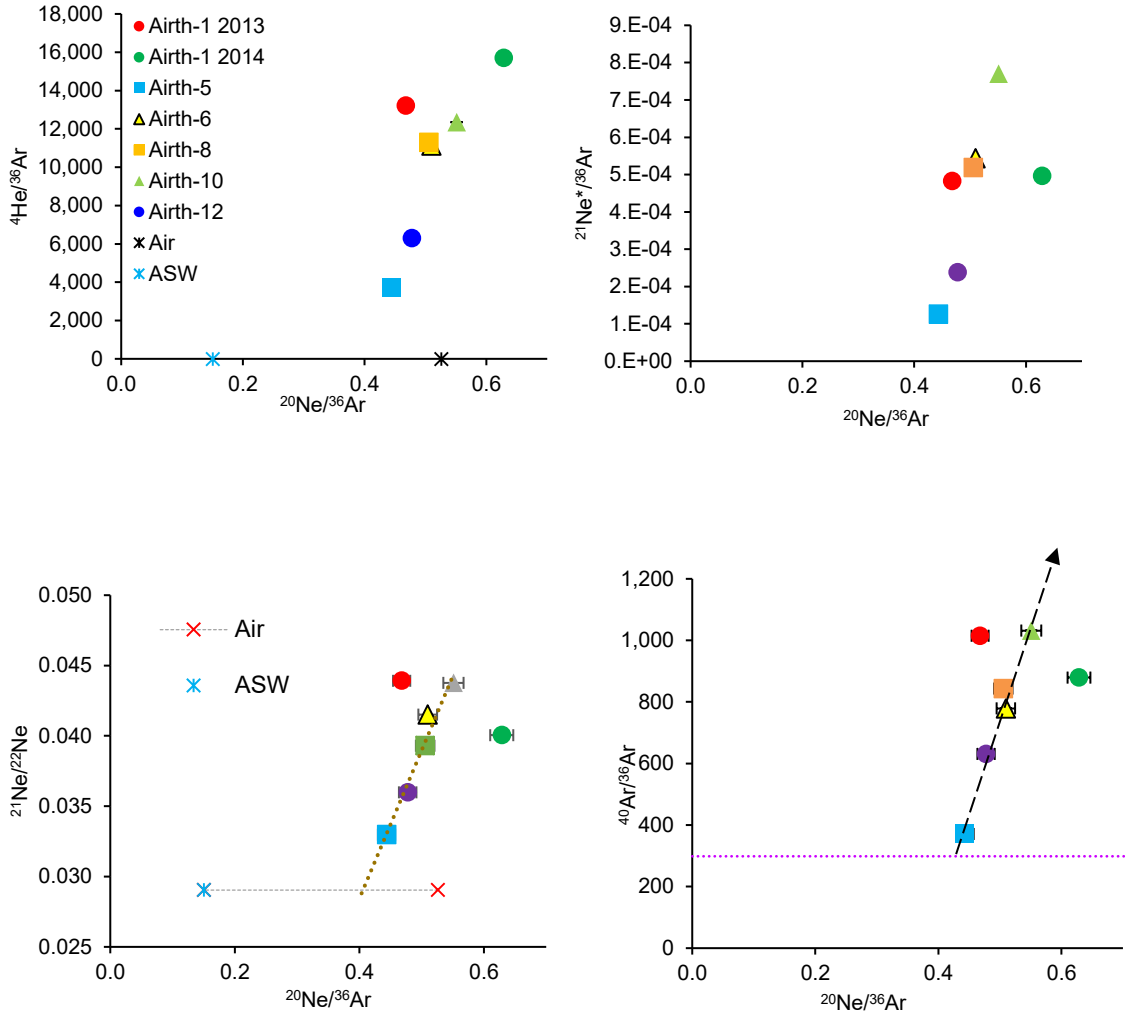

Figure 3-35 – Plots of various crustal/ANG ratios vs. $^{20}Ne/^{36}Ar$, showing increasing crustal components correlating with $^{20}Ne/^{36}Ar$. The correlations are less coherent for $^{20}Ne_{(atmosphere)}/^{36}Ar$ (not shown) which is consistent with a mixing trend.

A) (upper left) Plot of $^{4}He/^{36}Ar$ vs. $^{20}Ne/36$ Ar.

B) (upper right) Plot of $^{21}Ne^{*}_{(crust)}/^{36}Ar$ vs. $^{20}Ne/^{36}Ar$.

C) (lower left) Plot of $^{21}Ne/^{22}Ne$. Extrapolating the trend to $^{21}Ne/^{22}Ne$ = air (dashed grey line) gives a resultant $^{20}Ne/^{36}Ar$ of ~0.40.

D) (lower right) Plot of $^{40}Ar/^{36}Ar$ vs. $^{20}Ne/^{36}Ar$. Extrapolating the $^{40}Ar/^{36}Ar$ trend to the air ratio (dashed red line) results in a $^{20}Ne/^{36}Ar$ value of ~0.43.

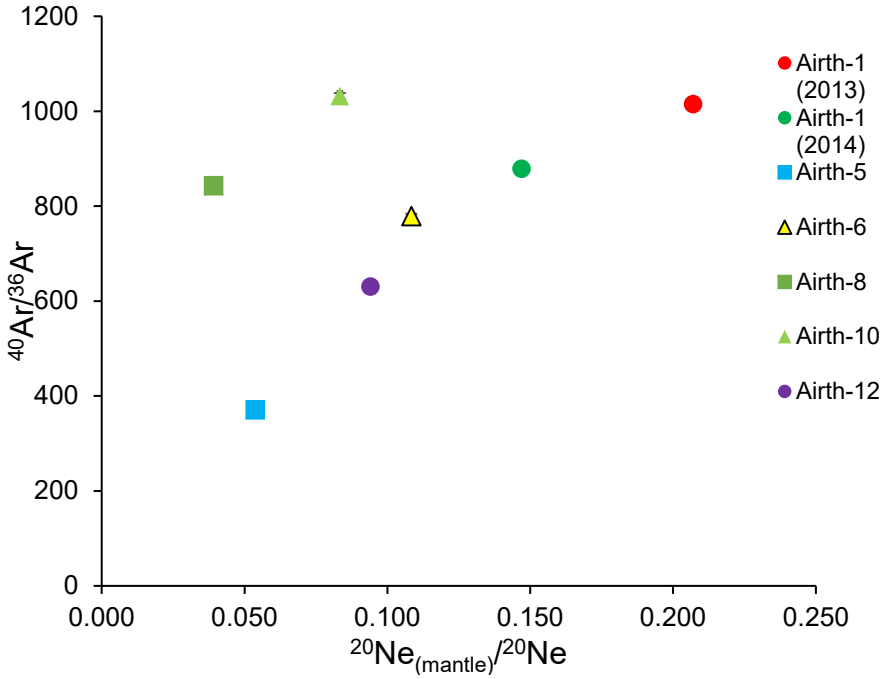

Figure 3-36 – Plot of $^{40}Ar/^{36}Ar$ vs. $^{20}Ne_{(mantle)}/^{20}Ne_{(total)}$. The neon isotopic ratio is effectively the percentage of mantle ^{20}Ne in the system. Perfect correlation cannot be expected, as neon isotope values show there is differing mantle input into different wells (notably Airth-8 being relatively depleted), nonetheless a general trend of increasing mantle ^{20}Ne correlates with increasing crustal $^{40}Ar^*$, showing that the mantle component resides within the coals along with the crustal component.

When crustal $^{4}He/^{21}Ne_{(total)}$ is plotted *vs.* $^{20}Ne/^{36}Ar$ (Figure 3-37), no clear fractionation pattern can be seen. However, when the purely crustal components ($^{4}He/^{21}Ne^*_{(crust)}$) are plotted against $^{20}Ne/^{36}Ar$, an unusual but clear correlation can be seen that is not present in the $^{4}He/^{21}Ne$ system. This highlights a coherence between these purely crustal components and the atmospheric components. However, this trend cannot be a result of mass-fractionation or solubility, as each mechanism would result in a positive gradient. This again is interpreted to be the result of mixing between two sources; an ASW-like groundwater which is rich in helium and atmospheric neon, and a more crustal end-member rich in $^{21}Ne^*_{(crust)}$. Increasing dewatering degasses and depletes the water of ^{4}He and $^{21}Ne_{(total)}$ (mainly atmosphere derived) components. This allows greater degassing from the coal, which has a lower ^{4}He inventory (due to smaller volumes associated with lower porosity) and a greater inventory of accumulated $^{21}Ne^*_{(crust)}$ (and other crustal noble gases).

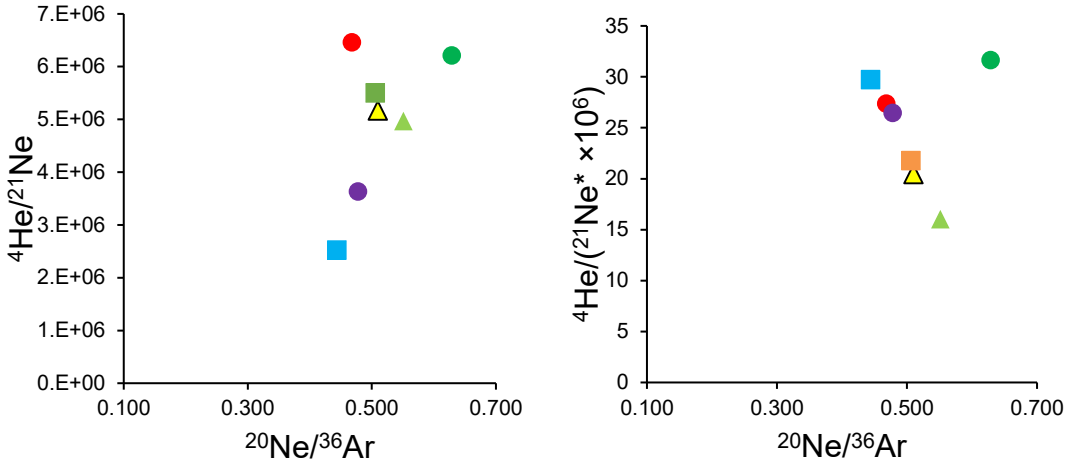

Figure 3-37 – Plot of $^{4}He/^{21}Ne$ vs $^{20}Ne/^{36}Ar$ and $^{4}He/^{21}Ne_{(crust)}$ vs. $^{20}Ne/^{36}Ar$. The first plot is measured data, the second plots only the crustally derived $^{21}Ne^{*}$. The trend in the data is the 'opposite' to what would be expected

$^{4}He/^{40}Ar^{*}$ ratios range from 16.8 to 51.6, exhibiting an average of 25.3. These are much higher than calculated for the average continental crust of 4.9 (Ballentine and O'Nions, 1992), and arguably also higher than 'typical' shallow crustal regions (CBM data from Zhou *et al.,* 2005 (0.084 – 12) and the Panhandle field (6.88 to 16.6, mean 12±2.4 (Ballentine and Lollar, 2002)), though comparable with a mean of 27.3 from Carboniferous-Permian Polish gases (Kotarba *et al.*, 2014). Normalising both ^{4}He and $^{40}Ar^{*}$ components to groundwater derived ^{36}Ar (see Figure 3-33) allows a local crustal $^{4}He/^{40}Ar^{*}$ end-member of 15.8 to be calculated by taking the gradient of the correlation-line, and is similar to the other published CBM dataset of 15.5 (Zhou *et al.,* 2005). Although this value is affected by the mantle contributions to ^{4}He and $^{40}Ar^{*}$, these are likely to be small in the case of ^{4}He (<3%) and small but unquantifiable in the case of $^{40}Ar^{*}$. This high value can either be attributed to preferential release of ^{4}He from minerals compared to ^{40}Ar in cooler shallow crustal rocks (Ballentine *et al.,* 1994), 1994), possibly higher (U+Th)/K ratio in surrounding rocks (but no data is available), or a lower $^{40}Ar^{*}$ contribution from the underlying basement relative to more diffusive and mobile helium. Using a similar technique to calculate the $^{4}He/^{21}Ne^{*}_{(excess)}$ end-member (Figure 3-34) results in $1.56x10^{7}$, which fits the average crustal production ratio of $(1\text{-}3)x10^{7}$ (Ballentine and Burnard., 2002), slightly lower than the $2.2x10^{7}$ (Grove *et al.,* 2017) and almost exactly $1.5x10^{7}$ (Kennedy *et al.,* 1990). This is juxtaposed to the higher than crustal average $^{4}He/^{40}Ar^{*}$ ratio. Furthermore, the Airth field $^{40}Ar^{*}/^{21}Ne^{*}$ is 1.06×10^{6}, or 1.23×10^{6} (depending on whether $^{21}Ne^{*}_{excess}$ or $^{21}Ne^{*}_{crust}$

is used) which is slightly lower than the $^{40}Ar^*/^{21}Ne^*$ crustal average = 3.05×10^6 (Ballentine and Lollar, 2002). As the $^4He/^{21}Ne^*$ ratio fits the crustal average, $^4He/^{40}Ar^*$ is well above the crustal average, and $^{40}Ar^*/^{21}Ne^*$ is below the crustal average, thus this suggests a factor only affecting $^{40}Ar^*$. The lower $^{40}Ar^*$ than expected also suggests that the mantle $^{40}Ar^*$ contributions to the field are very small. Low relative $^{40}Ar^*$ could be related to factors such as low detrital mineral content in coals (thus depleting sources of ^{40}K which typically resides in clays and feldspars), or reflect the shallow nature of the coals. ^4He release from minerals occurs at low temperatures, $^{21}Ne^*$ is released from minerals ~80°C and ^{40}Ar at >~220°C (Ballentine and Burnard, 2002; Hunt *et al.,* 2012)(Ballentine and Burnard, 2002; Hunt *et al.,* 2012), both of these temperatures are higher than the current temperatures in the field of <~50°C (Berrow *et al.,* 2014). Entrapment of ^{40}Ar within the coal matrix is also possible, and $^4He/^{40}Ar^*$ generally decrease with increasing $^{40}Ar/^{36}Ar$, interpreted to being a greater contribution to a greater trapped 'coal-gas' component. The crustal components show good correlation with the ANG components, especially ^4He and $^{21}Ne^*_{(crust)}$. ^4He and ^{21}Ne have similar solubility in water, so their ratios are less affected by solubility fractionation between phases than ^4He and $^{40}Ar^*$. Cao *et al.,* (2017) reported variations in ^4He and $^{40}Ar^*$ concentrations between horizontal and vertical wells in Longmaxi shales attributed to vertical heterogeneity in the shale, and at Airth this could be a factor for $^{40}Ar^*$ contributions as certain wells target more permeable areas (as negligible variation is seen in the helium system). Figure 3-38 shows little coherency between the crustal components, suggesting the $^{40}Ar^*$ was not well mixed with the other crustal components prior to degassing (Ballentine and Lollar, 2002).

Alternatively, non-steady-state processes could be playing a role (Sathaye *et al.,* 2016; Torgersen *et al.,* 2004), possibly as a result of fluctuating bottom-hole-pressures during dewatering stages. Such processes could also explain the apparent inconsistencies in the heavier ANG ratios relative to the lighter $^{20}Ne/^{36}Ar$ ratios.

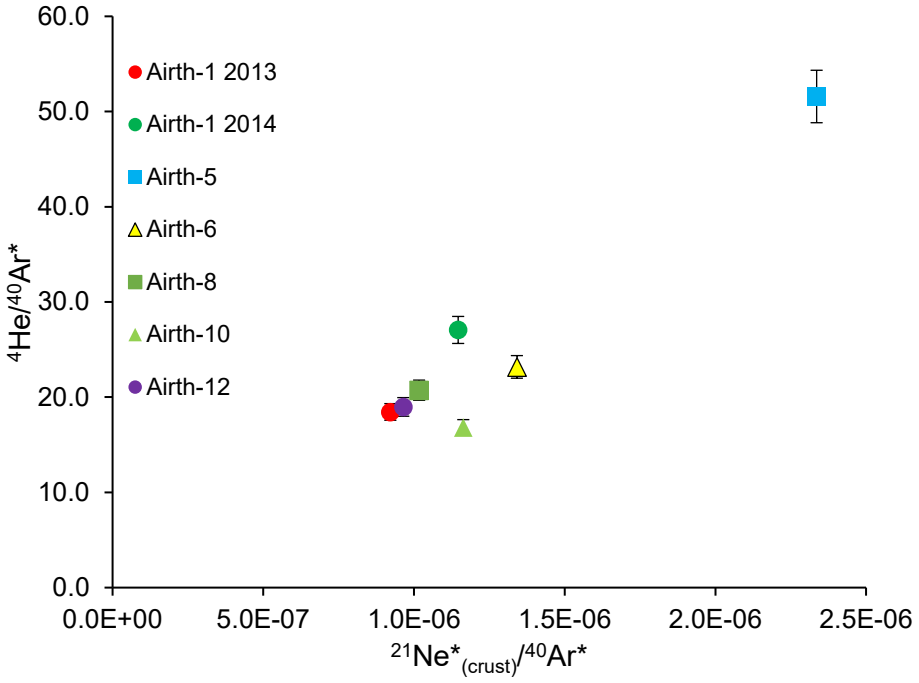

Figure 3-38 – Plot of crustal components; $^{4}He/^{40}Ar^{*}$ vs. $^{21}Ne^{*}/^{40}Ar^{*}$. There is no clear pattern in the ratios, suggesting all the crustal components were not mixed prior to gas production. This is attributed to factors mainly affecting $^{40}Ar^{*}$.

3.4.4.6 Origin of Noble Gases at the Airth CBM Field

The noble gas inventory of conventional hydrocarbon systems is a dynamic mixture of gases entrained from a diverse geographical and temporal range, as gases migrate from source to trap. Sources of noble gases include source rocks (Kennedy *et al.,* 2002), formation waters, external inputs such as mantle gas, deep crustal components, crustal radiogenic and nucleogenic gases produced *in situ*, as well as entrained from the various systems they have contacted (Ballentine and Burnard, 2002; Ballentine *et al.,* 2002). Trapped hydrocarbons may be subsequently affected by continued interaction with groundwater.

In contrast with conventional systems, in CBM deposits the gas reservoir is also the gas source. Initially, a discrete gaseous phase is non-existent in coals (or is present in very small volumes), and the coals and surrounding formations are water-saturated. When the CBM well is initially dewatered by pumping, the coals and surrounding formations undergo a reduction in pressure. The gas phase does not exist at depth until the dewatering process lowers the pressure to allow methane and other species to degas from formation waters, and then the coal matrix. This free-gas phase has not had a diverse migration history compared to conventional gas accumulations, and so the

CBM gas should contain only noble gases that are present in the vicinity of the wellbores at the time of gas desorpsion. These are derived from formation waters or coals, and diluted with desorbed methane. Hence the noble gas inventories in the gas phase should be related directly to the conditions in vicinity of the field (such as formation water temperature and salinity), or a result of physical processes that occur during gas extraction (release of gas from the coals *in situ*).

The degree to which a deep-sourced gas phase has interacted with groundwater is commonly assessed with $^{4}He/^{20}Ne$ ratios, which are regarded as a proxy for groundwater interaction. The dominant source of ^{20}Ne in the typical subsurface is groundwater containing dissolved atmosphere-derived neon. In the case of a *hypothetical* gas phase migrating from depth, possessing an elevated radiogenic ^{4}He concentration relative to ASW (*i.e.* $R_a < 1$), the migrating gas will strip noble gases from the water phase it contacts. Assuming this water has a composition of ASW, increasing gas-groundwater interaction will increasingly:

a) raise the $^{3}He/^{4}He$ ratio via ^{3}He addition from ASW, so $(^{3}He/^{4}He)_{gas} \rightarrow \sim 1$

b) reduce the $^{4}He/^{20}Ne$ of the gas phase, occurring due to the increase in ^{20}Ne content relative to ^{4}He from ASW, as typical ASW has neon concentrations an order of magnitude higher than helium concentrations.

At the Airth Field however, the gases are not 'migrating' great distances, and the formation water has *considerable* helium content from radiogenic ingrowth, so the typical model of decreasing $^{4}He/^{20}Ne$ being a result of increasing gas-water contact does not apply.

The dominant control on $^{4}He/^{20}Ne$ ratios is neon concentration which is generally proportional to helium concentration, with the relationship being non-linear (Figure 3-14). The highest ^{4}He concentrations correspond to the lowest $^{4}He/^{20}Ne$ ratios. Helium and neon have similar solubilities in water which is believed to be their greatest reservoir in the subsurface (Ozima and Podosek, 2001), and are hypothesised to have little inventory adsorped to solid surfaces. Considering the relatively homogenous distribution of the $^{3}He/^{4}He$ isotopes over the field (Figure 3-39), it could be assumed that neon might exhibit similar homogenous distributions to helium due to their relatively similar physical behaviours and solubilities. Therefore the $^{4}He/^{20}Ne$ ratio of gases derived from these waters should be reasonably uniform if helium and neon were sourced primarily (and completely degassed) from this water (*e.g.* Ballentine and Sherwood Lollar, (2002)), because $^{4}He/^{20}Ne$ ratios should be independent of methane

dilution in a closed system. However the $^{4}He/^{20}Ne$ ratios vary significantly, and are not correlated with $^{3}He/^{4}He$ ratios, suggesting the system is more complicated than simple degassing of water within the coals.

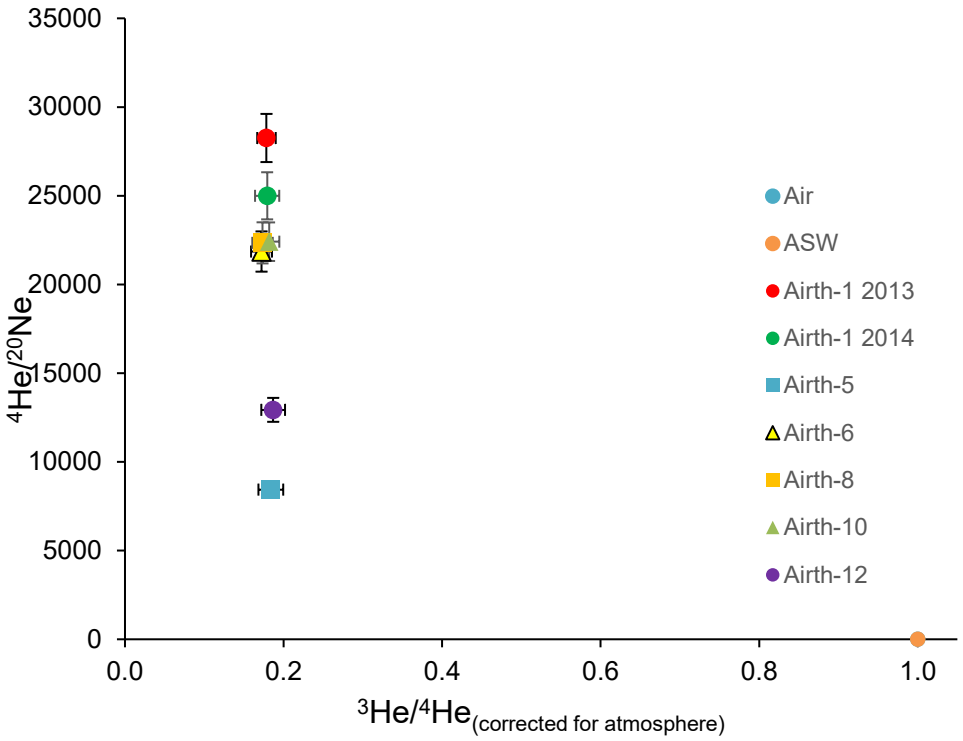

Figure 3-39 – Graph of $^{4}He/^{20}Ne$ vs. $^{3}He/^{4}He$.The $^{3}He/^{4}He$ ratio is remarkably uniform across the field, and independent of the $^{4}He/^{20}Ne$ ratio, showing the two ratios are unrelated. Typically subsurface systems will show a correlation with $^{4}He/^{20}Ne$ ratios and $^{3}He/^{4}He$ ratios, as a more crustal end-member is diluted by ASW, bringing the $^{3}He/^{4}He$ ratio closer to 1, and lowering the $^{4}He/^{20}Ne$ ratio (e.g. Ballentine et al., 1996; Zhou et al., 2005)

Wells that have never been pumped (Airth-5, Airth-6) show the lowest $^{4}He/^{20}Ne$ ratios, which would in most systems typically imply the greatest interaction with groundwater (via uptake of ^{20}Ne). Airth-1 (2013) is known to have been the most extensively pumped and shows the highest $^{4}He/^{20}Ne$ ratio, which normally implies the least groundwater contribution. However, this is seemingly counter-intuitive to the CBM production process, as greater dewatering exposes larger formation water volumes to a pressure drop and resulting degassing, which would lead to lower $^{4}He/^{20}Ne$ ratios, and this was observed in a CBM field by Zhou *et al.,* (2005).

It is observed that there is a pattern between decreasing overall noble gas concentrations and an increase in crustal noble gas enrichments relative to ANG components:

- The isotopic ratios of $^{40}Ar/^{36}Ar$ and $^{21}Ne/^{22}Ne$ increase (become more crustal) with decreasing argon and neon concentration (Figure 3-18, Figure 3-16)
- The elemental ratio of $^{4}He/^{20}Ne$ increases (becomes more crustal) with decreasing neon concentration (Figure 3-14)
- Crustal components fractionate coherently, showing this trend is not limited to a particular isotope system (Figure 3-19, Figure 3-33, Figure 3-34)

Fundamentally these observations cannot be a result of solubility fractionation or mass-dependent fractionation due to the coherence between crustal isotopic ratios and elemental ratios; solubility fractionation would not significantly affect isotopic ratios, and mass-fractionation can only fractionate isotopes dependent on relative mass (i.e. if $^{40}Ar/^{36}Ar$ *increases* then $^{21}Ne/^{22}Ne$ must *decrease*). This phenomenon then has to be a result of mixing between two components. Furthermore:

- The mantle component is generally correlated with crustal component, as observed in the neon isotope system (Figure 3-28), and when $^{20}Ne_{(mantle)}/^{20}Ne$
- is plotted vs $^{40}Ar/^{36}Ar$. Figure 3-36
- The $^{20}Ne/^{36}Ar$ ratios increase coherently with decreasing ^{20}Ne or ^{36}Ar concentrations, and appear air-like or above with an end-member ratio of ~0.45. Increasing $^{20}Ne/^{36}Ar$ ratios also correlate with increasing crustal noble gas ratios.

Again, these observations cannot readily be explained by simple solubility or mass-dependent fractionation of ASW. This shows that the mantle component and a $^{20}Ne/^{36}Ar$-enriched component must reside with the crustal end-member.

The co-variation of crustal components and atmospherically-derived noble gases suggest a mixing trend between a crustally-enriched end-member, and an ANG-enriched end-member. These are proposed to be:

- A water-derived component. This has a large concentration of all noble gases, particularly ANG's, small enrichments of crustal components (but nonetheless with isotopic ratios close to the air ratios), and with an enriched $^{20}Ne/^{36}Ar$ end-member of ~0.4. This is hypothesised to be a partly fractionated ancient ASW-like water with a residence time long enough to have accumulated a small radiogenic component.
- A residual coal-derived component. This is enriched in crustally derived ^{4}He, $^{21}Ne^*$ and $^{40}Ar^*$, which shows it had had a longer residence time than the surrounding groundwater, as radiogenic components are age accumulative. It displays small volume of gas with air-like $^{20}Ne/^{36}Ar$, $^{84}Kr,^{36}Ar$, and $^{132}Xe/^{36}Ar$ ratios, possibly 'fossil' sedimentary ANG's, or a previously fractionated ASW trapped within the coal matrix. Within the coals there is also a variable mantle component to different parts of the field.

The conceptual noble gas model of the Airth Field is proposed:

3.4.4.7 Conceptual Noble Gas Model of the Airth System

The coal fracture system, or cleats, are naturally more permeable than the coal matrix and any water-flow through the coal will occur primarily through the cleat system, so cleats are more likely to have a greater ASW contribution in response to any water flow through the system. Deep groundwater flow is known in the formations, as a band of warm 63°C freshwater in the Limestone Coal Formation in nearby exploration well Inch-of-Ferryton-1 (Berrow *et al.*, 2014). Ancient preserved isotopic signatures, especially those developed by the *in situ* production of radiogenic/nucleogenic isotopes are more likely to be trapped within the coal matrix.

The degree of degassing is related to the pressure gradient, which decreases away from the wellbore. The cleat/fracture system is the most permeable space, and water is preferentially degassed surrounding the wellbore and outwards throughout the cleat network. The result is a produced gas rich in all noble gas components, primarily those from the formation water which is most likely to have experienced slow water recharge over time.

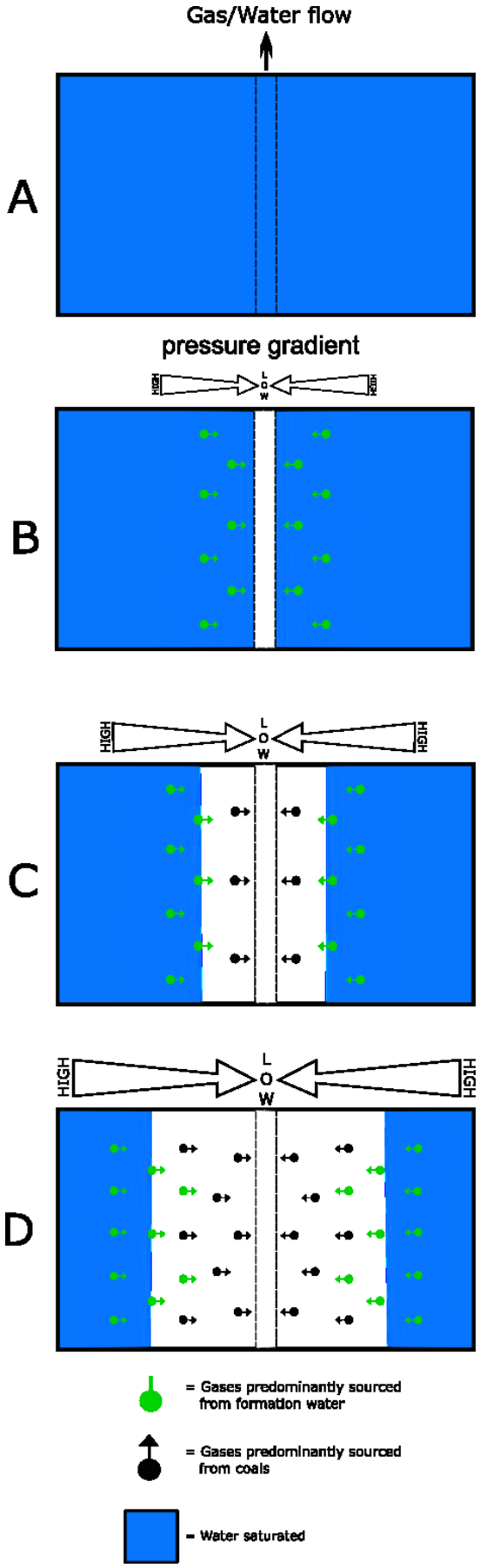

Figure 3-40 – Schematic illustrating the mechanisms behind the change in noble gas geochemistry at the Airth Field. Diagrams show a plan view of a section of well bore (dashed lines, centre) in a coal seam. Blue colour represents water saturation.

Stage A – Prior to dewatering; the initial state of a CBM coal seam. The seam is water-saturated, and no pressure gradient exists.

Stage B –Initial dewatering causes a pressure reduction at the well bore. This creates a pressure gradient from the pressurised coal seams towards the well-bore, resulting in the degassing of formation waters in the vicinity of the well. Gases are derived almost exclusively from formation waters, at high concentration.

Stage C – Further dewatering increases the pressure gradient, and extends the zone of influence further from the well. Formation water continues to degas distally. Proximal to the well bore, dewatering occurrs and gases begin desorbing from coal. Gases are primarily sourced from degassed formation water, with a smaller component of desorbed coal gases. Concentrations of noble gases are lower due to increasing dilution with methane, and the removal of the gases produced in stage B.

Stage D – More dewatering further extends the zone of influence of the pressure gradient. Dewatering is more complete, and a greater volume of coals near to the well bore desorb gases. Formation water continues to degas further from the wellbore, but it's volumetric contribution is smaller due to the increased volumes of desorbing coal gas. Coal-derived gases now make up a significant volume of the produced gas, and are less diluted by formation-water derived gases. The noble gas ratios appear more crustally-rich as a result of less formation water dilution.

This degassing progressively strips the more ASW-like component from the water, which is removed from the system. The water is eventually physically removed by pumping, and the hydrostatic head is considerably lowered, and the pressures surrounding the wellbore are reduced further. In wells that have been more extensively pumped and produced, concentrations of all noble gases are all lower as a result of a) increasing dilution with methane and b) removal of part of the noble gas inventory from the system via produced gas.

The resulting pressure decrease upon dewatering causes methane to desorb from coal surfaces (representing a greater volume of methane than that present in formation water), and diffusion of methane and noble gas species from within the coal matrix towards the cleat-gas interface following the pressure gradient. A greater crustal component is then measured in the produced gas, as desorbing methane carries noble gases embedded in the coals and pore spaces with it.

This process occurs on multiple scales:

- The major permeable fracture networks surrounding wellbore(s): waters degas following a concentration gradient away from the wellbore (the zone of influence is estimated to be ~250 m by Sinayuc *et al.,* (2011)).
- Lesser permeable fractures/cleats, small fractures, surfaces, and open pore space *etc*. connected to these major pathways.
- Unconnected pore space and microfractures within the coal matrix, where diffusion will play a significant role.

The degree to which each 'compartment' will degas and the rate of degassing will be proportional to the pressure gradient. Degassing of these compartments will occur concurrently as the reduced pressure 'front' moves outwards from the wellbore, with areas further outwards being subject to a lower pressure reduction than areas proximal to the wellbore (see Figure 3-40). Continued dewatering and gas production will produce a shift from part B to part C to part D. The initial gas compositions will be enriched in higher concentrations of formation water noble gases, and the later stages will show fewer formation water derived gases and a greater component degassed from the coal matrix. The coal-gas component becomes more prominent as a) the formation water component is removed from the system (*i.e.* less dilution), and b) coals more readily desorb gas as pressure is reduced (*i.e.* greater volumetric

contribution from coal). This is manifested in initial ASW-like noble gas ratios, trending to more crustal ratios.

The helium inventory is hypothesised to be homogenously distributed throughout the subsurface, as shown by the uniform $^{3}He/^{4}He$ ratio, and is contained in both the formation water and the coals. Major permeable pathways comprise the largest helium reservoir (in fracture porosity) which are degassed first, and non-pumped wells show the highest helium concentrations along with the greatest ANG components, but lower crustal $^{21}Ne^{*}_{(crust)}$ and $^{40}Ar^{*}$. Helium is also distributed throughout the coal matrix, but the low permeability of coals and low internal coal porosity of coals *vs.* fracture porosity results in a lower volumetric potential. Hence wells that have been subjected to a greater degree of dewatering show lower helium concentrations as a result of helium depletion, a smaller available helium reservoir available in porosity, and noble gas dilution with methane.

The Airth field has been pumped for gas flowrate testing in anticipation of commercial development, but has not so far been extensively put on production. Thus, the field represents a more pristine state of initial noble gas signatures than one which has been extensively dewatered and depleted. Airth represents a near 'end member' scenario for the start of the dewatering stage.

The gases sampled at Airth are hypothesised to be a mix between formation-water-derived and coal-derived components, controlled primarily by the stages of dewatering.

The most extreme end-members in the Airth Field being Airth-5, which has a significant contribution from the water component, and Airth-1 (2013) which shows the least water-derived influence and the highest crustal/atmospheric noble gas ratios. Both wells are believed to have experienced both the least dewatering (Airth-5, *i.e.* none), and the most dewatering (Airth-1 (2013), the oldest well, dewatered intermittently over years, and sampled several months after a flow test). The other wells show ranges of ASW-derived and crustal components between these pseudo end-members.

This mechanism proposes no issues for helium, which is assumed to be homogenously distributed due to its high diffusivity and constant observed $^{3}He/^{4}He$ ratio. In addition, it can also be applied to argon, as the $^{40}Ar^{*}$ concentrations are broadly speaking within the same order of magnitude regardless of $^{40}Ar/^{36}Ar$, suggesting a higher $^{40}Ar^{*}$-rich end-member in coals is being diluted by ASW with a more ASW-like component. However it is potentially problematic to imagine neon,

which also shows a high degree of diffusivity and similar solubility in water to helium, being compartmentalised in low porosity rock. Grove *et al.,* (2017) observed that low volumes of fluid flow are suggested to aid to the preservation of radiogenic He and nucleogenic Ne components within minerals, as the concentration gradient from within the mineral to the fluids will remain low where the fluids are not continually replaced. Such a mechanism where fluid flow is minimal could aid preservation of trapped components in restricted pore space/microfractures in coals over geological time. This has important implications for the storage of both *in-situ* radiogenic/nucleogenic components and *ex-situ* derived mantle volatiles over geological time periods. Furthermore, the observation that mantle components correlate closely with crustal components sequestered within the coals (rather than in mobile waters) shows that mantle input is not an ongoing phenomenon.

3.5 Field Development

The transition from ASW-like gases to more crustal/mantle signature as a result of pumping could be used as a tool to assess pumping history; wells with higher ASW components are not fully dewatered and thus more gas potential could exist. The large enrichments in $^{84}Kr/^{36}Ar$ and $^{132}Xe/^{36}Ar$ relative to ASW often seen in hydrocarbon fields are not seen here. If there is a sorbed component on coals it could be that a degree of coal 'destruction' would be necessary to release it, possibly via coal matrix shrinkage due to gas desorpsion as suggested by Zhou *et al.,* (2005), or it may have been expulsed with methane during the coalification process or oil/kerogen interaction, resulting in the depleted values measured. It would be an interesting temporal experiment to resample the gases in several years if extensive production is acheieved to assess the sedimentary heavy noble gas inventories. Grove *et al.,* (2017) also investigated the use of crustal noble gases as tracers for fluid flow in shales, which could have utility in similar closed systems such as UK coal beds characterised by low-permeabilities, both in assessing sorbed components and regional groundwater flow.

Cao *et al.,* (2017) reported a negative correlation in the Weiyuan gases of the Longmaxi shales between $^{40}Ar/^{36}Ar$ and ^{40}Ar over 3 years of gas production, with $^{40}Ar/^{36}Ar$ decreasing with an increasing ^{40}Ar concentration, interpreted to a decrease in radiogenic ^{40}Ar input from a diminishing free gas phase in the shales. The only temporal measurement at Airth (Airth-1 2013 *vs.* Airth-1 2014) shows a decrease in

$^{40}Ar/^{36}Ar$ but a decrease in argon concentration. The other samples however show a similar trend to Cao *et al.,* (2017) with argon, but spatially instead of temporally. This is attributed here to lesser dilution of the radiogenic component with ANG derived ^{36}Ar, and perhaps an increased contribution of $^{40}Ar^*$ derived from the coal matrix itself as dewatering progresses. Cao *et al.,* (2017) proposed the trend in the argon inventory could be used as a marker for 'productive' shale gases with a greater free gas supply. It is possible that argon measurements could be used in CBM fields as a marker for the dewatering process and remaining gas-in-place, as $^{40}Ar^*$ is hypothesised to reside mainly in the coal matrix and thus could be a marker for gas desorpsion.

3.6 Conclusions

The Airth CBM field in Central Scotland is one of only two commercial schemes in the UK extracting CBM. The site is located close to several sites where hydrocarbon contamination of the shallow subsurface could occur, such as abandoned coal mines, oil refineries and pipeline infrastructure, and natural oil and gas seepages. This text has characterised the baseline geochemistry of the Airth field in order to help determine the origins of any gases found in the shallow subsurface.

The gas is mainly composed of methane, with trace quantities of ethane and propane, and negligible N_2 and CO_2 contents. Carbon and hydrogen stable isotopes along with ethane concentrations show that the gas is unambiguously thermogenic in origin, with $\delta^{13}C_{CH4}$ and δD_{CH4} which overlap the range of UK North Sea gas. The coal gases show no traces of modern radiocarbon, which is expected from a fossil gas source.

Helium concentrations are the highest recorded onshore in the UK, and are mainly (>96%) sourced from the decay of U and Th series minerals, with negligible atmospheric contribution. A small mantle helium input is present within the coals, possibly sourced from deep-seated faults in the region. The $^{3}He/^{4}He$ ratios are unusually uniform at $0.18_{(Ra)}$, showing the helium inventory is well mixed across the field. Neon measurements show enrichments in crustal nucleogenic $^{21}Ne^*$ and a resolvable mantle ^{20}Ne signature which varies between wells.

Coalbed methane differs from conventional hydrocarbon accumulations in that there is a small initial fluid and/or gas phase for groundwater-derived gases and

crustal noble gases to equilibrate with (the formation water within pore spaces, and the cleat and fracture network of the coal).

This field has been pumped for gas flowrate testing in anticipation of commercial development, but has not so far been extensively put on production. Thus, the field represents a more pristine state of initial noble gas signatures than one which has been extensively dewatered and depleted. Dewatering of a well will cause a pressure reduction, causing degassing and depletion of noble gases and methane dissolved in the formation water. Further dewatering will degas methane sorbed onto coal surfaces (representing a greater proportion of dissolved methane than that present in formation water) and the concomitant degassing of noble gases also sorbed onto these surfaces (present from formation water, remnant sedimentary gases and radiogenic gases formed in situ within the coal).

Enrichments of crustal components increase with the removal of the air-derived components from formation water, hypothesised to be a result of the dewatering process. Dewatering removes ANG components from the more permeable cleats, fractures and open porespaces, and reduces the dilution of a crustal/mantle rich component contained within the coals.

The $^{20}Ne/^{36}Ar$ ratios appear air-like or above with an end-member ratio of ~0.45. This cannot readily be explained by simple solubility or mass-dependent fractionation of ASW at current reservoir conditions. The high $^{20}Ne/^{36}Ar$ is attributed to either 'fossil' sedimentary ANG gases trapped in the coal matrix, or possibly a trapped component within the coals consisting of older, previously fractionated ASW that has had its noble gas inventory modified by an oil/kerogen phase. ASW contributions and overall noble gas concentrations decrease as a function of dewatering, resulting in gases increasingly enriched in crustal components and higher $^{20}Ne/^{36}Ar$ ratios that are contained in the coal matrix.

The local $^{4}He/^{40}Ar^{*}$ end-member ratio is ~15.5, higher than the crustal average, attributed to cooler, shallow crust preferentially retaining ^{40}Ar in rocks. Crustal components and the modified ANG end-member gases fractionate coherently, suggesting these components were well mixed prior to gas production.

3.7 Bibliography

Bacon, M. J. (1995) 'Development and Techniques used on the Airth #1 well in Scotland.', in *Conference Documentation 'Planning for Profit: Coalbed Methane in the UK and Europe. 30-31st March*. London:

IBC Technical Services.
Badenszki, E., Daly, J. S., J. Whitehouse, M. and Upton, B. (2015) 'The mystery of the Scottish Midland Valley basement: Solved!', in *58th Irish Geological Research Meeting*. Belfast.
Ballentine, C. ., Mazurek, M. and Gautschi, A. (1994) 'Thermal constraints on crustal rare gas release and migration: Evidence from Alpine fluid inclusions', *Geochimica et Cosmochimica Acta*, 58(20), pp. 4333–4348. doi:10.1016/0016-7037(94)90337-9.
Ballentine, C. J., O'Nions, R. K., Oxburgh, E. R., Horvath, F. and Deak, J. (1991) 'Rare gas constraints on hydrocarbon accumulation, crustal degassing and groundwater flow in the Pannonian Basin', *Earth and Planetary Science Letters*, 105(1–3), pp. 229–246. doi:10.1016/0012-821X(91)90133-3.
Ballentine, C. J., Burgess, R. and Marty, B. (2002) 'Tracing Fluid Origin, Transport and Interaction in the Crust', *Reviews in Mineralogy and Geochemistry*, 47(1), pp. 539–614. doi:10.2138/rmg.2002.47.13.
Ballentine, C. J. and Burnard, P. G. (2002) 'Production, Release and Transport of Noble Gases in the Continental Crust', *Reviews in Mineralogy and Geochemistry*, 47(1), pp. 481–538. doi:10.2138/rmg.2002.47.12.
Ballentine, C. J. and O'Nions, R. K. (1992) 'The nature of mantle neon contributions to Vienna Basin hydrocarbon reservoirs', *Earth and Planetary Science Letters*, 113(4), pp. 553–567. doi:10.1016/0012-821X(92)90131-E.
Ballentine, C. J., O'Nions, R. K. and Coleman, M. L. (1996) 'A Magnus opus: Helium, neon, and argon isotopes in a North Sea oilfield', *Geochimica et Cosmochimica Acta*. Elsevier, 60(5), pp. 831–849. doi:10.1016/0016-7037(95)00439-4.
Ballentine, C. J. and Sherwood Lollar, B. (2002) 'Regional groundwater focusing of nitrogen and noble gases into the Hugoton-Panhandle giant gas field, USA', *Geochimica et Cosmochimica Acta*, 66(14), pp. 2483–2497. doi:10.1016/S0016-7037(02)00850-5.
Battani, A., Sarda, P. and Prinzhofer, A. (2000) 'Basin scale natural gas source, migration and trapping traced by noble gases and major elements: The Pakistan Indus basin', *Earth and Planetary Science Letters*, 181(1–2), pp. 229–249. doi:10.1016/S0012-821X(00)00188-6.
Baxby, M., Patience, R. L. and Bartle, K. D. (1994) 'THE ORIGIN AND DIAGENESIS OF SEDIMENTARY ORGANIC NITROGEN', *Journal of Petroleum Geology*, 17(2), pp. 211–230. doi:10.1111/j.1747-5457.1994.tb00127.x.
Bernard, B. B., Brooks, J. M. and Sackett, W. M. (1978) 'Light hydrocarbons in recent Texas continental shelf and slope sediments', *Journal of Geophysical Research*, 83(C8), p. 4053. doi:10.1029/JC083iC08p04053.
Berrow, A., Goold, D., Westerman, R., Code, P., Berrow, A., Goold, D., Westerman, R., Natural, C. and Plc, R. (2014) *UCG Potential of CNR's Kincardine Licence, Firth of Forth, Scotland*. Belltree Group.
Bluck, B. J. (2000) 'Old Red Sandstone basins and alluvial systems of Midland Scotland', *Geological Society, London, Special Publications*, 180(1), pp. 417–437. doi:10.1144/GSL.SP.2000.180.01.22.
Bosch, A. and Mazor, E. (1988) 'Natural gas association with water and oil as depicted by atmospheric noble gases: case studies from the southeastern Mediterranean Coastal Plain', *Earth and Planetary Science Letters*, 87(3), pp. 338–346. doi:10.1016/0012-821X(88)90021-0.
Cameron, I. B. and Stephenson, D. (1985) *British regional geology: the Midland Valley of Scotland*. British Geological Survey. ISBN: 978-0118843652.
Cao, C., Zhang, M., Tang, Q., Yang, Y., Lv, Z., Zhang, T., Chen, C., Yang, H. and Li, L. (2018) 'Noble gas isotopic variations and geological implication of Longmaxi shale gas in Sichuan Basin, China', *Marine and Petroleum Geology*, 89, pp. 38–46. doi:10.1016/j.marpetgeo.2017.01.022.
CEC (1988) *INVESTIGATION OF FIREDAMP AND ITS EMISSION IN COAL SEAMS*, *Technical Coal Research - EUR 11474 EN*. Commission of The European Communities. Available at: https://publications.europa.eu/en/publication-detail/-/publication/d48faada-31ce-4173-a9cb-f5b2ddff8453/language-en.
Clayton, J. . (1998) 'Geochemistry of coalbed gas – A review', *International Journal of Coal Geology*, 35(1–4), pp. 159–173. doi:10.1016/S0166-5162(97)00017-7.
Composite Energy Ltd. (2006) *Composite Energy Field Development Plan - Airth Pilot*. Composite Energy Ltd.
Craig, H., Lupton, J. E., Welhan, J. A. and Poreda, R. (1978) 'Helium isotope ratios in Yellowstone and Lassen Park volcanic gases', *Geophysical Research Letters*, 5(11), pp. 897–900. doi:10.1029/GL005i011p00897.
Creedy, D. P. (1988) 'Geological controls on the formation and distribution of gas in British coal measure strata', *International Journal of Coal Geology*, 10(1), pp. 1–31. doi:10.1016/0166-5162(88)90002-X.
Creedy, D. P. (1991) 'An introduction to geological aspects of methane occurrence and control in British deep coal mines', *Quarterly Journal of Engineering Geology and Hydrogeology*, 24(2), pp. 209–220. doi:10.1144/GSL.QJEG.1991.024.02.04.
Creedy, D. P. and Pritchard, F. W. (1983) 'Nitrogen and carbon dioxide occurrence in UK coal seams', *International Journal of Mining Engineering*, 1(1), pp. 71–77. doi:10.1007/BF00881263.
Crosdale, P. J., Beamish, B. B. and Valix, M. (1998) 'Coalbed methane sorption related to coal composition',

International Journal of Coal Geology, 35(1–4), pp. 147–158. doi:10.1016/S0166-5162(97)00015-3.

Crovetto, R., Fernández-Prini, R. and Japas, M. L. (1982) 'Solubilities of inert gases and methane in H2O and in D2O in the temperature range of 300 to 600 K', *The Journal of Chemical Physics*, 76(2), pp. 1077–1086. doi:10.1063/1.443074.

DECC (2013) *the Unconventional Hydrocarbon Resources of Britain's Onshore Basins - Coalbed Methane (CBM)*. Department of Energy and Climate Change. Available at: https://www.ogauthority.co.uk/media/1694/promote_uk_cbm_2012.pdf.

Dunai, T. J. and Baur, H. (1995) 'Helium, neon, and argon systematics of the European subcontinental mantle: Implications for its geochemical evolution', *Geochimica et Cosmochimica Acta*, 59(13), pp. 2767–2783. doi:10.1016/0016-7037(95)00172-V.

Envoi (2013) *Unconventional UK Asset Package of DART Energy Ltd.*, *Project Synopsis P213*. London: Envoi Ltd.

Flores, R. M. (1998) 'Coalbed methane: From hazard to resource', *International Journal of Coal Geology*, 35(1–4), pp. 3–26. doi:http://dx.doi.org/10.1016/S0166-5162(97)00043-8.

Gallagher, M. J., Michie, U. M., Smith, R. T. and Haynes, L. (1971) 'NEW EVIDENCE OF URANIUM AND OTHER MINERALIZATION IN SCOTLAND', *Trans. Inst. Min. Metall.* Inst. of Geological Sciences, London, 3(01), pp. 150–173.

Gan, H., Nandi, S. P. and Walker, P. L. (1972) 'Nature of the porosity in American coals', *Fuel*, 51(4), pp. 272–277. doi:10.1016/0016-2361(72)90003-8.

Gautheron, C. and Moreira, M. (2002) 'Helium signature of the subcontinental lithospheric mantle', *Earth and Planetary Science Letters*, 199(1–2), pp. 39–47. doi:10.1016/S0012-821X(02)00563-0.

Gilfillan, S. M. V., Ballentine, C. J., Holland, G., Blagburn, D., Lollar, B. S., Stevens, S., Schoell, M. and Cassidy, M. (2008) 'The noble gas geochemistry of natural CO2 gas reservoirs from the Colorado Plateau and Rocky Mountain provinces, USA', *Geochimica et Cosmochimica Acta*, 72(4), pp. 1174–1198. doi:10.1016/j.gca.2007.10.009.

Gold, T. and Held, M. (1987) 'HELIUM-NITROGEN-METHANE SYSTEMATICS IN NATURAL GASES OF TEXAS AND KANSAS', *Journal of Petroleum Geology*, 10(4), pp. 415–424. doi:10.1111/j.1747-5457.1987.tb00582.x.

Golding, S. D., Boreham, C. J. and Esterle, J. S. (2013) 'Stable isotope geochemistry of coal bed and shale gas and related production waters: A review', *International Journal of Coal Geology*, 120, pp. 24–40. doi:10.1016/j.coal.2013.09.001.

Gray, I. (1987) 'Reservoir Engineering in Coal Seams: Part 1-The Physical Process of Gas Storage and Movement in Coal Seams', *SPE Reservoir Engineering*, 2(01), pp. 28–34. doi:10.2118/12514-PA.

Grove, B. S., Walsh, T. B. and Darrah, T. H. (2017) 'Using Radiogenic Noble Gases to Trace the Conditions of Crustal Fluid Migration', *Procedia Earth and Planetary Science*, 17, pp. 818–821. doi:10.1016/j.proeps.2017.01.050.

Györe, D., Stuart, F. M., Gilfillan, S. M. V. and Waldron, S. (2015) 'Tracing injected CO 2 in the Cranfield enhanced oil recovery field (MS, USA) using He, Ne and Ar isotopes', *International Journal of Greenhouse Gas Control*. Elsevier Ltd, 42, pp. 554–561. doi:10.1016/j.ijggc.2015.09.009.

Györe, D., McKavney, R., Gilfillan, S. M. V. and Stuart, F. M. (2018) 'Fingerprinting coal-derived gases from the UK', *Chemical Geology*, 480, pp. 75–85. doi:10.1016/j.chemgeo.2017.09.016.

Hitchman, S. P., Darling, W. G. and Williams, G. M. (1989) *STABLE ISOTOPE RATIOS IN METHANE CONTAINING GASES IN THE UNITED KINGDOM*, *Technical Report WE/89/30*. Nottingham: British Geological Survey. Available at: http://nora.nerc.ac.uk/id/eprint/502528/1/WE89030.pdf.

Hiyagon, H. and Kennedy, B. . (1992) 'Noble gases in CH4-rich gas fields, Alberta, Canada', *Geochimica et Cosmochimica Acta*, 56(4), pp. 1569–1589. doi:10.1016/0016-7037(92)90226-9.

Hooper, M. D. (2003) *The Carboniferous evolution of the Central Coalfield Basin, Midland Valley of Scotland: implications for basin formation and the regional tectonic setting*. University of Leicester. Available at: https://lra.le.ac.uk/handle/2381/27768.

Hunt, A. G., Darrah, T. H. and Poreda, R. J. (2012) 'Determining the source and genetic fingerprint of natural gases using noble gas geochemistry: A northern Appalachian Basin case study', *AAPG Bulletin*, 96(10), pp. 1785–1811. doi:10.1306/03161211093.

Jones, N. S., Holloway, S., Smith, N. J. P., Browne, M. a E., Creedy, D. P., Garner, K. and Durucan, S. (2004) *UK Coal Resource for New Exploitation Technologies: Final Report*, *CR/04/015N*. Nottingham, U.K.: British Geological Survey. Available at: http://nora.nerc.ac.uk/id/eprint/509526/.

Kennedy, B. M., Hiyagon, H. and Reynolds, J. H. (1990) 'Crustal neon: a striking uniformity', *Earth and Planetary Science Letters*, 98(3–4), pp. 277–286. doi:10.1016/0012-821X(90)90030-2.

Kennedy, B. M., Torgersen, T. and van Soest, M. C. (2002) 'Multiple atmospheric noble gas components in hydrocarbon reservoirs: A study of the Northwest Shelf, Delaware Basin, SE New Mexico', *Geochimica et Cosmochimica Acta*, 66(16), pp. 2807–2822. doi:10.1016/S0016-7037(02)00883-9.

Kharaka, Y. K. and Specht, D. J. (1988) 'The solubility of noble gases in crude oil at 25–100°C', *Applied Geochemistry*, 3(2), pp. 137–144. doi:10.1016/0883-2927(88)90001-7.

Kirstein, L. A., Dunai, T. J., Davies, G. R., Upton, B. G. J. and Nikogosian, I. K. (2004) 'Helium isotope signature

of lithospheric mantle xenoliths from the Permo-Carboniferous magmatic province in Scotland — no evidence for a lower-mantle plume', *Geological Society, London, Special Publications*, 223(1), pp. 243–258. doi:10.1144/GSL.SP.2004.223.01.11.

Kotarba, M. J., Nagao, K. and Karnkowski, P. H. (2014) 'Origin of gaseous hydrocarbons, noble gases, carbon dioxide and nitrogen in Carboniferous and Permian strata of the distal part of the Polish Basin: Geological and isotopic approach', *Chemical Geology*, 383, pp. 164–179. doi:10.1016/j.chemgeo.2014.06.012.

Krooss, B. M., Littke, R., Müller, B., Frielingsdorf, J., Schwochau, K. and Idiz, E. F. (1995) 'Generation of nitrogen and methane from sedimentary organic matter: Implications on the dynamics of natural gas accumulations', *Chemical Geology*, 126(3–4), pp. 291–318. doi:10.1016/0009-2541(95)00124-7.

Langmuir, I. (1918) 'THE ADSORPTION OF GASES ON PLANE SURFACES OF GLASS, MICA AND PLATINUM.', *Journal of the American Chemical Society*, 40(9), pp. 1361–1403. doi:10.1021/ja02242a004.

Levine, J. R. (1993) 'Coalification: The Evolution of Coal as Source Rock and Reservoir Rock for Oil and Gas', in *Hydrocarbons from Coal*. Tulsa, OK: AAPG, pp. 39–77. doi:10.1306/St38577C3.

Lippmann-Pipke, J., Sherwood Lollar, B., Niedermann, S., Stroncik, N. A., Naumann, R., van Heerden, E. and Onstott, T. C. (2011) 'Neon identifies two billion year old fluid component in Kaapvaal Craton', *Chemical Geology*. Elsevier B.V., 283(3–4), pp. 287–296. doi:10.1016/j.chemgeo.2011.01.028.

Liu, G., Zhao, Z., Sun, M., Li, J., Hu, G. and Wang, X. (2012) 'New insights into natural gas diffusion coefficient in rocks', *Petroleum Exploration and Development*. Research Institute of Petroleum Exploration & Development, PetroChina, 39(5), pp. 597–604. doi:10.1016/S1876-3804(12)60081-0.

Mackay, L. M., Turner, J., Jones, S. M. and White, N. J. (2005) 'Cenozoic vertical motions in the Moray Firth Basin associated with initiation of the Iceland Plume', *Tectonics*, 24(5), p. n/a-n/a. doi:10.1029/2004TC001683.

Mamyrin, B. W., Annufriev, G., Kamenskiy, G. S. and Tolstikhin, I. L. (1970) 'Determination of the isotopic composition of atmospheric helium', *Geochem. Int.*, 7, pp. 498–505.

Marshall, J. E. A., Haughton, P. D. W. and Hillier, S. J. (1994) 'Vitrinite reflectivity and the structure and burial history of the Old Red Sandstone of the Midland Valley of Scotland', *Journal of the Geological Society*, 151(3), pp. 425–438. doi:10.1144/gsjgs.151.3.0425.

Meslé, M., Dromart, G. and Oger, P. (2013) 'Microbial methanogenesis in subsurface oil and coal', *Research in Microbiology*, 164(9), pp. 959–972. doi:10.1016/j.resmic.2013.07.004.

Monaghan, A. A. A. (2014) *The Carboniferous shales of the Midland Valley of Scotland : geology and resource estimation*. London, UK. Available at: https://www.ogauthority.co.uk/media/2765/bgs_decc_mvs_2014_main_report.pdf.

Moore, T. a. (2012) 'Coalbed methane: A review', *International Journal of Coal Geology*. Elsevier B.V., 101(0), pp. 36–81. doi:10.1016/j.coal.2012.05.011.

Nuccio, V. (2000) *USGS Fact Sheet FS–123–00*. Denver, CO: United States Geological Survey. Available at: https://pubs.usgs.gov/factsheet/fs123-00/.

Okolo, G. N., Everson, R. C., Neomagus, H. W. J. P., Roberts, M. J. and Sakurovs, R. (2015) 'Comparing the porosity and surface areas of coal as measured by gas adsorption, mercury intrusion and SAXS techniques', *Fuel*, 141(0), pp. 293–304. doi:10.1016/j.fuel.2014.10.046.

Oxburgh, E. R., O'Nions, R. K. and Hill, R. I. (1986) 'Helium isotopes in sedimentary basins', *Nature*, 324(6098), pp. 632–635. doi:10.1038/324632a0.

Ozima, M. and Podosek, F. A. (2001) *Noble Gas Geochemistry*. 2nd edn. Cambridge: Cambridge University Press. doi:10.1017/CBO9780511545986 ISBN: 9780511545986.

Pinti, D. L., Wada, N. and Matsuda, J. (1999) 'Neon excess in pumice: volcanological implications', *Journal of Volcanology and Geothermal Research*, 88(4), pp. 279–289. doi:10.1016/S0377-0273(99)00006-2.

Podosek, F. A., Honda, M. and Ozima, M. (1980) 'Sedimentary noble gases', *Geochimica et Cosmochimica Acta*, 44(11), pp. 1875–1884. doi:10.1016/0016-7037(80)90236-7.

Polyak, B. G. and Tolstikhin, I. N. (1985) 'Isotopic composition of the earth's helium and the problem of the motive forces of tectogenesis', *Chemical Geology: Isotope Geoscience section*, 52(1), pp. 9–33. doi:10.1016/0168-9622(85)90005-3.

Prinzhofer, A. (2013) 'Noble Gases in Oil and Gas Accumulations', in *The Noble Gases as Geochemical Tracers*. Berlin, Heidelberg: Springer Berlin Heidelberg, pp. 225–247. doi:10.1007/978-3-642-28836-4_9.

Radlinski, A. ., Mastalerz, M., Hinde, A. ., Hainbuchner, M., Rauch, H., Baron, M., Lin, J. ., Fan, L. and Thiyagarajan, P. (2004) 'Application of SAXS and SANS in evaluation of porosity, pore size distribution and surface area of coal', *International Journal of Coal Geology*, 59(3–4), pp. 245–271. doi:10.1016/j.coal.2004.03.002.

Rice, D. D. (1993) 'Composition and Origins of Coalbed Gas', *AAPG Bulletin*, 77(1), pp. 159–184. doi:10.1306/D9CB61EB-1715-11D7-8645000102C1865D.

Rightmire, C. T., Eddy, G. E. and Kirr, J. N. (1984) 'Coalbed Methane Resources of the United States', *AAPG Studies in Geology*, 17. doi:10.1306/St17437.

Rippon, J. H., Ellison, R. a. and Gayer, R. a. (2006) 'A review of joints (cleats) in British Carboniferous coals: indicators of palaeostress orientation', *Proceedings of the Yorkshire Geological Society*, 56(1), pp. 15–30. doi:10.1144/pygs.56.1.15.

Rippon, J., Read, W. A. and Park, R. G. (1996) 'The Ochil Fault and the Kincardine basin: key structures in the tectonic evolution of the Midland Valley of Scotland', *Journal of the Geological Society*, 153(4), pp. 573–587. doi:10.1144/gsjgs.153.4.0573.

Robinson, N., Parnell, J. and Brassell, S. (1989) 'Hydrocarbon compositions of bitumens from mineralized Devonian lavas and Carboniferous sedimentary rocks, central Scotland', *Marine and Petroleum Geology*, 6(4), pp. 316–323. doi:10.1016/0264-8172(89)90028-7.

Rodrigues, C. . and Lemos de Sousa, M. . (2002) 'The measurement of coal porosity with different gases', *International Journal of Coal Geology*, 48(3–4), pp. 245–251. doi:10.1016/S0166-5162(01)00061-1.

Sano, Y., Urabe, A., Wakita, H. and Wushiki, H. (1993) 'Origin of hydrogen-nitrogen gas seeps, Oman', *Applied Geochemistry*, 8(1), pp. 1–8. doi:10.1016/0883-2927(93)90053-J.

Sathaye, K. J., Larson, T. E. and Hesse, M. A. (2016) 'Noble gas fractionation during subsurface gas migration', *Earth and Planetary Science Letters*, 450, pp. 1–9. doi:10.1016/j.epsl.2016.05.034.

Schoell, M. (1980) 'The hydrogen and carbon isotopic composition of methane from natural gases of various origins', *Geochimica et Cosmochimica Acta*, 44(5), pp. 649–661. doi:10.1016/0016-7037(80)90155-6.

SEPA (2014) *Unconventional Gas Development - Monitoring of Produced Water*. Scottish Environmental Protection Agency.

Sherwood Lollar, B., Ballentine, C. J. and Onions, R. K. (1997) 'The fate of mantle-derived carbon in a continental sedimentary basin: Integration of relationships and stable isotope signatures', *Geochimica et Cosmochimica Acta*, 61(11), pp. 2295–2307. doi:10.1016/S0016-7037(97)00083-5.

Sinayuc, C., Shi, J.-Q. Q., Imrie, C. E., Syed, S. A., Korre, A. and Durucan, S. (2011) 'Implementation of horizontal well CBM/ECBM technology and the assessment of effective CO2 storage capacity in a Scottish coalfield', *Energy Procedia*. Elsevier, 4, pp. 2150–2156. doi:10.1016/j.egypro.2011.02.100.

Smythe, D. K. (2013) *Precognition by Professor David K. Smythe*. Available at: https://www.davidsmythe.org/fracking/cuadrilla sussex critique V1.pdf.

Strąpoć, D., Picardal, F. W., Turich, C., Schaperdoth, I., Macalady, J. L., Lipp, J. S., Lin, Y. S., Ertefai, T. F., Schubotz, F., Hinrichs, K. U., Mastalerz, M. and Schimmelmann, A. (2008) 'Methane-producing microbial community in a coal bed of the Illinois Basin', *Applied and Environmental Microbiology*, 74(8), pp. 2424–2432. doi:10.1128/AEM.02341-07.

Stuart, F. M., Ellam, R. M., Harrop, P. J., Fitton, J. G. and Bell, B. R. (2000) 'Constraints on mantle plumes from the helium isotopic composition of basalts from the British Tertiary Igneous Province', *Earth and Planetary Science Letters*, 177(3–4), pp. 273–285. doi:10.1016/S0012-821X(00)00050-9.

Tang, X., Ripepi, N. and Gilliland, E. (2016) 'Isothermal adsorption kinetics properties of carbon dioxide in crushed coal', *Greenhouse Gases: Science and Technology*, 6(2), pp. 260–274. doi:10.1002/ghg.1562.

Thomas, L. (2013) *Coal Geology*. II. Oxford, UK: Wiley-Blackwell. ISBN: 9781119990444.

Thwaites, N. and James, L. (2014) 'Well Design Evolution Towards the First Commercial Unconventional Gas Flowrate in Europe - SPE 167701', in *SPE/EAGE European Unconventional Resources Conference and Exhibition*. Vienna, Austria: Society of Petroleum Engineers. doi:10.2118/167701-MS.

Torgersen, T. and Kennedy, B. M. (1999) 'Air-Xe enrichments in Elk Hills oil field gases: Role of water in migration and storage', *Earth and Planetary Science Letters*, 167(3–4), pp. 239–253. doi:10.1016/S0012-821X(99)00021-7.

Torgersen, T., Kennedy, B. M. and van Soest, M. C. (2004) 'Diffusive separation of noble gases and noble gas abundance patterns in sedimentary rocks', *Earth and Planetary Science Letters*, 226(3–4), pp. 477–489. doi:10.1016/j.epsl.2004.07.030.

Underhill, J. R., Monaghan, A. A. and Browne, M. A. E. (2008) 'Controls on structural styles, basin development and petroleum prospectivity in the Midland Valley of Scotland', *Marine and Petroleum Geology*, 25(10), pp. 1000–1022. doi:10.1016/j.marpetgeo.2007.12.002.

Vermeesch, P. (2008) 'Three new ways to calculate average (U–Th)/He ages', *Chemical Geology*, 249(3–4), pp. 339–347. doi:10.1016/j.chemgeo.2008.01.027.

Vincent, C. J., Rowley, W. J. and Monaghan, A. A. (2010) 'Thermal and burial history modelling in the Midlothian-Leven syncline in the Midland Valley of Scotland using BasinMod and HotPot', *Scottish Journal of Geology*, 46(2), pp. 125–142. doi:10.1144/0036-9276/01-376.

Wang, G., Wang, K. and Ren, T. (2014) 'Improved analytic methods for coal surface area and pore size distribution determination using 77K nitrogen adsorption experiment', *International Journal of Mining Science and Technology*, 24(3), pp. 329–334. doi:10.1016/j.ijmst.2014.03.007.

Wells, C. B. M., Field, A., Thwaites, N., Energy, D., Suh, A. and International, S. D. (2014) 'SPE 167700 Use of Near Bit Azimuthal Gamma Ray and Inclination Tool Improves'.

Whiticar, M. J. (1994) 'Correlation of natural gases with their sources', in *The Petroleum System - from Source to Trap*. AAPG Special Edition, pp. 261–283.

Yatsevich, I. and Honda, M. (1997) 'Production of nucleogenic neon in the Earth from natural radioactive

decay', *Journal of Geophysical Research: Solid Earth*, 102(B5), pp. 10291–10298. doi:10.1029/97JB00395.

Yi, J., Akkutlu, I. Y., Karacan, C. Ö. and Clarkson, C. R. (2009) 'Gas sorption and transport in coals: A poroelastic medium approach', *International Journal of Coal Geology*, 77(1–2), pp. 137–144. doi:10.1016/j.coal.2008.09.016.

Zaikowski, A. and Spangler, R. R. (1990) 'Noble gas and methane partitioning from ground water: An aid to natural gas exploration and reservoir evaluation', *Geology*, 18(1), p. 72. doi:10.1130/0091-7613(1990)018<0072:NGAMPF>2.3.CO;2.

Zartman, R. E., Wasserburg, G. J. and Reynolds, J. H. (1961) 'Helium, argon, and carbon in some natural gases', *Journal of Geophysical Research*, 66(1), pp. 277–306. doi:10.1029/JZ066i001p00277.

Zhao, Y., Liu, S., Elsworth, D., Jiang, Y. and Zhu, J. (2014) 'Pore Structure Characterization of Coal by Synchrotron Small-Angle X-ray Scattering and Transmission Electron Microscopy', *Energy & Fuels*, 28(6), pp. 3704–3711. doi:10.1021/ef500487d.

Zhou, Z., Ballentine, C. J., Kipfer, R., Schoell, M. and Thibodeaux, S. (2005) 'Noble gas tracing of groundwater/coalbed methane interaction in the San Juan Basin, USA', *Geochimica et Cosmochimica Acta*, 69(23), pp. 5413–5428. doi:10.1016/j.gca.2005.06.027.

Zhou, Z. and Ballentine, C. J. (2006) '4He dating of groundwater associated with hydrocarbon reservoirs', *Chemical Geology*, 226(3–4), pp. 309–327. doi:10.1016/j.chemgeo.2005.09.030.

4 Noble Gas and Stable Isotope Characterisation of Gases from Abandoned Mine Methane Sites in Central England

4.1 Introduction

Coal Mine Methane (CMM) refers to any gas associated with the coal production process. One component of this is Abandoned Mine Methane (AMM), an unconventional gas source associated with abandoned mine workings. Methane in abandoned mines occurs in the collapsed areas of workings from which coal has been removed (termed 'gob'), and adjacent unmined seams that have been destressed by mining. This gas is often vented to the atmosphere, but can be utilised in AMM schemes by extraction with vacuum pumps.

Historic coal production has left a legacy of abandoned mines across the UK which are maintained by the Coal Authority. Coal mines are often located near to homes and industry, and many cases of stray gas from mines have been recorded; the entire town of Arkwright in Derbyshire was relocated 1 mile away in the early 1990's due to elevated methane concentrations recorded in buildings (Appleton, 2011). Coal gases may accumulate in old workings, and migrate to the surface along fractures, faults, boreholes, vents, shafts, or bedding planes, *etc*. which can be numerous in mined areas. Episodic releases of mine gases can be caused by changes in barometric pressure, or the rising water table in mines after abandonment (Krause and Pokryszka, 2013).

Elevated concentrations of methane present a hazard as concentrations between 5 – 15% in air are highly explosive, and can be an asphyxiant at greater concentrations. This problem is compounded in confined spaces such as cellars, caves or tunnels. Elevated CO_2 concentrations arising from mines also pose a threat as it is heavier than air and sinks into depressions such as cellars and trenches and can cause asphyxiation,

a problem particularly prone to NE England's coalfields due to their high CO_2 content (Appleton *et al.*, 1995; Appleton, 2011). Utilisation of AMM helps to reduce greenhouse emissions, can aid in preventing stray gas migration, and turns a potentially hazardous 'waste' by-product into a valuable commodity.

Primarily, the aim of this project is to characterise AMM gas geochemistry to define geochemical 'fingerprints', which can be used in source-to-sink models of gas migration to help solve real-world problems of identifying stray gases in the shallow subsurface. Other key advantages include determining hydrocarbon origin in coals (thermogenic vs. biogenic), predicting the evolution of gas geochemistry over time, and evaluating unprofitable air ingress to allow improved utilisation of AMM gases.

Sources of methane in the UK include carbonaceous shales, peat, landfills and other accumulated organic matter (*e.g.* buried ponds, lake sediments), but the greatest hazard is coal bearing rocks and abandoned mines (Appleton, 2011). The geochemistry of abandoned mine gases can change over time, overlap with other methane sources, and is often ambiguous as to its generation pathway which can problematic when ascribing a cause to any stray gas detected in the shallow subsurface.

Abandoned mines represent a more altered environment than typical Coal Bed Methane (CBM) deposits as the mining process exposes the subsurface to the oxic atmosphere, leading to significant chemical changes and redox conditions atypical of the subsurface. Furthermore, the more weathered environment and extensive fracture networks expose greater volumes of rock and enhance the potential for contemporaneous microbial activity through the greater availability of microbial substrates and inoculation of strata.

In this study, 6 samples of AMM gases from the East Pennine coalfield were collected and analysed for major gas composition, stable isotopes of methane and carbon dioxide, noble gases, and radiocarbon content. AMM gases were found to vary in methane, ethane, carbon dioxide, and nitrogen contents, as a result of the mixing between coalification gas desorbing from coals and atmospheric ingress into the mines. The presence of thermogenically generated higher molecular weight hydrocarbons ($C_1/(C_2+C_3)$ = 21 to 69) distinguish AMM gases from other potential sources of shallow methane, such as landfill gas.

The stable isotope values fall in a relatively narrow range ($\delta^{13}C_{CH4}$ = 47.4 to 51.0‰; δD_{CH4} = -211 to -238‰) and suggest a mixed thermogenic-biogenic methane system, overlapping with previous coal gas and landfill measurements in the area. Radiocarbon

measurement shows that AMM does not contain modern carbon, which is generally expected of fossil coal gases. The helium concentrations were high (350 - 1506 ppm) which appears to be ubiquitous in UK Paleozoic strata. The concentrations were considerably above the atmospheric value, and dominated by radiogenic ^{4}He. The noble gases showed a dilution of crustally derived components with a mixture of atmospheric air sources and degassed air saturated water. Some samples show elevated Kr and Xe which is attributed to interaction with an oil phase.

Several commonly used diagnostic plots used to determine hydrocarbon origins do not take into consideration the complexities of coal systems, and their caveats are discussed. The nature and origin of gases is explained, and the possibility of ongoing microbial methanogenesis is evaluated.

4.2 Longwall Mining

As AMM by definition requires a mine to exploit, it is pertinent to discuss the mine environment and primary method of coal extraction in order to understand the AMM process. Almost all modern mechanised deep coal mines employ some form of longwall mining; a process where two parallel access roads are cut into a coal seam, typically spaced ~250 m apart in British mines, and a mechanically driven cutter is propelled across the coalface removing the coal in long strips about ~0.7 m wide from the rectangular 'panel' (Creedy, 1991; Thomas, 2013). The coal is then loaded onto a conveyor and carried to an access road for removal from the mine. Both 'advance' and 'retreat' methods can be used; advance, where the machinery advances against the coalface driving the access tunnels as mining progresses, or retreat, where the access roads are driven first and the cutting face retreats back along the unmined coal panel (Creedy, 1991), see Figure 4-1.

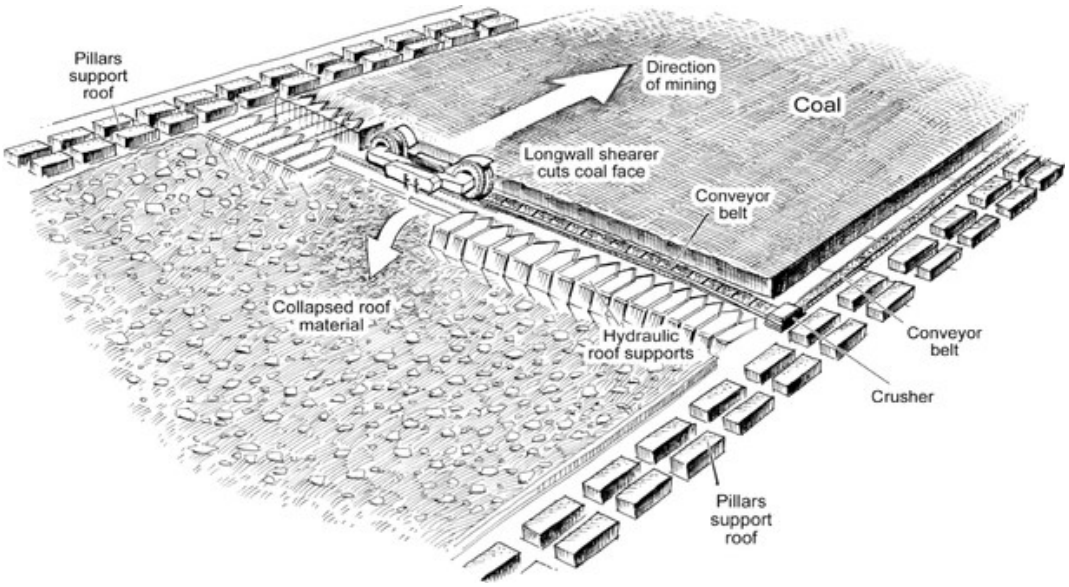

Figure 4-1 – Cartoon of retreat longwall coal mining. The coal cutter/shearer traverses upper-left to lower right, perpendicular to the two access roads. Diagram from US Gov. SEC, (2011).

The roof above the cutter is propped up with hydraulic jacks, and after a strip is cut away the machinery advances to the uncut face, unpropping the roof behind and allowing it to collapse into the void space (see Figure 4-2). The longwall method of mining results in a more complete extraction of coal compared to other methods as little to no coal is left in place to prop up the roof, consequently it is responsible for significant surface subsidence and seismic activity (Thomas, 2013). The subsided mass of rock debris behind the machinery is known as “waste”, “gob” or “goaf”; a permeable mass of collapsed rubble consisting of unmined coal originally at the base and top of the coal unit (sometimes deliberately unmined due to impurities), and overlying rock units. The collapsed zone is estimated to be 3-6 times the thickness of the mined seam, possibly up to 12 times where rocks are weak and porous (Palchik, 2003, and references therein). Directly above the gob area, vertical and horizontal fractures form in the overburden, possibly extending up to 200 m above and 100 m below the worked seam in UK coals (Creedy, 1991, and references therein), that can extend to another mined areas, major faults, or the surface, which increases the risk of fugitive gas migration (Palchik, 2003).

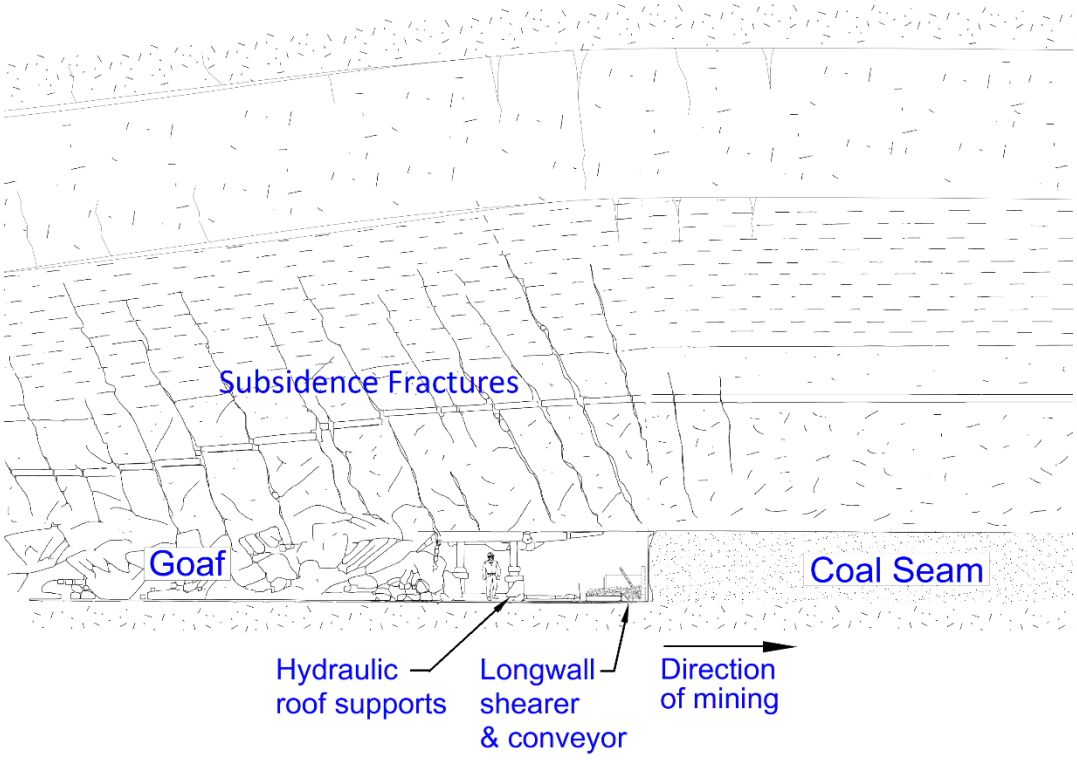

Figure 4-2 – Cartoon of longwall mining cross-section, depicting the unmined seam, the collapse of the roof behind the advancing coalface, and the stresses and fractures imparted on the strata. Image modified from: http://www.minesubsidence.com/index_files/files/Intro_Longwall_Mining_and_Subs.pdf

The low permeability of coals in the UK means gas is not easily desorbed from coals further from the worked coal face, typically requiring physical disturbance to degas into the cleat system, mined sections, or natural or induced fractures (CEC, 1988). The permeability of coals and surrounding strata is greatly increased via stress reduction, which creates and relaxes fractures. This increased permeability decreases the pressure in the surrounding rocks by exposing them directly to the atmospheric pressure in the mine, and leads to gas release (Creedy *et al.*, 2001; DTI, 2004). This makes longwall mining a powerful factor in UK mine gas emissions. During the mining process 85-90% of methane in longwall mines is from adjacent units, with lesser amounts from the working face (Creedy, 1991). Adjacent seams may be permeable sands with not-insignificant gas reserves, or thin un-mineable coal seams with significant gas generation potential (Creedy, 1991). "Gob gas"; gas from the collapsed workings behind mined faces can be 30% to 90% methane usually mixed with air during the mining process (Creedy, 1988, 1991).

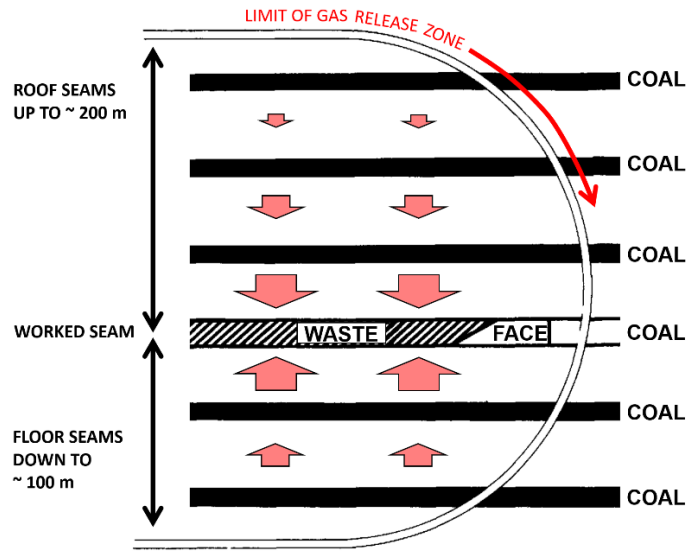

Figure 4-3 – Schematic of coal gas contributions to mine atmospheres during longwall mining, modified from Creedy, (1991). Major contributions to the mine emanate from surrounding strata, especially those in the overburden above the workings that are heavily fractured due to subsidence.

Much of the gas within the mine area will have been drained via boreholes prior to mining or vented to the atmosphere during the lifetime of the mine. The amount of gas remaining for an AMM scheme will depend on initial gas content and the proximity to any destressed workings. Coal units furthest away from the workings will have retained the most gas, however they are unlikely to provide significant contributions to gas output, as the suction pressure from the vacuum pumps is unlikely to be experienced far away from the main roadways and major fracture networks (Creedy, 1991; Creedy *et al.*, 2001; DTI, 2004).

British coal mines often have a long history of production and have employed a variety of mining methods over the life of the mine. Other forms of mining than longwall *e.g.* pillar and stall workings are less prone to subsidence and leave more coal unmined underground. More modern mines will typically employ only longwall mining, which creates more developed fracture networks which may potentially reach the surface. In the UK, the mining of several coal seams within a vertical succession is common especially in older mines, where seams were exhausted and work started at greater depths adding complexity and volume to the mine structures, *e.g.* Figure 4-4.

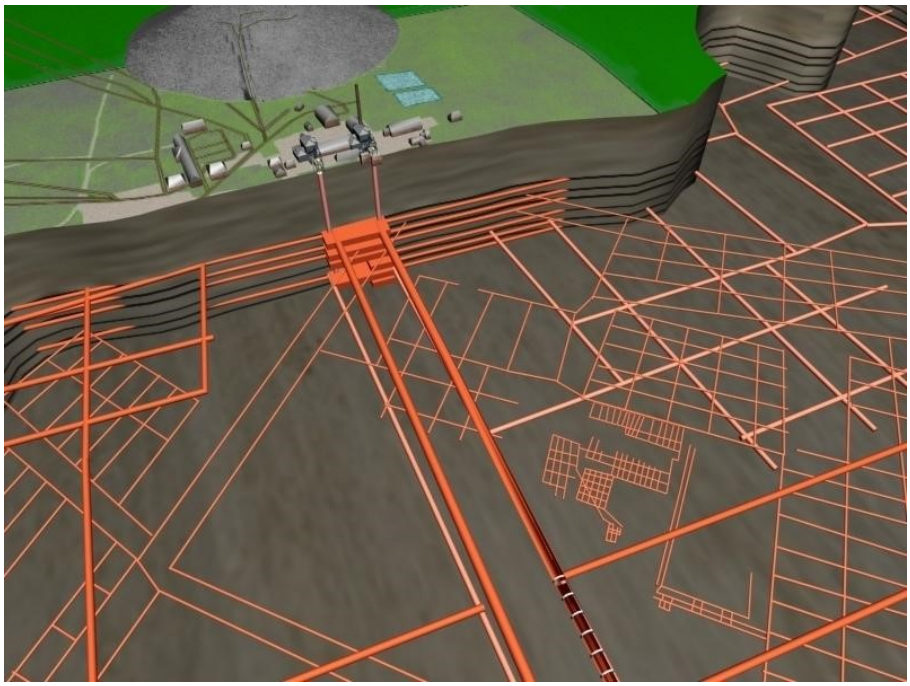

Figure 4-4 – Left: CGI render of longwall workings at Woodhouse Colliery, Northumberland. Workings were sunk to 6 seams over an extensive lateral area. Image © Durham County Council, reproduced from http://www.pastperfect.org.uk.

In a typical CBM development, the strata are minimally disturbed and gas is typically produced from a single seam per lateral well. In contrast, gases from AMM schemes come from much larger volumes, with much more developed major fracture networks, where an extensive network of linked roadways, goaf areas, and heavily fractured surrounding strata form the boundary of the reservoir.

4.3 AMM Processes

After mining operations cease at an underground coal mine air, water pumping to prevent mine flooding is stopped, the ventilation systems are shut down, and the shafts are sealed and abandoned (DTI, 2004). This results in the build-up of coal gases in the mine atmosphere and a rise in the groundwater table in the period of months to years (Thomas, 2013). In some cases this can result in a "water piston" effect, whereby the rising water forces the mine gases into connected workings, along bedding planes and faults, and upwards into shafts and fractures, which can extend to the surface in shallower mines (Kotarba and Korus, 2002; Krause and Pokryszka, 2013; Sechman *et al.*, 2013). Fluctuations in atmospheric pressure can also lead to enhanced degassing at low pressures (Hemp, 1998), and incidents of ingress of mine gas into homes can be

correlated with low barometric pressure weather conditions. Mine gas drainage vents are purposefully located in safe and strategic locations to allow the effective mitigation of this hazard. When coals are re-submerged under rising water, their ability to desorb methane and for this methane to migrate is significantly diminished (Krause and Pokryszka, 2013).

Methane leakage from abandoned mines in the UK produced an estimated 31 kilotons/year in 2015 and will continue to be emitted for decades (Kershaw and Whitworth, 2005). AMM schemes help to mitigate problems with methane by both utilising what would normally be vented to the atmosphere, and creating subsurface conditions where the control of gas flow can be managed preventing fugitive emissions to the surface.

AMM is extracted by the effective sealing of mine shafts, or by directional drilling into old workings or destressed gob areas (DTI, 2004). Suction pumps are installed at the wellhead or vent to lower the mine atmosphere's pressure, providing a pressure gradient to aid further methane desorpsion from coals, and this vacuum pressure is conveyed to other areas of the mine by the network of roadways and shafts (Creedy *et al.*, 2001; DTI, 2004). The primary source of gas is derived from worked coal seams in gob/goaf areas and destressed areas surrounding the workings, and the whole unflooded section of the mine and surrounding destressed area can be considered the reservoir boundary (Creedy *et al.*, 2001; DTI, 2004). It is possible that some gas could also be derived from secondary microbial action degrading the coals as well as the significant amounts of timber left in the mine after abandonment (Beckmann, Krüger, *et al.*, 2011; Sechman *et al.*, 2013; Kang *et al.*, 2016).

Creedy et al., (2001) and Ren, (2004) identified several criteria for effective AMM scheme, which excluding economic factors are:

- Large area of subterranean workings, pneumatically connected by roadways and shafts.
- Large destressed rock volume surrounding workings.
- Suitable connection from the surface to the subsurface *e.g.* unfilled shaft or drift, a specially drilled well, or pipework installed prior to mine abandonment (*e.g.* Prince of Wales colliery).
- Sufficient residual methane content in surrounding unmined seams.
- No connections to surface, either via connections to shallow workings or fractures to the surface to prevent air ingress.

- Minimal groundwater rebound and little chance for water to pool in roadways, reducing connectivity between areas.

The primary use for AMM gases in the UK is fuelling electrical generators connected to the National Grid in so called "gas-to-wire" schemes.

4.4 East Pennine Coalfield and Sample Locations

The West Yorkshire and Nottinghamshire coalfields are located in the north east of the Midlands region of England (Figure 4-6, Table 8). The coalfields belong to the East Pennine Coalfield, the most productive of all the UK coal measures (Allen, 1995). The majority of mines exploit the Top Hard (a.k.a. Barnsley) coal seam, with various other seams contributing to mined output depending on local coal seam stratigraphy. A generalised stratigraphy of the commonly mined coals is given in Figure 4-5.

The majority of mined seams lie in the Westphalian Pennine Middle Coal Measures Group (313 to 304 Ma). The coals were deposited in cycles typically grading upwards from mudstone, siltstone, sandstone and coal (Waters, 2009). In general, the coals crop out in an NNW-SSE orientated band west of Doncaster and Nottingham, and dip gently to the east under Permian sandstones where they form the significant resources of the concealed coalfields. There is an increase in coal seam gas contents and the thickness of the Westphalian coal measures towards the NW (Creedy and Pritchard, 1983; DECC, 2013)

The maturity of UK coals observed today is believed to have been attained prior to the uplift caused by the Variscan orogeny in the late Carboniferous (Creedy, 1988). The Carboniferous maturity pattern and its effect on gas content and permeability have been modified subsequently by Variscan and later uplifts, which have led to degasification and migration of gas into conventional reservoirs. This has occurred in the Southern North Sea and Cleveland Basin, although a Westphalian source for other onshore gas fields and discoveries is not proven (DECC, 2013). Subsequent reburial in Permian and Mesozoic times has not produced equivalent burial depths, except in the Cheshire and Cleveland basins (DECC, 2013). The post-Carboniferous subsidence has preserved the gas content downhole gradients and coal ranks as these are both related, unless methane has migrated back into coal seams subsequently. This seems unlikely,

given the very low permeability of the coals, but it is more likely where mining has taken place. The gas contents of seams where no mining has taken place are known to be higher. Dawson (1954) showed that in the Haig Mine, Cumberland, the gas content of the Bannock seam was between 3 to 7 times lower where the Main seam had been mined 37 m below, 8 years previously.

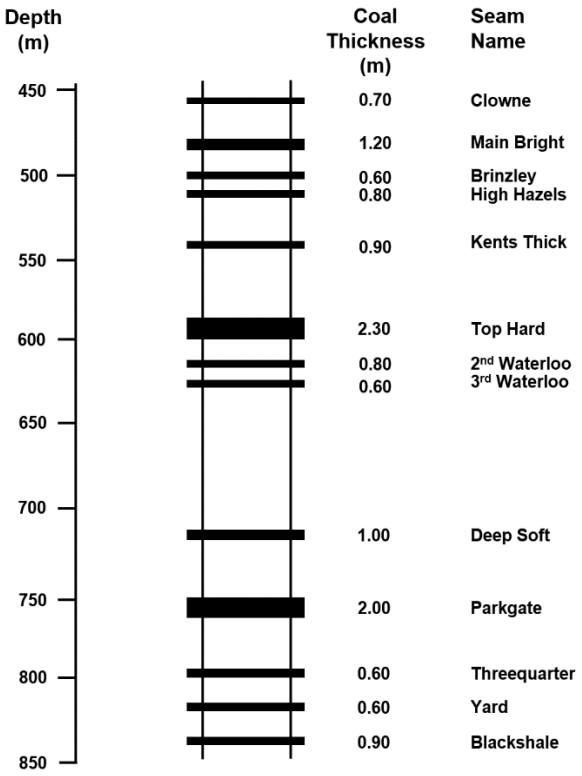

Figure 4-5 – Generalised stratigraphic sequence of named coal seams in the Coal Measures, length units in metres (modified from Allen, (1995))

The AMM wells sampled in this study target individual collieries, details of which are given below. All AMM sites were operated by Alkane Energy Ltd. who provided some mine information on-site. Depth data are after the UK Onshore Geophysical Library (www.ukogl.org.uk), completion dates are after the BGS Borehole Record, (http://www.bgs.ac.uk/data/boreholescans/home.html).

Site	Latitude	Longitude
Old Mill Lane-1	53.15268	-1.18381
Prince-of-Wales-1	53.69743	-1.31276
Warsop-1	53.20794	-1.17647
Crown-Farm-1	53.14918	-1.14945
Bevercotes-1	53.26255	-0.95882
Newmarket-Lane-1	53.72546	-1.44914

Table 8 – List of sample locations

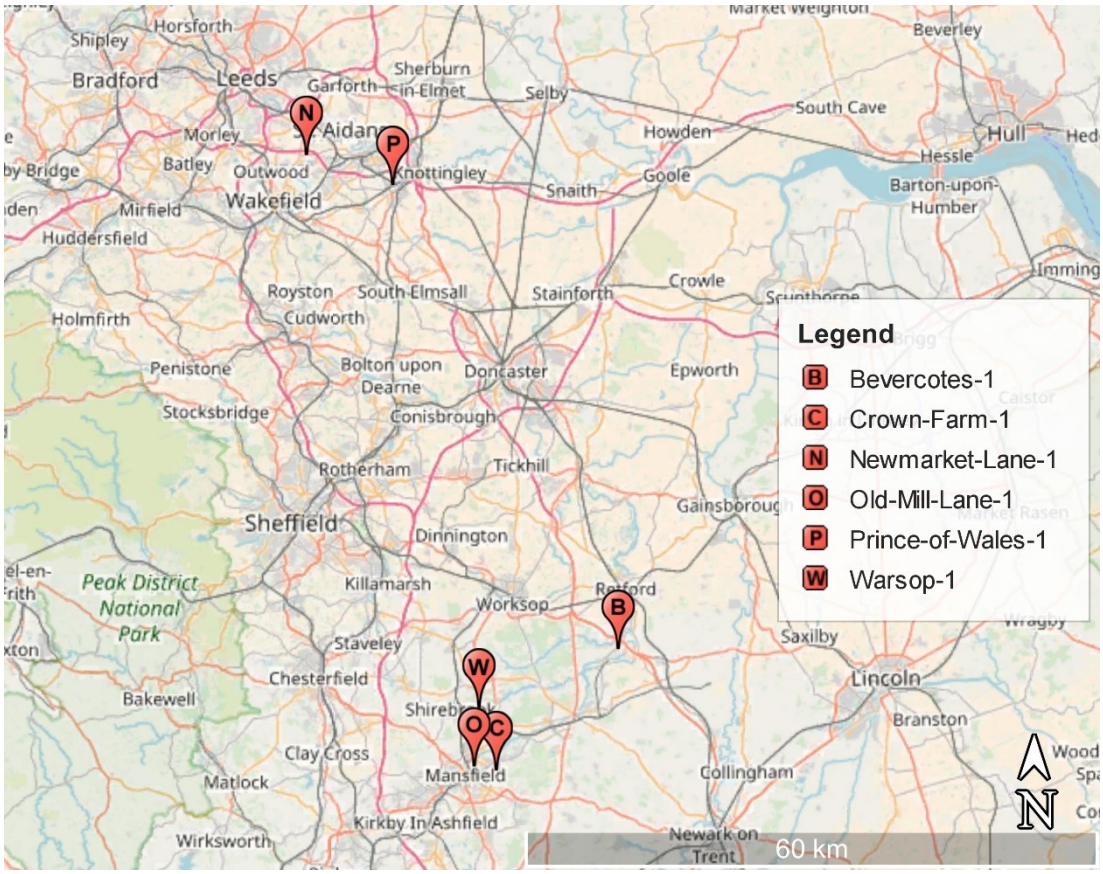

Figure 4-6 – Map of sampled AMM sites (red pins) in relation to larger towns. Map © OpenStreetMap.

4.4.1 Prince of Wales

The Prince of Wales Colliery was constructed on the site of an existing mine, on the northern edge of Pontefract in West Yorkshire. Work on the drift tunnels was started in 1975 and production commenced in the Castleford Four Foot (known elsewhere as "Clowne"/"Newhill") seam in 1980 and three other seams were exploited. The colliery closed in 2002, after producing some 1.5 million tonnes of coal per year. As part of UK

Coal closure plans, Alkane Energy were permitted to install a 4.7 km pipe from the surface to the deep drifts, which is now connected to a 1.5 MW electricity generating plant (Alkane Energy, 2008). The last seam to be worked was the Warren House (part of Top Hard) seam, at ~500 m depth (*Prince of Wales Colliery History*, 2002).

4.4.2 Sherwood (Old-Mill-Lane)

The Sherwood colliery was developed by the Bolsover company in 1902 to a depth of 421 m. Output was initially mainly from the Top Hard Seam and Dunsil Seam, abandoned in 1959, then further production coming from the Deep Hard, Piper, Yard and Blackshale seams. The colliery closed in 1992 (Mansfield Heritage, 2015). Old Mill Lane-1 is a vertical well intersecting the worked seams ~1 km from the shaft location, spud on 18th November2001, reaching 393 m MDBGL (300 m TVDSS) (UKOGL, 2017).

4.4.3 Warsop

The Warsop Main Colliery, located near the town of Warsop, opened in 1893 to exploit the Top Hard seam. The High Hazel, Main Bright, Clowne and Deep Soft seams were also exploited during the mine's long life, before closure in 1989 (*Warsop Vale Local History Society*, 2002). The Warsop-1 well is comprised of a vertical section (222 m MDBGL) with lateral (345 m MDBGL), which reaches the Coal Measures at 69 m MDBGL. It was spud on 12the March 2002 and completed by the 10th April 2002 (UKOGL, 2017).

4.4.4 Mansfield Colliery (Crown Farm)

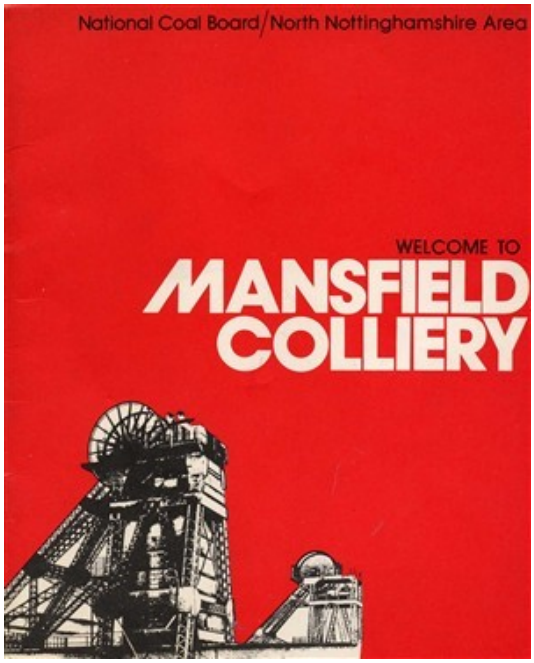

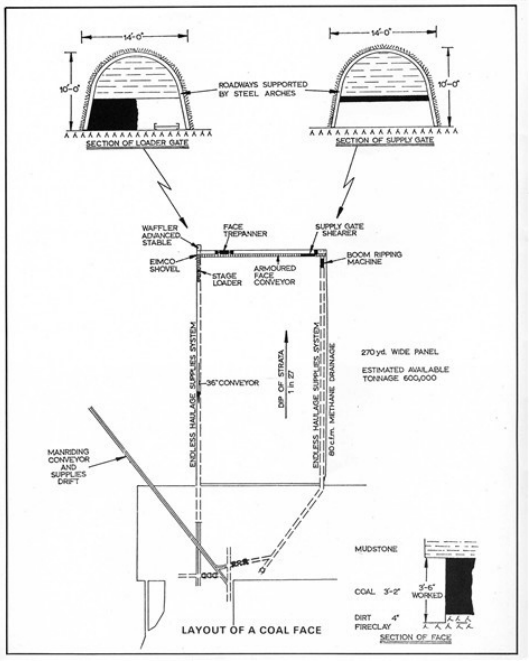

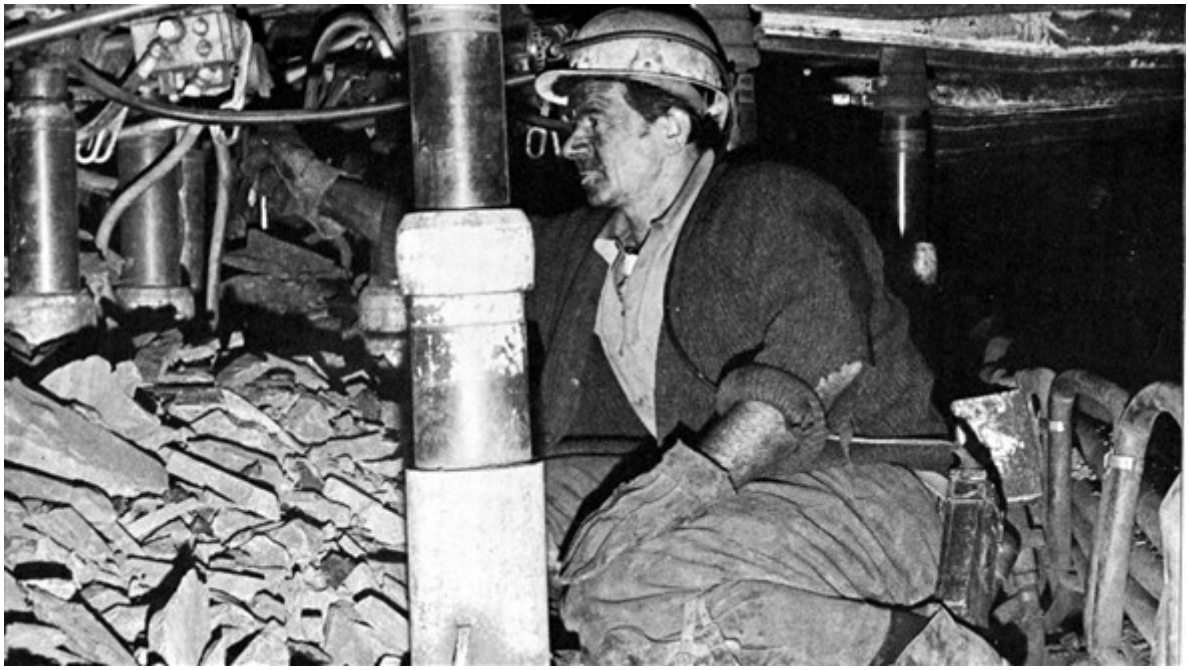

Upper left: cover for NCB brochure for Mansfield Colliery. Upper right: schematic of roadways and longwall panels at Mansfield Colliery. Lower: A miner advancing hydraulic chocks at Mansfield colliery circa ~1970's. The normal working height of the seams was ~4 ft (1.2 m). Photos © NCB and www.ourmansfieldandarea.co.uk, and reproduced here with kind permission.

The Mansfield colliery (unofficially named Crown Farm colliery due to proximity to a local farm) was sunk by the Bolsover Colliery Company in 1904, where the Top Hard

seam (~1.6 m thick) was reached at 487 m depth. Development of the Hazel seam started in 1930 and of the Lower Seam in 1940. Production continued to 1988 and the shaft was infilled and colliery closed in 1989 (Marples, 2009). Crown-Farm-1 was spud on 3rd February 2006, and is one of the 2 vertical wells reaching the Coal Measures at 184 MDBGL, and terminating at 417 MDBGL (310 MTVDSS) (UKOGL, 2017). The gas feeds 4 generators and provides gas for a local textile mill.

4.4.5 Bevercotes Colliery

Shearer cutting the Top Hard seam at Bevercotes, circa ~1990's. © forum user "Bones"; https://www.aditnow.co.uk/ and reproduced here with kind permission.

Bevercotes colliery is located near to the village of Bevercotes in Nottinghamshire. The first shaft was sank in 1953 and briefly abandoned a few years later, before the mine re-opened with state-of-the-art equipment in 1963, and closed in 1993. The target seam for the mine (Top Hard) was found to be locally washed out, so the shaft was sunk to the lower Dukeries seam (aka. Parkgate), which is known to be oil-prone (Huxley, 1983). Oil is known to persistently emanate from faults at Bevercotes (Creedy, 1988),

and reportedly caused issues, with more oil being produced than coal in early years that was sold to BP. The mine is not far from the Bothamsall and Eakring oil fields.

Bevercotes-1 was spud on 14the September 2002 and completed on the 8th November 2002. The well enters the Coal Measures unit at 384 m MDBGL and targets the deepest seam at 724 m MDBGL (700 m TVDSS) (UKOGL, 2017).

4.4.6 Newmarket Lane

The Newmarket Lane Colliery, located near Stanley in West Yorkshire opened in 1837 and closed in 1983, making it one of the oldest mines in the UK (*Newmarket Colliery History*, 2009). Newmarket-Lane-1 is a deviated well 273 m in length, spud 19/11/2008, and targets a Silkstone seam roadway, which ceased to be mined in 1940 (*Newmarket Colliery History*, 2009; Alkane Energy, 2009).

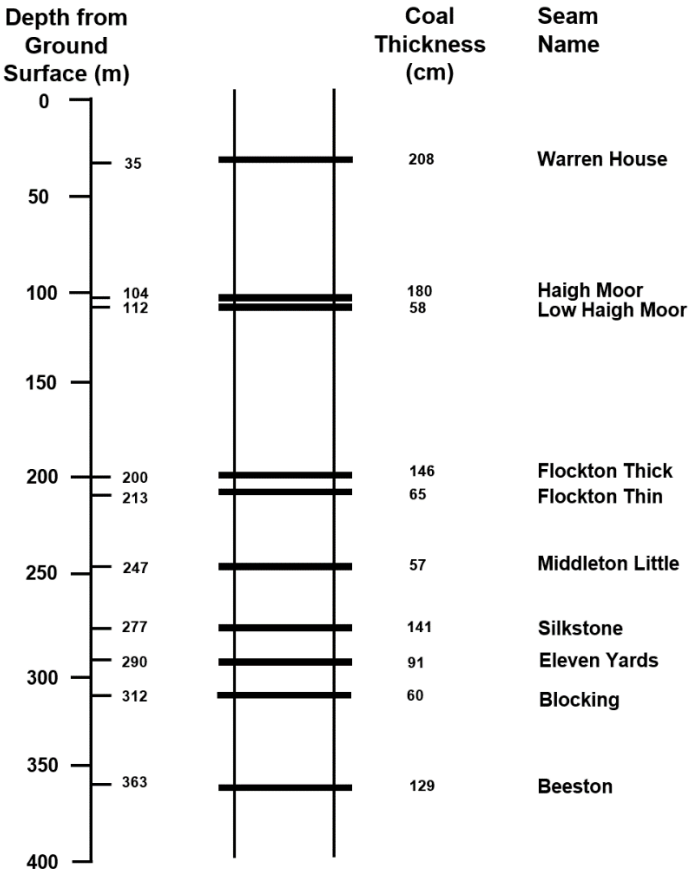

Figure 4-7 – Section at Newmarket Colliery Shaft indicating coal seams, data from Alkane Energy (2009).

4.5 Results

6 samples from English AMM schemes operated by Alkane Energy Ltd. were collected in July 2014, and analysed for bulk gas composition, carbon and hydrogen stable isotopes (February 2017), noble gases (March 2016), and 1 sample for radiocarbon of methane (March 2016). See Methodology (this volume) for descriptions of analytical procedures.

4.5.1 Bulk Gases

Major gases in most AMM samples consisted mainly of methane, with appreciable nitrogen and carbon dioxide contents, with minor ethane and propane. Methane in samples ranged from 35% to 79% (see Table 9). Methane was the dominant species in all samples except for Old-Mill-Lane-1, where the methane concentration was ~35%, and high percentages of N_2 were calculated, suggesting dilution with the atmosphere. CO_2 concentrations ranged from 1.9% to 26.1%. No carbon monoxide, ethylene, oxygen, or acetylene were detected.

The gases are considered 'wet', with $C_1/(C_2+C_3)C_2+C_3 < 50$, excepting Prince-of-Wales-1 (Whiticar, 1999; Strąpoć *et al.*, 2011). These levels are significantly 'wetter' than biogenically derived gas (where typically $C_1/(C_2+C_3)$ = >1000), and indicate a significant thermogenic component (Rice, 1993; Strąpoć *et al.*, 2008). Prince-of-Wales-1 shows the highest C_1/C_2+C_3 ratio (69), indicating the lowest relative C_{2+} hydrocarbon contents. Bevercotes-1 and Warsop-1 show the lowest C_1/C_2 and $C_1/(C_2+C_3)$ ratios showing greater higher-hydrocarbon content (Table 10). Oil shows are observed in the Bevercotes mine, and this sample shows a wetter character, but no oil association is documented at Warsop. Overall, the samples are not overly enriched with heavier hydrocarbons compared with average UK coal gas samples (*e.g.* Figure 4-20). CH_4/CO_2 ranges from 2.5 (Crown-Farm-1) to 43 (Prince-of-Wales-1). There is no observed correlation between CH_4 concentration and hydrocarbon ratios (C_1/C_2 or $C_1/[C_2+C_3]$), between hydrocarbon ratios and C_1/CO_2 ratios, or between CO_2 and nitrogen content.

	Methane %	Ethane %	Propane %	CO_2 %	N_2 %
Prince-of-Wales-1	79	1.03	0.10	1.9	18
Bevercotes-1	70	2.88	0.62	7.6	19
Old-Mill-Lane-1	49	1.40	0.26	11.0	39
Warsop-1	62	2.66	0.34	26.1	9
Newmarket-Lane-1	74	1.86	0.26	9.8	15
Crown-Farm-1	35	0.74	0.13	14.3	49

Table 9 – Approximate absolute concentrations of major gas species in AMM samples. N.B. These values are taken and calculated from a single analysis of each gas, and certain caveats apply, see GC section in Methodology

	C_1/C_2	d	C_1/C_3	d	$C_1/(C_2+C_3)$	d	C_1/CO_2	d
Prince-of-Wales-1	76	0.12	752	3.3	69	0.22	43	0.22
Bevercotes-1	24	0.04	110	0.5	20	0.06	9.1	0.05
Old-Mill-Lane-1	35	0.05	208	0.9	30	0.10	4.4	0.02
Warsop-1	23	0.04	186	0.8	21	0.07	26	0.13
Newmarket-Lane-1	39	0.06	279	1.2	35	0.11	7.5	0.04
Crown-Farm-1	48	0.08	258	1.1	40	0.13	2.5	0.01

Table 10 – Table of bulk gas ratios for AMM samples. C_1, C_2, and C_3 refer to methane, ethane, and propane respectively.

4.5.2 Stable Isotopes

The carbon ($\delta^{13}C_{CH4}$) and hydrogen (δD_{CH4}) isotopic ranges of the methane in the AMM gases (Table 10) fall firmly in the thermogenic range as defined by Schoell (1980) (See Figure 4-8).

	$\delta^{13}C$	δD	$\delta^{13}C_{(CO2)}$
Prince-of-Wales-1	-49.62	-232.8	-24.52
Bevercotes-1	-46.54	-219.4	N/A
Old-Mill-Lane-1	-50.43	-238.2	N/A
Warsop-1	-51.08	-230	-7.94
Newmarket-Lane-1	-47.41	-223.3	-13.79
Crown-Farm-1	-48.83	-210.5	-11.14

Table 11 – Table of stable $\delta^{13}C_{CH4}$, δD_{CH4}, and $\delta^{13}C_{CO2}$ for AMM gases. 1σ standard deviation of carbon isotopes is 0.3‰, and 3‰ for hydrogen.

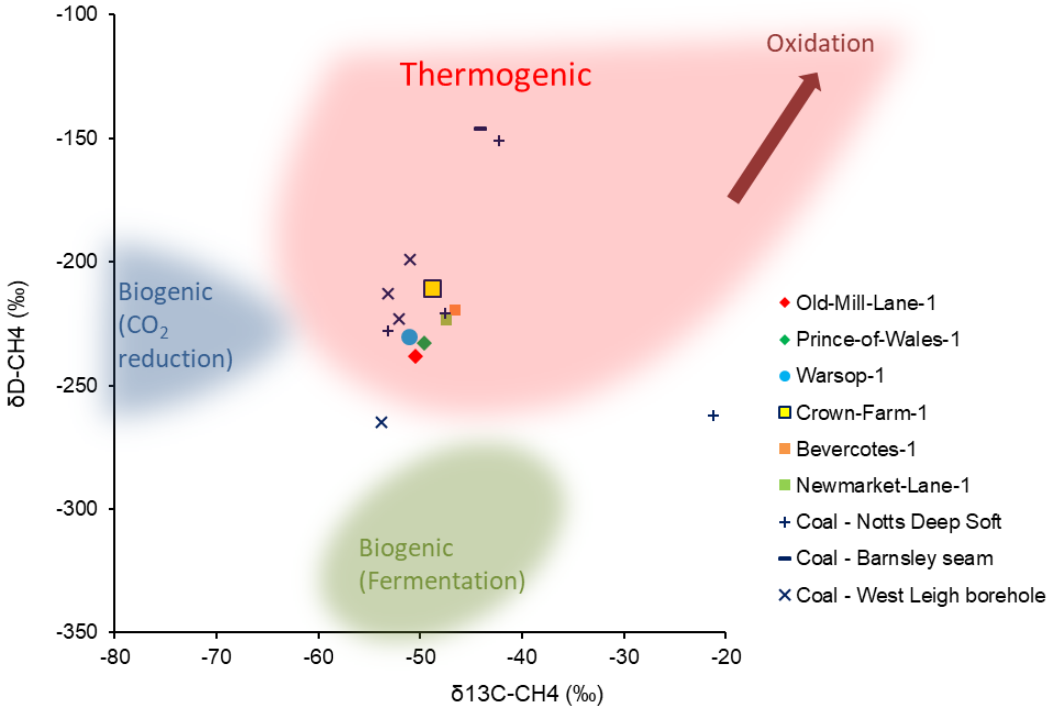

Figure 4-8- Plot of $\delta^{13}C_{CH4}$ vs. δD_{CH4} for English AMM gases, after Schoell, (1980). Data from individual mines (this study). Data from Coal – Notts Deep Soft, Barnsley seam, and West Leigh borehole from Hitchman et al., (1989).

A "Bernard" plot (Figure 4-9) shows the samples also falling into or very close to the thermogenic regime, with Old-Mill-Lane-1 and Warsop-1 displaying slightly lighter isotope values just outside the thermogenic boundary, but falling within the bounds of thermogenic gases for hydrocarbon composition. There is no significant relationship within this dataset between $\delta^{13}C_{CH4}$ isotope values and major gas composition, which would be suggestive of thermal maturity trends or varying microbial input.

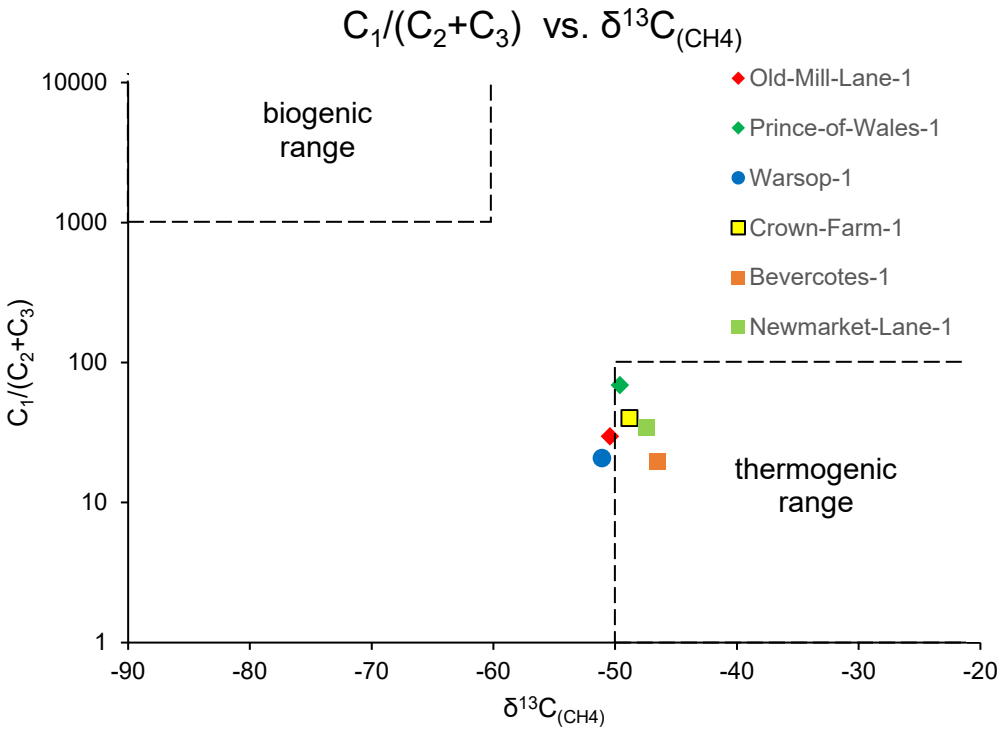

Figure 4-9 - The 'Bernard plot' of molecular and C isotope composition of English AMM gases. Redrawn after Hachikubo et al. (2015) (Fields modified after Bernard et al., (1978)).

4 of 6 samples were analysed for $\delta^{13}C_{CO2}$. The $\delta^{13}C_{CO2}$ values are heavier than the $\delta^{13}C_{CH4}$ values, with the maximum value of -7.9‰ (Warsop-1) and a minimum of -24.5‰ (Prince-of-Wales-1). There is a correlation between the concentration of the CO_2 and $\delta^{13}C_{CO2}$ values, with greater CO_2 concentrations becoming enriched in ^{13}C (see Figure 4-10). There is no apparent correlation between C_1/CO_2 and $\delta^{13}C_{CO2}$ values.

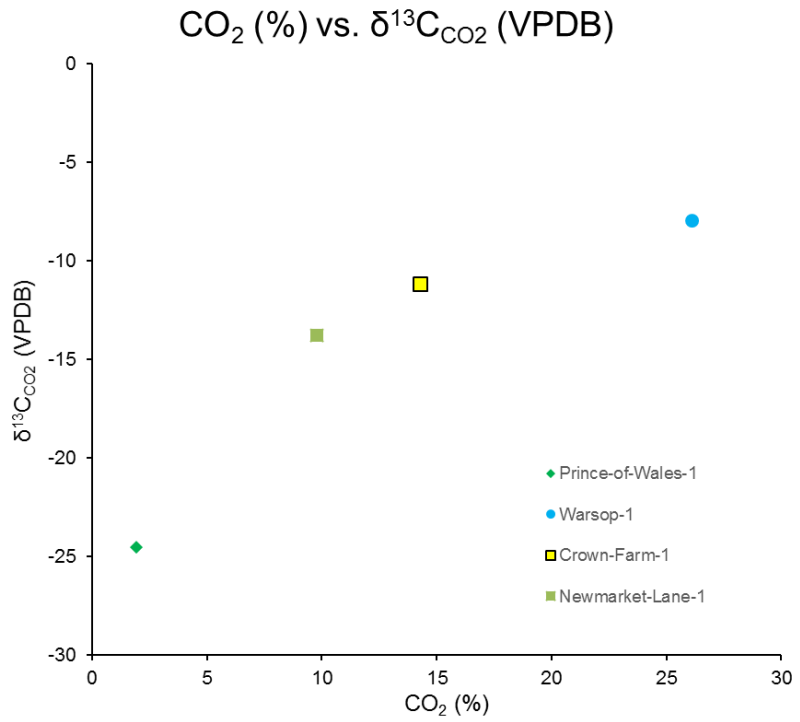

Figure 4-10 – Plot of $\delta^{13}C_{CO2}$ vs. CO_2 content. The CO_2 becomes isotopically heavier with increasing concentration.

4.5.3 Radiocarbon

Radiocarbon analysis for methane at Warsop-1 (Analysis: SUERC-71502) was indistinguishable from background, showing that there is no resolvable modern carbon input to the sampled methane.

4.6 Air Saturated Water (ASW) Calculations

Generic ASW ratios are calculated for the AMM samples assuming recharge of fresh (meteoric) water, and surface recharge temperature and altitude (10°C, Nottingham average - climate-data.org, 50 m above mean sea level) using Henry's constants from Crovetto et al., (1982) with no excess air component.

4.7 Noble Gases

4.7.1 Helium

^{4}He concentrations range from 337 ppm to 1506 ppm, orders of magnitude above the air value of 5.24 ppm (Ozima and Podosek, 2001). ^{3}He/^{4}He ratios range from 0.0019 to 0.043 R_a (where Ra refers to the atmospheric ^{3}He/^{4}He ratio of the atmosphere of 1.399 x 10^{-6}), highlighting the significant radiogenic component to all the gases, with no external mantle input and negligible input from the atmosphere or ASW to the helium inventory (see Figure 4-11).

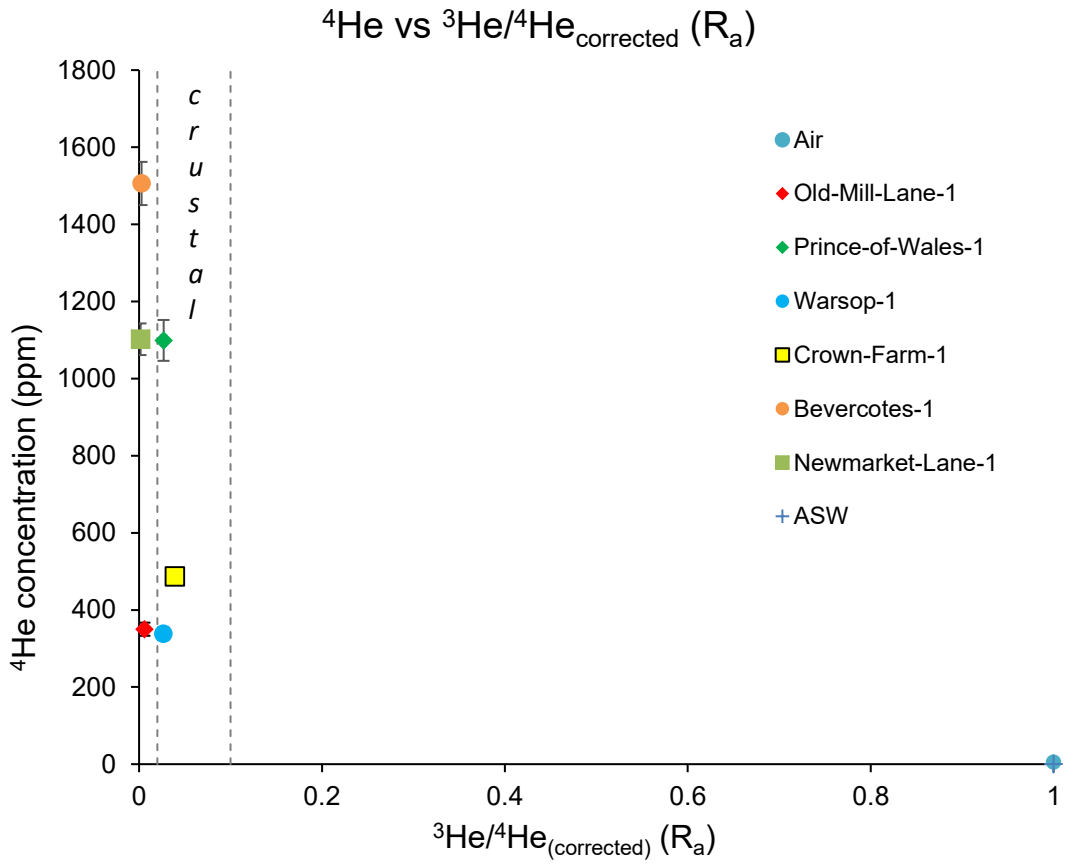

Figure 4-11 – Plot of ^{4}He vs. ^{3}He/^{4}He$_{(Ra)}$, illustrating the significantly above atmospheric levels of ^{4}He, and radiogenic ^{3}He/^{4}He ratios measured in the AMM samples. Some samples have such significant ^{4}He excesses that they fall below the typical continental crust ^{3}He/^{4}He values of 0.02 to 0.1 (Ozima and Podosek, 2002), shown between the dashed lines.

Concentration data

Well	^{4}He ($x10^{-4}$)		^{20}Ne ($x10^{-7}$)		^{40}Ar ($x10^{-3}$)		^{84}Kr ($x10^{-8}$)		^{132}Xe ($x10^{-9}$)	
Old-Mill-Lane-1	3.50	(0.17)	50.185	(0.337)	4.399	(0.163)	40.30	(1.68)	17.53	(0.092)
Prince-of-Wales-1	10.99	(0.53)	2.359	(0.100)	0.305	(0.011)	2.50	(0.10)	1.081	(0.006)
Warsop-1	3.38	(0.16)	3.197	(0.136)	0.390	(0.014)	12.72	(0.53)	13.76	(0.072)
Crown-Farm-1	4.87	(0.18)	76.872	(0.437)	5.384	(0.199)	47.80	(1.99)	14.55	(0.076)
Bevercotes-1	15.06	(0.56)	1.136	(0.048)	0.156	(0.006)	1.70	(0.07)	1.777	(0.009)
Newmarket-Lane-1	11.02	(0.41)	13.251	(0.562)	1.054	(0.039)	11.41	(0.47)	7.165	(0.038)

Units: cm^3 STP/cm^3 - (Standard T (0°C) and P (0.101 Mpa) after Ozima and Podosek (2002))

1 σ uncertainty shown in parentheses

Isotopic ratios

Well	$^{3}He/^{4}He$ (R/R_a)	$^{20}Ne/^{22}Ne$	$^{21}Ne/^{22}Ne$	$^{40}Ar/^{36}Ar$	$^{38}Ar/^{36}Ar$
Old-Mill-Lane-1	0.0094 (6)	9.80 (5)	0.0284 (0)	300 (1)	0.186 (3)
Prince-of-Wales-1	0.0268 (6)	9.64 (5)	0.0305 (0)	327 (1)	0.187 (3)
Warsop-1	0.0267 (8)	9.75 (5)	0.0288 (0)	308 (1)	0.186 (3)
Crown-Farm-1	0.0429 (9)	9.79 (5)	0.0280 (0)	300 (1)	0.186 (4)
Bevercotes-1	0.0027 (1)	9.70 (5)	0.0316 (3)	367 (1)	0.187 (3)
Newmarket-Lane-1	0.0019 (1)	9.62 (6)	0.0285 (0)	303 (2)	0.192 (5)

1 σ uncertainty shown as last significant figures in parentheses

ntrations and isotopic ratios for English AMM gases measured in this study.

4.7.2 Neon

Neon concentrations range from 0.1136 ppm ± 0.0048 (Bevercotes-1) to 7.687 ± 0.004 ppm (Crown-Farm-1). All samples except Bevercotes-1 have a greater ^{20}Ne concentration than that expected from ASW (0.183 ppm), suggesting a mix with atmospheric air. This air-mixing is observed in the $^{4}He/^{20}Ne$ ratios which range from 63 (Crown-Farm-1) to 13262 (Bevercotes-1), reflecting the different degrees of interaction with atmosphere-derived components. Lower $^{4}He/^{20}Ne$ ratios correspond to increased atmospheric air inputs, as atmospheric ^{20}Ne dilutes the radiogenic ^{4}He component ($^{4}He/^{20}Ne$ ratio of the atmosphere = 0.32). There is no correlation between $^{4}He/^{20}Ne$ and $^{3}He/^{4}He$, owing to the negligible helium component in the atmosphere compared to the concentrations of radiogenic helium in the samples (Figure 4-12).

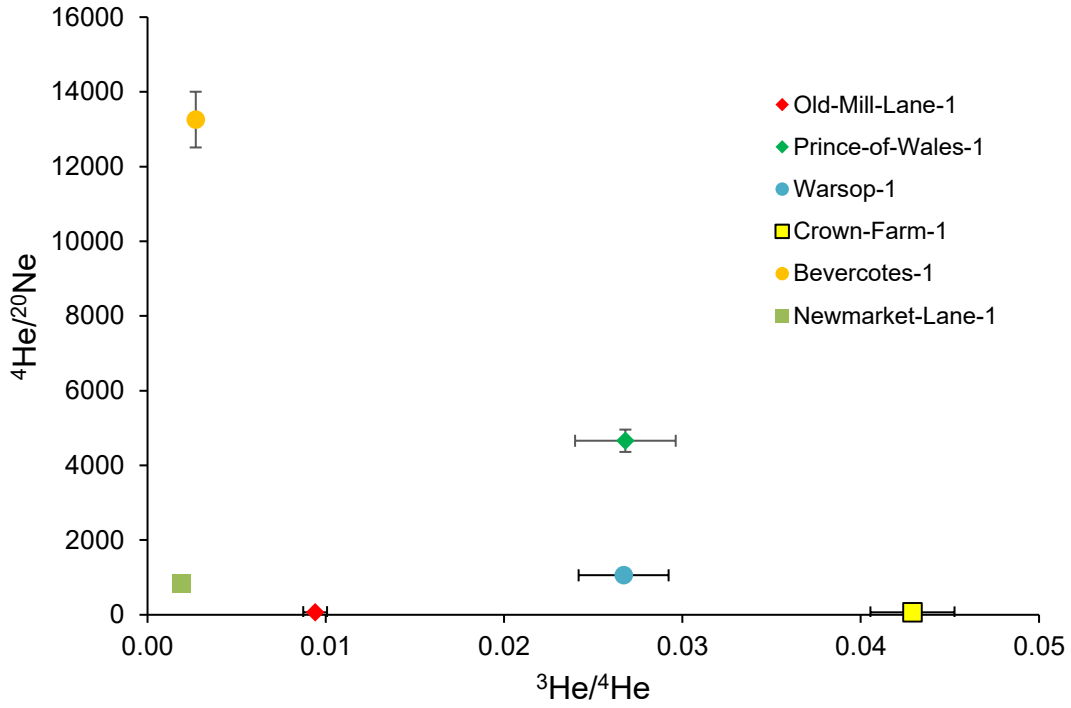

Figure 4-12 – Plot of $^{4}He/^{20}Ne$ vs. $^{3}He/^{4}He_{(Ra)}$. High $^{4}He/^{20}Ne$ ratios reflect mixing with atmospheric component. There is no correlation between $^{4}He/^{20}Ne$ and $^{3}He/^{4}He_{(Ra)}$ ratios due to the low helium concentration in the atmosphere relative to the crustal component. Air and ASW are off-chart to the right ($^{3}He/^{4}He$ = 1; $^{4}He/^{20}Ne$ = 0.318 (air) ~0.261 (ASW).

Most of the $^{20}Ne/^{22}Ne$ values plot within 1σ uncertainty of the air ratio, except for Newmarket Lane-1 (9.62 ± 0.06) which sits on the mass-fractionation line from air, and Prince of Wales (9.64 ± 0.05) mines (see Figure 4-13). $^{21}Ne/^{22}Ne$ ratios are generally air-like, but Prince-of-Wales-1 and Bevercotes-1 show an enrichment in excess crustal

$^{21}Ne^*$. Crown-Farm-1 shows a small depletion in $^{21}Ne/^{22}Ne$ that cannot be explained by mass fractionation, but is very likely air-derived. Newmarket-Lane-1 and Warsop-1 represent air values, but plot on the mass fractionation line from the air value. Newmarket-Lane-1 also shows a slight decrease in $^{38}Ar/^{36}Ar$, confirming isotopic mass-fractionation. Prince-of-Wales-1 and Bevercotes-1 appear to be a mix between crustally derived neon and air, subsequently affected by mass fractionation. These 2 wells correlate closely with lower overall ANG concentrations and higher $^{4}He/^{20}Ne$ ratios, showing they are less diluted with ANG's which allows the resolution of a more crustal end-member. In summary, all samples show neon ratios similar to air with some modification by mass-fractionation, except for Bevercotes-1 and Prince-of-Wales-1 which show a component of crustal $^{21}Ne^*$ and a degree of alteration by mass-fractionation. No trace of mantle neon can be resolved, as anticipated by the highly radiogenic $^{3}He/^{4}He$ ratios.

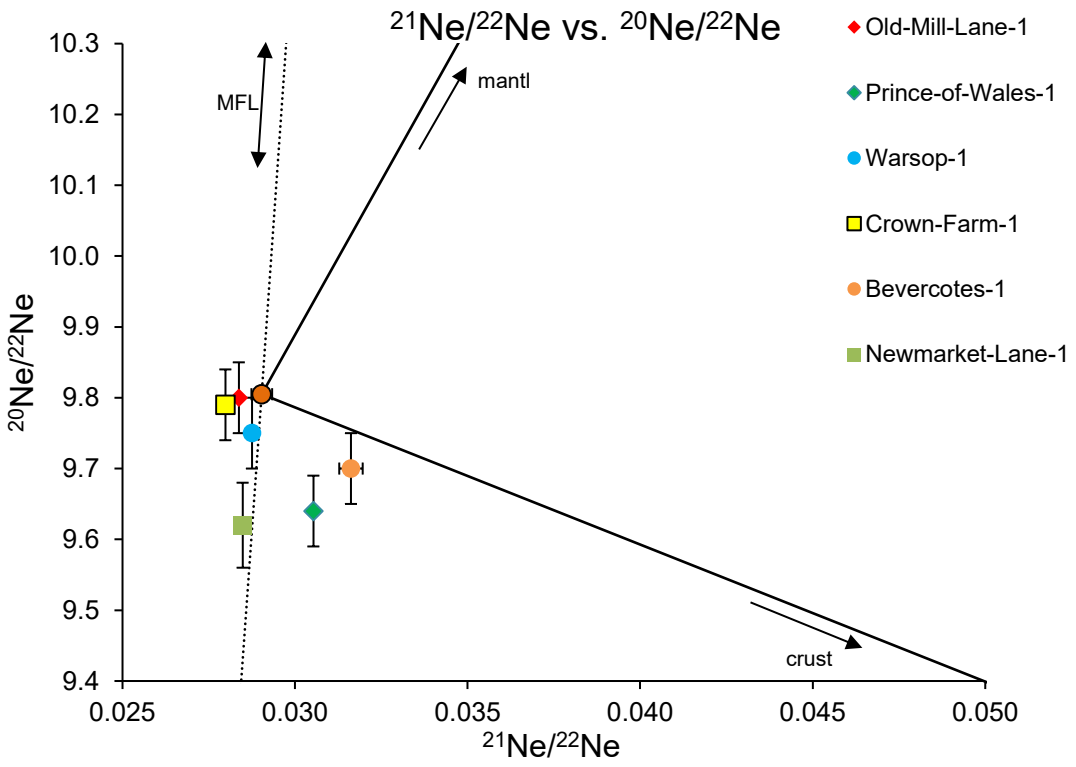

Figure 4-13 – Plot of $^{20}Ne/^{22}Ne$ vs. $^{21}Ne/^{22}Ne$. All samples show neon ratios similar to air with modification by mass-fractionation (along the Mass Fractionation Line (MFL), except for Bevercotes-1 and Prince-of-Wales-1 which show a component of crustal $^{21}Ne^*$ and a degree of alteration by mass-fractionation.

4.7.3 Argon

^{40}Ar concentrations range from 156 ppm (Bevercotes-1) which is below the ASW value of ~384 ppm, to 5384 ppm (Crown-Farm-1) which far exceeds the ASW value, and is over half the concentration found in atmospheric-air of 9300 ppm. ^{40}Ar/^{36}Ar ratios range from 300±1 at Crown-Farm-1, which is slightly above the air value of 298.6 (Mark *et al.*, 2011) to 367±1 (Bevercotes-1) showing a small ^{40}Ar* excess. All ^{38}Ar/^{36}Ar values are within error of the air value of 0.189 (Mark *et al.*, 2011).

The ^{40}Ar/^{36}Ar ratios in air and ASW are practically identical (298.5; (Mark *et al.*, 2011) but the concentrations of argon are different (^{36}Ar = 16.5 ppm in air, ~0.176 in ASW). A plot of ^{40}Ar/^{36}Ar vs. [^{36}Ar] concentrations (

Figure 4-14) shows that generally, air-like argon ratios are found in samples with large argon concentrations orders of magnitude above ASW values, indicating significant atmospheric-air input in 3 samples. Samples with a more radiogenic ^{40}Ar/^{36}Ar ratio are generally much lower in total argon concentrations indicating little or no dilution with atmospheric air. This clear mixing trend between an atmospheric end-member and a crustal end-member can also be seen in a plot of ^{4}He/^{20}Ne vs. ^{40}Ar/^{36}Ar (Figure 4-15).

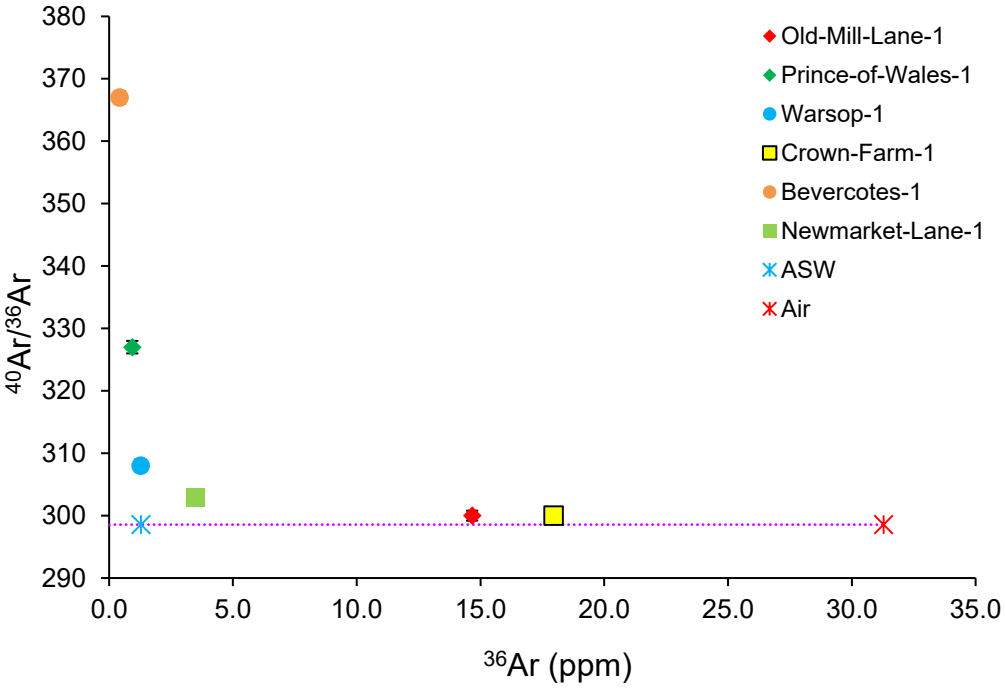

Figure 4-14 – Plot of ^{40}Ar/^{36}Ar vs. ^{36}Ar. Samples with increasing ^{36}Ar above ASW concentrations (a proxy for atmospheric air) show air-like ^{40}Ar/^{36}Ar ratios.

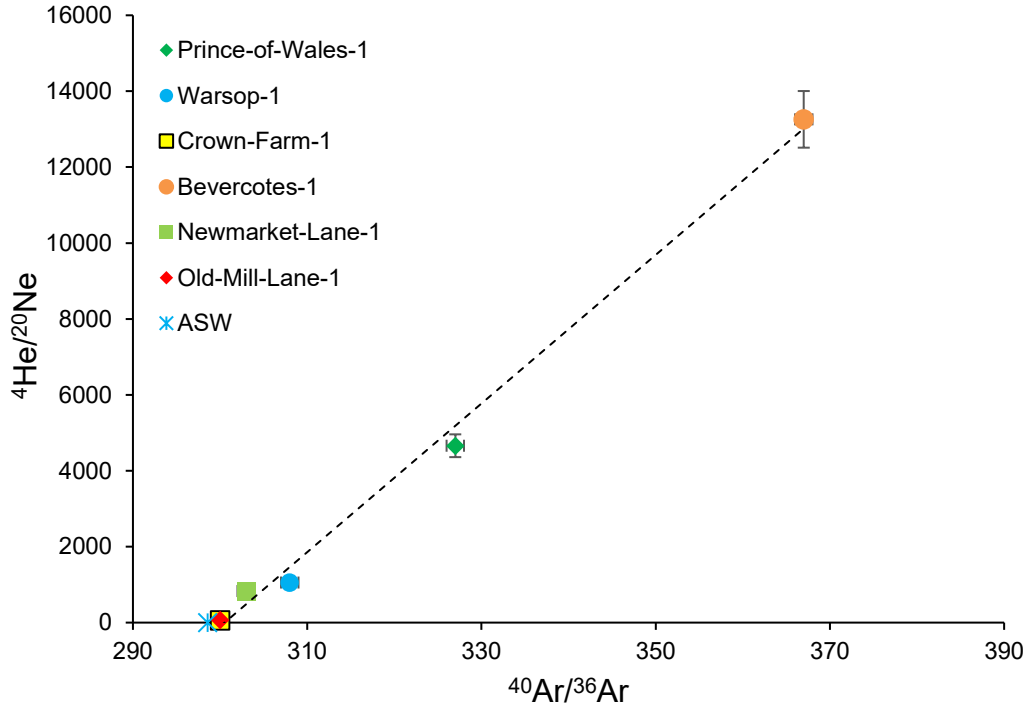

Figure 4-15 – Plot of $^{4}He/^{20}Ne$ vs. $^{40}Ar/^{36}Ar$. Note the clear mixing trend between a crustal-rich end-member characterised by Bevercotes-1 and the atmospheric end-member.

4.7.4 Krypton and Xenon

^{84}Kr concentrations range from 0.0170 ±0.0007 ppm (Bevercotes-1) to 0.478 ±0.020 (Crown-Farm-1). These values are all below the air concentration of 0.65 ppm (Ozima and Podosek, 2001) and both above and below the ASW ratio of 0.052 ppm. ^{132}Xe concentrations range from 0.00108 ±0.000006 ppm (Prince-of-Wales-1) to 0.01753 ±0.00092 ppm (Old-Mill-Lane-1), and mirror the ^{84}Kr system in being both greater than and below the ASW concentration of 0.00357 ppm.

Figure 4-16 shows that generally ANG ratios fall between the values of ASW and air, with the exception of heavy noble has enrichment seen at Warsop-1. The same distribution of data is repeated in the $^{132}Xe/^{36}Ar$ system.

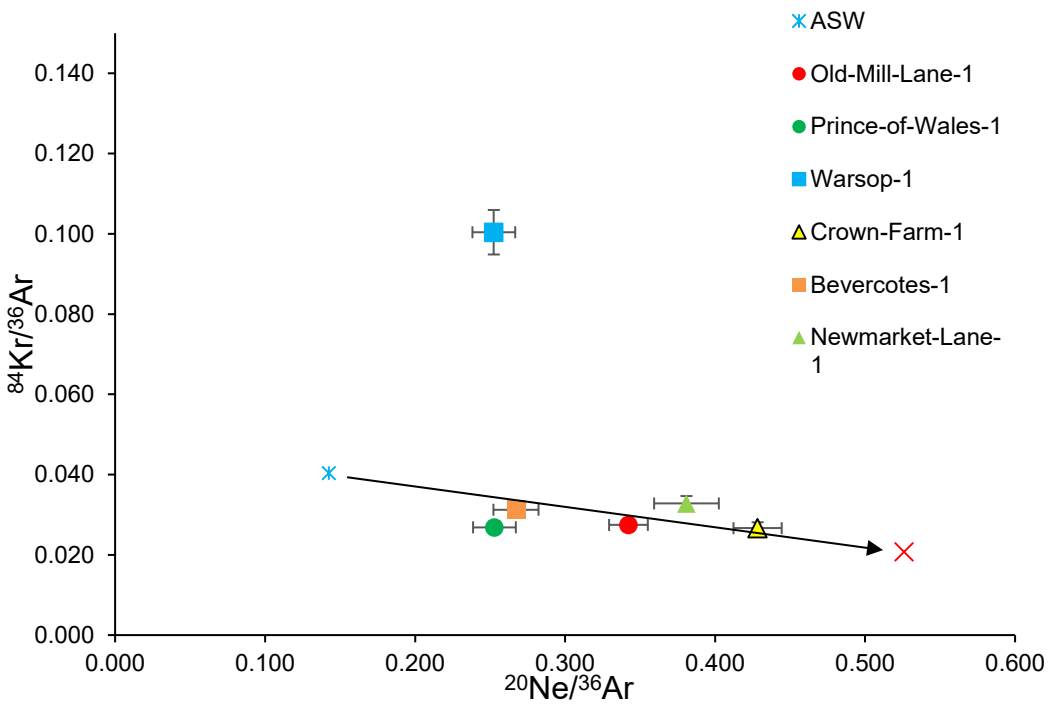

Figure 4-16 – Plot of $^{84}Kr/^{36}Ar$ vs. $^{20}Ne/^{36}Ar$. Most samples generally show an ANG inventory between that of air and ASW, with the exception of Warsop-1 which shows an excess of heavy noble gases (Kr, Xe).

4.8 Discussion

The samples are all obtained from mines that target the Carboniferous Coal Measures in Central England, but it is important to note that they cannot be regarded as a continuous dataset like a typical gas/oil field as the mines are all unique, owing to different construction methods, depths, coal seams targeted, age since closure, mine-water rebound status, and the resultant effects on exploitable area for AMM gas generation. The AMM wells/shafts are connected to heterogeneous voids in the subsurface strata, physically linked by tunnels, roadways, and collapsed gob areas, all of which are intensively cross-cut by mining-induced fractures which can extend tens of metres below workings into virgin seams, and hundreds of meters above, potentially even to the surface. These voids are actively pumped to produce gas, so measurable parameters like well/shaft depth cannot be intrinsically linked to gas properties (*e.g.* reservoir pressure), as much larger volumes both above and below the well bore are being exploited.

4.8.1 GC Measurements

Hydrocarbon and CO_2 data are reported as ratios of species, averaged over a minimum of three repeat analyses and show good reproducibility between repeated sample runs. Direct quantification of N_2 by GC was not possible (see Methodology), but was calculated by subtracting the absolute concentrations of other major species (CH_4, ethane, propane, CO_2) from 100% using data from the first analysis of a sample. The GC column chosen was able to resolve between O_2 and N_2, and it was seen that samples that contained larger percentages of N_2 (tens of percent) did not contain resolvable concentrations of oxygen, showing a modified air component where O_2 has been removed in the mine environment. The nitrogen calculation thus assumes that N_2 is the only other species in the gas; while higher hydrocarbons are unlikely to make up a significant proportion of the gas, hydrogen concentration determinations were not attempted and could potentially make up several % v/v of mine gases (Rice, 1993). Nevertheless, the calculated nitrogen concentrations are included to add to the discussion on atmospheric input to AMM gases.

4.8.2 Bulk Gases

4.8.2.1 Atmospheric Ingress

During operation, mines are ventilated to maintain a safe breathing atmosphere for workers and to remove build-up of methane gas to prevent explosions. When ventilation ceases, this atmospheric component is most likely expelled with continued degassing of coals, but some may remain.

AMM schemes are subjected to suction to aid degassing of coal and provide enough gas flux to provide economic quantities of gas (DTI, 2004). Air ingress can be a problem where the mine is not successfully sealed, either as a result of poor barriers around ventilation shafts and openings, or drawn down from the surface through fractures in shallower mines (DTI, 2004). Quantifying the atmospheric ingress can help assess the sealing and ultimate economics of an AMM resource.

Nitrogen composes 78% of the atmosphere but also occurs naturally at lower concentrations within coal gases (Creedy and Pritchard, 1983; Rice, 1993). Nitrogen concentrations were sometimes quite high, and at Old-Mill-Lane-1 and Crown-Farm-1 were in excess of the 25% maximum expected of UK coal gases (Creedy, 1988). While nitrogen is common in coal gases and generally derived from the degradation of

nitrogen-bearing macerals in coal during the coalification process, the concentrations generated and retained by this process are generally low (Creedy and Pritchard, 1983; Rice, 1993). The bulk of the nitrogen in gases with high nitrogen content in this case is not a result of coalification or thermal breakdown, but clearly derived from atmospheric air leading also to coherent enrichments in atmosphere-derived ^{36}Ar (see Figure 4-17).

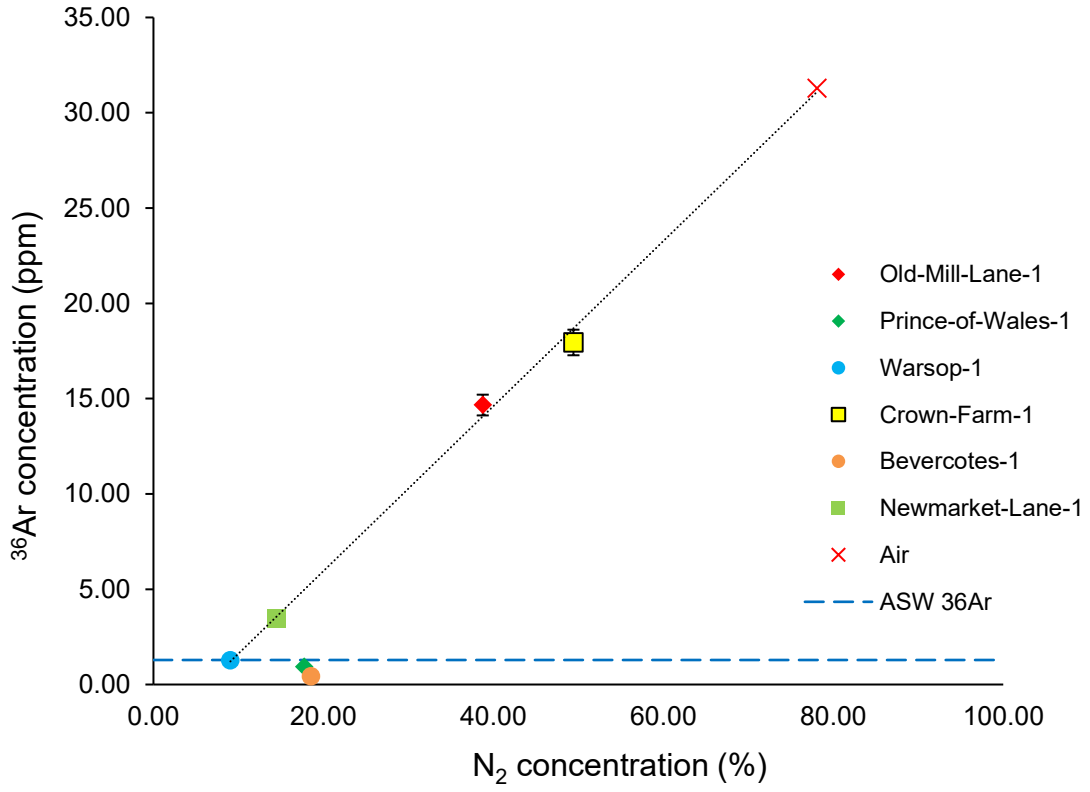

Figure 4-17 – Plot of ^{36}Ar vs N_2 content. There is a clear correlation between atmosphere-derived N_2 and ^{36}Ar as the air fraction in the gases increases. The dotted blue line represents typical ASW ^{36}Ar concentration calculated for the region; ^{36}Ar concentrations far in excess of this value have to be atmospherically-derived and not degassed from groundwater. Bevercotes-1 and Prince-of-Wales-1 show below-ASW values of ^{36}Ar, but elevated N_2 content.

This atmospheric component must have been present in the sampled mine gases rather than introduced via sampling error, as qualitative GC measurements show a lack of oxygen that would have been entrained if samples were incorrectly captured. Copper tube leakage is also unlikely, as leaks large enough to allow significant ingress of a large molecule like nitrogen would not have maintained the elevated concentrations of helium or below-atmospheric neon compositions.

Prince-of-Wales-1, Bevercotes-1 and Warsop do not show elevated ^{36}Ar with respect to ASW, and all display low nitrogen contents. These samples also show low $^{20}Ne/^{36}Ar$ ratios closer to ASW rather than to the air-ratio. This shows that these samples do not have a component derived directly from the atmosphere.

Prince-of-Wales-1 and Bevercotes-1 show higher nitrogen content than Warsop at similar ^{36}Ar concentrations. This could be due to be incorrect nitrogen data (see GC), but at these lower concentrations (<20%) could also be related to varying coalification nitrogen, or nitrogen cycling from groundwater infiltration as observed by Flores et al. (2008). Further investigation could make use of nitrogen isotope determination as a useful discriminant.

The lack of associated oxygen with the nitrogen contents is likely due to it's removal from gases either by bacterial oxidation of organic matter in the mines (Whiticar, 1996) or inorganic processes such coal, iron, or pyrite oxidation producing 'black damp', a nitrogen and CO_2 rich, oxygen-deficient mine atmosphere (Burrell *et al.*, 1916; Creedy and Pritchard, 1983; Sechman *et al.*, 2013; Thomas, 2013). The absence of oxygen in gases could be utilised in locating poor mine seals, as the residence time of atmospheric air in these samples must be long enough for chemical processes to have removed the oxygen; this situation may not occur if a seal failure were nearer to the vacuum pumping apparatus.

Despite the air ingress introducing oxygen, there is no clear connection between atmospheric nitrogen and CO_2 which might be expected to form from atmospheric oxygen as a product of oxidation; this is either because the CO_2 has numerous sources unrelated to reduction of atmospheric oxygen into CO_2, or that the processes do not evolve equimolar quantities of CO_2 from coals due to solubility in water, adsorption on coals, and formation of other oxides (Burrell *et al.*, 1916; Creedy and Pritchard, 1983).

It is problematic to quantitively estimate air ingress, as air-derived components are sourced both directly from the atmosphere (in some samples) as well as indirectly from the atmosphere via degassed ASW. For the two most air-diluted samples (Crown-Farm-1: $^{4}He/^{20}Ne = 63$; Old-Mill-Lane-1: $^{4}He/^{20}Ne = 70$) which show high concentrations of ANG's; then the ^{36}Ar concentration in the samples in excess of ASW concentrations (~1.29 ppm) can be expressed as a fraction of the air ^{36}Ar concentration (31.3 ppm) (Mark *et al.*, 2011). From this a rough approximation for the percentage of air can be calculated, resulting in 43% (Old-Mill-Lane-1) and 53% (Crown-Farm-1).

If the lowest nitrogen content observed (Warsop-1; 9%) is used as the baseline coalification nitrogen content, then estimates of air ingress based on nitrogen content (subtracting 9% coalification nitrogen from the sample, and dividing by the air value of 78%) then air ingress is estimated as 38% (Old-Mill-Lane-1) and 52% (Crown-Farm-1), which are similar to ^{36}Ar-based estimates, providing confidence in these assessments.

4.8.2.2 Carbon Dioxide

There are numerous sources of CO_2 in the subsurface environment, both organic and inorganic. CO_2 can be generated in the geological past and stored within coals, or generated more recently due to chemical reactions in a disturbed mined environment. Furthermore, source determination is complicated because subsurface CO_2 is commonly of mixed origins.

CO_2 can be a significant asphyxiant hazard and negatively affects the operation of gas turbines, so understanding its sources and generation can aid in the prediction of future CO_2 concentration trends. Additionally, CO_2 is common in biological settings, and is both utilised by and produced by microbes that degrade coal, and consume and produce methane (Whiticar, 1999; Golding *et al.*, 2013; Meslé *et al.*, 2013), so understanding the sources and sinks of CO_2 can highlight important biological processes occurring in the subsurface.

Isotopic investigations into CO_2 source determination are problematic, because the absolute isotopic composition of CO_2 is not diagnostic of gas origin in of itself. Moreover, particular diagnostic plots *e.g.* $\delta^{13}C_{CO2\text{-}CH4}$ - a commonly used tool in many studies to investigate gas origins (Whiticar, 1999; Strąpoć *et al.*, 2011), are not valid when there are significant external gas contributions (*e.g.* Vinson et al., 2017). The same applies where other non-methanogenic bacterial processes compete for substrates; the mass balance between CH_4 and CO_2 is affected and the net isotopic signatures of gas present are masked.

$\delta^{13}C_{CO2}$ values (-7.9 to -24.9‰) were measured in 4 of the 6 AMM samples. All are heavier than the $\delta^{13}C_{CH4}$ from the same sample. CH_4/CO_2 varies from 2.5 (Crown Farm-1) to 42 (Prince of Wales), and there is no correlation with CH_4/CO_2 and higher hydrocarbon contents ($C_1/(C_2+C_3)$).

In coals, significant volumes of primary coalification CO_2 are generated at lower thermal maturities due to the microbial degradation of coal organic matter and the subsequent thermal decarboxylation of kerogens at greater depths (Rice, 1993;

Whiticar, 1996; Thomas, 2013), however the coal structure at low coal ranks is not suitably developed to adsorb large volumes of gas (Kotarba, 2001), and most coalification CO_2 is expulsed during its formation (Thomas, 2013). In the UK the remainder has been mostly removed over geological time by groundwater flow due to the high solubility of CO_2, resulting in the low in-seam CO_2 contents observed today (Creedy, 1988; Thielemann *et al.*, 2004). Concentrations of CO_2 in UK coal seams are commensurate with CO_2 saturation in water at atmospheric pressure and temperature, and tentatively attributed to carbonate cleat mineralisation post-uplift by Creedy (1988), however isotopic evidence for this is lacking.

The $\delta^{13}C_{CO2}$ of AMM samples are isotopically heavier ($\delta^{13}C_{CO2}$ = -7.9‰ to -24.5‰) than those previously reported for UK coals taken from the similar geographic area ($\delta^{13}C_{CO2}$ = -38.1 to -54‰) (Hitchman *et al.*, 1989). These previously reported $\delta^{13}C_{CO2}$ measurements were much closer in value to the corresponding methane $\delta^{13}C_{CH4}$, and can reasonably be attributed to CH_4 oxidation. CO_2 concentrations in this study are generally greater than the ~5% previously measured in UK coal gases (Creedy and Pritchard, 1983; Hitchman *et al.*, 1989), and also often higher than typically expected in coalbed gases (<~6%) (Creedy, 1988; Rice, 1993). The previously measured samples were drainage gases from coal boreholes, which can be presumed to be mainly desorbed from undisturbed coals rather than from a disturbed mined environment. AMM samples (this study) also show a trend of $\delta^{13}C_{CO2}$ becoming isotopically heavier with increasing CO_2 concentration (Figure 4-10). Because measured concentrations of CO_2 in AMM gases are both variable and isotopically heavier than previously reported, it is probable that the source of CO_2 is secondary and introduced relatively recently as a direct result of the mining process and abandonment.

Potential sources of CO_2 in coals could then include atmospheric components entrained in the coals from the period of mining, microbial degradation of organic materials in the mine (coals and timbers), oxidation of methane, and thermal/chemical degradation of carbonates (Rice, 1993; Baldassare and Laughrey, 1997; Golding *et al.*, 2013). These are investigated further:

Thermal decomposition of carbonates (Hunt, 1996) is not expected, as the coals are relatively low maturity (primarily sub-bituminous/bituminous), and the main source of carbonate was precipitated in the cleat system after maximum burial *i.e.* highest temperature (Creedy and Pritchard, 1983).

CO_2 generated by thermal decarboxylation and coal oxidation is shown to possess a $\delta^{13}C_{CO2}$ similar to the source coal $\delta^{13}C_{coal}$ (Smith and Pallasser, 1996), which ranges from -21‰ to -27‰ (Whiticar, 1996; Rimmer *et al.*, 2006; Hamilton *et al.*, 2014; Warwick and Ruppert, 2016). Aerobic CO_2 generation is expected to occur in mines when ventilation introduces O_2 and water (Thielemann *et al.*, 2004). Bituminous coals with high pyrite contents often contain greater volumes of CO_2, as pyrite-rich coals absorb more oxygen when moist (Thomas, 2013). This oxygen reacts with hydrogen and carbon in coals to produce H_2O and CO_2, and could lead to elevated CO_2 concentrations outside the range of 'typical' unmined coal gases. Prince-of-Wales-1 has a lower concentration of CO_2 (<5%) and is isotopically lighter ($\delta^{13}C_{CO2}$ = -24.5‰), which is indicative of either remnant coalification gas, or inorganic coal oxidation.

CO_2 can also be generated by the oxidation of methane, which is a common fate for methane migrating through shallow sediments. Aerobic methane oxidation is believed to be very unlikely in subsurface environments such as CBM due to excessive oxygen requirements (Head *et al.*, 2003), but is a possible scenario in the more open and oxidised AMM environment, and methylotrophic bacteria are known from Polish coal seams (Stępniewska *et al.*, 2013). The $\delta^{13}C_{CO2}$ formed via CH_4 oxidation is expected to lie close to, or lighter than, the $\delta^{13}C_{CH4}$ of the oxidised methane (Whiticar, 1999; Vinson *et al.*, 2017) and this is not observed in AMM samples, though the process could be occurring locally on a small scale and mixed with heavier CO_2. Significant CH_4 oxidation may enrich the residual CH_4 in ^{13}C, but the similarity in $\delta^{13}C_{CH4}$ temporally (Hitchman et al., 1989) and spatially over the wider geographic area suggests that the $\delta^{13}C_{CH4}$ signature is persistent and not significantly affected by oxidation. Moreover, the lack of correlation between CO_2 and N_2 concentrations suggests that the degree of air ingress currently observed has no influence on CO_2 generation in the mines, but does not preclude previous atmospheric (*i.e.* oxygen) influence on the coals in the long histories of the collieries having an effect on CO_2 generation.

The isotope values for Warsop-1 ($\delta^{13}C_{CO2}$ = -7.9‰) is similar to the atmosphere (atmospheric $\delta^{13}C_{CO2}$ =~ -7‰ (Ohmoto, 1986)). Due to several orders of magnitude difference between atmospheric CO_2 levels and those found in AMM gases, *direct* addition of atmospheric CO_2 cannot be responsible for the CO_2 observed. However, significant atmospheric CO_2 addition is potentially plausible because CO_2 has a high affinity for adsorbing onto coals, and will even displace CH_4 in the coal matrix (a phenomenon fundamental to Enhanced-CBM). Decades of ventilation during mining

could have allowed significant CO_2 to adsorb onto coals to be released at a later date. Thielemann et al., (2004) observed lower concentration (<5%) of atmospherically dominated CO_2 in active mines in the Ruhr Basin, with increasing CO_2 concentrations (up to 19.5%) becoming isotopically lighter, which was attributed to microbial CO_2 formation. English AMM gases show the opposite trend, with isotopically heavier $\delta^{13}C_{CO2}$ correlating with greater CO_2 concentrations. The lack of isotopically enriched CO_2 in all AMM mines, all of which have been subject to decades of atmospheric ventilation, and a trend which appears to be the opposite of that observed elsewhere excludes atmospheric CO_2 as a significant source of CO_2 in AMM gases.

In some fields, isotopically heavy CO_2 ($\delta^{13}C_{CO2}$ = >-5‰) is indicative of microbial methanogenesis via CO_2 reduction (Whiticar, 1999; Golding *et al.*, 2013). The enrichments of $\delta^{13}C_{CO2}$ arise as a product of substrate (*i.e.* CO_2) depletion, whereby lighter CO_2 is preferentially utilised by microbes leaving the residual CO_2 enriched in ^{13}C. This process is unlikely to be active in this scenario as a concentration of 26% cannot be regarded as 'depleted'. Radiocarbon measurements on CO_2 in the Ruhr Basin coal mines suggested a modern input to microbially produced CO_2, probably derived from mine timbers or DIC introduced from groundwater rebound (Thielemann *et al.*, 2004), but unfortunately radiocarbon was not analysed on CO_2 in this study and so cannot be evaluated. Crucially, Thielemann et al., (2004) observed greater microbial CO_2 inputs were also correlated with lighter $\delta^{13}C_{CH4}$ values, hypothesised to be a result of recent microbial methanogenesis, but English AMM gases show no coherence with and little variation in $\delta^{13}C_{CH4}$ despite a wide range in $\delta^{13}C_{CO2}$ values, suggesting the CO_2 and CH_4 systems are not microbially linked. In coal spoil heaps, CO_2 can be produced by the chemical neutralisation of acid mine waters with carbonate materials which leads to isotopically heavier $\delta^{13}C_{CO2}$ (*e.g.* -5.5‰ to -3‰) (Laughrey and Baldassare, (2003); and references therein). Acid Mine Drainage (AMD) waters are characterised by low alkalinity (Karacan *et al.*, 2011; Thomas, 2013), and are primarily produced by the oxidation of sulphide minerals (predominantly pyrite in coals) by the reaction:

$$2FeS_{2(s)} + 7O_{2(g)} + 2H_2O_{(l)} = 2Fe^{2+}_{(aq)} + 4SO_4^{2-}{}_{(aq)} + 4H^+_{(aq)}$$

This highly acidic water further reacts with carbonate minerals (*e.g.* $CaCO_3$/calcite, ankerite, siderite) to produce bicarbonate, and ultimately CO_2. Due to the $\delta^{13}C$ of carbonate minerals, the generated CO_2 is isotopically heavy (Laughrey and Baldassare, 2003). Pyrite (FeS_2) is commonly abundant in UK coals (*e.g.* Parkgate seam) (Spears and Tewalt, 2009), and mine outflow waters are commonly supersaturated with CO_2

with partial pressures sometimes exceeding x100 that of the atmosphere (Jarvis, 2006; McAllan *et al.*, 2009). This suggests that large concentrations of isotopically-heavy CO_2 are derived from chemical carbonate dissolution within the mines.

In the absence of co-variation between $\delta^{13}C_{CO2}$ and $\delta^{13}C_{CH4}$ suggesting CO_2 is unrelated to methanogenesis, then the CO_2 present in English AMM gases can be reasonably explained by varying mixtures between smaller concentrations of isotopically lighter CO_2 derived from coalification or coal oxidation (*e.g.* $\delta^{13}C_{CO2}$ = ~-25‰), and larger concentrations of isotopically heavier CO_2 (*e.g.* $\delta^{13}C_{CO2}$ = ~-5‰) produced recently from chemical carbonate dissolution.

4.8.2.3 Hydrocarbons

The hydrocarbons in coals are produced during the deposition of organic material, through to the processes of coalification and metamorphosis, and can be both inorganic and microbial. Due to the capability of coals to retain hydrocarbons (Whiticar, 1996; Golding *et al.*, 2013), the resultant suite of gases measured in a coal sample can range across geological time and method of production. This makes it difficult to define a 'coal' type gas (Golding *et al.*, 2013).

Gas content in coals can be a complex mixture of:

- Primary microbial gases generated during sediment deposition and early burial
- Thermogenic coalification gases (linked to thermal maturity - R_o)
- Exogenous migrated and retained gases
- Secondary microbial gases

The molecular and isotopic composition of gases can be further modified by preferential retention and expulsion during subsequent uplift, degassing, and *ex situ* hydrocarbon migration into coals (Creedy, 1988; Rice, 1993; Whiticar, 1996; Golding *et al.*, 2013).

The gaseous hydrocarbon content of coal is dependent on the initial composition of the kerogen present, assumed in coals to be primarily type III humic (Van Krevelen, 1961). In the early stages of coal formation, the hydrocarbons consist solely of methane generated via primary microbial methanogenesis in sediments, with significant volumes of CO_2. At higher maturities kerogens are partly transformed into gaseous hydrocarbons via heat and pressure during coalification thermal catalysis; the degree

of thermal maturity affects the type of gas and volumes of gas generated. At low coal-ranks, the ranges of thermogenic gas generation overlap with biogenic.

Early thermogenic gas generation is believed to start at R_o = 0.5% (Whiticar, 1996; Strąpoć *et al.*, 2011), but some authors propose R_o = 0.4% as the onset of 'early mature' or 'low mature' gases (Xu *et al.*, 2008). The transition between biochemical and thermo-catalytic processes is suggested to be R_o = 0.4% - 0.6% (Xu *et al.*, 2008), 0.4% - 0.7% (Galimov, 1988), or 0.8% (Liu and Xu, 1999). Microbial methane production is maximised in low maturity coals (~0.3% - ~0.8% R_o) (Gao *et al.*, 2014), but is still able to be utilised by methanogens at lower rates in higher rank coals (Strąpoć *et al.*, 2011). The majority of the gas generation occurring from R_o = 0.7% to 1.6% (Strąpoć *et al.*, 2011)

CO_2 is the dominant gas produced by coalification at early stages, with methane dominating along with appreciable contents of C_{2+} ($C_1/C_2 < 10$) in bituminous stages as the coals go through the equivalent of the oil window (Whiticar, 1994; Golding et al., 2013). Maximum gas generation occurs simultaneously with wet gas (C_{2+}) generation, which peaks at R_o = 0.6% - 0.8% which closely corresponds with the oil window for sapropelic - type I/II kerogens. Wet gas generation declines at around R_o = 1.8% (Scott et al., 1994) and gases become increasingly dry ($C_1/C_2 > 1000$). Thermal cracking of bitumens occurs as the coals enter the gas window around the anthracite stage. The onset of thermogenic gas production occurs at a later stage in type III kerogens vs. type I/II, and both the yield of CH_4 and C_{2+} components is less. These processes are summarised in Figure 4-18 and Figure 4-19.

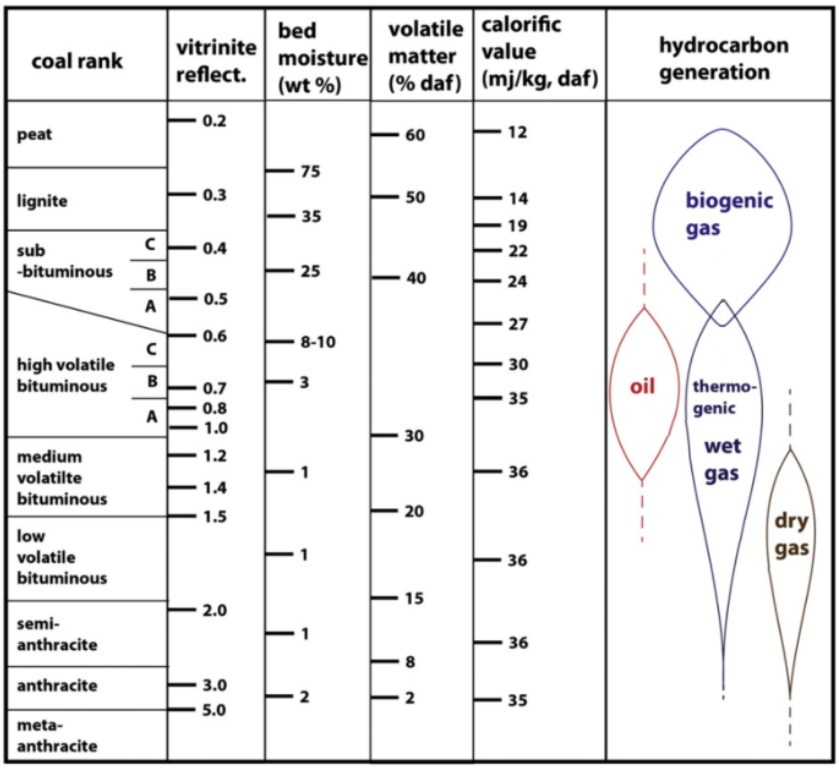

Figure 4-18 – Approximate correlation of rank parameters vs. measurable coal properties and hydrocarbon generation window, reproduced from Moore, (2012).

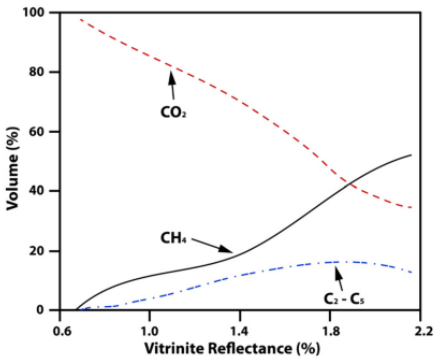

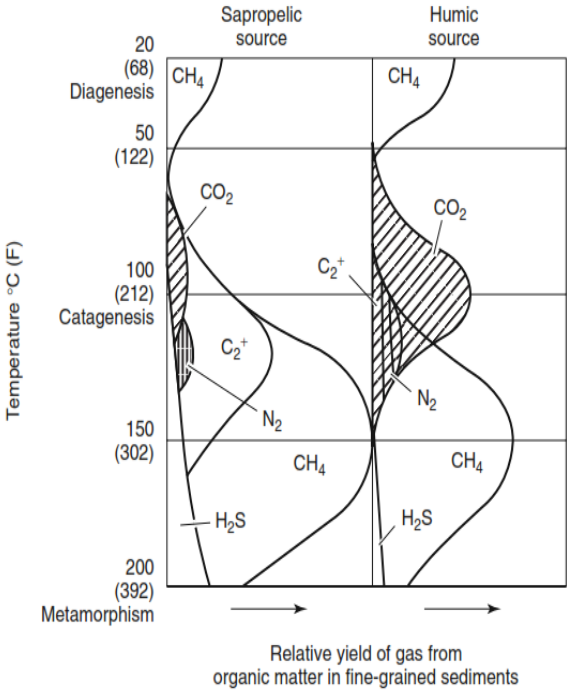

Figure 4-19 – Left: Total volumes of gases generated by coalification vs. vitrinite reflectance, based on experimental coal pyrolysis data from Zhang et al., (2008). Reproduced from Moore et al., (2012). Right: Relative volumes of generated gas with increasing temperature, including biogenic production. Reproduced from Thomas (2013).

The thermogenic gas content ($C_1/(C_2+C_3)$) generated by a coal is then influenced by the maximum thermal maturity of the coals reached at maximum burial, plus any retained components from previous stages of biogenic/thermogenic gas production. Other factors involve biogenic gas production (addition of methane), and non-coal source inputs.

Data on coal maturity for the individual coals within the collieries in this study is not known, however it is acknowledged that they targeted subbituminous to high-volatile bituminous coals. Using mean vitrinite reflectance (R_o) data from nearby collieries that mined the same seams in the East Pennine coalfield, the range of vitrinite reflectivities in the AMM coals can be estimated at ~0.5% to ~1.1% R_o (BCURA, 2002). This closely corresponds with the oil window for higher maturity coals, and both microbial and thermal catagenic gas production for the lowest maturity coals.

Hydrocarbon contents in AMM samples are in line with previously reported measurements in UK coals believed to be the retained products of coalification by Creedy (1988), and are well within the bounds of typical coal gases (Rice, 1993). Methane was expected as the dominant gas species, especially considering the AMM developments were designed and installed to extract it. The total methane concentrations bear no correlation to the hydrocarbon compositions (C_1/C_2, or $C_1/[C_2+C_3]$). Methane is assumed to be the dominant gas in the mine atmosphere, and the variation in methane concentrations then is likely a result of dilution from air ingress into the workings from pumping operations, along with additional CO_2 input.

There is significant variation in the $C_1/(C_2+C_3)$ contents, and Bevercotes-1 shows the highest $C_1/(C_2+C_3)$ and is known to have oil present, which could be the cause of higher C_{2+} contents. However, it is impossible to ascertain whether these variations are related to coal maturity, biogenic gas input, external hydrocarbon input, or preferential desorpsion of lighter methane. A closer look at the East Pennine coalfield may help to explain the variation.

4.8.2.4 Regional variation

As shown earlier, the AMM gases show a clear contribution from thermogenic sources because the concentrations of heavier hydrocarbons (C_{2+}) are much larger than would be expected from biogenic sources (where $C_1/C_2 > 1000$). Based on compositional data from British Coal measurements of borehole and degassed core samples, Creedy (1988) regarded the hydrocarbons in the East Pennine coalfield to be products of coalification, with minor localised addition from petroleum-derived hydrocarbons.

As is common to many coalfields, coal seam gas contents generally increase with depth, mostly as a function of the increasing thermal gradient and therefore increase in coal rank with depth (Hilt, 1873; Creedy, 1988). In the East Pennine coalfield, regional gas contents correlated with in-seam measurements have shown that overall hydrocarbon gas contents and compositions can in some areas also be related to the distance from the Permo-Carboniferous unconformity (Creedy, 1988, 1991). Gas content and methane/ethane ratios are believed to have been initially established by coalification related to the parameters of rank/depth, but subsequent diffusion-related degassing from the Permo-Carboniferous erosion surface caused by the Variscan uplift has overprinted the coalification trends in certain regions. For example, in the Witham prospect to the East, gas content decreases towards the unconformity following in-seam diffusion to the atmosphere resulting in seam gas contents close to zero at the unconformity, before being subsequently reburied (Creedy, 1988, 1991). Furthermore, the greater diffusivity of methane relative to ethane resulted in greater relative ethane concentrations towards the unconformity as the methane was preferentially lost. As the in-seam gas contents appear to correlate with proximity to the unconformity, the implication is that little to no gas migration, subsequent coalification, or migration along post-Permian faults occurred after reburial, probably due to mineralisation of the cleat system preventing significant gas migration (Creedy, 1988).

Other large-scale structures across the coalfield affect local seam-gas contents such as the Variscan related Eakring anticline, where gas content decreases towards the anticlinal crest attributed to a decrease in rank, suggesting folding and coalification were contemporaneous. Similarly, in the Gainsborough anticline, gas content increases towards the anticlinal crest attributed to free gas movement along interbedded permeable sand units (Creedy, 1988). This highlights the complexity of the geology and its effect on gas content and compositions, but also highlights that the observed trends have been preserved over long periods of geological time, showing that significant gas migration has not occurred since at least the Miocene when the dips of the strata were reversed (CEC, 1988).

As well as maturity, the methane/ethane ratios in coals are governed by retention as most of the gas generated is expulsed, with coals commonly retaining heavier hydrocarbons within the coal matrix (Whiticar, 1996). As methane is more diffusive than ethane and higher hydrocarbons, it is preferentially lost over ethane during any subsequent degassing of coals, which can occur due to of uplift or faulting (Creedy,

1991). The higher diffusivity of methane is also the reason why gases in both AMM and CBM can become both compositionally and isotopically heavier over time as the reservoir is depleted (Rice, 1993; Moore, 2012; Thomas, 2013).

Bevercotes-1 and Warsop-1 show the lowest $C_1/(C_2+C_3)$ ratios and therefore the largest higher hydrocarbon content. While these gases are not particularly 'wet' and fall within the range of expected C_{2+} contents observed in coalification gases (Rice, 1993) as well as predictive models based on coal maturity (see Figure 4-19), Creedy (1988) noted that in the East Pennine coalfields, higher C_{2+} hydrocarbon content increased in seams around faults with oil shows, demonstrating a degree of migrated gas is locally present (Creedy, 1988, 1991). However, the overall external contribution of C_{2+} contribution from oil vs. humic kerogen cannot be resolved.

Coals in the Bevercotes mine are known to have oil shows (Huxley, 1983) that affected coal production, with the Parkgate seam being particularly oil-prone. The nearby Maltby colliery temporarily shut down production in 2012 for safety reasons due to striking oil-prone seams. No comprehensive study has been found on whether this oil is generated within the coals or surrounding sediments or migrated from elsewhere such as the Eakring oilfield, though various nearby collieries also experienced localised oil shows in fault zones, coal cleat, and surrounding porous sandstones, and it's presence is thought to be related to faults (Creedy, 1988). The throw of the faults has no apparent bearing on oil volumes, so it was tentatively suggested that the oil had not migrated a significant distance (Creedy, 1988).

Despite the known presence of oil in the Coal Measures and its influence on localised C_{2+} contents, all the samples in this study are more methane-rich than the majority of previously reported datasets from the region (see Figure 4-20). Given the geographic range of the mine sites, this is suggestive either of a limited effect of migrated oil on overall C_{2+} gas concentrations, or possible subsequent addition of methane from microbial methanogenesis masking the additional petroleum related signature.

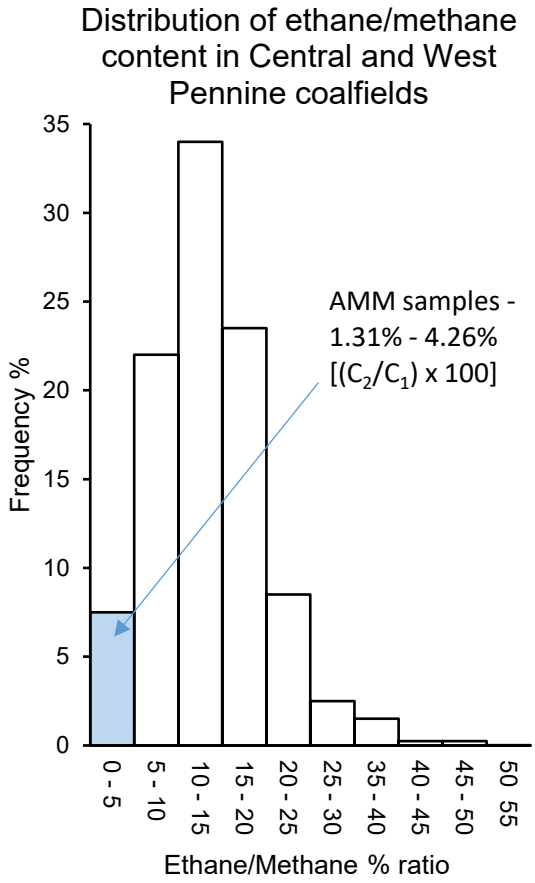

Figure 4-20 – Plot of the frequency of methane/ethane ratios in Central and West Pennine coalfields. Central England AMM samples (from this study) possessed C_2/C_1 percentage ratios of 1.31% - 4.26% C_2/C_1, which is at the lower end of previously reported Pennine coalfield data, denoted by the blue box. Reproduced after (CEC, 1988).

4.8.3 Stable Isotopes

Isotope geochemistry of hydrocarbons from humic sources is especially problematic as coals retain hydrocarbons in pore space or adsorbed onto coal surfaces which makes mixtures of different gas sources more likely (*e.g.* microbial and thermogenic) (Whiticar, 1996). A coal may retain components of pre-coalification gases along with early-mature thermogenic gases, or show a strong thermogenic component when active microbial methanogenesis is occurring, which masks the isotopic and compositional signatures of gas generation types (Rice, 1993; Whiticar, 1996; Strąpoć *et al.*, 2011; Dias *et al.*, 2014). Furthermore, the desorption of coal gases can cause significant compositional and isotopic fractionation (Rice, 1993; Whiticar, 1994, 1996; Niemann and Whiticar, 2017). Heavier hydrocarbons are preferentially retained over methane, and $\delta^{12}C_{CH4}$ has a higher diffusivity than $\delta^{13}C_{CH4}$; for example $\delta^{13}C_{CH4}$ may shift

by as much as -43.4‰ over time in core desorption experiments (Niemann and Whiticar, 2017). This has hampered the reliable characterisation of coal gases vs. type I/II derived hydrocarbons that have a more defined geochemistry.

Identification of thermogenic gases is commonly based on the presence of C_2+ components which are generally absent in microbial gases (Bernard *et al.*, 1976; Oremland *et al.*, 1988; Whiticar, 1999), combined with stable isotope compositions of carbon and hydrogen. Thermal catagenesis is less selective than microbes in fractionating carbon and hydrogen when producing methane from source material, and microbial gases are hence lighter than thermogenic (Whiticar, 1994, 1999). The 'Bernard Diagram' (Figure 4-9) modified after the papers of Bernard et al. (1978), and Faber and Stahl, (1984) defines thermogenic gas as $\delta^{13}C_{CH4} > -50‰$ and $C_1/(C_2+C_3) < 100$, and biogenic gas as $\delta^{13}C_{CH4} < -60‰$ and $C_1/(C_2+C_3) > 1000$. Values outside this range are considered mixed microbial-thermogenic.

AMM samples (Figure 4-9) plot in the thermogenic range in terms of C_2+ content, but on the boundary for thermogenic/mixed carbon stable isotopes. These definitions are somewhat arbitrary and some authors prefer different ranges depending on the gas type being studied. This is because maturity affects the molecular and isotopic compositions of produced gases from separate kerogen types differently, with type III kerogens typically producing characteristically heavier hydrocarbons than type I/II (Whiticar, 1996; Martini *et al.*, 1998; Strąpoć *et al.*, 2008; Golding *et al.*, 2013). As some samples fall outside of the thermogenic boundary, this suggests there could be a small component of lighter microbial gas.

Microbial gas is typically dry ($C_1/(C_2+C_3) > 1000$) being devoid of C_2+ components, but coal maturity also affects the $C_1/(C_2+C_3)$ ratios. So the resultant $\delta^{13}C_{CH4}$ and $C_1/(C_2+C_3)$ of a mixed biogenic-thermogenic system depends both on the degree of mixing as well as the thermal maturity. Strąpoć et al., (2011) produced revised plots to determine biogenic gas content in CBM with compensation for thermal maturity (see Figure 4-21). This suggests there is potentially up to 30% biogenic gas in some AMM samples. It should be noted however that the low-maturity end-member ($\delta^{13}C_{CH4} = -50‰$ and $C_1/(C_2+C_3) = 10$ at $R_o = 0.5\%$) may not be representative, especially when considering the possibility of early mature gases. The utility of these plots is diminished for high maturity (*e.g.* anthracite) gases which are typically isotopically heavy and compositionally dry.

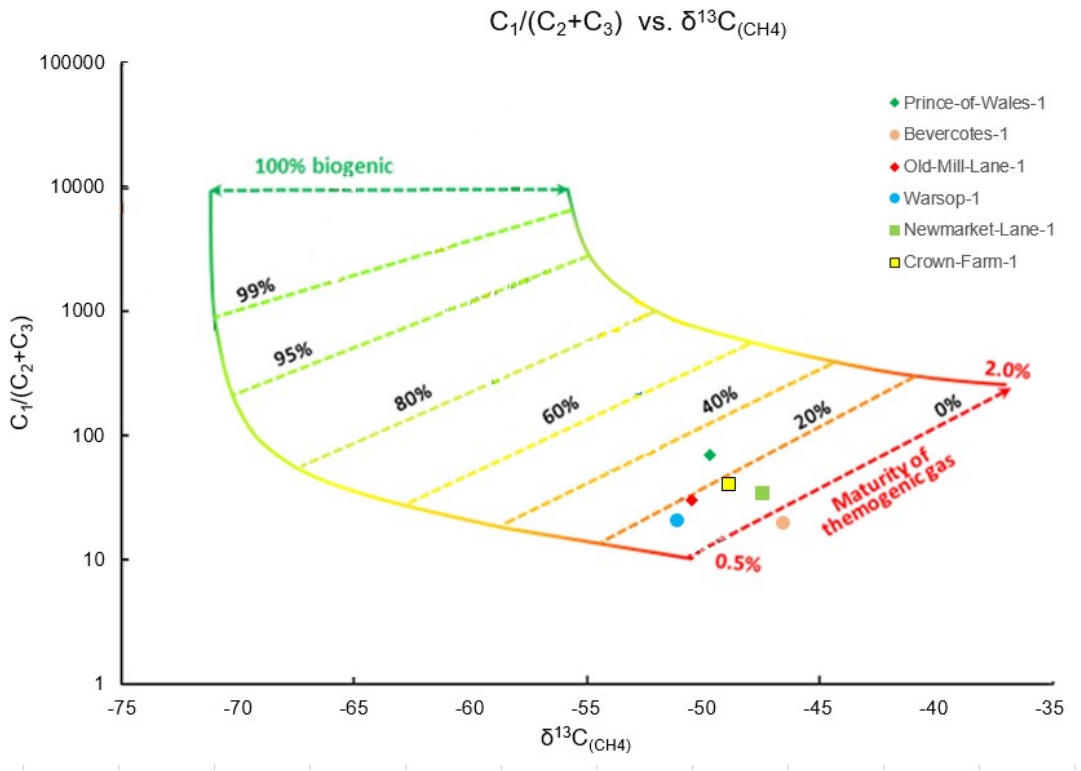

Figure 4-21 – Plot of $C_1/(C_2+C_3)$ vs. $\delta^{13}C_{CH4}$ (modified after Strąpoć et al., 2011). Plot is essentially a modified Bernard plot, between thermogenic and biogenic end-members, with compensating lines for thermal maturity. AMM gases appear to show <30% biogenic gas.

The gases plot in the 'thermogenic' field of a Whiticar style plot (Whiticar, 1996), specifically in the 'Early-Mature' thermogenic field (Figure 4-22). The diagnostic fields of the Whiticar plots are based on numerous sources, and 'Early-Mature' is based on early-mature methane derived from type I/II kerogens, while humic sourced methane plots to the lower right with isotopically heavier $\delta^{13}C_{CH4}$ and δD_{CH4} values. As thermogenic gases from type III kerogen are typically heavier than those sourced from type I/II kerogen (Whiticar, 1994, and references therein), the AMM samples are isotopically lighter than should be expected if a purely thermogenic coal source is assumed. While this could be a result of isotopic fractionation or type I/II kerogen input into the coals, the majority of gas is clearly generated by the coals, which suggests modification to a lighter isotopic signature. This could be the addition of an isotopically lighter microbial methane component.

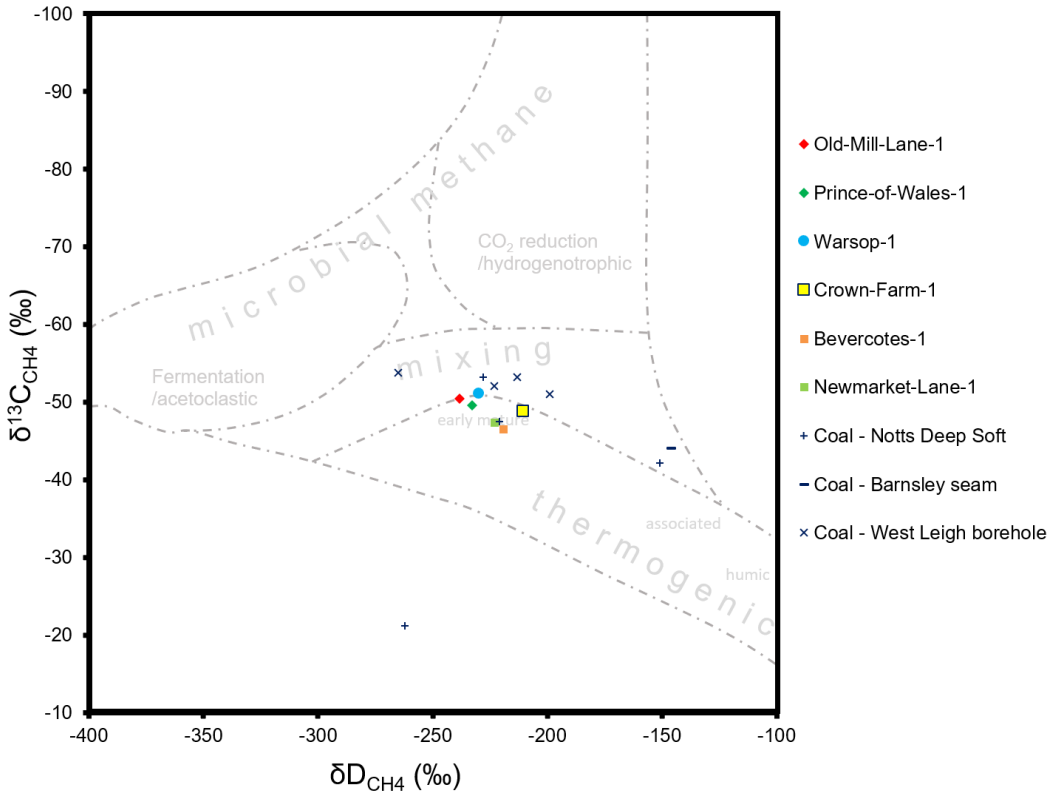

Figure 4-22 – Plot of $\delta^{13}C_{CH4}$ vs. δD_{CH4}, after Whiticar (1994), plotting data from AMM gases (this study), and UK coal gases reported by Hitchman (1989).

In light of the probability of an external component(s) to AMM gases, the relatively tight isotopic and compositional grouping within AMM samples was not expected given the varied geography and history of the sites. The AMM $\delta^{13}C_{CH4}$ and δD_{CH4} measurements overlap with some of the previous methane samples from the Deep Soft seam (Nottinghamshire, mine unspecified) and other coals in the UK (Hitchman *et al.*, 1989) (see Figure 4-22), but there is a wide spread in values, especially in δD_{CH4}. Most gases do not show unambiguous coal-type sources using $\delta^{13}C_{CH4}$ - δD_{CH4} diagnostic fields as per Whiticar (1994), nor are they isotopically distinct from other sources of methane such as landfill or wet North Sea gas (Hitchman *et al.*, 1989), possibly because the coal maturities observed correspond to the oil-window in type I/II kerogens.

The $\delta^{13}C_{CH4}$ observed alone in AMM however are in good agreement with most previous coal samples (Hitchman *et al.*, 1989) and also regional measurements of Nottinghamshire and Yorkshire mine emissions of 45.4 - 48.3 % (Zazzeri *et al.*, 2016). This shows a regional East Pennine trend to the coal gases of 53.8‰ > $\delta^{13}C_{CH4}$ > -40‰ (mean = -49.4‰, ±3.3 to 1σ; n=20). This is lighter than Scottish CBM gases (mean $\delta^{13}C_{CH4}$ = -41‰; this volume) and Welsh anthracites ($\delta^{13}C_{CH4}$ = -30.9‰ to -41.2‰;

mean = -36.5‰) (Zazzeri *et al.*, 2016), probably representing a difference in coal maturity in the different areas.

The hydrocarbon compositions and isotopic ratios occupy a fairly narrow range; more variation is seen within basins in other studies which is unexpected considering the widespread geographic locations and histories of the mine sites. AMM gases show a thermogenic $\delta^{13}C_{CH4}$ signature if thermogenic gases are defined as $\delta^{13}C_{CH4} > -50‰$ (Bernard *et al.*, 1976; Schoell, 1980; Burruss and Laughrey, 2010; Osborn and McIntosh, 2010; Tao *et al.*, 2012), despite the probable input of biogenic gas.

δD_{CH4} values show a much greater degree of variation. There is a wide range of δD values in coals, especially early-mature coals, which can make the distinctions between gas types fairly arbitrary and subject to varied interpretation. δD_{CH4} of thermogenic natural gases are sensitive to various processes such as thermal maturity, hydrogen exchange between water and organic matter during thermal maturation, source organic material δD, depositional water δD, formation water δD, and other factors (Schoell, 1980; Dai, 1993; Ni *et al.*, 2013), and are most likely basin-specific (Ni *et al.*, 2013). This feature could be useful for gas tracing purposes if they had a narrow range or were broadly constrained, however isotopic values have a wide range and overlap with landfill gas and North Sea gas. This demonstrates that 'coal gases' do not have unique $\delta^{13}C_{CH4}$ and δD_{CH4} identifiers, especially at lower ranks.

The $\delta^{13}C_{CH4}$ of purely thermogenic methane derived from type III kerogen for a given thermal maturity can be calculated using predictive models based on peat pyrolysis experiments. For the thermal maturities observed in East Pennine coals (Ro = 0.50% to 1.03%), thermogenic gases are calculated to -26.2‰ to -34.5‰ (see Appendix). It can be seen that all of the AMM gases are isotopically lighter than would be expected for a purely thermogenic gas. Simple binary mixing of these isotopic values with an assumed biogenic end-member of -70‰ allows an estimate of the contribution of biogenic gas (see Appendix). Thus 34% to 57% of the methane in AMM samples is derived from a non-thermogenic source. This component would have to be ancient microbial CH_4 related to primary biogenic gas, or produced more recently.

Thermogenic end-member = -34.5‰		Thermogenic end-member = -26.2‰	
Min biogenic	Max biogenic	Min biogenic	Max biogenic
34%	47%	47%	57%

Table 13 – Table of estimated biogenic gas component using different thermogenic gas end-members. Please see the Appendix for detailed calculations.

4.8.4 Radiocarbon

Several samples were submitted for radiocarbon analysis, but only 1 sample had sufficient methane for radiocarbon analysis to be performed. Warsop was determined as radiocarbon 'dead', indicating no resolvable inputs of modern carbon into methane above the baseline. The hydrocarbons at Warsop were 'wetter' than the other samples indicating a strong thermogenic origin, so the radiocarbon dead nature of these gases is perhaps unsurprising. Warsop was however high in CO_2 content, and it could be possible that oxidation of modern carbon (*e.g.* mine timbers) formed CO_2 which may have a resolvable modern carbon input. This was observed in abandoned mines in the Ruhr basin, where radiocarbon ages for CO_2 of ~13 ka were observed (Thielemann *et al.*, 2004).

4.8.5 Methanogenesis in Abandoned Mines

Isotopic evidence suggests the presence of microbial methane, but does not constrain the timing or type of any methanogenesis. In other areas, mine gas hydrocarbon and isotopic compositions have been observed to change over time related to microbial degradation of coals and timbers (Thielemann *et al.*, 2004). If the processes driving these changes are known it could be possible to predict the evolution of mine gases and future emissions, support the mitigation of hazardous mine gases, and even assist the generation of additional methane via the stimulation of microbes by enhancing certain nutrients.

Two stages of methanogenesis are known from various coalfields; primary and secondary (Levine, 1993; Whiticar, 1994; Smith and Pallasser, 1996; Golding *et al.*, 2013). Primary microbial methane is predominantly generated at low ranks (< 0.3 R_o) and generally expelled with further burial (Levine, 1993; Kaiser *et al.*, 1994), although probably continues to form at higher ranks alongside low-mature thermogenic gases (Meslé *et al.*, 2013). Secondary microbial methanogenesis can occur at any point post-coalification. Generation of secondary microbial methane is commonly associated with

the 'inoculation' of the seams with microbes, as elevated temperatures and pressures associated with coalification sterilise the coals (Wilhelms *et al.*, 2001). The onset of secondary microbial methanogenesis can sometimes be tied to an 'inoculation' event such as groundwater infiltration (Flores *et al.*, 2008). Variations in the pathway of microbial methanogenesis (CO_2 reduction vs. acetoclastic methanogenesis) have been reported across basins, hypothesised to be related to nutrient availability/groundwater recharge *e.g.* Powder River Basin CBM (Flores *et al.*, 2008; Green *et al.*, 2008).

The rates of 'typical' secondary microbial methane generation in coal basins are assumed to be geologically slow (Vinson *et al.*, 2017), but abandoned mines can show a recent phase of methanogenesis initiated by the weathering and degradation of coals and timbers left in the mine (Krüger *et al.*, 2008; Beckmann, Krüger, *et al.*, 2011). This post-mining secondary methanogenesis could be considered a separate process to the microbial methanogenesis that occurs in unmined CBM basins. Studies on the relatively dynamic environment of abandoned mines have seen increasing interest with the advent of enhanced microbial methane production.

The isotopic difference between $\delta^{13}C_{CH4}$ and $\delta^{13}C_{CO2}$ can be expressed as a simple difference *i.e.* $\Delta\ \delta^{13}C_{CO2\text{-}CH4}$ (a.k.a. ε_c) or as an alpha factor (Whiticar, 1996) via the equation:

$$\alpha^{13}C_{CO2-CH4} = (\delta_{13}C_{CO2} + 1000)/(\delta_{13}C_{CH4} + 1000)$$

Variations in this carbon isotope fractionation have been utilised in many studies as a proxy measurement for determining methanogenic pathways and are a common tool in fingerprinting gas genetic types (Whiticar, 1999; Strąpoć *et al.*, 2011; Vinson *et al.*, 2017). Methanogenesis via CO_2 reduction produces a greater offset in $\Delta\ \delta^{13}C_{CO2\text{-}CH4}$ than acetate fermentation due to the greater isotopic fractionation of CO_2 associated with that pathway (Whiticar, 1999; Vinson *et al.*, 2017). Previously measured UK coal gas samples showed $\Delta\ \delta^{13}C_{CO2-CH4}$ plotting in the methane oxidation field (see Figure 4-23), and were distinct from other sources of gas (landfill, *etc*.). This offset was believed to be a diagnostic fingerprint of coal gases where $\delta^{13}C_{CH4}$ and δD_{CH4} had overlap with other sources *e.g.* landfill (Hitchman *et al.*, 1989). Gases in this study plot partly in the acetoclastic methanogenesis field (

Figure 4-23 - though with caveats discussed below), but crucially appear more similar to gases measured in some UK landfills, which shows the mine gas composition is probably temporal in nature, and that $\Delta\ \delta^{13}C_{CO2\text{-}CH4}$ is not a useful discriminant for

characterising AMM gases. This is possibly due to the similar nature of microbial pathways in gas generation.

An issue with the diagnostic fields in $\delta^{13}C_{CO2}$ vs. $\delta^{13}C_{CH4}$ plots (

Figure 4-23) is the assumption of an ideal methanogenic system. Non-methanogenic processes affect the isotopic composition and mass-balance of gases (Vinson *et al.*, 2017), and are likely to include:

- External (non-microbial) inputs of CO_2 or CH_4 from thermogenic gas or inorganic processes
- Competitive substrate utilisation by bacteria such as sulphate/iron reducers producing CO_2 with $\delta^{13}C_{CO2}$ closer to the original organic substrate
- Methane oxidation and non-methanogenic CO_2 utilisation
- Formation water interaction (gas loss and mineral interactions)

Addition of thermogenic gases results in the shift of observed isotope values to the lower right (Figure 4-23), which could imply CO_2 reduction as the dominant methanogenic pathway with added thermogenic gas. Moreover, CO_2 in this system may be inorganically derived (*e.g.* carbonate dissolution) and unrelated to methanogenesis, yet driving the differences in apparent $\Delta\delta^{13}C_{CO2\text{-}CH4}$. Most importantly however, it demonstrates the cautious use of this technique to mixed-gas systems.

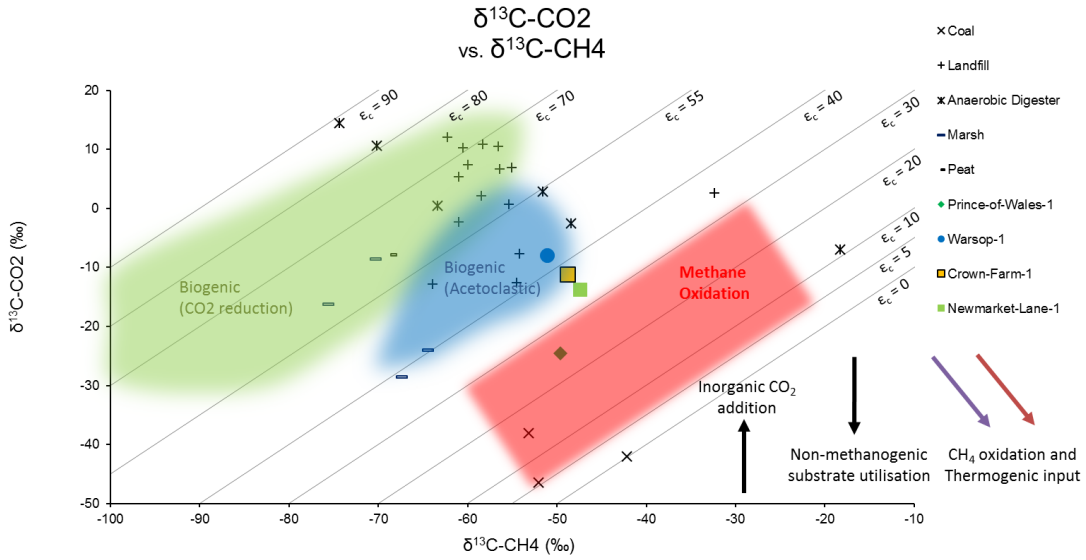

Figure 4-23 – Plot of $\delta^{13}C_{CO2}$ vs. $\delta^{13}C_{CH4}$. Methanogenesis by CO_2 reduction has a larger isotopic difference than acetoclastic. Where $\varepsilon_c = \delta^{13}C_{CO2} - \delta^{13}C_{CH4}$. Diagnostic fields after Whiticar (1999). Arrows depict effects of non-methanogenic effects on the observed isotope systems (Vinson et al., 2017), and carbonate-dissolution CO_2 addition. Addition of thermogenic gas can shift the apparent $\Delta\ \delta^{13}C_{(CO2-CH4)}$ away from the isotopic values associated with gas generation type. Coloured data samples from this study. Other data from Hitchman et al., (1989).

Thielemann et al., (2004) analysed gases from abandoned mines in the Ruhr basin, Germany, and found a mixed thermogenic-biogenic system with similar $\delta^{13}C_{CH4}$ to this study data ($\delta^{13}C_{CH4}$ = -40.0‰ to -57.3‰) where ethane became progressively isotopically heavier with time, yet methane remained unchanged. The microbial component was more apparent in active mines and abandoned mined areas than unmined coals. They found living methanogenic archaea in AMM waters, and postulated that at least some microbial methane was possibly being actively generated in mines, hypothesised to be via CO_2 reduction based on $\delta^{13}C_{CH4}$ and δD_{CH4}. The pattern of isotopic separation between methane and ethane suggested ongoing microbial methanogenesis coupled with a gradual depletion of thermogenic ethane desorbing from coals.

Krüger et al., (2008) also found a mixed thermogenic-biogenic gas system from a mine in the Ruhr basin shut in the 1960's, and cultured methanogenic microbes and fungi from timbers and hard coal samples. The methanogens were found to be from the *Methanosarcinales* order which utilise the acetate fermentation pathway. Analysis of $\delta^{13}C_{CH4}$ from methane generated from cultured samples indicated $\delta^{13}C_{CH4}$ = -47.4±1.31‰ from hard coals and $\delta^{13}C_{CH4}$ = -55.8±3.25‰ from timbers,

while the overall mine atmosphere was slightly heavier at 45.6±4.32‰ which indicated both an ongoing mix with thermogenic gas, and also discrepancies with the typical isotopic boundaries associated with biogenic and thermogenic gases (Bernard *et al.*, 1976; Whiticar, 1996). From this it was concluded that microbial methanogenesis is probably a current process in the abandoned mines studied. Beckmann et al., (2011a), (2011b), and Wei et al., (2014) also highlighted the role of acetoclastic methanogenesis in abandoned coal mines. Other authors suggest CO_2 reduction as the methane formation mechanism (Thielemann *et al.*, 2004; Flores *et al.*, 2008; Strąpoć *et al.*, 2008), and this seems the dominant pathway for 'traditional' (non-mined) CBM deposits (Vinson *et al.*, 2017).

Coals are traditionally considered fairly resistant to microbial degradation due to their refractory nature, and are more resistant at higher ranks (Strąpoć *et al.*, 2011). The nature of the breakdown processes are poorly understood and subject to ongoing research (Furmann *et al.*, 2013; Sekhohola *et al.*, 2013). Oxidative weathering is known to solubilise the humic components in lignites and coals into humic acids, which are more bioavailable to microbes and have the potential for greater substrate production for methanogenesis (Sekhohola *et al.*, 2013; Tamamura *et al.*, 2015). Oxygen is present in the mines for the duration of mining which may initiate the oxidation and weathering of the coals and timbers facilitating further microbial degradation under anaerobic conditions (Krüger *et al.*, 2008).

This enhanced bioavailability of coal provides a different environment with greater availability of substrates and nutrients not seen in unworked coal seams, and the oxygen-poor environment (but not strictly anaerobic) is likely to affect the microbial consortium. The detection of acetogenic bacteria and fungi degrading coals and timbers in abandoned mines can provide the acetate for methanogenesis (Beckmann, Krüger, *et al.*, 2011), favouring acetoclastic methanogenesis over CO_2 reduction where H_2 would be the limiting factor, whereas in unmined seams or 'typical' CBM, CO_2 reduction is a more common methanogenic pathway where nutrients and substrate availability is extremely limited (Vinson *et al.*, 2017).

$\delta^{13}C_{CH4}$ and δD_{CH4} isotope values are fairly uniform despite the different mine environments and wide geographic range, and are similar to previously measured samples of East Pennine coal gases time (Hitchman *et al.*, 1989). If methanogenesis were occurring the production rates would be expected to differ significantly between the sites and over time due to environmental conditions, and differences would be

observed in the volumes of microbial gas generated and the volumes of thermogenic gases degassing from the mines, and would lead to variations in resultant methane stable isotope values (*e.g.* Thielemann *et al.*, (2004)), but this is not observed. There is some correlation between $\delta^{13}C_{CO2}$ and $\delta^{13}C_{CH4}$ indicating possible acetoclastic methanogenesis, but this could be related to inorganic CO_2 addition. The microbial consortium of East Pennine coal waters is unknown, but methanogenic archaea (*Methanomassiliicoccus luminyensis*) are known in Welsh mine water drainage (Falagán *et al.*, 2016)

The observation of no modern ^{14}C in methane has implications for recent methanogenesis; modern ^{14}C could be incorporated into methane either by CO_2 reduction (CO_2 derived from oxidation of mine timbers), or acetate fermentation (acetate derived from microbial breakdown of timber, or derived from CO_2 by acetogenic pathways). If methanogenesis were occurring, timbers would provide more bioavailable substrates than hard coal and so detectable ^{14}C could be expected in generated methane. At least at Warsop, the methane was radiocarbon dead, so no modern day methanogenesis is thought to be occurring. As methanogens are obligate anaerobes (Formolo, 2010), it could be that oxygen partial pressures are too high for methanogens. Another significant factor would be competitive substrate utilisation; bacteria that reduce iron or sulphate can extract higher energy yields from substrates than methanogens and will outcompete them. Mine waters are known to be high in sulphates and iron as a result of the oxidation of pyrite which is abundant in UK coals in the East Pennine coalfield (Spears and Tewalt, 2009; Karacan *et al.*, 2011) which would retard methanogenesis in favour of other non-methanogenic microbial pathways.

Too little information is available to determine if any current microbial methanogenesis is occurring at AMM sites; mine gases plot within, or near to, the diagnostic field of acetoclastic methanogenesis on a $\delta^{13}C_{CH4}$ vs. $\delta^{13}C_{CO2}$ plot (Whiticar, 1999), but a radiocarbon measurement from Warsop exhibited ^{14}C 'dead' methane. This indicates that microbial methanogenesis from mine timbers (which is the most bioavailable substrate for methanogenesis) is not occurring in that sample. This does not preclude microbial methanogenesis from ^{14}C-dead coal substrates, nor from methanogenesis in the other mines, but the narrow range in $\delta^{13}C_{CH4}$ and δD_{CH4} across all samples do not indicate recent methanogenic activity that is known to produce significant isotopic fractionation effects. Thus, the biogenic gas component identified is probably preserved from a much earlier age, anywhere from the peat deposition period

and diagenesis to post-coalification secondary microbial methanogenesis. The apparent preservation of in-seam gas contents related to the Permo-Carboniferous unconformity in parts of the coal basin (Creedy, 1988), and the relatively narrow range of stable isotope values observed in this study and Hitchman *et al.*, (1989), would suggest that the biogenic addition occurred prior to that period.

A temporal study would be required to track changes which may indicate modern microbial activity; if purely fossil gases are emanated (such as thermogenic gas or ancient microbial-mixed) then it would be expected that the mine gases would become gradually isotopically and compositionally heavier with time as the reservoir is depleted (*e.g.* Rice, 1993; Thielemann et al., 2004). Whereas, an increase in microbial methanogenesis would trend towards isotopically and compositionally lighter gases, and a greater separation between methane and ethane isotopes. Radiocarbon measurements on CO_2 as well as methane would help constrain any contributions of microbial gases to the mine atmosphere.

4.8.6 Air Saturated Water Calculations

As many mines are continually pumped of water to maintain access to coal seams, the water table is artificially lowered and kept in that state for several decades. It is then assumed that recharge water into mines is fresh meteoric water having originated at the surface most likely during or after the working lifetime of the mines, as formation water is removed early in the process. This is corroberated by Caphouse colliery (West Yorkshire) coal mine pumping operations which vary with rainfall, and $\delta^{18}O_{H2O}$ and δD_{H2O} measurements which suggest meteoric water input (Burnside *et al.*, 2016) and other UK mine dewatering operations (Younger *et al.*, 2015).

The surface elevation of the mine shafts have a limited range from 33 m to 110 m above sea level so a general value of 50 m was chosen to represent elevation in ASW calculations. Such small differences in elevation have negligible effect on the outcome of ASW calculations. The mean weather temperature is assumed to be identical over the geographic area.

4.8.7 Noble Gases

4.8.7.1 Atmospheric Noble Gases (ANGs)

Subsurface hydrocarbons typically have ANG inventories derived from ASW that may have been subsequently affected by various fractionation processes. In some AMM samples, there can also be a component of atmospheric air.

AMM gas samples typically have an order of magnitude higher ANG concentrations than Scottish CBM (this volume), and are two orders higher in samples that show atmospheric ingress.

ANG's can be expressed as ratios relative to ^{36}Ar (*e.g.* $i/^{36}Ar$), and these ratios can be normalised to the air ratio to give a fractionation factor F:

$$F = [(i/^{36}Ar)_{sample} / (i/^{36}Ar)_{air}]$$

These are listed in Table 14, and plotted graphically on Figure 4-24, along with the calculated maximum solubility patterns for gas/water/oil systems after Bosch and Mazor, (1988). This plot references the ANG ratios relative to the ratios found in air, in ASW, and oil, based on calculated solubilities. This allows a graphical representation of where the samples fall in relation to solubility-based distribution patterns with gas-water or gas-oil interactions (for a more in-depth description please see ANG section of Chapter 3).

All samples except Warsop-1 and Bevercotes-1 show a typical pattern of a gas/water interaction where ANG's are stripped from the water phase. Crown-Farm-1 and Old-Mill-Lane-1 have the largest atmospheric ingress, and so plot close to the air-value (= 1; horizontal line). Samples with significantly elevated $^{20}Ne/^{36}Ar$ ratios relative to ASW (Crown-Farm-1, Old-Mill-Lane-1, Newmarket-Lane-1) have atmospheric air ingress, and the other samples show $^{20}Ne/^{36}Ar$ that can easily be explained by solubility fractionation from ASW as water is degassed.

Warsop-1 and Bevercotes-1 show an excess of heavy ANG's ($^{84}Kr/^{36}Ar$ and $^{132}Xe/^{36}Ar$) which are at or above ASW ratios, which is above the typical solubility of gas/water interaction. This indicates either possible interaction with an oil phase possessing enrichments of heavy ANG's, or the release of trapped sedimentary heavy noble gases (*e.g.* Torgersen and Kennedy (1999); Zhou *et al.*, (2005)). These two samples also exhibit the lowest $C_1/(C_2+C_3)$ ratios which suggests an oil association. Bevercotes colliery is known to have oil shows, though there is little documentation available on Warsop colliery. Oil interaction is therefore believed to have caused the enrichments of $^{84}Kr/^{36}Ar$ and $^{132}Xe/^{36}Ar$ of ANG's observed in these samples.

Bevercotes-1 shows the most crustal signatures and the least air contribution. Other samples show less crustal signatures and greater ANG contributions, highlighting the dilution of the crustal components with ANG's.

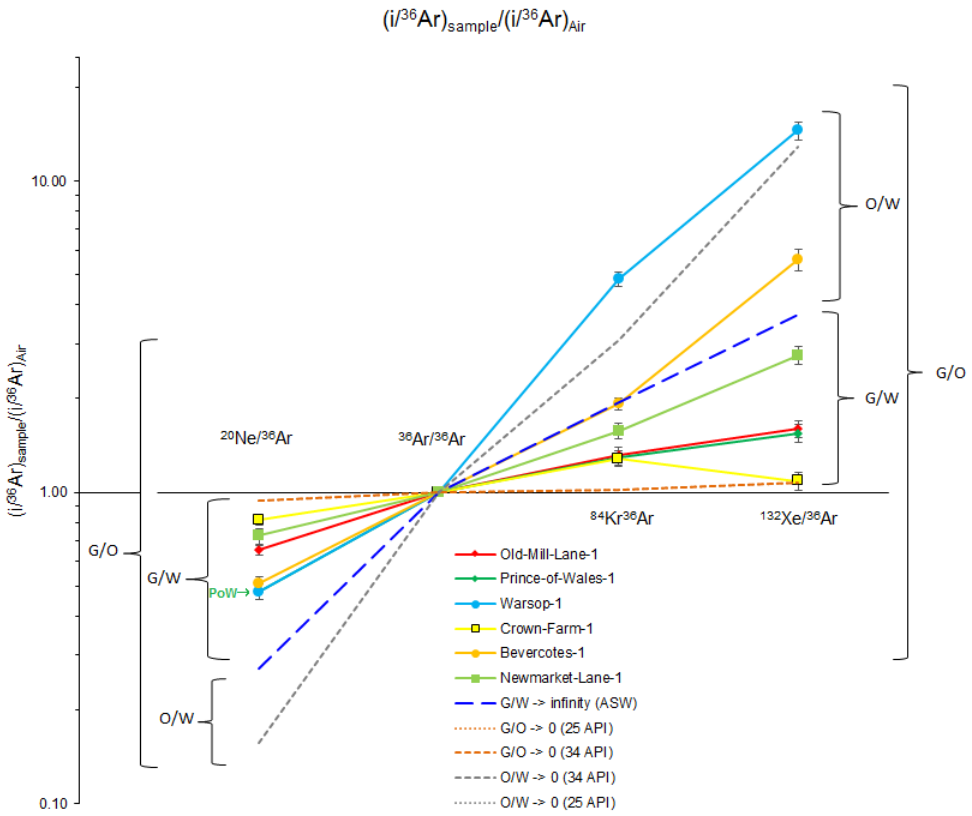

Figure 4-24 – Plot of $i/^{36}Ar$ (sample) normalised to the $i/^{36}Ar$ air-ratio, after Bosch and Mazor (1988). The x-axis line represents the air-ratios (and consequently is the hypothetical non-solubility-controlled gas/water ratio → 0), while the gas-water maximum solubility fractionation line (gas/water → ∞) calculated for generalised P-T conditions for the mines is represented by the dashed blue line (ASW). Thus, a system where gas equilibrates with water would be expected to fit between the ASW and air lines (labelled G/W). Oil/Water and Gas/Oil maximum fractionation lines are also calculated for 2 crude oils of different densities using the solubility data from Kharaka and Specht (1988) and generalised P-T conditions for the mines, representing extreme examples of possible solubility fractionation (labelled O/W). Gas equilibrated with an oil-phase which has been previously equilibrated with ASW is also calculated (labelled G/O).

	$(^{20}Ne/^{36}Ar)_{sample}/(^{20}Ne/^{36}Ar)_{Air}$	$(^{36}Ar/^{36}Ar)_{sample}/(^{36}Ar/^{36}Ar)_{Air}$	$(^{84}Kr/^{36}Ar)_{sample}/(^{84}Kr/^{36}Ar)_{Air}$	$(^{132}Xe/^{36}Ar)_{sample}/(^{132}Xe/^{36}Ar)_{Air}$
Old-Mill-Lane-1	0.65	1.00	1.32	1.60
Prince-of-Wales-1	0.48	1.00	1.29	1.55
Warsop-1	0.48	1.00	4.84	14.53
Crown-Farm-1	0.81	1.00	1.28	1.08
Bevercotes-1	0.51	1.00	1.92	5.59
Newmarket-Lane-1	0.72	1.00	1.58	2.75

Table 14 – Table of fractionation factors (F) relative to the air ratios.

4.8.7.2 Crustal Noble Gases

All samples show low $^{3}He/^{4}He_{(Ra)}$ similar to other sedimentary basins in the UK (Oxburgh *et al.*, 1986), and an order of magnitude lower than Scottish CBM (this volume), which indicates the purely radiogenic nature of the helium with negligible mantle or atmospheric/ASW addition. Old-Mill-Lane-1, Bevercotes-1, and Newmarket-Lane-1 have total ^{3}He concentrations that are lower than the atmospheric value (69.3%, 77.6%, 40.0% respectively). Prince-of-Wales-1, Warsop-1 and Crown-Farm-1 show concentrations of ^{3}He above atmospheric (562%, 172%, 398% respectively). Crown-Farm-1 and Old-Mill-Lane-1 show the highest atmospheric ingress yet have ^{3}He concentrations an order of magnitude apart, and therefore direct atmospheric ingress has an insignificant effect on $^{3}He/^{4}He_{(Ra)}$ due to the negligible concentration of helium in the atmosphere relative to the ^{3}He concentrations found in AMM gases. There is also no correlation between $^{3}He/^{4}He_{(Ra)}$ and $^{4}He/^{20}Ne$ which might be expected in samples that have seen varying degrees of groundwater or air interaction.

Györe *et al.*, (2018) calculated the *in situ* radiogenic ^{4}He production from the uranium & thorium concentrations in UK coals (1.6±0.7 and 4.7±1.7 mg/kg; (Hamilton, 1974)) and a mean coal age of 308.5 Ma to be a maximum of 141.7 cm^3/tonne. This would generate ^{4}He concentrations of 44.3 ppmv assuming all the ^{4}He was in the gas phase and diluted with methane from the coals (at 3.8 to 4.1 m^3/tonne in Nottinghamshire and Yorkshire (Creedy, 1991)), which corresponds to only 14% of the measured ^{4}He, thus showing the bulk of the helium does not originate from coals (Györe *et al.*, 2018). This is not surprising as coals are not particularly rich in uranium or thorium relative to other rock types due to their lack of clays or other detrital minerals in comparison to other rock types (Rider, 2002). Thorium is mainly contained in the clay/detrital fraction of coals, while uranium being more mobile in the subsurface (Rider, 2002) is found in both clays and the organic matter fractions. The uranium/thorium ratios in the Parkgate seam are thought to to be controlled by

seawater (Spears and Tewalt, 2009). Additionally, the helium storage capacity of UK coals is small due to very low porosities (Creedy, 1988). It is probable that the majority of helium is sourced from adjacent more porous units *e.g.* sandstones that are connected to the mine void space by extensive fractures, and the helium is mainly generated within rocks with higher uranium & thorium content such as shales, or migrated from the deep crustal basement.

Helium is not believed to adsorp onto coals at geological temperatures and pressures (Ozima and Podosek, 2001; Rodrigues and Lemos de Sousa, 2002) and is not believed to have a significant inventory within coals due to low fracture porosity (Creedy, 1988). Unlike in a typical hydrocarbon reservoir where helium accumulates over geological periods of time in a physical trap and produced alongside hydrocarbons, in AMM a quantity of the helium originally in the formations must have been removed during mine dewatering and then also removed over time with continued mine ventilation, so observed concentrations are only what has accumulated in the mine atmosphere since closure, and concentrations must be regarded as minima of their original values. Nonetheless high concentrations are observed in coal gases, which suggests a significant 'trapped' component. The vitrinite maceral is rich in micropores which are are defined as <2 nm, compared with the molecular diameter of helium being 0.186 nm (Rodrigues and Lemos de Sousa, 2002). These micropores could have the potential to store quantities of helium which allow the concentrations of helium observed, which is released along with desorbed methane from coals, and allow elevated methane contents over time which are an ideal tracer for tracking mine gas migration to the subsurface.

Even higher concentrations of helium (0.1 - 0.2%) were observed in drainage gases from nearby Harworth colliery (N. Notts) and Yorkshire Main colliery (Creedy, 1988). This shows high helium contents are regionally pervasive, and also observed in Scottish coals (this volume). High helium content is probably ubiquitous in Paleozoic strata, related to the age of the formations as radiogenic components are age accumulative. Similarly aged Paleozoic gases contain high concentrations of helium (Kotarba, 2001; Kotarba and Rice, 2001).

Concentrations of ^{4}He are broadly similar to those previously measured in the coalfield, with 3 samples showing over 1000 ppm; however atmospheric ingress has diluted ^{4}He concentrations significantly in Crown-Farm-1 and Old-Mill-Lane-1.

If the estimates for the percentage of air ingress values (see Bulk Gases-Atmospheric Ingress) are used to correct the ^{4}He values for dilution (ignoring atmospheric helium), this results in 'undiluted' ^{4}He values of 611 ppm (Old-Mill-Lane-1) and 1042 ppm (Crown-Farm-1) which are similar to the other samples. Interestingly, Warsop-1 shows the lowest measured helium content (338±16 ppm) but has not experienced significant dilution via atmospheric ingress, as the ANG concentrations and $^{20}Ne/^{36}Ar$ ratio are closer to ASW values than air, and $^{4}He/^{20}Ne$ = 1057±67 which shows the gas has little atmospheric component.

There is a clear correlation between $^{4}He/^{36}Ar$ and $^{40}Ar/^{36}Ar$ (Figure 4-25). Due to mass-fractionation, absolute $^{21}Ne^{*}$ cannot be calculated for most samples. However, a similar trend exists with $^{21}Ne/^{22}Ne$ and $^{4}He/^{36}Ar$ (Figure 4-26) and $^{21}Ne/^{22}Ne$ vs. $^{40}Ar^{*}/^{36}Ar$ (not shown). These show that the crustal components are well mixed and show a clear two component mixing between a crustal and an atmospheric end-member.

AMM gases contain 12 ppm $^{40}Ar^{*}$ (Warsop-1) to 37 ppm $^{40}Ar^{*}$ (Bevercotes-1), and $^{40}Ar^{*}$ generally comprises less than 10% of the total ^{40}Ar (except Bevercotes-1; 24%). $^{40}Ar/^{36}Ar$ ratios are lower than those observed in Scottish CBM (this volume), owing to both lower absolute concentrations of $^{40}Ar^{*}$, and higher dilutions with ANG's. *In situ* generated $^{40}Ar^{*}$ is primarily age-accumulative, however East Pennine coals are not hugely dissimilar in age (average: ~308.5 Ma) to the Scottish coals studied (~320 Ma), so the lower $^{40}Ar^{*}$ contents in the East Pennine coalfield are possibly due to lesser *ex situ* input (*i.e.* mantle or deep crustal basement) into the English coal gases.

The $^{4}He/^{40}Ar^{*}$ ratios range from 17.0±1 (Old-Mill-Lane-1) to 40.5±2 (Bevercotes-1), with an average of 36.3. A plot of $^{4}He/^{36}Ar$ vs. $^{40}Ar/^{36}Ar$ can be used to determine the local $^{4}He/^{40}Ar^{*}$ ratio (Zhou et al., 2005), resulting in a local end-member of 33.2 (see Figure 4-25), much higher than the crustal average of 4.8 (Ballentine and O'Nions, 1992), San Juan CBM (15.5) (Zhou et al., 2005), and CBM from central Scotland (15.8, this volume). This could be due to increased U+Th abundance (producing ^{4}He) in the mined environment, e.g. greater interaction with detrital minerals in adjacent sediments. The lower $^{40}Ar^{*}$ absolute concentrations compared with Scottish CBM (this volume) could also suggest lower K content in surrounding rocks, but could also be an artefact of lower ex situ $^{40}Ar^{*}$ inputs (i.e. deep crustal or mantle component).

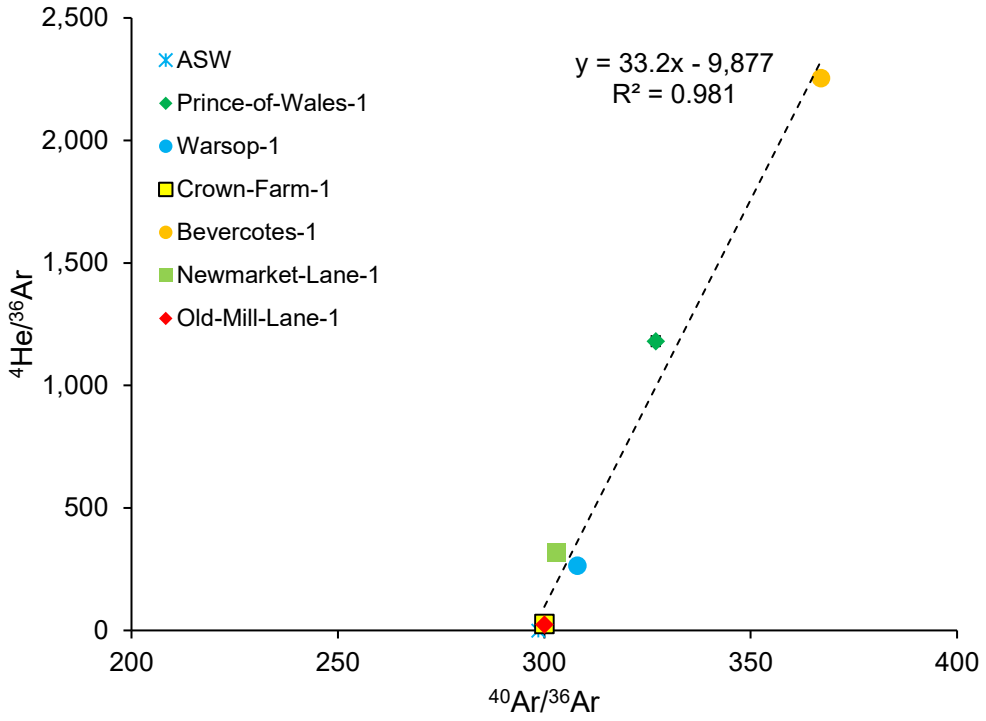

Figure 4-25 – Plot of 4He/36Ar vs. 40Ar/36Ar. Errors may be smaller than symbols.

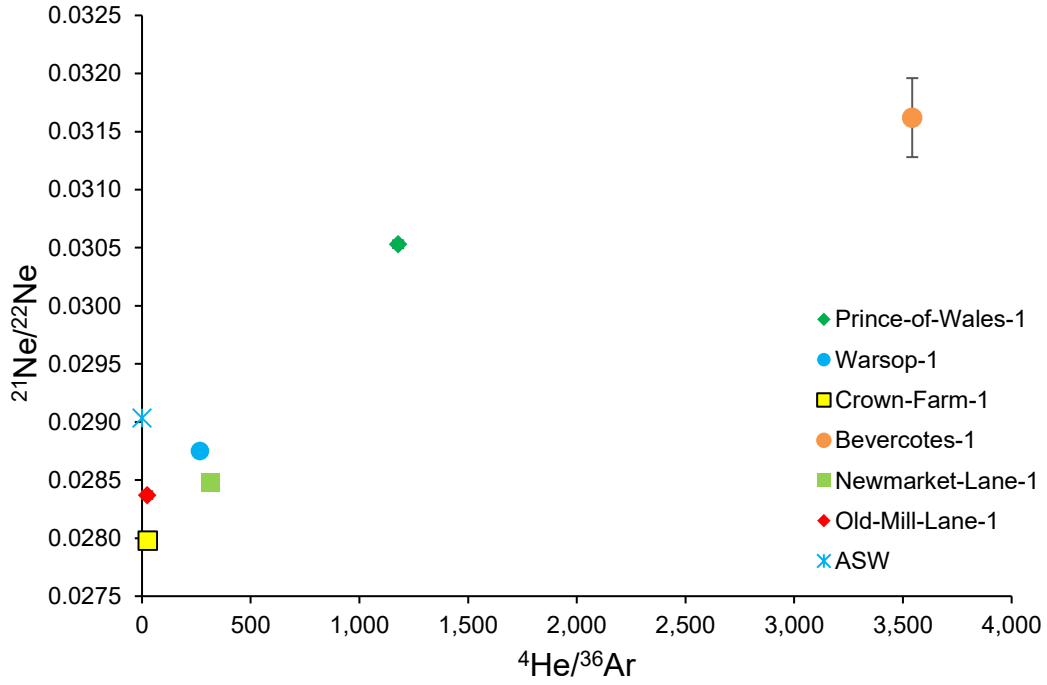

Figure 4-26 – Plot of $^{21}Ne/^{22}Ne$ vs. $^{40}Ar/^{36}Ar$. As ^{22}Ne and ^{36}Ar are primordial, their ratio can be assumed constant and thus a correlation between ^{21}Ne and ^{4}He can be observed.

Preferential release of ^{4}He from minerals at lower temperatures (Ballentine et al., 1994) is also a distinct possibility, especially considering that the mines will have had a component of their crustal noble gases released during the mining process, and current observations have accumulated in the mine atmosphere since closure. Current mine temperatures are well below the argon closure temperature for minerals, and will facilitate ^{4}He release from minerals over $^{40}Ar^{*}$.

Hydrocarbons with a greater thermogenic signature are often associated with a greater radiogenic noble gas component, as generally higher maturities are associated with deeper systems (Hilt, 1873; Ballentine and Burnard, 2002). In AMM gases there is no obvious correlation between $C_1/(C_2+C_3)$ and any crustal noble gas concentration or ratio (*e.g.* $^{4}He/^{21}Ne^{*}$, $^{4}He/^{40}Ar^{*}$), indicating the two factors are unconnected. This is probably due to the basin history of UK Paleozoic coals, where maximum burial depth and therefore hydrocarbon composition was defined early on (Carboniferous-Permian), with subsequent uplift, degassing, and reburial of strata. Thus, the observed modern hydrocarbon composition is overprinted by secondary processes of migration and differential retention of methane/ethane rather than primary factors related to thermal maturity. In conventional hydrocarbon accumulations, noble gases and hydrocarbons are trapped in a system which may persist and be preserved over geological time, where noble gases will preferentially remain in the gas or oil due to their lower solubility in water.

In coal systems, there is little trapped gaseous component as hydrocarbons are retained by adsorption in the coal matrix and the coals remain water saturated. Groundwater flushing over geological time probably limits the extent of preservation of crustal noble gases from the time of hydrocarbon gas formation, as lighter noble gases (He, Ne, Ar) are not believed to adsorb onto or be retained in coals or other materials. An analogous situation would be the preferential loss of primary coalification CO_2 from coals due to dissolution in water over geological time. Furthermore, unlike in conventional hydrocarbon deposits or typical CBM, much of the water in the mines was removed for several decades. This could remove a component of preserved crustal components present in formation waters, and subject coals to atmospheric pressures which facilitates degassing of components within coals, ultimately depleting the crustal noble gas inventory.

The noble gas inventory represents an assemblage of remnant formation waters, modern meteoric recharge waters, admixtures with air in some samples, and

radiogenic components that have been recently released from parent minerals/macerals; and these cannot be correlated with the Paleozoic hydrocarbons.

Krause and Pokryszka (2013) recognise three phases in mine gas emissions: during mining, a 1 – 3 month period after a longwall mining ceases in a panel, and a ~15 year period post-mining phase where methane diminishes. AMM schemes operate in the latter stage. The volumes of methane desorbed into the mines decrease as coals become depleted of gas, and also as they become water saturated with the rising water table after pumping ceases.

It is hypothesised that components associated with degassing coals (methane, ^{4}He, $^{40}Ar^{*}$) will decrease relative to the ANG components as this occurs, *i.e.* lower $^{4}He/^{36}Ar$ or $^{4}He/^{20}Ne$ ratios. This could be an indicator of the remaining potential of a reservoir. Tracking the atmosphere-derived components via elevated ANG components could be used to trace air ingress from unsealed mine entries that reduce AMM scheme effectiveness.

4.9 Conclusions

Abandoned Mine Methane (AMM) gases from the East Pennine coalfield in Nottinghamshire and South Yorkshire possess methane contents from 35% to 79%, with the remaining volume mainly composed of N_2, CO_2, and trace noble gases. The N_2 is atmospherically-derived, with O_2 having been depleted in the mine workings, and introduced by vacuum pumping equipment used to produce gas. N_2 concentration in some samples increases linearly with the air-derived atmospheric noble gases. Mansfield and Sherwood colliery gases show significant atmospheric air ingress of up to ~53% and ~43% respectively. The source of CO_2 is mix of coal oxidation, and chemical carbonate dissolution when present at higher concentrations.

The methane exhibits a narrow range of $\delta^{13}C_{CH4}$ and δD_{CH4} values (mean: $\delta^{13}C_{CH4}$ = -49‰; δD_{CH4} = -226‰) which can be considered characteristic of the gases. These represent a primarily thermogenic origin sourced from the coal, but up to a third of the methane could be microbially derived. These isotopic ranges however overlap with other coal and non-coal sources (*e.g.* landfill), which makes stable isotope analysis an ambiguous tracing tool. One sample of methane was analysed for radiocarbon and was determined to be radiocarbon 'dead' as would be expected of fossil thermogenic methane. Previous studies however show mine gases may possess modern ^{14}C from

mine timbers (Thielemann *et al.*, 2004), so radiocarbon may not be a useful discriminant for coal mine gases.

All AMM samples, along with British coals in general, possess elevated ethane and higher hydrocarbon contents ($C_1/(C_2+C_3)$ = 23 – 76), which are products of the coalification process and localised interaction with oil. This property can be used to distinguish AMM gases from other gas sources with overlapping stable isotope signatures such as landfill.

Coals in abandoned mines have experienced a shift in redox conditions and chemical equilibria away from their undisturbed anoxic state. This leads to oxidative effects on coal chemistry and carbonate dissolution that affects the mass balance and isotopic signatures of mine gases. Thus several diagnostic tests based on stable isotope data (*e.g.* Bernard diagrams, Whiticar plots (Figure 4-8, Figure 4-9)), used to determine gas origin do not take into account the complexities of mixed thermogenic-biogenic systems, or other complexities of coal mine systems. This is partly because external inputs affecting the flux of both methane and CO_2 in mines (*e.g.* thermogenic methane, and CO_2 from carbonate dissolution) alter the isotopic signatures. Moreover, mine gases observed in other studies can be temporal with regards to hydrocarbon composition and stable isotopic signature due to desorption effects, microbial alteration, and possible concurrent microbial methanogenesis (Thielemann *et al.*, 2004; Krüger *et al.*, 2008; Niemann and Whiticar, 2017).

The atmospheric noble gases in samples without direct atmospheric ingress were introduced via air saturated water (ASW), and follow typical gas/water interaction patterns as mine gases interact with the ASW that is infiltrating the mines after closure. Bevercotes and Warsop colliery gases show $^{84}Kr/^{36}Ar$ and $^{132}Xe/^{36}Ar$ enrichments, which probably indicate interaction with an oil phase. Resolvable excess crustal $^{21}Ne^*$ and $^{40}Ar^*$ can be observed where samples have a smaller atmospheric dilution.

AMM gas samples contain significant concentrations of helium (350 - 1506 ppm), which are higher concentrations than could have been generated within the coals themselves from U and Th decay chains, and is likely mainly sourced from surrounding formations as well as the crustal flux of ^4He from depth. The helium shows a strongly radiogenic character (0.006 – 0.039 R_a) which is sometimes below the average crustal ratio, but in line with previously reported UK measurements (Oxburgh *et al.*, 1986). The coals and/or interbedded units have stored high concentrations of helium even in

shallow mines, and this makes helium an excellent tool for tracing coal gases to surface receptors.

4.10 Bibliography

Alkane Energy (2008) *Prince of Wales Alkane Development Plan*.

Alkane Energy (2009) 'Newmarket Alkane development Plan.pdf'. Available at: https://ukogl.org.uk/map/php/pdf.php?subfolder=industry_reports&filename=40984.pdf.

Allen, M. J. (1995) 'Exploration and exploitation of the East Pennine Coalfield', *Geological Society, London, Special Publications*, 82(1), pp. 207–214. doi:10.1144/GSL.SP.1995.082.01.14.

Appleton, J. D., Hooker, P. J., Smith, N. J. P. and Britain, G. (1995) *Methane, Carbon Dioxide and Oil Seeps from Natural Sources and Mining Areas: Characteristics, Extent and Relevance to Planning and Development in Great Britain: British Geological Survey, Analytical Geochemistry Series, Technical Report WP/95/1*. Technical. Keyworth, Nottingham: British Geological Survey.

Appleton, J. D. (2011) *User Guide for the BGS Methane and carbon dioxide from natural sources and coal mining dataset for Great Britain*, *OR/11/054*. Nottingham: British Geological Survey. Available at: http://nora.nerc.ac.uk/17444/1/OR11054.pdf.

Baldassare, F. J. and Laughrey, C. D. (1997) 'Identifying the sources of stray methane by using geochemical and isotopic fingerprinting', *Environmental Geosciences*, 4(2), pp. 85–94. doi:10.1111/j.1526-0984.1997.00005.pp.x.

Ballentine, C. ., Mazurek, M. and Gautschi, A. (1994) 'Thermal constraints on crustal rare gas release and migration: Evidence from Alpine fluid inclusions', *Geochimica et Cosmochimica Acta*, 58(20), pp. 4333–4348. doi:10.1016/0016-7037(94)90337-9.

Ballentine, C. J. and Burnard, P. G. (2002) 'Production, Release and Transport of Noble Gases in the Continental Crust', *Reviews in Mineralogy and Geochemistry*, 47(1), pp. 481–538. doi:10.2138/rmg.2002.47.12.

Ballentine, C. J. and O'Nions, R. K. (1992) 'The nature of mantle neon contributions to Vienna Basin hydrocarbon reservoirs', *Earth and Planetary Science Letters*, 113(4), pp. 553–567. doi:10.1016/0012-821X(92)90131-E.

BCURA (2002) *BCURA Database*. Cheltenham: British Coal Utilisation Research Association. Available at: http://www.bcura.org/coalbank.html.

Beckmann, S., Lueders, T., Krüger, M., von Netzer, F., Engelen, B. and Cypionka, H. (2011) 'Acetogens and Acetoclastic Methanosarcinales Govern Methane Formation in Abandoned Coal Mines', *Applied and Environmental Microbiology*, 77(11), pp. 3749–3756. doi:10.1128/AEM.02818-10.

Beckmann, S., Krüger, M., Engelen, B., Gorbushina, A. a. and Cypionka, H. (2011) 'Role of Bacteria , Archaea and Fungi involved in Methane Release in Abandoned Coal Mines', *Geomicrobiology Journal*, 28(4), pp. 347–358. doi:10.1080/01490451.2010.503258.

Bernard, B. B., Brooks, J. M. and Sackett, W. M. (1976) 'Natural gas seepage in the Gulf of Mexico', *Earth and Planetary Science Letters*, 31(1), pp. 48–54. doi:10.1016/0012-821X(76)90095-9.

Bernard, B. B., Brooks, J. M. and Sackett, W. M. (1978) 'Light hydrocarbons in recent Texas continental shelf and slope sediments', *Journal of Geophysical Research*, 83(C8), p. 4053. doi:10.1029/JC083iC08p04053.

Bosch, A. and Mazor, E. (1988) 'Natural gas association with water and oil as depicted by atmospheric noble gases: case studies from the southeastern Mediterranean Coastal Plain', *Earth and Planetary Science Letters*, 87(3), pp. 338–346. doi:10.1016/0012-821X(88)90021-0.

Burnside, N. M., Banks, D. and Boyce, A. J. (2016) 'International Journal of Coal Geology Sustainability of thermal energy production at the fl ooded mine workings of the former Caphouse Colliery , Yorkshire , United Kingdom', *International Journal of Coal Geology*. Elsevier B.V., 164, pp. 85–91. doi:10.1016/j.coal.2016.03.006.

Burrell, G. A., Robertson, I. and Oberfell, G. (1916) *Black Damp in Mines*. Washington D.C.: US Department of the Interior.

Burruss, R. C. and Laughrey, C. D. (2010) 'Carbon and hydrogen isotopic reversals in deep basin gas: Evidence for limits to the stability of hydrocarbons', *Organic Geochemistry*. Elsevier Ltd, 41(12), pp. 1285–1296. doi:10.1016/j.orggeochem.2010.09.008.

CEC (1988) *INVESTIGATION OF FIREDAMP AND ITS EMISSION IN COAL SEAMS*, *Technical Coal Research - EUR 11474 EN*. Commission of The European Communities. Available at: https://publications.europa.eu/en/publication-detail/-/publication/d48faada-31ce-4173-a9cb-f5b2ddff8453/language-en.

Creedy, D. P. (1988) 'Geological controls on the formation and distribution of gas in British coal measure

strata', International *Journal of Coal Geology*, 10(1), pp. 1–31. doi:10.1016/0166-5162(88)90002-X.
Creedy, D. P. (1991) 'An introduction to geological aspects of methane occurrence and control in British deep coal mines', *Quarterly Journal of Engineering Geology and Hydrogeology*, 24(2), pp. 209–220. doi:10.1144/GSL.QJEG.1991.024.02.04.
Creedy, D. P., Garner, K., Holloway, S. and Ren, T. X. (2001) *A Review of the Worldwide Status of Coalbed Methane Extraction and Utilisation*, *Report No. COAL R210 DTI/Pub URN 01/1040*. Department of Trade and Industry.
Creedy, D. P. and Pritchard, F. W. (1983) 'Nitrogen and carbon dioxide occurrence in UK coal seams', *International Journal of Mining Engineering*, 1(1), pp. 71–77. doi:10.1007/BF00881263.
Dai, J. (1993) 'Carbon and hydrogen isotopic compositions and origin identification of different types natural gas', *Natural Gas Geoscience*, 4(2–3), pp. 1–40.
DECC (2013) *the Unconventional Hydrocarbon Resources of Britain's Onshore Basins - Coalbed Methane (CBM)*. Department of Energy and Climate Change. Available at: https://www.ogauthority.co.uk/media/1694/promote_uk_cbm_2012.pdf.
Dias, R. F., Lewan, M. D., Birdwell, J. E. and Kotarba, M. J. (2014) 'Differentiation of pre-existing trapped methane from thermogenic methane in an igneous-intruded coal by hydrous pyrolysis', *Organic Geochemistry*. Elsevier Ltd, 67, pp. 1–7. doi:10.1016/j.orggeochem.2013.11.010.
DTI (2004) *METHANE EXTRACTION AND UTILISATION FROM ABANDONED COAL MINES - CHINA/UK TECHNOLOGY TRANSFER*, *Report No. COAL R251 DTI/Pub URN 03/1609*. Department of Trade and Industry.
Falagán, C., Smail, I., Grail, B. M. and Johnson, D. B. (2016) 'Microbial communities in passive remediation systems at three abandoned coal mine sites in the United Kingdom', in *IMWA 2016 – Mining Meets Water – Conflicts and Solutions*. Leipzig, Germany, pp. 796–803. Available at: https://www.imwa.info/docs/imwa_2016/IMWA2016_Falagan_29.pdf.
Flores, R. M., Rice, C. a., Stricker, G. D., Warden, A. and Ellis, M. S. (2008) 'Methanogenic pathways of coal-bed gas in the Powder River Basin, United States: The geologic factor', *International Journal of Coal Geology*, 76(1–2), pp. 52–75. doi:10.1016/j.coal.2008.02.005.
Formolo, M. (2010) 'The Microbial Production of Methane and Other Volatile Hydrocarbons', in Timmis, K. N. (ed.) *Handbook of Hydrocarbon and Lipid Microbiology*. Berlin, Heidelberg: Springer Berlin Heidelberg, pp. 113–126. doi:10.1007/978-3-540-77587-4_6.
Furmann, A., Schimmelmann, A., Brassell, S. C., Mastalerz, M. and Picardal, F. (2013) 'Chemical compound classes supporting microbial methanogenesis in coal', *Chemical Geology*. Elsevier B.V., 339, pp. 226–241. doi:10.1016/j.chemgeo.2012.08.010.
Galimov, E. M. (1988) 'Sources and mechanisms of formation of gaseous hydrocarbons in sedimentary rocks', *Chemical Geology*, 71(1–3), pp. 77–95. doi:10.1016/0009-2541(88)90107-6.
Gao, L., Mastalerz, M. and Schimmelmann, A. (2014) 'The Origin of Coalbed Methane', *Coal Bed Methane: From Prospect to Pipeline*, pp. 7–29. doi:10.1016/B978-0-12-800880-5.00002-4.
Golding, S. D., Boreham, C. J. and Esterle, J. S. (2013) 'Stable isotope geochemistry of coal bed and shale gas and related production waters: A review', *International Journal of Coal Geology*, 120, pp. 24–40. doi:10.1016/j.coal.2013.09.001.
Green, M. S., Flanegan, K. C. and Gilcrease, P. C. (2008) 'Characterization of a methanogenic consortium enriched from a coalbed methane well in the Powder River Basin, U.S.A.', *International Journal of Coal Geology*, 76(1–2), pp. 34–45. doi:10.1016/j.coal.2008.05.001.
Györe, D., McKavney, R., Gilfillan, S. M. V. and Stuart, F. M. (2018) 'Fingerprinting coal-derived gases from the UK', *Chemical Geology*, 480, pp. 75–85. doi:10.1016/j.chemgeo.2017.09.016.
Hamilton, E. I. (1974) 'The chemical elements and human morbidity—water, air and places—a study of natural variability', *Science of The Total Environment*, 3(1), pp. 3–85. doi:10.1016/0048-9697(74)90040-0.
Hamilton, S. K., Golding, S. D., Baublys, K. A. and Esterle, J. S. (2014) 'Stable isotopic and molecular composition of desorbed coal seam gases from the Walloon Subgroup, eastern Surat Basin, Australia', *International Journal of Coal Geology*. Elsevier B.V., 122(0), pp. 21–36. doi:10.1016/j.coal.2013.12.003.
Head, I. M., Jones, D. M. and Larter, S. R. (2003) 'Biological activity in the deep subsurface and the origin of heavy oil.', *Nature*, 426(6964), pp. 344–52. doi:10.1038/nature02134.
Hemp, R. (1998) 'The effect of changes in barometric pressure on mines in the highveld of South Africa', *Journal of the Mine Ventilation Society of South Africa*, 51(2), pp. 41–52.
Hilt, C. (1873) 'Die Beziehungen zwischen der Zusammensetzung und den technischen Eigenschaften der Steinkohle', *Ver. Dtsch. Ing. Z*, 17(2), pp. 194–202.
Hitchman, S. P., Darling, W. G. and Williams, G. M. (1989) *STABLE ISOTOPE RATIOS IN METHANE CONTAINING GASES IN THE UNITED KINGDOM*, *Technical Report WE/89/30*. Nottingham: British Geological Survey. Available at: http://nora.nerc.ac.uk/id/eprint/502528/1/WE89030.pdf.
Hunt, J. M. (1996) *Petroleum Geochemistry and Geology*. 2nd edn. W.H. Freeman. ISBN: 9780716724414.
Huxley, J. (1983) *Britain's Onshore Oil Industry*. London: Palgrave Macmillan UK. doi:10.1007/978-1-349-

06597-4 ISBN: 978-0-333-34526-9.

Jarvis, A. P. (2006) 'THE ROLE OF DISSOLVED CARBON DIOXIDE IN GOVERNING DEEP COAL MINE WATER QUALITY AND DETERMINING TREATMENT PROCESS SELECTION', in *7th International Conference on Acid Rock Drainage (ICARD)*. St. Louis: American Society of Mining and Reclamation (ASMR), pp. 833–843.

Kaiser, W. R., Hamilton, D. S., Scott, a. R., Tyler, R. and Finley, R. J. (1994) 'Geological and hydrological controls on the producibility of coalbed methane', *Journal of the Geological Society*, 151(3), pp. 417–420. doi:10.1144/gsjgs.151.3.0417.

Kang, M., Christian, S., Celia, M. A., Mauzerall, D. L., Bill, M., Miller, A. R., Chen, Y., Conrad, M. E., Darrah, T. H. and Jackson, R. B. (2016) 'Identification and characterization of high methane-emitting abandoned oil and gas wells', *Proceedings of the National Academy of Sciences*, 113(48), p. 201605913. doi:10.1073/pnas.1605913113.

Karacan, C. Ö., Ruiz, F. a., Cotè, M. and Phipps, S. (2011) 'Coal mine methane: A review of capture and utilization practices with benefits to mining safety and to greenhouse gas reduction', *International Journal of Coal Geology*. Elsevier B.V., 86(2–3), pp. 121–156. doi:10.1016/j.coal.2011.02.009.

Kershaw, S. and Whitworth, K. (2005) *Development of a Methodology for Estimating Methane Emissions from Abandoned Coal Mines in the UK Environmental Consultancy*. DEFRA - Department for Environment and Rural Affairs.

Kharaka, Y. K. and Specht, D. J. (1988) 'The solubility of noble gases in crude oil at 25–100°C', *Applied Geochemistry*, 3(2), pp. 137–144. doi:10.1016/0883-2927(88)90001-7.

Kotarba, M. J. (2001) 'Composition and origin of coalbed gases in the Upper Silesian and Lublin basins, Poland', *Organic Geochemistry*, 32(1), pp. 163–180. doi:10.1016/S0146-6380(00)00134-0.

Kotarba, M. J. and Korus, A. (2002) 'Origin of coalbed and near-surface gases in Wałbrzych Coal Distric', *Gas hazard in the near-surface zone of the Wałbrzych Coal District caused by coal mine closure: geological and geochemical controls. In: Kotarba MJ (Ed.) Gas hazard in the near-surface zone of the Wałbrzych Coal District caused by coal mine closure: geological and geochemical controls*.

Kotarba, M. J. and Rice, D. D. (2001) 'Composition and origin of coalbed gases in the Lower Silesian basin, southwest Poland', *Applied Geochemistry*, 16(7–8), pp. 895–910. doi:10.1016/S0883-2927(00)00058-5.

Krause, E. and Pokryszka, Z. (2013) 'Investigations on Methane Emission from Flooded Workings of Closed Coal Mines', *Journal of Sustainable Mining*, 12(2), pp. 40–45. doi:10.7424/jsm130206.

Van Krevelen, D. W. (1961) *Coal*. Amsterdam: Elsevier Scientific Publishing Company. ISBN: 0444895868.

Krüger, M., Beckmann, S., Engelen, B., Thielemann, T., Cramer, B., Schippers, A. and Cypionka, H. (2008) 'Microbial Methane Formation from Hard Coal and Timber in an Abandoned Coal Mine', *Geomicrobiology Journal*. Taylor & Francis, 25(6), pp. 315–321. doi:10.1080/01490450802258402.

Laughrey, C. D. and Baldassare, F. J. (2003) 'Some applications of isotope geochemistry for determining sources of stray carbon dioxide gas', *Environmental Geosciences*, 10(3), pp. 107–122. doi:10.1306/eg100303003.

Levine, J. R. (1993) 'Coalification: The Evolution of Coal as Source Rock and Reservoir Rock for Oil and Gas', in *Hydrocarbons from Coal*. Tulsa, OK: AAPG, pp. 39–77. doi:10.1306/St38577C3.

Liu, W. and Xu, Y. (1999) 'A two-stage model of carbon isotopic fractionation in coal-gas', *Geochimica et Cosmochimica Acta*, 28(4), pp. 359–365.

Mansfield Heritage (2015) *Mansfield Heritage*. Available at: http://www.mansfieldwoodhouseheritagelink.co.uk/author/holly/ (Accessed: 12 May 2017).

Mark, D. F., Stuart, F. M. and de Podesta, M. (2011) 'New high-precision measurements of the isotopic composition of atmospheric argon', *Geochimica et Cosmochimica Acta*. Elsevier Ltd, 75(23), pp. 7494–7501. doi:10.1016/j.gca.2011.09.042.

Marples, P. (2009) *Mansfield Colliery History*. Available at: http://www.ourmansfieldandarea.org.uk/page_id__56_path__0p2p20p.aspx (Accessed: 12 May 2017).

Martini, A. M., Walter, L. M., Budai, J. M., Ku, T. C. W., Kaiser, C. J. and Schoell, M. (1998) 'Genetic and temporal relations between formation waters and biogenic methane: Upper Devonian Antrim Shale, Michigan Basin, USA', *Geochimica et Cosmochimica Acta*, 62(10), pp. 1699–1720. doi:10.1016/S0016-7037(98)00090-8.

McAllan, J., Banks, D., Beyer, N. and Watson, I. (2009) 'Alkalinity, temporary CO2 and permanent acidity: an empirical assessment of the significance of field and laboratory determinations on mine waters', *Geochemistry: Exploration, Environment, Analysis*, 9(4), p. 299 LP-312.

Meslé, M., Dromart, G. and Oger, P. (2013) 'Microbial methanogenesis in subsurface oil and coal', *Research in Microbiology*, 164(9), pp. 959–972. doi:10.1016/j.resmic.2013.07.004.

'Microbial communities in passive remediation systems at three abandoned coal mine sites in the United Kingdom' (2016) in *IMWA 2016 – Mining Meets Water – Conflicts and Solutions*. Leipzig, Germany, pp. 796–803. Available at: https://www.imwa.info/docs/imwa_2016/IMWA2016_Falagan_29.pdf.

Moore, T. a. (2012) 'Coalbed methane: A review', *International Journal of Coal Geology*. Elsevier B.V.,

101(0), pp. 36–81. doi:10.1016/j.coal.2012.05.011.

Newmarket Colliery History (2009). Available at: http://www.stanleyhistoryonline.com/Local-Collierys.html (Accessed: 12 May 2017).

Ni, Y., Dai, J., Zhu, G., Zhang, S., Zhang, D., Su, J., Tao, X., Liao, F., Wu, W., Gong, D. and Liu, Q. (2013) 'Stable hydrogen and carbon isotopic ratios of coal-derived and oil-derived gases: A case study in the Tarim basin, NW China', *International Journal of Coal Geology*. Elsevier B.V., 116–117, pp. 302–313. doi:10.1016/j.coal.2013.06.006.

Niemann, M. and Whiticar, M. (2017) 'Stable Isotope Systematics of Coalbed Gas during Desorption and Production', *Geosciences*, 7(2), p. 43. doi:10.3390/geosciences7020043.

Oremland, R. S., Whiticar, M. J., Strohmaier, F. E. and Kiene, R. P. (1988) 'Bacterial ethane formation from reduced, ethylated sulfur compounds in anoxic sediments', *Geochimica et Cosmochimica Acta*, 52(7), pp. 1895–1904. doi:10.1016/0016-7037(88)90013-0.

Osborn, S. G. and McIntosh, J. C. (2010) 'Chemical and isotopic tracers of the contribution of microbial gas in Devonian organic-rich shales and reservoir sandstones, northern Appalachian Basin', *Applied Geochemistry*. Elsevier Ltd, 25(3), pp. 456–471. doi:10.1016/j.apgeochem.2010.01.001.

Oxburgh, E. R., O'Nions, R. K. and Hill, R. I. (1986) 'Helium isotopes in sedimentary basins', *Nature*, 324(6098), pp. 632–635. doi:10.1038/324632a0.

Ozima, M. and Podosek, F. A. (2001) *Noble Gas Geochemistry*. 2nd edn. Cambridge: Cambridge University Press. doi:10.1017/CBO9780511545986 ISBN: 9780511545986.

Palchik, V. (2003) 'Formation of fractured zones in overburden due to longwall mining', *Environmental Geology*, 44(1), pp. 28–38. doi:10.1007/s00254-002-0732-7.

Prince of Wales Colliery History (2002). Available at: http://www.minersadvice.co.uk/princeofwales.htm (Accessed: 12 May 2017).

Rice, D. D. (1993) 'Composition and Origins of Coalbed Gas', *AAPG Bulletin*, 77(1), pp. 159–184. doi:10.1306/D9CB61EB-1715-11D7-8645000102C1865D.

Rider, M. H. (2002) *The Geological Interpretation of Well Logs*. 2nd edn. Rider-French Consulting Limited. ISBN: 9780954190606.

Rimmer, S. M., Rowe, H. D., Taulbee, D. N. and Hower, J. C. (2006) 'Influence of maceral content on ??13C and ??15N in a Middle Pennsylvanian coal', *Chemical Geology*, 225(1–2), pp. 77–90. doi:10.1016/j.chemgeo.2005.08.012.

Rodrigues, C. . and Lemos de Sousa, M. . (2002) 'The measurement of coal porosity with different gases', *International Journal of Coal Geology*, 48(3–4), pp. 245–251. doi:10.1016/S0166-5162(01)00061-1.

Schoell, M. (1980) 'The hydrogen and carbon isotopic composition of methane from natural gases of various origins', *Geochimica et Cosmochimica Acta*, 44(5), pp. 649–661. doi:10.1016/0016-7037(80)90155-6.

Scott, A. R., Kaiser, W. R. and Ayers Jr, W. B. (1994) 'Thermogenic and secondary biogenic gases, San Juan Basin, Colorado and New Mexico - implications for coalbed gas producibility', *American Association of Petroleum Geologists Bulletin*. Bureau of Economic Geology, Univ of Texas at Austin, Austin, TX, USA, 78(8), pp. 1186–1209.

Sechman, H., Kotarba, M. J., Fiszer, J. and Dzieniewicz, M. (2013) 'Distribution of methane and carbon dioxide concentrations in the near-surface zone and their genetic characterization at the abandoned "Nowa Ruda" coal mine (Lower Silesian Coal Basin, SW Poland)', *International Journal of Coal Geology*. Elsevier B.V., 116–117(0), pp. 1–16. doi:10.1016/j.coal.2013.05.005.

Sekhohola, L. M., Igbinigie, E. E. and Cowan, A. K. (2013) 'Biological degradation and solubilisation of coal', *Biodegradation*, 24(3), pp. 305–318. doi:10.1007/s10532-012-9594-1.

Smith, J. W. and Pallasser, R. J. (1996) 'Microbial origin of Australian coalbed methane', *AAPG Bulletin*, 80(6), pp. 891–897. doi:10.1306/64ED88FE-1724-11D7-8645000102C1865D.

Spears, D. A. and Tewalt, S. J. (2009) 'The geochemistry of environmentally important trace elements in UK coals, with special reference to the Parkgate coal in the Yorkshire-Nottinghamshire Coalfield, UK', *International Journal of Coal Geology*, 80(3–4), pp. 157–166. doi:10.1016/j.coal.2009.08.010.

Stępniewska, Z., Pytlak, A. and Kuźniar, A. (2013) 'Methanotrophic activity in Carboniferous coalbed rocks', *International Journal of Coal Geology*, 106(0), pp. 1–10. doi:10.1016/j.coal.2013.01.003.

Strąpoć, D., Picardal, F. W., Turich, C., Schaperdoth, I., Macalady, J. L., Lipp, J. S., Lin, Y. S., Ertefai, T. F., Schubotz, F., Hinrichs, K. U., Mastalerz, M. and Schimmelmann, A. (2008) 'Methane-producing microbial community in a coal bed of the Illinois Basin', *Applied and Environmental Microbiology*, 74(8), pp. 2424–2432. doi:10.1128/AEM.02341-07.

Strąpoć, D., Mastalerz, M., Schimmelmann, A., Drobniak, A. and Hedges, S. (2008) 'Variability of geochemical properties in a microbially dominated coalbed gas system from the eastern margin of the Illinois Basin, USA', *International Journal of Coal Geology*, 76(1–2), pp. 98–110. doi:10.1016/j.coal.2008.02.002.

Strąpoć, D., Mastalerz, M., Dawson, K., Macalady, J., Callaghan, A. V., Wawrik, B., Turich, C. and Ashby, M. (2011) 'Biogeochemistry of Microbial Coal-Bed Methane', *Annual Review of Earth and Planetary Sciences*. Annual Reviews, 39(1), pp. 617–656. doi:10.1146/annurev-earth-040610-133343.

Tamamura, S., Ueno, A., Aramaki, N., Matsumoto, H., Uchida, K., Igarashi, T. and Kaneko, K. (2015) 'Effects of oxidative weathering on the composition of organic matter in coal and sedimentary rock', *Organic Geochemistry*. Elsevier Ltd, 81, pp. 8–19. doi:10.1016/j.orggeochem.2015.01.006.

Tao, M., Li, J., Li, X., Ma, Y., Li, Z., Wang, Z., Gao, Z., Zhang, X. and Wang, Y. (2012) 'New approaches and markers for identifying secondary biogenic coalbed gas', *Acta Geologica Sinica*, 86(1), pp. 199–208. doi:10.1111/j.1755-6724.2012.00622.x.

Thielemann, T., Cramer, B. and Schippers, A. (2004) 'Coalbed methane in the Ruhr Basin, Germany: a renewable energy resource?', *Organic Geochemistry*, 35(11–12), pp. 1537–1549. doi:10.1016/j.orggeochem.2004.05.004.

Thomas, L. (2013) *Coal Geology*. II. Oxford, UK: Wiley-Blackwell. ISBN: 9781119990444.

Torgersen, T. and Kennedy, B. M. (1999) 'Air-Xe enrichments in Elk Hills oil field gases: Role of water in migration and storage', *Earth and Planetary Science Letters*, 167(3–4), pp. 239–253. doi:10.1016/S0012-821X(99)00021-7.

UKOGL (2017) *U.K. Onshore Geophysical Library*. Available at: https://ukogl.org.uk (Accessed: 12 May 2017).

US Gov. SEC (2014) *Arch Coal - Form 10K - ANNUAL REPORT PURSUANT TO SECTION 13 OR 15(d) OF THE SECURITIES EXCHANGE ACT OF 1934*. Available at: https://www.sec.gov/Archives/edgar/data/1037676/000104746915001419/a2223254z10-k.htm.

Vinson, D. S., Blair, N. E., Martini, A. M., Larter, S., Orem, W. H. and McIntosh, J. C. (2017) 'Microbial methane from in situ biodegradation of coal and shale: A review and reevaluation of hydrogen and carbon isotope signatures', *Chemical Geology*, 453, pp. 128–145. doi:10.1016/j.chemgeo.2017.01.027.

Warsop Vale Local History Society (2002). Available at: http://www.warsopvale.org/history2.htm (Accessed: 12 May 2017).

Warwick, P. D. and Ruppert, L. F. (2016) 'Carbon and oxygen isotopic composition of coal and carbon dioxide derived from laboratory coal combustion: A preliminary study', *International Journal of Coal Geology*. Elsevier B.V., 166, pp. 128–135. doi:10.1016/j.coal.2016.06.009.

Wei, M., Yu, Z., Jiang, Z. and Zhang, H. (2014) 'Microbial diversity and biogenic methane potential of a thermogenic-gas coal mine', *International Journal of Coal Geology*, 134–135, pp. 96–107. doi:10.1016/j.coal.2014.09.008.

Whiticar, M. J. (1994) 'Correlation of natural gases with their sources', in *The Petroleum System - from Source to Trap*. AAPG Special Edition, pp. 261–283.

Whiticar, M. J. (1996) 'Stable isotope geochemistry of coals, humic kerogens and related natural gases', *International Journal of Coal Geology*, 32(1–4), pp. 191–215. doi:10.1016/S0166-5162(96)00042-0.

Whiticar, M. J. (1999) 'Carbon and hydrogen isotope systematics of bacterial formation and oxidation of methane', *Chemical Geology*, 161(1–3), pp. 291–314. doi:10.1016/S0009-2541(99)00092-3.

Wilhelms, A., Larter, S. R., Head, I., Farrimond, P., Di-Primio, R. and Zwach, C. (2001) 'Biodegradation of oil in uplifted basins prevented by deep-burial sterilization', *Nature*, 411(6841), pp. 1034–1037. doi:10.1038/35082535.

Xu, Y. C., Wang ZhiYong, Z. Y., Wang, X. F., Zheng, J. J. and Du, H. Y. (2008) 'Low-mature gases and typical low-mature gas fields in China', *Science in China, Series D: Earth Sciences*, 51(2), pp. 312–320. doi:10.1007/s11430-008-0011-x.

Younger, P. L., Boyce, A. J. and Waring, A. J. (2015) 'Proceedings of the Geologists ' Association Chloride waters of Great Britain revisited : from subsea formation waters to onshore geothermal fluids', *Proceedings of the Geologists' Association*. The Geologists' Association., 126(4–5), pp. 453–465. doi:10.1016/j.pgeola.2015.04.001.

Zazzeri, G., Lowry, D., Fisher, R. E., France, J. L., Lanoisell??, M., Kelly, B. F. J., Necki, J. M., Iverach, C. P., Ginty, E., Zimnoch, M., Jasek, A. and Nisbet, E. G. (2016) 'Carbon isotopic signature of coal-derived methane emissions to the atmosphere: From coalification to alteration', *Atmospheric Chemistry and Physics*, 16(21), pp. 13669–13680. doi:10.5194/acp-16-13669-2016.

Zhou, Z., Ballentine, C. J., Kipfer, R., Schoell, M. and Thibodeaux, S. (2005) 'Noble gas tracing of groundwater/coalbed methane interaction in the San Juan Basin, USA', *Geochimica et Cosmochimica Acta*, 69(23), pp. 5413–5428. doi:10.1016/j.gca.2005.06.027.

5 Regional Case Studies and Tracing Workflow

5.1 Introduction

Elevated methane concentrations in soils or shallow aquifers can cause safety and environmental issues. In order to direct efforts to prevent or mitigate the effects of stray gases, the source of the gas must be determined. Source-to-sink models require the baseline geochemistry of both end-members, and knowledge of the processes which affect the gases along the migration path.

This chapter reports and characterises the disparate individual hydrocarbon samples not associated with the other hydrocarbon fields to provide additional baseline measurements for UK deep gases. These include the first noble gas analyses of UK shale gas exploration well Preese-Hall-1, a nearby hydraulically fractured tight gas well Elswick-1, shale oil exploration well Balcombe-1, and a natural gas seep in the Midland Valley. Several water samples from Scotland and England were also analysed, and where possible are compared with deep gases in the subsurface using helium and neon isotopes.

The geochemical attributes of gases are assessed and discussed, and the characteristic 'fingerprints' of gases are described. Finally, a workflow methodology is laid out, where the effectiveness and limitations of different analytical methods is evaluated.

5.2 Results

Results of noble gas measurements are given in Table 15 and Table 16, and bulk gas ratios and stable isotopes are given in Table 17 to save repetition in later sections.

Concentration data

Well	^{4}He ($x10^{-3}$) cc/ccSTP		^{20}Ne ($x10^{-8}$) cc/ccSTP		^{40}Ar ($x10^{-5}$) cc/ccSTP		^{84}Kr ($x10^{-9}$) cc/ccSTP		^{132}Xe ($x10^{-11}$) cc/ccSTP	
Balcombe-2Z	1.166	(0.057)	6.03	(0.131)	9.091	(0.502)	5.36	(0.22)	34.98	(1.83)
Preece-Hall-1	0.095	(0.0005)	657.3	(3.46)	390.28	(17.32)	283.44	(1.49)	800.4	(4.2)
Torry Bay	0.831	(0.040)	778.5	(4.09)	542.1	(5.652)	304.55	(1.60)	1104.0	(5.7)
Elleswick-1	0.715	(0.014)	254.3	(5.50)	76.023	(1.445)	46.02	(0.24)	229.8	(1.2)
Sheffield Mains Gas*	0.128	(0.006)	3.3	(0.14)	6.310	(0.233)	5.23	(0.22)	40.4	(2.1)

Units: cm^3 STP/cm^3 - (Standard T (0°C) and P (0.101 Mpa) after Ozima and Podosek (2002))
1σ uncertainty shown in parentheses

Isotopic ratios

Well	$^{3}He/^{4}He$ (R/R_a)	$^{20}Ne/^{22}Ne$	$^{21}Ne/^{22}Ne$	$^{40}Ar/^{36}Ar$	$^{38}Ar/^{36}Ar$
Balcombe-2Z	0.018 (1)	9.85 (9)	0.0363 (8)	490 (3)	0.191 (2)
Preece-Hall-1	0.066 (4)	10.01 (9)	0.0285 (7)	280 (2)	0.192 (2)
Torry Bay	0.199 (8)	9.67 (10)	0.0282 (6)	303 (2)	0.190 (1)
Elleswick-1	0.075 (2)	10.16 (9)	0.0299 (6)	300 (2)	0.186 (1)
Sheffield Mains Gas*	0.061 (4)	9.57 (8)	0.0310 (10)	443 (2)	0.185 (3)

concentrations and ratios for UK conventional and unconventional gas samples.
r data from this study, measured by the author at SUERC, East Kilbride.

Table 16 - Table of noble gas concentrations, noble gas ratios, and dissolved methane, nitrogen and oxygen concentrations in UK water samples. All data from this study, measured by the University of Ohio.

Concentration data

Well	^{4}He ($x10^{-6}$) cc/ccSTP	^{20}Ne ($x10^{-8}$) cc/ccSTP	^{40}Ar ($x10^{-5}$) cc/ccSTP	^{84}Kr ($x10^{-9}$) cc/ccSTP	^{132}Xe ($x10^{-10}$) cc/ccSTP	CH_4 mg/l	N_2 mg/l	O_2 mg/l
Leadburn House	0.63 (0.005)	26.2 (0.29)	35.5 (0.07)	46.66 (0.75)	22.9 (0.7)	2.65	17.72	0.0018
Balcombe Water 1	31.82 (0.255)	60.0 (0.66)	39.8 (0.08)	46.87 (0.75)	19.5 (1.3)	1.71	16.65	0.0005
Balcombe Water 2	23.90 (0.191)	39.0 (0.43)	32.6 (0.07)	37.43 (0.60)	15.6 (1.1)	17.66	12.62	0.0047
Balm Well	0.06 (0.000)	14.6 (0.16)	43.1 (0.09)	53.61 (0.86)	25.4 (1.1)	14.79	18.79	0.0004

Units: cm^3 STP/cm^3 - (Standard T (0°C) and P (0.101 Mpa) after Ozima and Podosek (2002))
1σ uncertainty shown in parentheses

Isotopic ratios

Well	$^{3}He/^{4}He$ (R/R_a)	$^{20}Ne/^{22}Ne$	$^{21}Ne/^{22}Ne$	$^{40}Ar/^{36}Ar$	$^{38}Ar/^{36}Ar$
Leadburn House	0.1368 (0)	9.81 (5)	0.0289 (3)	296 (2)	0.189 (2)
Balcombe Water 1	0.0281 (0)	9.81 (5)	0.0289 (3)	297 (2)	0.189 (2)
Balcombe Water 2	0.0254 (0)	9.94 (5)	0.0289 (3)	298 (2)	0.184 (2)
Balm Well	0.7081 (0)	9.79 (5)	0.0288 (3)	296 (2)	0.189 (2)

.

	C_1/C_2	d	C_1/C_3	d	$C_1/(C_2+C_3)$	d	C_1/CO_2	d	$\delta^{13}C_{CH4}$ ‰	δD_{CH4} ‰
Balcombe-2	31	0.05	98	0.4	24	0.08	671	3.4	-51.5	-220.5
Preese-Hall-1	22	0.04	83	0.4	18	0.06	163	0.8	-21.7	-220.5
Torry Bay	1082	1.71							-30.9	-222
Elswick	37	0.06	351	1.5	33	0.11	68	0.3	-32.6	-134.9
Sheffield Mains Gas									-40.6	

Table 17 – Table of bulk gas ratios and carbon and hydrogen stable isotopes for gas samples. Sheffield Mains Gas from Flude et al., (2017). All other data measured by the author.

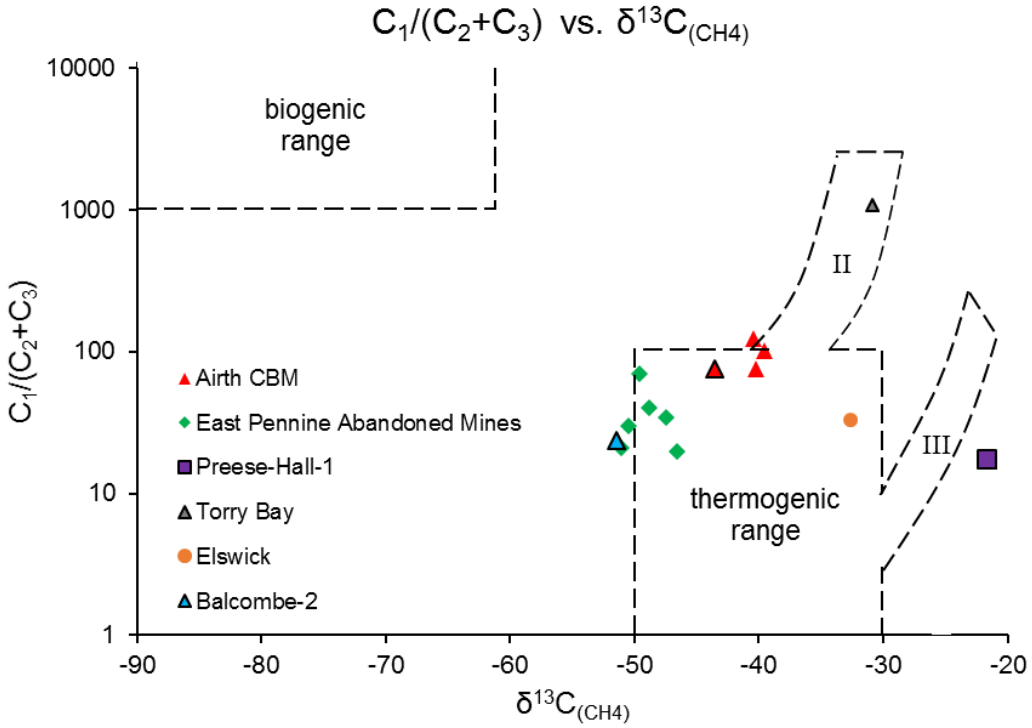

Figure 5-1 – 'Bernard' plot of $C_1/(C_2+C_3)$ vs. $\delta^{13}C_{CH4}$ for all available samples in this study. II refers to the maturation trend for type II kerogen, III refers to the maturation trend for type III kerogen.

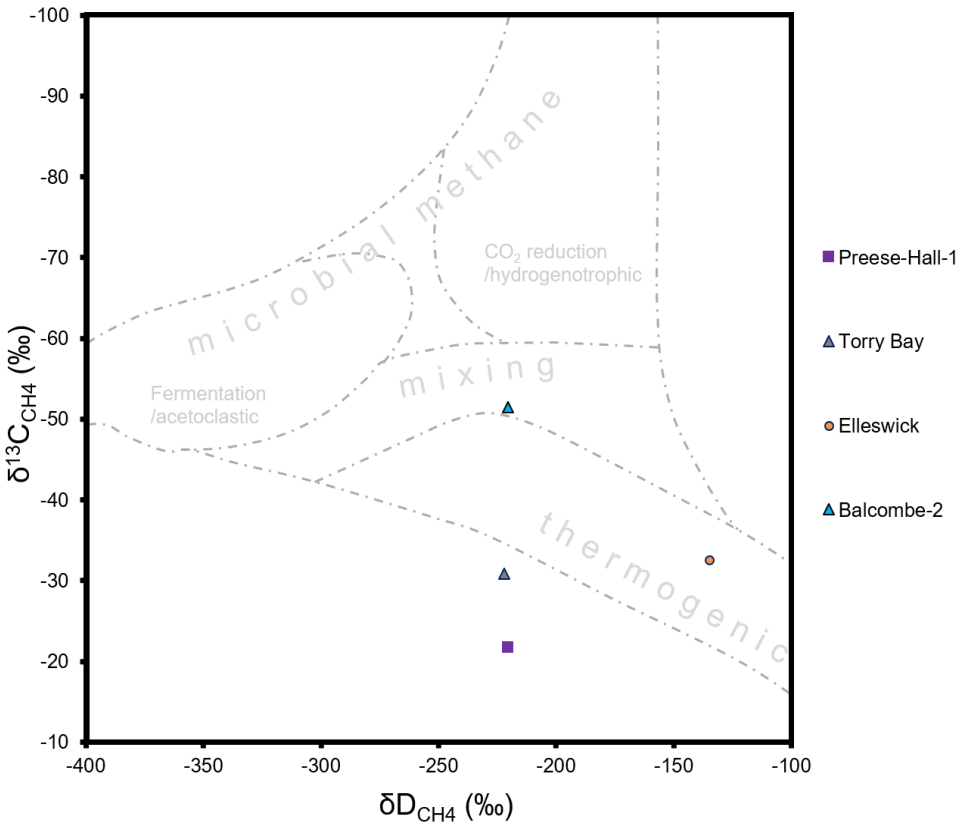

Figure 5-2 – 'Whiticar' style plot of $\delta^{13}C_{CH4}$ vs. δD_{CH4} for samples in this study. Balcombe-2 shows mixed thermogenic-biogenic; Elswick-1 shows a thermogenic signature, and Torry Bay and Preese-Hall-1 do not plot within a diagnostic field.

5.3 UK Pipeline Gas

Methane contamination of the shallow subsurface can involve numerous natural and anthropogenic sources. Potential sources of contamination include the numerous cross-country pipelines and smaller pipes into domestic and industrial buildings. Another source of 'geological' scale contamination is from underground gas storage schemes, of which 4 currently operate onshore with more in the pipeline (BGS, 2010). These developments face many of the challenges associated with Carbon Capture and Storage schemes. It is therefore pertinent to discuss the geochemistry of typical pipeline gas.

Natural gases are produced from various sources and blended to produce a basic quality standard before entering the National Transmission System for gas distribution. Over the 2016 period, 46% of natural gas in the UK was domestically supplied from the UK North Sea fields. The remainder (54%) was imported, primarily supplied from Norway (35%) via pipeline (primarily North Sea gas), with increasing imports from

Qatari LNG tanker (11%), and the remainder sent via pipeline from the Netherlands (~0.05%), Belgium (~0.02%) and non-Qatari LNG shipments (0.01%) (BEIS, 2017). These sources would be expected to possess elevated helium concentrations with respect to air, with a crustally dominated $^{3}He/^{4}He$ ratio (e.g. Ballentine et al., 1996), with the exception of Qatari LNG which may be processed for helium before exporting and have little helium inventory.

Gas was sampled from a domestic supply in Sheffield in 2016 by Flude *et al.*, (2017). It should be noted that this is merely a geochemical snapshot of the regional pipeline supply at this point in time, and reflects a mix of the various sources that comprise the pipeline gas. The composition will not be homogenous across different gas sources, and is sure to change over time, however for the immediate future the gas supply will remain composed primarily of North Sea gas (combined UK and Norwegian reserves) and thus this will be assumed representative of pipeline gas.

The gas was determined to possess a helium content of 128±6.2 ppm, two orders of magnitude above air (5.25 ppm; (Mamyrin *et al.*, 1970)) with a typical crustal $^{3}He/^{4}He$ signature ($0.061_{(Ra)}$±0.004), and a radiogenic argon signature ($^{40}Ar/^{36}Ar$ = 443±2). The neon isotopes show a small crustal $^{21}Ne^{*}$ addition, and mass fractionation reducing the $^{20}Ne/^{22}Ne$ below the air ratio. The $^{4}He/^{20}Ne$ = 3832±248, indicating little atmospheric interaction. Other noble gases were determined to be low in concentration. The $\delta^{13}C_{CH4}$ was determined to be -40.6‰.

The high helium contents, low neon contents, and thermogenic $\delta^{13}C_{CH4}$ are ideal for tracing fugitive gas from pipelines. Pipeline gas could be distinguished from AMM or CBM gases by their lower relative ^{4}He component and the typical crustal $^{3}He/^{4}He$ ratio. Scottish CBM samples have an order of magnitude higher ^{4}He content, and characteristically higher $^{3}He/^{4}He$ ratio (~$0.18_{(Ra)}$), and East Pennine coal gas samples typically also have higher ^{4}He and show very low crustal $^{3}He/^{4}He$ signatures ($0.0019 - 0.043_{(Ra)}$, but typically <$0.02_{(Ra)}$).

5.4 Airth and Torry Bay

Gas seeps at Torry Bay on the intertidal zone of the Firth of Forth were initially observed in 1989 (Judd *et al.*, 2002), and they are still present at the time of writing. Gas seeps around the Torry Bay/Torryburn/Culross region have been reported as far back as 1829; when sinking the engine pit for a new colliery on Preston Island (near

Torry Bay), Bald (1829) reports in *Observations on the spontaneous emissions of inflammable Gas, in particular of Carburetted Hydrogen:*

"…the inflammable gas issued through the fissures and beds of the sandstone rock, and made the water in the pit boil like a pot, or not unlike liquor in a violent state of fermentation"

And meanwhile, on the tidal flats away from the pit:

"…it was a common amusement of the workmen to make cones of clay, each perforated with a small hole, and put them over the places where the gas issued. These they ignited, and they flamed like large coal-gas burners"

The history of gas seeps may go back even further to St. Mungo in the 6th Century, whose miraculous escapades with eternal fire at Culross may have had a more earthly genesis (Grealy, 2011).

Torry Bay is located 13 kilometres to the East of the Airth CBM field (Figure 5-3), and < 1.5 km from the former Valleyfield and Preston Island collieries. The presence of gas in a common occurrence in the surrounding region:

Preston Island was an artificial island build by Sir. Robert Preston in ~1800 to extract shallow coals for salt panning. The shallow workings (<30 fathoms; ~55m) were abandoned in 1811 after a firedamp explosion killed the workforce (Gazetteer for Scotland, 2016). A fatal gas explosion during well drilling occurred in 1905 at Rosyth Dockyards (Judd *et al.*, 2002). The Valleyfield colliery required gas flares to be installed after abandonment (Mike Browne, BGS, *pers comms*), and was notable for a particularly gassy sandstone unit at ~60 m depth from BGS borehole records (well ref: NT08NW367). Methane authigenic carbonates are known on the opposite side of the Firth of Forth in the gardens of Hopetoun House (Andrews, 1988) (carbonate precipitations occurring where there is sulphate-dependent anaerobic oxidation of methane, common in marine methane seepages (Joseph *et al.*, 2013)). All of these cases point to a long history of shallow natural gas in the region, probably sourced from the numerous shallow coals (Judd *et al.*, 2002).

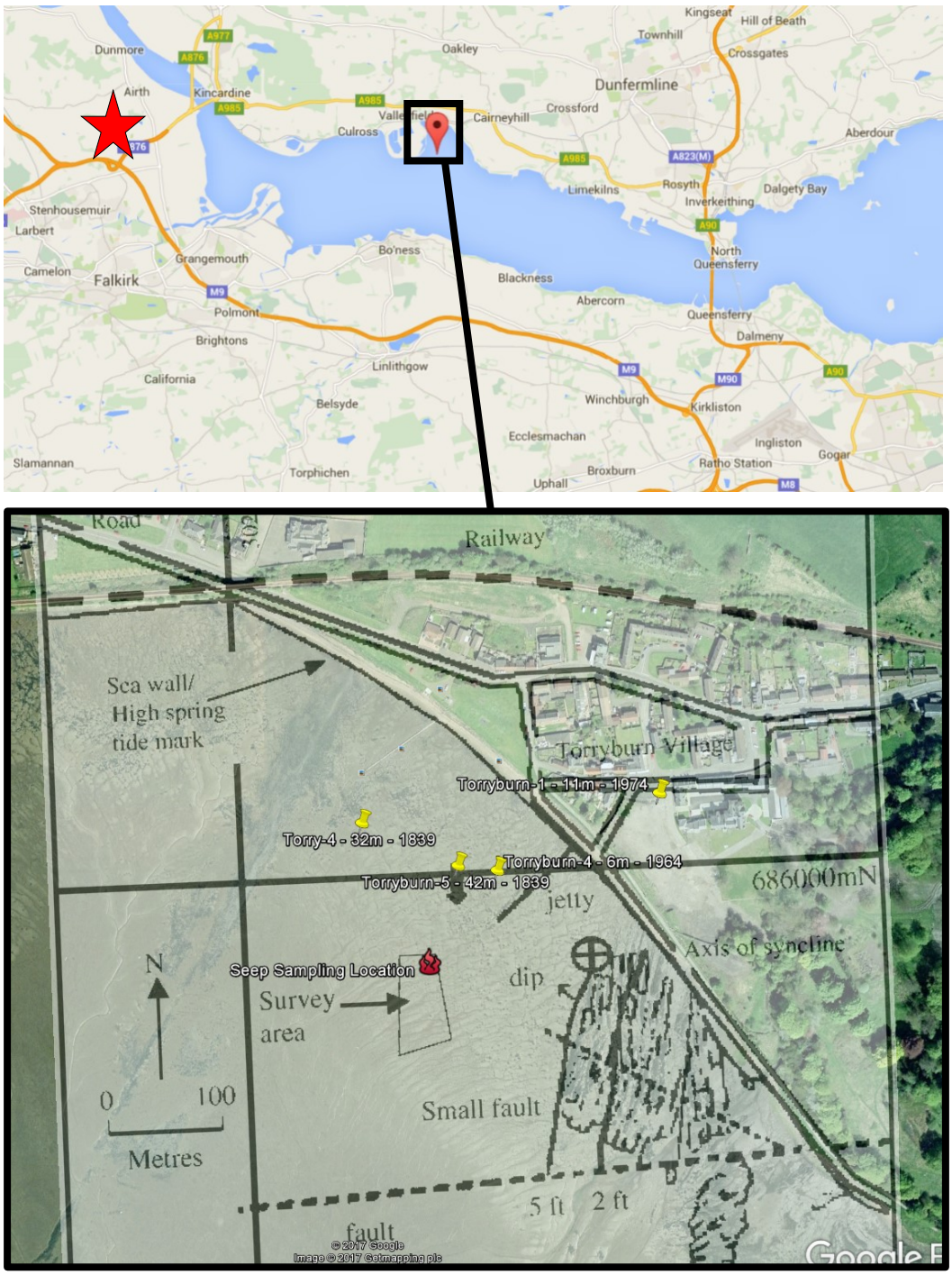

Figure 5-3 – Maps of Torry Bay. UPPER: Location map of the Firth of Forth with the Airth field (red star) and Torry Bay area (black box). LOWER: Expanded Torry Bay area with map overlay adapted from Judd et al., (2002). Seep area can be seen in the "survey area" box. Actual sample location is indicated by the red flame. Yellow pins represent a selection of nearby deep well borings for coal exploration, denoted by Name-depth(m)-year drilled.

The Torry Bay seeps emanate in patches in the mudflats and flow at several cc/min, estimated to add up to 1840 to 2630 m^3/year (Judd *et al.*, 2002). The surface

locations are related to topographic highs in the sandy gravel layer underlying the tidal muds, and appear spatially fixed over time (Judd *et al.*, 2002). The entire area is underlain with coal seams in the Limestone Coal Formation (LCF), which is the same strata targeted at the Airth field and formerly mined at the nearby Valleyfield Colliery. The Airth field targets the western limb on the Clackmannan syncline, and Torry Bay sits on the eastern limb where coals crop out at the surface and dip to the west. Shallow coals were worked in the area, but are not believed to undercut the seep site (Judd *et al.*, 2002), but no written records would have existed from early shallow mines in the early 1800's when these seams could have been worked *e.g.* Preston Island. Possible workings are indicated in the Torryburn-1 well by loss of drilling air-pressure ~250 m to the NE, and a small mine is recorded ~150 m to the east of the seeps, so it is unknown if these would have undercut the seep area. Several coal exploration boreholes were drilled in 1839 up to 80 m deep, the closest of which are shown in Figure 5-3, and are known to have intersected various coal beds, including the Parrot seam. These bores are plausible conduits for deeper gas migration to the surface at the Torry bay site.

5.4.1 Torry Bay Geochemistry

Judd et al., (2002) measured the bulk geochemistry and found:

Gas	**Concentration (%)**
Methane	74.12
Ethane	0.13
C_{2+}	Not detected
CO_2	<0.1%
UNKNOWN	25%
Therefore: C_1/C_2	571

Table 3– Bulk geochemistry of Torry Bay seeps as measured by Judd et al., (2002).

Bulk geochemistry of Torry Bay in this study was hampered by the aforementioned GC issues relating the sample tubes and vacuum (see Methodology), and only 12% methane was detected due to atmospheric dilution. Unfortunately, insufficient sample was available for radiocarbon determination. C_1/C_2 from this study was determined to be 1082, although the ethane at these low concentrations was near the limit of

detection for the equipment. No propane was detected, but this does not preclude its presence. The C_1/C_2 in this study and previously reported are much higher than the Airth field (average $C_1/C_2 = 99$). On a 'Bernard' plot, Torry Bay plots inside the type II high-maturity kerogen window (Bernard *et al.*, 1978; Whiticar, 1994). The $\delta^{13}C_{CH4} = -30.9‰$ and $\delta D_{CH4} = -222‰$, which places the methane in the "geothermal/ hydrothermal/crystalline" field of a Whiticar style plot, which is clearly an unrealistic interpretation. It is unlikely that this designation is compatible with the original source of the Torry Bay gases. This suggests either-:

- a large microbial methane contribution, low in C_{2+}
- microbial oxidation of C_2+
- high maturity humic-sourced gas
- a combination of the above

These values are isotopically heavier in $\delta^{13}C$ than the average for the Airth field (average Airth $\delta^{13}C_{CH4} = -40.4‰$), but isotopically lighter in δD_{CH4} (average Airth $\delta D_{CH4} = -183‰$), this does not fit thermogenic or microbial gases and does not fit between the two end-members, nor is it characteristic of oxidation.

The difference between Torry Bay and the Airth field cannot be caused by microbial oxidation, which would enrich both the $\delta^{13}C_{CH4}$ and δD_{CH4}. The differences could possibly be explained either by thermal maturity:

- The Clackmannan syncline was formed contemporaneously with deposition, so the Airth coals will have been buried deeper and have different thermal maturities)
- Localised heating affects from the Midland Valley Sill which has burnt/coked coal seams to the west of Torry Bay (BGS borehole records). Heavy carbon isotopes ($\delta^{13}C_{CH4} = -30.9‰$), and higher C_1/C_2 would be concordant with a high maturity humic-sourced gas.

Desorpsion effects may also play a significant role (e.g. Niemann and Whiticar, 2017) which affect both the compositional and isotopic ratios, as the seep has clearly been active for a long period unlike the Airth CBM field. The gas source cannot be unambiguously determined from C and H isotopic and compositional analysis, but it can reasonably be inferred to be sourced from the coals and to have a significant thermogenic component.

Microbial methanogenesis may be altering the isotopic ratios, in particular in lightening the $\delta D_{CH4.}$ The sediments on the Forth estuary are organic-rich, and leaves and other organic debris are found in muds in the seep area and the odour of hydrogen sulphide is reported at times (Judd *et al.*, 2002), which is indicative of anoxic conditions where microbial methanogenesis may be occurring. Radiocarbon and $\delta^{13}C_{CO2}$ measurements would help to determine the possible input of microbial gas.

^{4}He concentrations at Torry Bay were an unexpected 813±40 ppm. The sample showed elevated ^{20}Ne and ^{36}Ar concentrations significantly above ASW concentrations, suggesting atmospheric input probably entrained during sampling of these low-volume flows. The approximate percentage of air-contamination can be calculated using either the ^{20}Ne or ^{36}Ar excess relative to ASW, and results in 46% (^{20}Ne-method) and 54% (^{36}Ar-method) air contamination. Using the mean (50%), then the 'undiluted' concentration of ^{4}He is estimated to be 1662 ppm, which is in-line with the concentrations observed at the Airth field. Moreover, the ^{3}He/^{4}He ratio was determined to be $0.20\pm0.01_{(Ra)}$, which shows a clear radiogenic ^{4}He excess. Importantly, this is also a very similar ratio to that observed in the Airth field ($0.18_{(Ra)}$), showing a clear addition of mantle ^{3}He, as ASW or air contributions have a negligible effect on helium ratios when the helium concentrations are in such great excess of both ^{4}He and ^{3}He relative to ASW or air. Neon isotopes are slightly lower than the air ratio in both ^{20}Ne/^{22}Ne and ^{21}Ne/^{22}Ne, and are a result of mass fractionation from air. ^{40}Ar/^{36}Ar was 303±2, indicating a very small ^{40}Ar* excess. This crustal excess would be larger and more easily resolvable if not diluted with the atmosphere.

The helium data shows the gases at Torry Bay are sourced from deep with large ^{4}He excesses, and sourced from the same region as the Airth field gases as they share the characteristic mantle ^{3}He addition and similar ^{3}He/^{4}He ratios. This is not to say that the gases are from the Airth field itself, but that the processes which have added crustal and mantle helium into the coal beds must have been active in the same manner at the Torry Bay site.

Although the hydrocarbon composition and stable carbon and hydrogen isotopes are seemingly unconnected to the Airth field, Torry Bay gases have a significant thermogenic component sourced from the underlying coals and share a characteristic ^{3}He/^{4}He ratio with the Airth CBM field. The characteristic ^{3}He/^{4}He ratios distinguish this gas from English coal gas and 'typical' UK pipeline gases which both show a greater radiogenic signature.

Despite the sample being air contaminated, a clear connection to deep sourced gas can be seen in Figure 5-4.

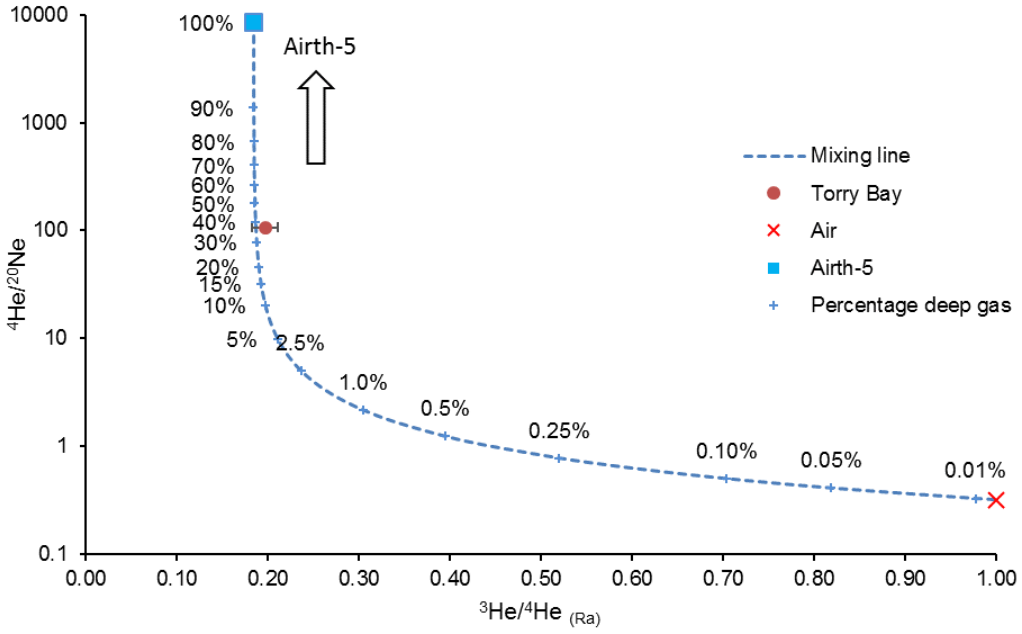

Figure 5-4 – Plot of $^{4}He/^{20}Ne$ vs. $^{3}He/^{4}He_{(Ra)}$. Airth-5 is plotted to the top, and air is plotted to the lower right. The blue dashed line represents binary mixing between Airth-5 and air, with percentage of deep gas marked on the line. Torry Bay sits on the mixing line showing a ~38% deep gas signature. This highlights the utility of noble gases as conservative tracers.

5.5 Leadburn House

Leadburn House is located near the Leadburn junction, on the border between Midlothian and the Borders, 55°47'17.87"N, 3°13'21.04"W. The domestic water well was identified from Scottish water data as having elevated methane concentrations (Ó Dochartaigh *et al.*, 2012). The well is artesian, and when sampling the water had a strong smell of hydrogen sulphide and white filamentous bacteria growing in and around the wellbore, which indicates strongly reducing conditions. The homeowner mentioned previously high Mn content which required extra filtering which no longer appears to be a problem, which suggests slowly changing redox conditions at the site.

Methane concentrations were determined to be elevated at 2.65 mg/l; methane in excess of >1.5mg/l can lead to a risk of explosion in confined spaces (Gooddy and Darling, 2005). Elevated methane is common in UK Carboniferous strata (Gooddy and

Darling, 2005; Darling and Gooddy, 2006), and Leadburn House is drilled into the Limestone Coal Group which is the same strata that Airth and Torry Bay interact with. The $^{3}He/^{4}He$ ratio was determined to be $0.137\pm0.00001_{(Ra)}$, but when corrected for ASW there is a strong radiogenic signature of $0.0035\pm0.0021_{(Ra)}$. ^{4}He concentrations were low at 0.626±0.005 ppm, but are still an order of magnitude higher than ASW. ^{20}Ne and ^{36}Ar were 0.262±0.003 ppm and 1.20±0.002 ppm, which are slightly above the ASW value of 0.176 ppm and 1.17 ppm. This corresponds to a $^{20}Ne/^{36}Ar$ of 0.218±0.0024 which is typical of ASW with a small excess air component. ^{84}Kr is typical of ASW and ^{132}Xe is slightly lower at 75% of the ASW value, possibly indicating a small degree of solubility fractionation. The ASW-like concentrations suggest no degassing has occurred prior to sampling, and the methane has been generated in or dissolved into the water before being produced at the well. The low helium concentrations are well above ASW values, and show a definite radiogenic excess. Both the corrected and uncorrected $^{3}He/^{4}He$ ratios are lower than the Airth field and Torry Bay, which defines a limit to the mantle input detected at those sites which lie ~38 km to the NW of Leadburn House. Unfortunately, stable carbon or hydrogen isotope data was unable to be analysed, however from the elevated ^{4}He concentrations and radiogenic $^{3}He/^{4}He$ ratio, it can be determined that the water has a significant residence time in the subsurface, and the elevated methane is slowly accumulated without causing the stripping of ASW noble gases from the formation water.

5.6 Balm Well

St. Catherine's well or the "Balm Well" is a natural petroleum seep in the Liberton area of Edinburgh. Oil has seeped into the well for centuries and was formerly used as a balm for skin ailments, being visited by King James IV of Scotland, rebuilt by King James VI (James I of England) in 1617, became a place of pilgrimage, was sacked by Oliver Cromwell's troops in 1650, and rebuilt in the 1880's (Underhill *et al.*, 2008). Today this iconic facet of British history is immortalised in the street names of a nearby housing development, and can be visited in the grounds of Toby Carvery.

Oil is believed to migrate up the Pentland Fault separating Carboniferous strata to the SE with Devonian to the NW (Underhill *et al.*, 2008). When sampling, a faint oily sheen could be observed. The methane concentration was determined at 1.7 mg/l,

however insufficient methane for isotopic analysis could be obtained from degassing 2 l of water.

^{4}He concentrations were determined to be only 0.057±0.0005 ppm, which is only ×0.25 greater than the ASW ratio. $^{3}He/^{4}He = 0.71_{(Ra)}$, which indicates a very small component of radiogenic ^{4}He mixing with ASW ($^{3}He/^{4}He = \sim 1$). Neon and argon isotopes are indistinguishable from the air ratios, and concentrations of other ANG species are broadly in line with the expected ASW concentrations.

Correcting the $^{3}He/^{4}He$ for ASW results in a $^{3}He/^{4}He_{(Ra)\text{-corrected}}$ of 0.135±0.029. This could suggest a small mantle ^{3}He input to the water, as is observed to the north in the Airth field. However, the low concentration of helium observed results in the $^{4}He/^{20}Ne$ ratios being the same order of magnitude as air and ASW. The resulting 'corrected' $^{3}He/^{4}He$ fundamentally relies on the assumed $^{4}He/^{20}Ne$ ratio of ASW. Any excess air input will change the ASW $^{4}He/^{20}Ne$ and thus changes the resultant corrected $^{3}He/^{4}He$ ratio, and so this is inherently unreliable for a single sample. More samples across the region would allow the resolution of the $^{3}He/^{4}He$ ratio.

The Balmwell sample contains resolvable radiogenic helium, so a small component can be traced to the deep subsurface, however all other noble gas ratios point to typical ASW.

5.7 Lancashire Conventional and Shale Gas

5.7.1 Preese-Hall-1 Exploration Well

Preese-Hall-1 was the first unconventional shale gas well drilled in the UK. It was located near the town of Singleton, NW of Preston in Lancashire, England (53°49'19.71"N, 2°57'2.00"W). It is a vertical well with lateral segment, spud by Cuadrilla Ltd. on the 16th August 2010 to drill and core the Sabden, Bowland, and Hodder shales to assess the potential for shale gas resources in the Bowland basin. 13-3/8" casing was installed down to 2021 ft (616 m), then 9-5/8" casing down to 4606 ft (1404 m), with a 5.5" casing string set to total depth (9100 ft; 2774 m).

The Preese-Hall-1 site caused controversy when hydraulic fracturing at the site was apparently the cause of 2 seismic events in 2011 which deformed the casing at depth, but no deformation of the upper sections was reported (Green, Christopher *et*

al., 2012). Operations at Preese Hall were suspended in 2012 when the well was plugged with cement and a steel bridge plug inserted above this. Since suspension, a 312 psi (2151 kPa/21.5 bar) pressure was detected between the 5.5" production casing and 9-5/8" borehole casing, believed to be derived from the Kinder Scout formation (Millstone Grit) which is located ~300ft (91 m) below the 9-5/8" casing shoe. As part of remedial measures before abandonment, Cuadrilla milled the production casing at the 9-5/8" casing shoe to complete a rock-to-rock cement bond, and a cement plug was placed above this. The wellbore was cemented to surface and welded shut. The site is now classed as plugged and abandoned, and no trace of the wellhead exists at the surface.

Figure 5-5 – Photograph of the workover rig at Cuadrilla's Preese Hall shale gas site. Gas sampling was undertaken while a cement packer was being drilled out as part of remedial operations.

5.7.2 Preese-Hall-1 Geochemistry

A sample of this migrated gas was collected, and the noble gas data are reported in Table 15. Compositional and isotopic data is given in Table 18. The $\delta^{13}C_{CH4}$ and δD_{CH4} do not plot within a specified field on a typical 'Schoell' type plot. The $\delta^{13}C_{CH4}$ is the

isotopically heaviest gas in the dataset, while δD_{CH4} is indicative of Balcombe-2 and East Pennine coal samples. More information could be gained from isotopic analysis of C_1 and C_2 components. Due to remedial operations it was not possible to take a sample of the shale gas from the wellbore, however GGS (2014) report $\delta^{13}C_{CH4}$ = 40.23‰ and $C_1/(C_2+C_3) < \sim 10$ from a sample given by Cuadrilla. The Preese-Hall-1 *shale* gas shows a typical thermogenic signature with elevated C_2+ contents, which is distinctly isotopically lighter and compositionally heavier than the gas sampled in this study from the intermediate formation (Kinderscout Formation), which is a useful diagnostic feature.

Preese-Hall-1 shows a wetter gas character ($C_1/(C_2+C_3)$) than Balcombe-2, but within the same region as East Pennine coal samples. CO_2 contents are still low, but higher than Balcombe-2 and East Pennine coal samples.

	C_1/C_2	d	C_1/C_3	d	$C_1/(C_2+C_3)$	d	C_1/CO_2	d	$\delta^{13}C_{CH4}$	δD_{CH4}
Preese-Hall-1	22	0.04	83	0.4	18	0.06	163	0.8	-21.7	-220.5

Table 18 – Compositional and isotopic data for Preese-Hall-1

The $^3He/^4He$ was determined to be 0.066±0.004, showing a typical crustal-radiogenic signature of helium. ^4He was 95±0.5 ppm, which is lower than the other unconventional samples measured. This is attributed to air-contamination; the ^{20}Ne and ^{36}Ar concentrations were an order of magnitude greater than ASW, $^{20}Ne/^{36}Ar$ = 0.47±0.02 (closer to the air ratio than to the ASW ratio), and a commensurately low $^4He/^{20}Ne$ ratio of 14±0.1 highlight the large atmospheric input. It is not known whether this atmospheric input is a result of:

- Copper tube leakage.
- Entrained air during sampling.
- A process connected to the drilling and remedial measures on-site.

Neon isotopes show mass fractionation away from the air value, being enriched in $^{20}Ne/^{22}Ne$. Curiously, the argon isotopes show an unusual pattern; the $^{40}Ar/^{36}Ar$ = 280±1.7 which is lower than the air ratio (air = 298.5), however the $^{38}Ar/^{36}Ar$ = 0.192±0.0023 is above the air-ratio (air = 0.1885), and so this cannot be accounted for by mass-fractionation.

The air contamination of the sample can be approximately determined by calculating the excess ANG's over the ASW concentration, which results in 38% (using

^{20}Ne) to 39% (using ^{36}Ar). This results in an 'undiluted' ^{4}He concentration of ~250 ppm, which is lower than other UK unconventional samples, but higher than UK Pipeline gas.

5.7.3 Elswick-1

The Elswick-1 well is a tight gas well <5 km from the Preese-Hall shale gas site (53°49'33.09"N, 2°52'37.88"W), near the town of Elswick, near Blackpool, Lancashire. It was completed and stimulated ("fracked") in 1993. The well is drilled to 1580 m and targets the Collyhurst Sandstone (Lower Permian), a low permeability sandstone capped by the Manchester Marl Formation.

Figure 5-6 – Photograph of the steel cage around the Elswick-1 wellhead. The wellhead is connected by a pipeline (yellow, in the background) to an electrical generator.

Elswick-1 was sampled on the 1st April 2014, and results given in Table 15 and Table 19.

	C_1/C_2	d	C_1/C_3	d	$C_1/(C_2+C_3)$	d	C_1/CO_2	d	$\delta^{13}C_{CH4}$	δD_{CH4}
Elswick-1	33.79	0.000	177.75	0.00	31.99	0.00	336.65	0.00	-32.6	-134.9

Table 19 – Table of compositional and isotopic parameters from Elswick-1.

As the Coal Measures do not exist in the subcrop beneath the Elswick field, this gas is assumed to be derived from the underlying shales (DECC, 2013). $\delta^{13}C_{CH4}$ and δD_{CH4} overlap with North Sea gases (Hitchman *et al.*, 1989). The Elleswick-1 well gas contains an elevated concentration of 715±14 ppm of ^4He at $^4He/^3He = 0.08_{(Ra)}$. This shows a strong crustal radiogenic signature, in line with the crustal average ratio (Ballentine and Burnard, 2002), and is similar to other samples in this study. Neon concentration was determined to be 2.54 ppm, which is ~x14 the concentration found in ASW, but below the air value of 16.5 ppm. The $^{20}Ne/^{22}Ne = 10.16±0.091$ and $^{21}Ne/^{22}Ne = 0.0299±0.00058$, which lie on the mass-fractionation line from the air-ratio.

The $^{40}Ar/^{36}Ar$ ratio was 295.5±2.2, which is abnormally slightly lower than the air-ratio of 298.5±0.31 (Mark *et al.*, 2011), and the ^{36}Ar concentration was 2.53±0.050 ppm, which is over twice the concentration in ASW (~1.17 ppm) but below the air value (31.3 ppm). The $^{20}Ne/^{36}Ar$ ratio is 1.00±0.030, which is unusually high (the air ratio being 0.526). ^{84}Kr and ^{132}Xe values are at or below ASW concentrations.

The well had been shut-in for period consisting of at least several months, and the relatively high ^{20}Ne concentration, high $^{20}Ne/^{36}Ar$ and the lower than air $^{40}Ar/^{36}Ar$ are hypothesized to be caused by air contamination by diffusion through seals in the wellhead, enriching the gas in lighter components but having little effect on heavy noble gases. Mass-fractionation is seen in both the neon isotopic system, $^{40}Ar/^{36}Ar$, and $^{38}Ar/^{36}Ar$ which is slightly lower than air (0.186±0.0014 vs. 0.189±0.0003 in air). This would also imply ^4He diffusion out of the wellhead, so the ^4He concentrations can be regarded as minima. This air contamination precludes a more detailed analysis of noble gases.

5.8 Balcombe, West Sussex

The Balcombe well pad was initially host to the well Balcombe-1, drilled by Conoco in 1986. At 170 ft (52 m) depth in the Ashdown bed, Balcombe-1 produced 150 bbl of formation water with elevated methane and ethane content (54,910 ppm CH_4 and

1335 ppm ethane) (therefore $C_1/C_2 = 41.1$), with minor gas quantities in the overlying Wadhurst clay. Shallow gas was also found in the Ashdown beds at Southwater-1 also drilled by Conoco 15 km to the west (Cuadrilla, 2013). The sediments of the Ashdown are very carbonaceous and several lignite beds are known which could potentially be a source of microbial gas. However, significant gas reserves (650,000 ft^3/day; 184059 m^3/day) were found in the upper Ashdown beds in the Bolney-1 well ~6 km to the south of the Balcombe site (Cuadrilla, 2013), and this suggests gas accumulations are sourced from elsewhere, and the gas generation capacity of the Ashdown beds is limited.

Shallow gas has a long history in the region; the nearby town of Heathfield was the site of the UK's first gas well when a water bore sank for steam engine boilers struck gas at 312 feet (Dawson, 1898). This was used to power the gas lights at Heathfield Station for decades (Dawson, 1898; Reeves, 1948). Sources of gas include the basal Ashdown beds or top Purbeck beds (hosting Kimmeridge clays), although lignite beds were also a possible gas source (Dawson, 1898; Reeves, 1948). A 'historical' analysis of this gas is given in Table 20.

Species	Percentage (Natural Gas Fields of England - 1902)	Percentage (Hewitt, 1898)
Methane	93.16	91.9
C_{2+}	2.94	-
Nitrogen	2.90	0.9
Hydrogen	-	7.2
Carbon Monoxide	1.00	-

Table 20 – Gas compositions of Heathfield Railway Bore gases. Data from Hewitt, (1898), and Reeves, (1948). Carbon monoxide is not expected in natural gases, and is a relic of the analytical techniques used which would have normally been used to analyse coal gas produced by destructive coal distillation, which would have yielded carbon monoxide.

5.8.1 Balcombe-2

Balcombe-2 is an unconventional well targeting a limestone layer between Kimmeridge clays and drilled by Cuadrilla. It was drilled to a vertical depth of 2700 ft (823 m), with a 1714 ft (522 m) lateral section and completed in September 2013.

Balcombe-2 gas shows a large concentration of helium typical of crustal ratios ($^3He/^4He = 0.02_{(Ra)}$ and [^4He] at 1166 ppm), which is two to three orders of magnitude above the air and ASW values (5.24 and ~0.046 ppm respectively). The ^{20}Ne concentration is 0.060±0.0013 ppm which is ~$^1/_3$ the concentration of ASW, and $^4He/^{20}Ne$ = 19328±1027 which is several orders of magnitude above the ASW and air

ratios of ~0.26 and 0.318, which shows the negligible atmospheric input in the sample. The $^{21}Ne/^{22}Ne$ ratio is higher than air, but the $^{20}Ne/^{22}Ne$ ratio is within error of air. This is due to a small excess of resolvable crustal-nucleogenic $^{21}Ne^*$, and a degree of mass fractionation increasing primarily the ^{20}Ne value. Balcombe-2 has low total argon concentrations (^{40}Ar = 90 ppm), an order of magnitude below the ASW value of 347 ppm, and $^{40}Ar/^{36}Ar$ = 490±2.9, indicating excess crustal $^{40}Ar^*$. The ^{84}Kr and ^{132}Xe concentrations are an order of magnitude below ASW, and along with neon and argon, are broadly in line with other UK unconventional gases (Airth field, this study).

The Balcombe-2 gases show high methane contents and appreciable C_2+ components (see Table 21). Gas wetness ($C_1/(C_2+C_3)$) is lower than some Abandoned Mine Methane samples from the East Midlands, although the C_1/C_3 is higher, probably a result of the different source kerogens in the Kimmeridge.; humic sourced thermogenic gases may be rich in C_2 but lower in C_3+ components (Whiticar, 1996; Golding *et al.*, 2013). C_1/CO_2 is very high, showing very little CO_2 input.

The single data point plotted on a Schoell-style ($\delta^{13}C_{CH4}$ vs. δD_{CH4}) diagram places the gas in the "early-mature thermogenic" field (Figure 5-7), which is consistent with compositional data and the thermal maturity of the shale. This value is very close to English AMM samples, which also overlap with landfill data from the UK (Hitchman *et al.*, 1989). This shows isotopic data is not particularly diagnostic.

	C_1/C_2	d	C_1/C_3	d	$C_1/(C_2+C_3)$	d	C_1/CO_2	d	$\delta^{13}C_{CH4}$	δD_{CH4}
Balcombe-2	31	0.05	98	0.4	24	0.08	671	3.4	-51.5	-220.5

Table 21 – Table of bulk gas composition and stable isotopes from the Balcombe-2 well.

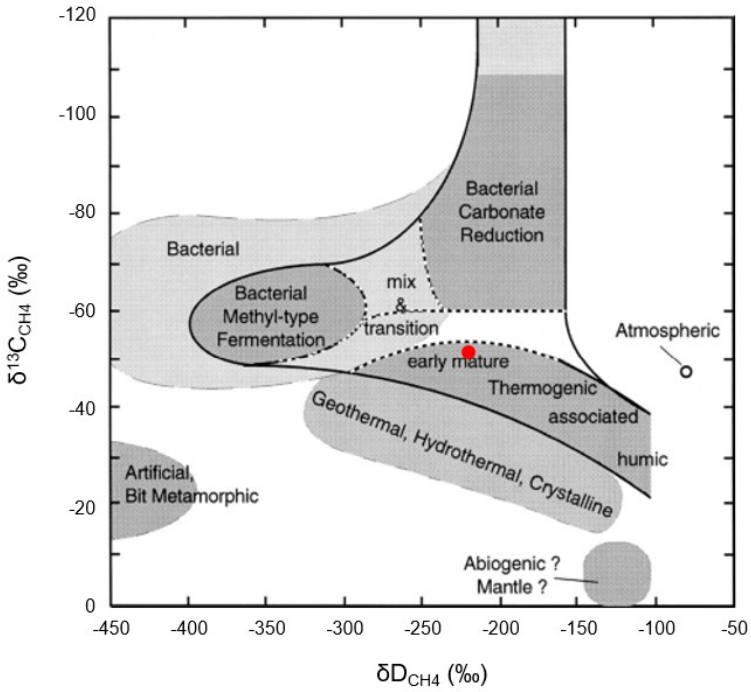

Figure 5-7 – 'Schoell' plot for Balcombe-2 sample, after Schoell, (1980). δ13CCH4 vs. δD_{CH4} for Balcombe-2 gas. Sample plots in the Early-Mature field.

5.8.2 Landfill

A former landfill site is located ~750 m away from the Balcombe well pad on Oldlands Avenue in Balcombe town (Figure 5-8). It was operated from 1962 – 1984 and is believed to have contained inert, commercial and household waste (EA, 2013), and reported to be off-gassing methane which prompted the EA's refusal for new housing developments on the site. The landfill is up-gradient of the Balcombe-2 site, but the geological connectivity is unknown. The landfill sits on the Tunbridge Wells Sands, but these are not present at the Balcombe-2 site. A water bore exists somewhere on the landfill plot (56 m deep; TQ32/32 - BGS wellbore records), which bores through the Tunbridge Wells Sands and into the Wadhurst Clays, which are the top unit at the Balcombe site. There may be continuity with the underlying Ashdown beds due to nearby faulting to the south; BGS maps place the Paddockhurst Fault, running NNE-SSW, between the landfill and Balcombe site. This down-throws the SE about ~30-40 m. It is unclear how this may affect the connectivity between the two sites.

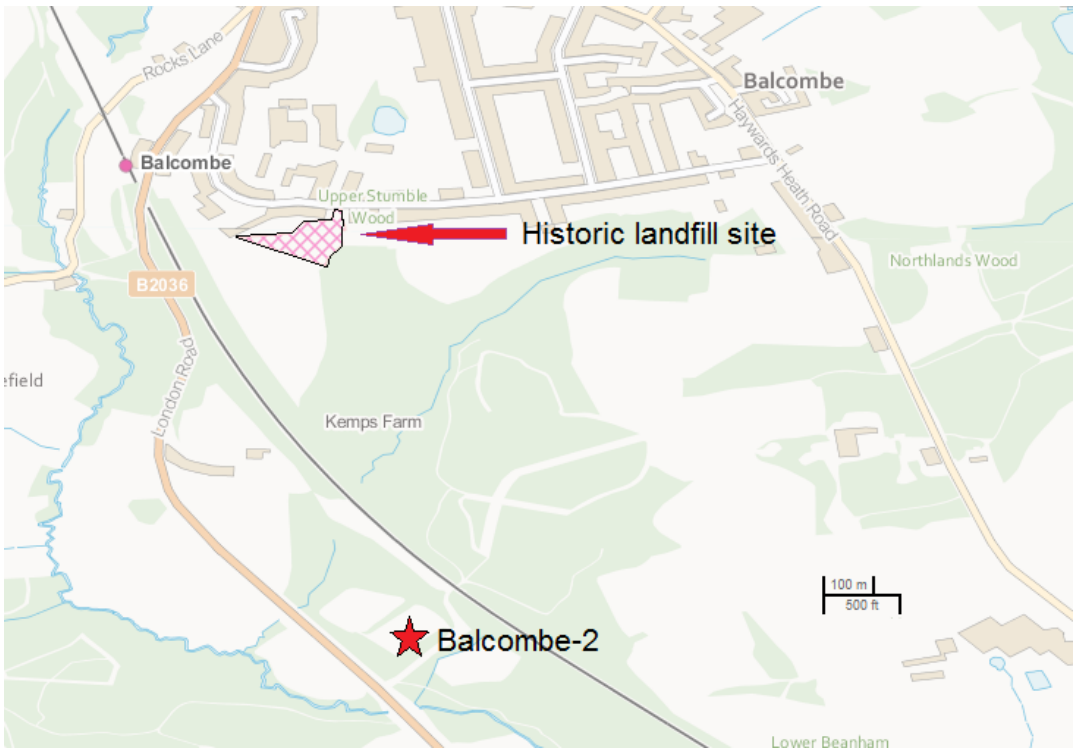

Figure 5-8 – Map of Balcombe-2 well and proximity to an old landfill site

5.8.3 Balcombe Water Monitoring Well Geochemistry (BALMW01)

Due to the known presence of gas in the Ashdown beds, before the Balcombe-2 well was spud a water monitoring well (BALMW01) was drilled onsite by GGS Ltd. to monitor shallow groundwaters. The artesian well was drilled to ~50 m and intersects the Ashdown beds.

Several samples were taken temporally from the water monitoring well BALMW01 over several months by Ground Gas Solutions Ltd. (GGS). Results from these and from sampling undertaken for this study are given in Table 22.

C_1/C_2 ratios vary from 4.7 to 42.8 from GGS samples, but C_2 was below detection methods at the University of Ohio for the samples collected for this study. The C_1/C_2 ratios in water samples show there is a significant thermogenic component to the gases, as purely microbial gases show minimal C_2+ components, *e.g.* C_1/C_2 = >1000 (Oremland *et al.*, 1988; Whiticar, 1994, 1999). All but one sample shows a *lower* C_1/C_2 than the deep gas collected from the Balcombe-2 well. Microbial oxidation of methane would result in a higher C_1/C_2 ratio because higher aliphatic hydrocarbons are preferentially oxidised over C_1 (Bernard *et al.*, 1978; Schoell, 1983); so the lower C_1/C_2

are seemingly incongruous with oxidation of gas from the Balcombe-2 well or addition of microbial CH_4.

The variations in C_1/C_2 content could be caused by temporal variations in microbial input to the system. The $\delta^{13}C_{CH4}$ range from -45.1‰ to -59‰. A plot of C_1/C_2 vs. $\delta^{13}C_{CH4}$ (Figure 5-9) shows that most of the samples do not fall in the thermogenic range with respect to isotopes, however neither does the deep gas sample from the Balcombe-2 well.

BALMW01

Date	Data Source	CH_4 (mg/l)	CO_2 (mg/l)	C_2H_6 (mg/l)	N_2 (mg/l)	C_1/C_2	C_1/CO_2	$\delta^{13}CH_4$ ‰	$\delta^{13}CO_2$ ‰
08/07/2013	*	12.4	2.3	0.29	ND	42.8	5.4	-53.3	-25.2
11/07/2013	*	6.84	1.92	0.97	ND	7.1	3.6	-45.1	-21.1
17/07/2013	*	7.42	1.48	1.1	ND	6.7	5.0	-45.2	-29.8
06/08/2013	~	11.16	1.76	1.28	ND	8.7	6.3	-51.70	ND
08/08/2013	~	11.41	0.55	1.85	ND	6.2	20.7	-52.80	ND
14/08/2013	~	11.78	2.53	2.01	ND	5.9	4.7	-54.80	ND
28/08/2014	† non-purged	17.68	ND	ND	20.8	ND	ND	-59	ND
28/08/2014	† purged	14.81	ND	ND	15.8	ND	ND	-52	ND
11/09/2013	~	7.00	0.95	1.50	ND	4.7	7.4	ND	ND

Balcombe-2

Date	Data Source	CH_4 (%)	CO_2 (%)	C_2H_6 (%)	N_2 (mg/l)	C_1/C_2	C_1/CO_2	$\delta^{13}CH_4$ ‰	$\delta^{13}CH_4$ ‰
12/09/2014	¤	89.07	0.13	2.82	ND	22.3	670	-51.5	-220.5
	†	ND	ND	ND	ND	ND	ND	-56.1	ND

Table 22 – Table of temporal data from the BALMW01 monitoring well.
** Measurements made by GGS for Interim Pre-Drill Environmental Monitoring Report 31st July 2013.*
~ Measurements made by GGS for Drill Phase Environmental Monitoring Report 25th October.
† CH_4 concentrations were determined by Tom Darrah at Ohio State University for this study, along with noble gas measurements from copper tube samples. Stable isotopes for these samples were collected separately in large glass bottles, and analysed at the radiocarbon lab at SUERC.
¤ concentration analysis performed at the University of Edinburgh, $\delta^{13}C_{CH4}$ at SUERC stable isotope lab.
Samples on 28/08/2014 were taken when the well was being purged of x3 well volumes (non-purged) and after purging this volume (purged).

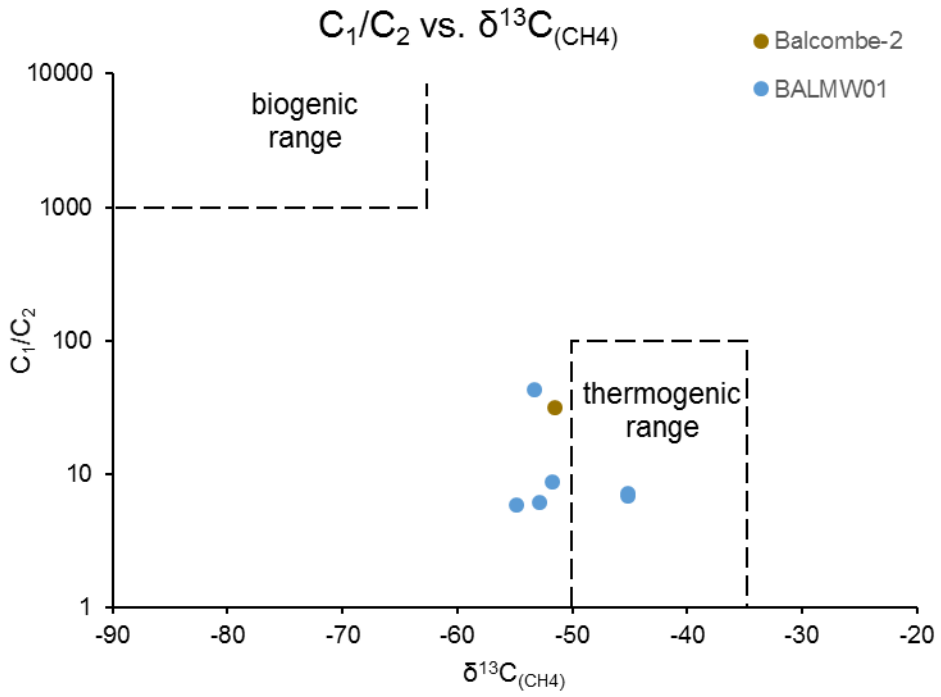

Figure 5-9 – 'Bernard'-styled plot of C_1/C_2 vs. $\delta^{13}C_{CH4}$ for Balcombe gas and water samples. Shows a modified Bernard-type plot, utilising C_1/C_2 instead of $C_1/(C_2+C_3)$, due to lack of C_3 data. Due to small C_3 contents of gases, diagnostic fields have been kept the same. "Balcombe-2" data from this study. Balcombe water ("BALMW01") from GGS data.

Nevertheless, the Balcombe-2 deep gas sits within the isotopic and compositional range of hydrocarbons found in the water monitoring well, which would indicate a deep source for these gases.

2 samples were taken from BALMW01 in 28/8/14 and analysed for radiocarbon. The first sample was taken early during well purging, and the second was taken after 3 well-volumes of water (2500 l) were removed from the artesian well. From the first sample to the second sample there was an increase in total dissolved solids (492 to 544 ppm), dissolved oxygen (4.43 to 8.12 ppm), stable carbon isotopes ($\delta^{13}C_{CH4}$ = -59‰ to -52‰), and enrichment of modern ^{14}C (27.27 to 47.17 percent-modern-carbon (pMC) ±1σ). For reference, the ^{14}C-conventional ages of these gases were 10,437±57 years before present and 6036±55 years before present respectively, however it should be noted that these represent relative inputs of ^{14}C into gases rather than absolute age. This was coupled with a decrease in pH (9.12 to 8.26).

As the Balcombe-2 deep gas sample was determined to be radiocarbon dead, this indicates the shallow gas is mixing with a significant contribution from a modern

carbon source. Active microbial methanogenesis of 'modern' (<60,000 years) organic matter must be occurring in the system and mixing with the deeper gas, although this seemingly does not reduce the $\delta^{13}C_{CH4}$ or increase the C_1/C_2 ratios due to biogenic input. Natural sources of methane from marshes and swamps will typically be derived from much older organic material than modern landfill and accumulated prior to thermonuclear testing, and should possess a lower percent modern carbon than anthropogenic methane from landfill. In the USA, 'drift gas' in common glacial tills shows typically <30 pMC while landfills contain 87-170 pMC (Coleman *et al.*, 1988, 1995; Hackley *et al.*, 1996; Mace *et al.*, 2016). Assuming a mix with radiocarbon-dead thermogenic gas, then the observed 47 pMC in methane in the shallow waters must be a result of 'modern' (<~50 y) carbon. The most probable source of this is the nearby landfill site, but other potential sources include a water treatment works to the south or various farm slurry tanks.

The difference in isotopic values between the 'un-purged' well sample and 'purged' sample is curious, and highlights the vagaries of sample collection when interpreting results. If mixing between a biogenic end-member and thermogenic end-member were occurring, then it might be expected that a radiocarbon-dead $\delta^{13}C$-enriched thermogenic end-member would be mixing with a $\delta^{13}C$-depleted radiocarbon-enriched biogenic end-member, and samples would show a lighter $\delta^{13}C$ signature with a younger radiocarbon age. The enrichment of $\delta^{13}C$ coupled with an increase in ^{14}C content between the non-purged and purged samples suggests a kinetic fractionation process rather than mixing between more/less of each component is driving these differences (both a relative increase in ^{13}C and ^{14}C in the gases in the 'purged' sample).

^{4}He concentrations in Balcombe groundwater range from 31.82 ppm to 23.90 ppm, which is greater than one order of magnitude higher than the ASW value of ~0.046 ppm and ~x4 higher than the air ratio of 5.24 ppm. The $^{3}He/^{4}He$ ratios were 0.028±0.000003 and 0.025±0.000003, and correcting for atmospheric neon results in $^{3}He/^{4}He$ of 0.022 and 0.020, which shows a strong radiogenic component concordant with the continental crust.

Neon and argon isotopes for both water samples are within error of the air ratios, indicating the dominance of ASW components in the waters. ^{20}Ne were 0.600±0.007 and 0.390±0.004, which is ×3.9 and ×2.2 the ASW concentration, and ^{36}Ar were 1.34±0.003 ppm and 1.10±0.002 ppm, which are ×1.1 and ×0.9 of the ASW

concentration. $^{84}Kr/^{36}Ar$ and $^{132}Xe/^{36}Ar$ show ratios lower than ASW, with $^{20}Ne/^{36}Ar$ slightly enriched. The enriched concentrations of ^{20}Ne relative to ASW, higher $^{20}Ne/^{36}Ar$ than ASW, and the lower $^{84}Kr/^{36}Ar$ and $^{132}Xe/^{36}Ar$ than ASW point to solubility-controlled degassing, and which clearly changes between subsequent samples. The samples were collected as liquid water, so should not display noble gas enrichment features of degassing. However, the well was artesian over-pressured and samples came from 50 m depth, and at the surface the large dissolved gas content caused 1000 l IBC containers of the produced water to visibly effervesce. The spread of heavier noble gases could represent partial degassing of sub-surface water during sampling as water samples are removed from 50 m hydrostatic head to 0 m, enriching water samples with a small component of gas, which may slightly enrich lighter noble gas components relative to heavier ones and result in the ratios observed. Nevertheless, noble gas concentrations at ASW concentrations or above do not suggest previous gas stripping of the formation water. The migration of free gases in the subsurface causes stripping of dissolved noble gases into the gas phase, and leaves the residual water depleted. Gas stripping has been observed in areas where well integrity failure has caused methane contamination in the shallow subsurface (Darrah *et al.*, 2014).

The concentrations of ANG's suggest a degree of degassing, attributed to partial degassing during sampling, but can nonetheless be attributed to typical ASW. This indicates that the elevated ^{4}He deep gas migrated slowly, accumulating in water rather than migrating as a free-phase which would strip ASW gases and leave residual waters depleted. It also suggests the ^{14}C enriched methane (attributed to landfill gas) migrated either dissolved in water or as a leachate plume which was degraded *in situ,* rather than as a free gas phase. This explanation may also explain the elevated heavy metals in the water (Cd, Cr, Fe, Pb, Ni, Zn, and Na). Heavy metal enrichment and elevated gas concentrations are not seen in the other nearby shallower water monitoring wells.

Landfills have been observed to be high in tritium (Coleman *et al.*, 1995; Hackley *et al.*, 1996); tritiated water enters landfill sites as meteoric water, and may also be introduced into the landfill directly in tritiated luminous paints in clocks, instrument dials, and noctilucent emergency lighting (Hackley *et al.*, 1996). Tritium (^{3}H) has a natural abundance of $<10^{-15}$% and decays to ^{3}He over a period of 12.4 years. It is naturally occurring as a result of cosmic ray bombardment of the upper atmosphere, but also produced from thermonuclear testing since the 1950's and the nuclear industry, and such can be used a tracer in modern water residence studies (Coleman *et*

al., 1988, 1995). The $^{3}He/^{4}He$ in the Balcombe water samples is very slightly elevated vs. the Balcombe-2 deep gas ($0.022\pm0.0004_{((Ra)\text{-corrected})}$ vs. $0.0180\pm0.0014_{(Ra)\text{-corrected}}$), but still shows a strongly radiogenic signal, showing that any ^{3}He ingrowth from tritium in this case must be negligible.

The observations that gas was encountered while drilling the Balcombe-1 in the 1980's, the stability of carbon and hydrogen isotopic signatures pre-to-post drilling activity, and the lack of atmospheric noble gas stripping indicate that drilling activity has not affected the shallow subsurface waters. Radiogenic $^{3}He/^{4}He$ fingerprints and ASW noble gas concentrations show that a significant proportion of the methane must be sourced from depth dissolved in water at low concentrations, and this gas has an identical hydrocarbon composition to the deep gas sampled from the Balcombe-2 well. A smaller component of 'modern' microbial methane enriched in ^{14}C is also present, but seemingly not at quantities which affect the $\delta^{13}C_{CH4}$ or C_1/C_2 composition. Resolution of the microbial component may be possible with δD_{CH4} data. This is hypothesised to have formed in the subsurface from a landfill leachate plume from a site located to the north.

5.9 Tracing Potential

5.9.1 Helium

Helium has a good track record as a tracing tool for deep gases (e.g. Gilfillan *et al.*, 2009; Darrah *et al.*, 2014; Wen *et al.*, 2016). In ths study, the Balm Well sample is a good example of the mixing between deep-sourced gas and shallow groundwater with an ASW noble gas inventory, as only a miniscule proportion of radiogenic helium from depth perturbes the $^{3}He/^{4}He$ ratio away from the ASW value to $\sim0.7_{(Ra)}$. The low solubility of helium in water means that crustal components can be resolved at a higher sensitivity than samples diluted with air (Mackintosh and Ballentine, 2012). This demonstrates that helium concentrations and isotopic ratios are a sensitive tracer for deep gas in the shallow subsurface, and that UK gases contain concentrations which are ideal for tracing.

High initial $^{4}He/^{20}Ne$ ratios in deep gases are ideal for tracing migrated gas, as a high initial $^{4}He/^{20}Ne$ end member is more easily resolved after interaction with ASW

during migration, as ^{20}Ne increases as it is stripped from groundwaters which migrating gas contacts, resulting in a decreasing $^{4}He/^{20}Ne$ ratio (Figure 5-10).

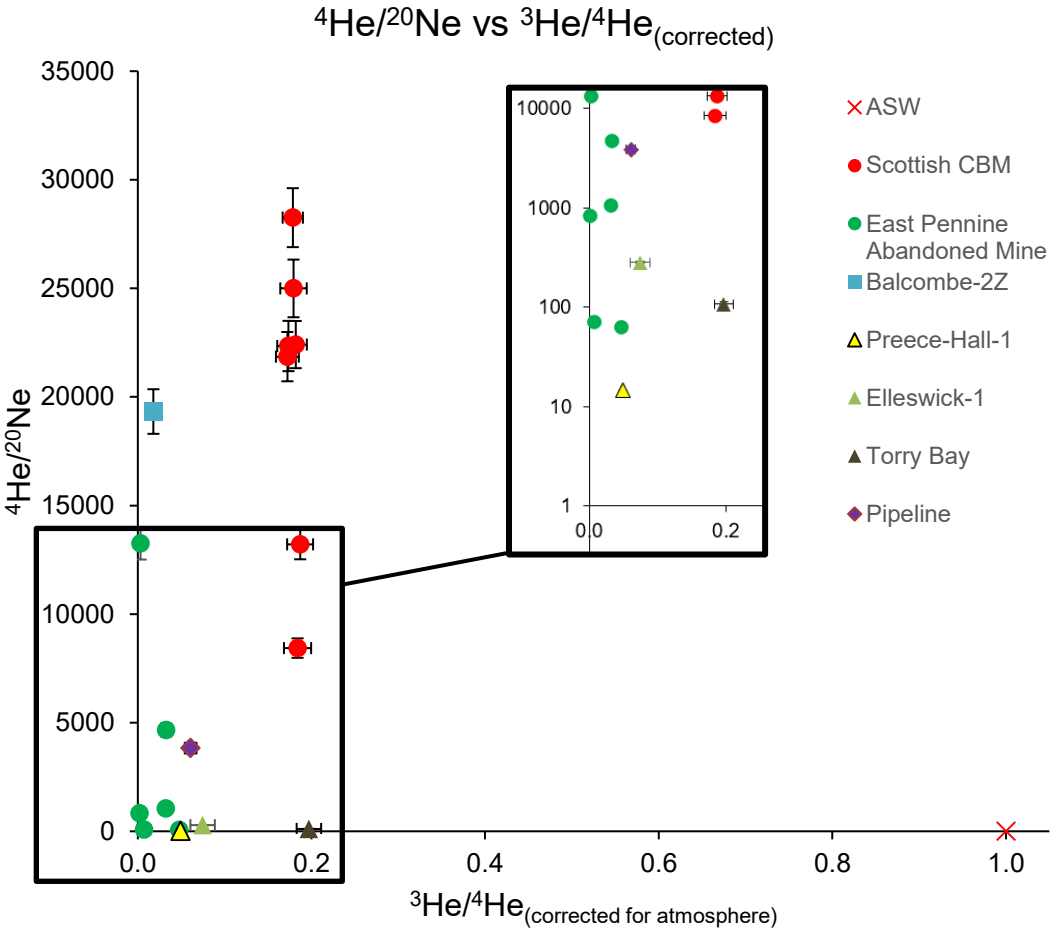

Figure 5-10 – Plot of $^{4}He/^{20}Ne$ vs. $^{3}He/^{4}He$ $_{(Ra)\text{-corrected}}$, with expanded view (logarithmic) of lower range. Plot shows most samples have $^{4}He/^{20}Ne$ above air (0.52) and ASW (~0.26).

5.9.2 Crustal Noble Gases

High values of excess argon $^{40}Ar^{*}$ and $^{21}Ne^{*}_{(crust)}$ can also be used as tracers of deep gases similar to helium, but are easily diluted with atmospheric components and thus have a lower sensitivity for gas tracing. This is evident in the Torry Bay sample, where excess ^{4}He is immediately obvious, but $^{40}Ar^{*}$ is only slightly above the atmospheric ratio.

The coal gases and shale gas studied have high $^{4}He/^{40}Ar^{*}$ ratios, significantly higher than the crustal average. This is possibly related to preferential release of ^{4}He from minerals at lower temperatures (Ballentine *et al.*, 1994), which could be pervasive in

unconventional gases (e.g. this study, and the only other CBM dataset in Zhou *et al.*, (2005)). The $^{4}He/^{40}Ar^{*}$ ratios are also higher than that found in conventional gases in the UK region (pipeline gas and the Magnus Field – North Sea (Ballentine *et al.*, 1996; Flude *et al.*, 2017)), and appear to be unique to each field (Table 23). As helium is ubiquitous in deep-sourced gases, utilising radiogenic $^{40}Ar^{*}$ in addition to helium could be used as a diagnostic feature when comparing different sources of deep gases.

The small concentrations of $^{40}Ar^{*}$ and $^{21}Ne^{*}$ are easily masked by atmospheric input which limits their utility as a tracer, especially at surface seeps. However, these crustal gases could be applied as tracers in the subsurface, for example mixing between gas types, rather than to identify deep gases in surface environments.

Location	Min $^{4}He/^{40}Ar^{*}$	Max $^{4}He/^{40}Ar^{*}$	Mean $^{4}He/^{40}Ar^{*}$	Local end-member $^{4}He/^{40}Ar^{*}$
English AMM (this study)	17	40.5	36.3	33.2
Scottish CBM (this study)	16.8	51.6	25.3	15.8
San Juan Basin CBM (*Zhou et al.*, 2005)	0.12	12.1	2.36	15.5
Balcombe-2 (this study)	-	-	32.8	-
Sheffield Mains Gas (Flude *et al.*, 2017)	-	-	6.2	-
Magnus Field – North Sea (Ballentine *et al.*, 1996)	3.2	15.6	10.6	-
Crustal Average (Elliot *et al.*, 1993)	-	-	-	4.9

Table 23 – Table of $^{4}He/^{40}Ar^{*}$ ratios for gases in this study, and selected UK and US Fields.

5.9.3 Composition and Carbon and Hydrogen Stable Isotopes

'Bernard' plots are very useful for determining gas origin, and groups of samples in this study typically fall in reasonably tight groupings (Figure 5-11). Unfortunately, there is limited compositional C_1/C_2 data for environmental samples in the UK for comparison.

Stable carbon and hydrogen isotope analysis is ambiguous as a tracing tool, as UK gas isotopic ranges overlap the ranges measured in landfill, coals, and North Sea gases

(Figure 5-12). The Torry Bay and Preese-Hall-1 shale gas sample had isotope values which do not fit the prescribed fields for hydrocarbons, which makes analysis difficult.

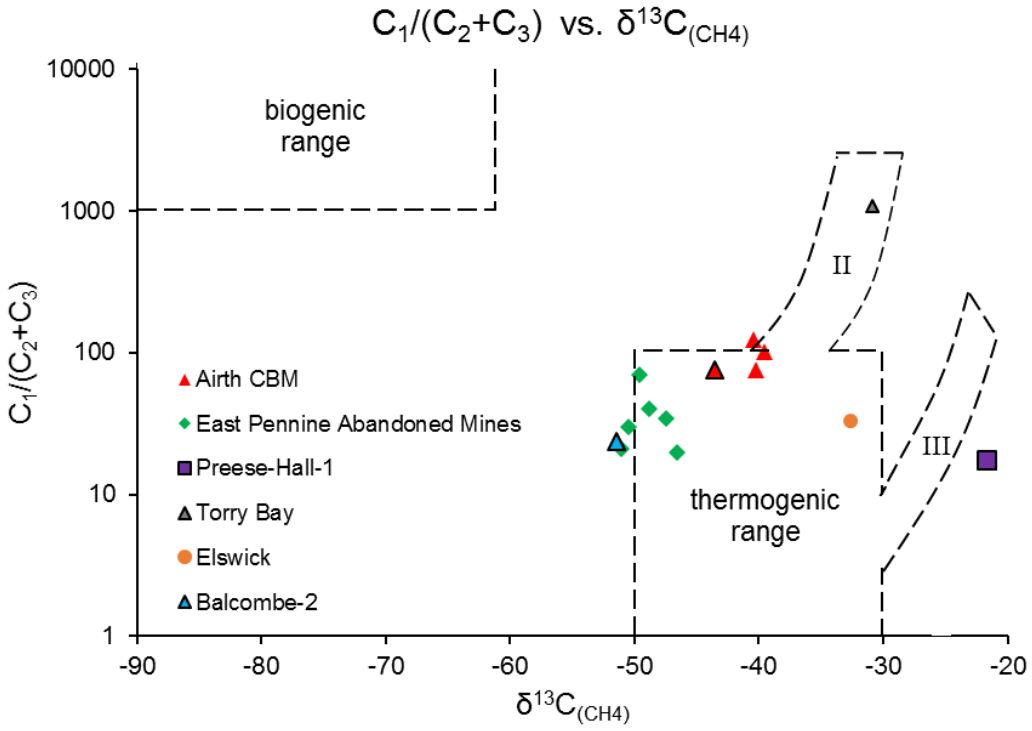

Figure 5-11 – 'Bernard' plot of $C_1/(C_2+C_3)$ vs. $\delta^{13}C_{CH4}$. II refers to the maturation trend for type II kerogen, III refers to the maturation trend for type III kerogen.

The overlapping of UK unconventional gases with landfill and other coal measurements is most likely due to certain generation mechanisms (*e.g.* early mature thermogenic) producing a similar isotopic ratio to microbial processes, as well as direct mixing with microbial gas in the case of AMM samples. H-isotopes can be used generally to help distinguish between thermogenic and biogenic CH_4, and be used in combination with δD from water to see if gases are related to that water or migrated from elsewhere. Whiticar (1999) observed that for methane produced by CO_2 reduction: $\delta D_{CH4} = \delta D_{H2O} - 160\ (\pm 10)$ ‰, *i.e.* the methane $\delta^{13}C_{CH4}$ is offset by -160‰ from the δD_{H2O} of the water. This is a fairly diagnostic test which should deduce the microbial pathway of methanogenesis, however rapidly formed methane where substrates are not limited may have larger offsets (Vinson *et al.*, 2017). Care must be taken when interpreting stable isotope data. Issues comparing the $\delta^{13}C_{CH4}$ with $\delta^{13}C_{CO2}$ will also arise in areas where there is significant non-biological external input to a sample, such as CO_2 generated by chemical carbonate dissolution in AMM samples.

Radiocarbon measurements have identified 'modern' ^{14}C in waters at the Balcombe site, which would otherwise have gone unnoticed as the C_1/C_2 and $\delta^{13}C_{CH4}$ values in the waters are indistinguishable from deep sourced gas in the region.

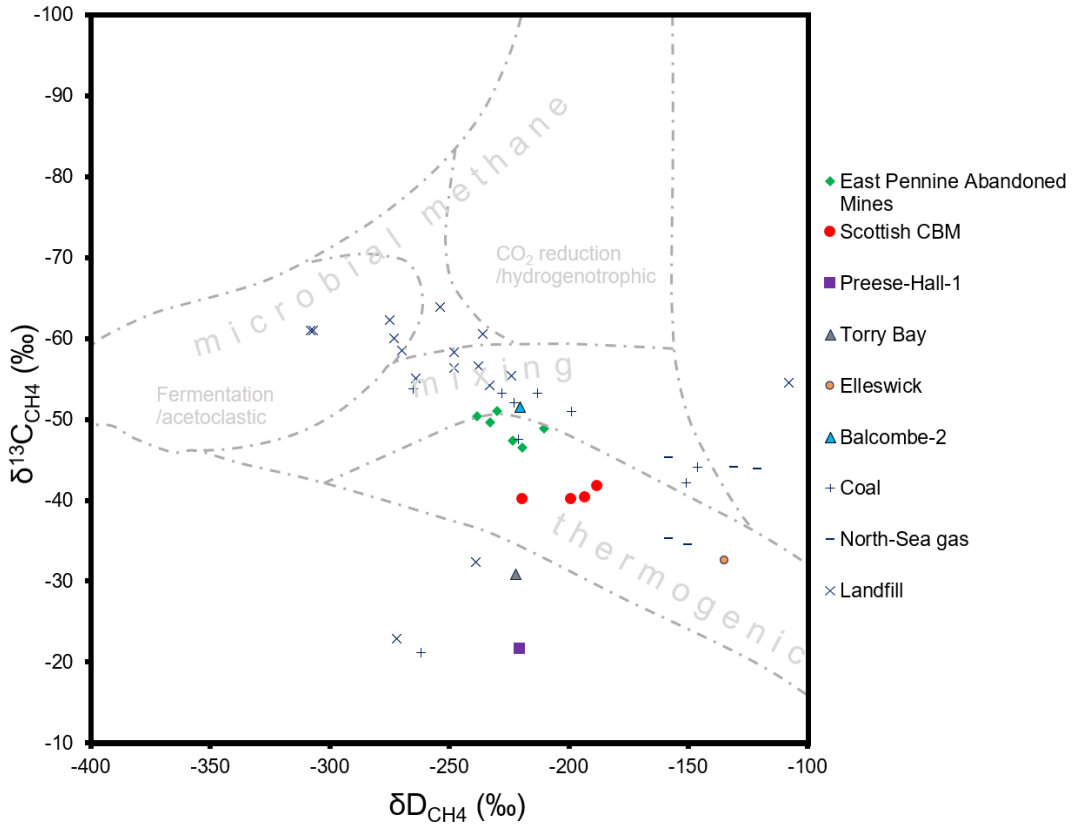

Figure 5-12 – 'Whiticar' style $\delta^{13}C_{CH4}$ vs. δD_{CH4} plot of sampled gases, and other UK samples measured by Hitchman et al., (1989).

Refined petrochemical products, such as oils, diesel, gases (*e.g.* blended for pipeline, commercial Qatari LNG, US shale ethane) are unlikely to retain any noble gas content, and thus would be difficult to trace with noble gases, however the lack of ^4He content can then distinguish between a geological source of deep gas, and one which may have a thermogenic molecular and isotopic signature but has been introduced into the subsurface by other means *e.g.* fuel spillage or tank leakage.

5.10 Tracing Workflow

Gas Fingerprinting is a term used to describe the process of utilising geochemical evidence to define and constrain a source of gas (Baldassare *et al.*, 2014). Source to receptor tracing requires the knowledge of the geochemistry of the end-members, and the processes which affect the gas on its way to the receptor. Five steps are normally undertaken when identifying a stray gas (Baldassare *et al.*, 2014):

1- Describe and characterise the gas at the receptor
2- Identify potential sources of the gas
3- Characterise the stable isotope and molecular composition of potential sources
4- Evaluate the potential for secondary effects on the stray gas
5- Identify the most likely source

The ultimate purpose of gas fingerprinting is to determine the origin of any stray gas so that the effects it has can be predicted and mitigated. A workflow methodology to fingerprint a stray gas should aim to identify the source of a gas in as few steps as possible, which aids fast turnaround of conclusions and minimises time and cost.

Any workflow methodology will ultimately depend on the equipment available to the researcher, the nature of the samples, time and funds available, and the requirements of the survey.

Sampling and analysis should be directed to answer specific questions about the geochemistry of a gas to point towards a source, and conducted in such a way to direct further sampling or analytical procedures if necessary. Hydrocarbons and the processes affecting them are best defined by assessing a range of samples and identifying trends, rather than analysis of limited discrete samples, but in some cases this is not possible. Some geochemical techniques are better suited than others to delineate between possible gas sources, and a brief overview of techniques and caveats is given:

5.10.1 Sampling

The sampling of gases and waters is the most important step in the gas fingerprinting process. Incorrect sampling, storage, and handing will mean any results will not be representative of the sampled gas. Methane and light noble gases are highly mobile, and correct sampling equipment and storage must be used to avoid losing or

fractionating samples (Schowalter *et al.*, 2010; Eby *et al.*, 2015; Molofsky *et al.*, 2016), as methane is known to diffusive through certain materials such as gas bags or the septa on glass sampling bottles (Eby *et al.*, 2015). The 'shelf-life' of methane in foil gas bags before isotopic fractionation occurs is less than a month (Eby *et al.,* 2015, T. Donnelly, *pers comms*), and this is reduced further after piercing the gas bag septum with gas needles to remove aliquots.

The types of sample and container required by different analytical techniques will determine how and when samples must be collected. Water samples must be kept refrigerated and/or acidified after collection to minimise bacterial alteration (Kampbell and Vandegrift, 1998; Molofsky *et al.*, 2016).

5.10.2 Compositional Analysis

Compositional analysis of bulk gases is the cheapest method of characterising gases, and possibly the most diagnostic of tests to distinguish the presence of thermogenic gases. All but the very lowest maturity coals (lignites to sub-bituminous) and very highest maturity coals (anthracites) will have an elevated C_2/C_1 relative to biogenic gas (Whiticar, 1994; Golding *et al.*, 2013). Biogenic gases will possess a low ethane content ($C_1/(C_2+C_3) > 1000$) (*e.g.* Bernard *et al.*, 1976) because microbial ethanogenesis is rare and probably restricted to recent marine sediments (Oremland *et al.*, 1988; Hinrichs *et al.*, 2006) (although both C_2 and C_3 can be a constituent component of landfill gas (Coleman *et al.*, 1995)). Gases associated with recent microbial activity also often have high CO_2 contents, *e.g.* landfill gases (Coleman *et al.*, 1995; Hackley *et al.*, 1996).

Compositional analysis is readily performed on gas samples by gas chromatography, and water samples by headspace gas chromatography. Mass-spectrometry is a poor choice for concentration determination as hydrocarbons fragment when ionised, resulting in a spread of ionised fragments with different m/z that will overlap with the ionised fragments from other homologous alkanes, and unpicking the mass-spectrum into the constituent concentrations of each component is problematic (de Hoffman and Stroobant, 2007).

A study which tracks changes in bulk composition over time may be more effective than discrete sampling which utilises a more technically complex analysis, for example temporal respective changes in extremely low concentrations of higher hydrocarbons

may prove to be a more sensitive parameter than $\delta^{13}C_{CH4}$ in methane when analysing mixed thermogenic-microbial systems in aquifers (*e.g.* Schloemer *et al.,* 2016).

Compositional analyses however require a well-defined database of end-members, and although they hint at a gas genetic type, there are numerous processes which can significantly shift the mass-balance of different gas species such as methane and CO_2.

5.10.3 Stable Carbon and Hydrogen Isotopes

For any sample which cannot be differentiated with just gas composition, isotopic analysis is beneficial. Isotopic analysis of carbon isotopes in CH_4 and CO_2, and hydrogen stable isotopes in CH_4 can help to elucidate gas types via the diagnostic fields in 'Schoell' (Schoell, 1980), and combined with gas composition in 'Bernard' plots (Bernard *et al.*, 1978).

Isotopic trends can be observed, such as substrate depletion during active methanogenesis which shifts $\delta^{13}C_{CO2}$ to values >0‰. Care must be taken in the sampling and storage of gas samples to avoid kinetic or solubility fractionation by following defined procedures and using correct materials.

CO_2 can easily be removed from gas samples with soda lime, but separating C_2+ components is more difficult, and the use of cryogenic separation may introduce unwanted isotopic fractionation (see Methodology, this text). The methodology used by any lab must be reviewed prior to interpreting results, as methods of methane isotopic analysis which do not separate the C_2+ components may influence the results. Caution must be exercised when directly comparing samples collected with different methods and analysed by different laboratories, as the results can be drastically different even for the same sample (e.g. Molofsky *et al.*, 2016).

Combined molecular-composition and isotopic measurements can be performed by combined GC-IRMS, where components are chromatographically separated and measured by GC. The individual gases can then be collected and combusted with in-line systems before entering the mass-spectrometer as CO_2 or H_2. This is the typical method used by larger commercial laboratories (e.g. Isotech Labs, IL, USA), as it allows the separation and cryo-focussing of low-concentration C_2+ components which can then be isotopically analysed.

$\delta^{13}C_{CH4}$ isotopes can reveal a lot about a sample, especially when combined with compositional data *i.e.* 'Bernard' type plots. δD_{CH4} on the other hand are often specific to

depositional basins for thermogenic gases (Golding *et al.*, 2013), which may or may not be useful as a tracer of gas in groundwater. δD_{CH4} measurements can be useful for distinguishing between microbial gas and thermogenic gases (Whiticar, 1994, 1999) or determining the microbial methanogenic pathway (Whiticar, 1999; Strąpoć *et al.*, 2011). However, it can be seen that many samples do not fit the diagnostic fields of these plots, and frequently overlap with thermogenic gases in the UK (Hitchman *et al.*, 1989). Analysis of methane $\delta^{13}C_{CH4}$ and δD_{CH4} requires combustion of methane into CO_2 and H_2O, with further reduction of H_2O into H_2. This extra step required for δD_{CH4} adds complexity (and cost) to the analysis. As various inorganic and microbial pathways have a dependence on water δD_{H2O} (Whiticar, 1999; Vinson *et al.*, 2017), δD_{CH4} measurements are probably best taken alongside water δD_{H2O} for comparison. The waters for some samples may be inaccessible (or even geologically ancient), and δD_{CH4} can still require careful interpretation to be informative. For a limited sample set, or point-source sampling, the usefulness of δD_{CH4} for gas tracing may be limited, and the time and cost of analysis (especially if water δD_{H2O} is also analysed) may be better focussed elsewhere, *e.g.* $\delta^{13}C_{CO2}$ measurements, which may be a better indicator of microbial activity when combined with $\delta^{13}C_{CH4}$ (Whiticar, 1999; Strąpoć *et al.*, 2011; Vinson *et al.*, 2017), or repeated sampling over time.

New portable analytical equipment is becoming routinely available that can analyse methane and CO_2 concentrations as well as carbon isotopic ratios utilising cavity down-ring spectroscopy or specialised optics (Crosson *et al.*, 2002; Zare *et al.*, 2009; Picarro Inc., 2017). While these offer lower precision measurements than standard GC or IRMS techniques, they have the advantage of onsite and low-cost analysis, and can be used to quickly direct further investigation if further technical analysis is required.

5.10.4 Radiocarbon

Microbial methanogenesis typically occurs via one of two pathways: acetate fermentation or CO_2 reduction (Schoell, 1980; Whiticar, 1999). The isotopic fractionation these processes exert on produced gas define the diagnostic fields in the δD_{CH4} vs. $\delta^{13}C_{CH4}$ 'Schoell' plots, but because these define microbial processes they are less able to distinguish between the different *sources* of organic material, *e.g.* microbial *coal* gas vs. microbial *landfill* gas *vs.* microbial *marsh* gas. While these sources of gas

may be generated in the modern environment, the ages of the methanogenic precursors can be used to distinguish between them.

The approximate age of the organic substrate can be assessed by radiocarbon in methane or CO_2, which can help to resolve gases from landfill, sewerage, swamps/peats, *etc*., from radiocarbon-dead thermogenic gases. Radiocarbon analysis via Accelerator Mass Spectrometry (AMS) used in this study is expensive and time consuming, but allows the resolution of very small quantities of ^{14}C to a high precision. For methane, the determination of any quantity of ^{14}C above 0 pMC (percent modern carbon) is a diagnostic trait, as it establishes that there must be a 'modern' component. Thus, the precision of AMS is probably unnecessary, and Liquid Scintillation Counting for ^{14}C may be a more economic option and possibly provide a faster turnaround of results. When collecting samples, it is important to know the volumes required; commercial ^{14}C measurement can require as much as 2 g of carbon, which could mean a sample collection of 4-65 litres (Hackley *et al.*, 1996).

5.10.5 Noble Gases

Noble gas measurements are both time consuming, expensive, and require specialist sampling equipment. Their conservative and unreactive nature however allows unique resolution of deep gas sources at the surface, fractionation processes which affected the gases, and migration history. Elevated ^{4}He is diagnostic of deep gases that have had a long residence time in the crust, and the low concentrations in the atmosphere and typical air-equilibrated-water (*i.e.* ASW) make ^{4}He an excellent and unequivocal tracer for deep gases in the shallow subsurface (Mackintosh *et al.*, 2006; Gilfillan and Haszeldine, 2011; Darrah *et al.*, 2014; Györe *et al.*, 2018). Most deep gas samples are limited to the number of point-source hydrocarbon wells, so noble gas analysis can be worth the effort. For shallow water samples however, the dilution of various crustal components when mixed with ASW means that a full isotopic analysis of helium to xenon is unnecessary if the purpose of the analysis is solely to identify the presence of deep-sourced of methane.

The migration of free gas through a water column can strip the dissolved noble gases, and depletions in the atmospheric noble gas inventory of water can be used to identify the mechanism of gas contamination (Darrah *et al.*, 2014). Such analysis could be performed without Kr or Xe data, or even without isotopic ratios. Where full isotope

resolution mass spectrometry is not required, helium, neon, and argon concentrations can be performed by gas chromatography if correct sampling procedures are followed.

Recent developments have been made so that is also possible to analyse helium, neon, argon, krypton, N_2, O_2, CO_2, and CH_4 *in situ* with a portable quadrupole mass spectrometer (Brennwald *et al.*, 2016). Routine onsite analysis of helium content could provide a fast determination of deep gas content, and guide further sampling collection to minimise time and expenditure for full IRMS isotopic analysis if required.

5.10.6 Other Techniques

Further analytical techniques such as methane isotopologue analysis are in their infancy (Stolper, Lawson, *et al.*, 2014; Stolper, Sessions, *et al.*, 2014; Stolper *et al.*, 2015), and may be best suited to shed light on the intricacies of thermogenic and biogenic production mechanisms.

5.11 Conclusions

All the samples of unconventional gas in this study (plus a sample of UK domestic pipeline gas) are characterised by high concentrations of ^4He, with a strong radiogenic component. This is similar to other UK gases (Oxburgh *et al.*, 1986), and other natural gas accumulations. Helium concentrations from sampled gases were higher than those found in pipeline gas (Flude *et al.*, 2017). This is excellent for tracing any fugitive gas, as the helium inventory of the atmosphere is low (5.24 ppm), allowing the resolution of small excesses of helium derived from deep-sourced gas in the shallow subsurface. Surficial sources of gas (landfill, marsh gas, peat bogs, *etc.*) are not expected to contain significant quantities of helium.

Geochemical analysis was applied to natural gas seeps and monitoring wells to test the efficacy of the methods. Helium and neon isotopes were used to prove the deep-sourced origin of methane-rich gas in a surface gas seep in Scotland (Torry Bay), as well as a shallow a groundwater located near a shale-oil exploration well (Balcombe Water Monitoring Well).

The Torry Bay ^4He concentration once adjusted for atmospheric contamination was 1662 ppm, with the $^3He/^4He = 0.20_{Ra}$, both observations are similar to the fingerprint of the Airth CBM Field which is located 13 km to the East. The Torry Bay

sample sits on a mixing line calculated between Air Saturated Water (ASW) and the Airth Field. Torry Bay also showed a small but resolvable excess of $^{40}Ar^*$, highlighting the radiogenic component of deep sourced gas.

The Balcombe Water sample has previously been interpreted as thermogenic gas which had migrated from the deep subsurface. This is confirmed by the elevated ^{4}He and a thermogenic ($C_1/(C_2+C_3)$) and $\delta^{13}C_{CH4}$ hydrocarbon composition. However, radiocarbon analysis revealed that there must also be a component of modern methane, hypothesised to be from a nearby landfill site which has previously not been noticed.

Trace levels of ^{4}He were found in water samples at Leadburn House, and St. Catherine's well, showing there is a small input of a deep-sourced component to these waters. Preese-Hall-1 shale gas appeared significantly air contaminated, however there was still significant quantities of ^{4}He present in the gas.

^{4}He, $^{21}Ne^*$, and $^{40}Ar^*$ have different production and release rates in the crust, and when combined these may be useful tracers for distinguishing between different sources of deep gas in the subsurface.

5.12 Bibliography

Andrews, J. E. (1988) 'Methane-related Mg-calcite cements in recent tidal flat sediments from the Firth of Forth', *Scottish Journal of Geology*, 24(3), pp. 233–244. doi:10.1144/sjg24030233.

Bald, R. (1829) 'Observations on the spontaneous emissions of in-flammable Gas, in particular of Carburetted Hydrogen', *The Edinburgh Journal of Science*, 1.

Baldassare, F. J., McCaffrey, M. a. and Harper, J. a. (2014) 'A geochemical context for stray gas investigations in the northern Appalachian Basin: Implications of analyses of natural gases from Neogene-through Devonian-age strata', *AAPG Bulletin*, 98(2), pp. 341–372. doi:10.1306/06111312178.

Ballentine, C. ., Mazurek, M. and Gautschi, A. (1994) 'Thermal constraints on crustal rare gas release and migration: Evidence from Alpine fluid inclusions', *Geochimica et Cosmochimica Acta*, 58(20), pp. 4333–4348. doi:10.1016/0016-7037(94)90337-9.

Ballentine, C. J. and Burnard, P. G. (2002) 'Production, Release and Transport of Noble Gases in the Continental Crust', *Reviews in Mineralogy and Geochemistry*, 47(1), pp. 481–538. doi:10.2138/rmg.2002.47.12.

Ballentine, C. J., O'Nions, R. K. and Coleman, M. L. (1996) 'A Magnus opus: Helium, neon, and argon isotopes in a North Sea oilfield', *Geochimica et Cosmochimica Acta*. Elsevier, 60(5), pp. 831–849. doi:10.1016/0016-7037(95)00439-4.

BEIS (2017) *Digest of UK Energy Statistics (DUKES): natural gas*.

Bernard, B. B., Brooks, J. M. and Sackett, W. M. (1976) 'Natural gas seepage in the Gulf of Mexico', *Earth and Planetary Science Letters*, 31(1), pp. 48–54. doi:10.1016/0012-821X(76)90095-9.

Bernard, B. B., Brooks, J. M. and Sackett, W. M. (1978) 'Light hydrocarbons in recent Texas continental shelf and slope sediments', *Journal of Geophysical Research*, 83(C8), p. 4053. doi:10.1029/JC083iC08p04053.

BGS (2010) *Underground natural gas storage in the UK*.

Brennwald, M. S., Schmidt, M., Oser, J. and Kipfer, R. (2016) 'A Portable and Autonomous Mass Spectrometric System for On-Site Environmental Gas Analysis', *Environmental Science & Technology*. American Chemical Society, 50(24), pp. 13455–13463. doi:10.1021/acs.est.6b03669.

Coleman, D. D., Liu Chao-Li, Hackley, K. C. and Pelphrey, S. R. (1995) 'Isotopic identification of landfill

methane', *AAPG Division of Environmental Geosciences Journal*, 2(2), pp. 95–103.
Coleman, D. D., Liu, C.-L. and Riley, K. M. (1988) 'Microbial methane in the shallow Paleozoic sediments and glacial deposits of Illinois, U.S.A.', *Chemical Geology*, 71(1), pp. 23–40. doi:http://dx.doi.org/10.1016/0009-2541(88)90103-9.
Crosson, E. R., Ricci, K. N., Richman, B. A., Chilese, F. C., Owano, T. G., Provencal, R. A., Todd, M. W., Glasser, J., Kachanov, A. A., Paldus, B. A., Spence, T. G. and Zare, R. N. (2002) 'Stable Isotope Ratios Using Cavity Ring-Down Spectroscopy: Determination of 13C/12C for Carbon Dioxide in Human Breath', *Analytical Chemistry*. American Chemical Society, 74(9), pp. 2003–2007. doi:10.1021/ac025511d.
Cuadrilla (2013) 'Statement from Cuadrilla Resources about Shallow Gas in West Sussex', May.
Darling, W. G. and Gooddy, D. C. (2006) 'The hydrogeochemistry of methane: Evidence from English groundwaters', *Chemical Geology*, 229(4), pp. 293–312. doi:10.1016/j.chemgeo.2005.11.003.
Darrah, T. H., Vengosh, a., Jackson, R. B., Warner, N. R. and Poreda, R. J. (2014) 'Noble gases identify the mechanisms of fugitive gas contamination in drinking-water wells overlying the Marcellus and Barnett Shales', *Proceedings of the National Academy of Sciences*, 111(39), pp. 14076–14081. doi:10.1073/pnas.1322107111.
Dawson, C. (1898) 'On the Discovery of Natural Gas in East Sussex', *Quarterly Journal of the Geological Society*, 54(1–4), pp. 564–571. doi:10.1144/GSL.JGS.1898.054.01-04.38.
DECC (2013) *the Unconventional Hydrocarbon Resources of Britain's Onshore Basins - Coalbed Methane (CBM)*. Department of Energy and Climate Change. Available at: https://www.ogauthority.co.uk/media/1694/promote_uk_cbm_2012.pdf.
EA (2013) *Environment Agency Historic Landfill Data*.
Eby, P., Gibson, J. J. and Yi, Y. (2015) 'Suitability of selected free-gas and dissolved-gas sampling containers for carbon isotopic analysis', *Rapid Communications in Mass Spectrometry*, 29(13), pp. 1215–1226. doi:10.1002/rcm.7213.
Elliot, T., Ballentine, C. J., O'Nions, R. K. and Ricchiuto, T. (1993) 'Carbon, helium, neon and argon isotopes in a Po basin (northern Italy) natural gas field', *Chemical Geology*, 106(3–4), pp. 429–440. doi:10.1016/0009-2541(93)90042-H.
Flude, S., Györe, D., Stuart, F. M., Zurakowska, M., Boyce, A. J., Haszeldine, R. S., Chalaturnyk, R. and Gilfillan, S. M. V. (2017) 'The inherent tracer fingerprint of captured CO2', *International Journal of Greenhouse Gas Control*, 65, pp. 40–54. doi:10.1016/j.ijggc.2017.08.010.
Gazetteer for Scotland (2016) *Preston Island History*. Available at: http://www.scottish-places.info/features/featurefirst22.html (Accessed: 3 March 2016).
GGS (2014) *Summary Report: Independent Environmental Monitoring - Natural Gas Exploration Site at Preese Hall, Weeton. GGS222-01-SR01*.
Gilfillan, S. and Haszeldine, S. (2011) *Report on Noble Gas, Carbon Stable Isotopes and HCO3 Measurements from the Kerr Quarter and Surrounding Area, Goodwater, Saskatchewan*. IPAC CO2 Research Incorporated. Available at: https://www.geos.ed.ac.uk/homes/sgilfil1/Kerrreport.pdf.
Gilfillan, S. M. V, Lollar, B. S., Holland, G., Blagburn, D., Stevens, S., Schoell, M., Cassidy, M., Ding, Z., Zhou, Z., Lacrampe-Couloume, G. and Ballentine, C. J. (2009) 'Solubility trapping in formation water as dominant CO2 sink in natural gas fields', *Nature*. Macmillan Publishers Limited. All rights reserved, 458(7238), pp. 614–618. doi:10.1038/nature07852.
Golding, S. D., Boreham, C. J. and Esterle, J. S. (2013) 'Stable isotope geochemistry of coal bed and shale gas and related production waters: A review', *International Journal of Coal Geology*, 120, pp. 24–40. doi:10.1016/j.coal.2013.09.001.
Gooddy, D. C. and Darling, W. G. (2005) 'The potential for methane emissions from groundwaters of the UK', *Science of The Total Environment*, 339(1–3), pp. 117–126. doi:10.1016/j.scitotenv.2004.07.019.
Grealy, N. (2011) *THOUSAND YEAR PLUS HISTORY OF METHANE AND UK WATER CONTAMINATION*. Available at: http://www.reimaginegas.com/?p=1755 (Accessed: 4 March 2016).
Green, Christopher, A., Styles, P. and Baptie, B. J. (2012) *Shale Gas Fracturing Review & Recommendations for Induced Seismic Migration*. Available at: https://www.gov.uk/government/uploads/system/uploads/attachment_data/file/48330/5055-preese-hall-shale-gas-fracturing-review-and-recomm.pdf.
Györe, D., McKavney, R., Gilfillan, S. M. V. and Stuart, F. M. (2018) 'Fingerprinting coal-derived gases from the UK', *Chemical Geology*, 480, pp. 75–85. doi:10.1016/j.chemgeo.2017.09.016.
Hackley, K. C., Liu, C. L. and Coleman, D. D. (1996) 'Environmental Isotope Characteristics of Landfill Leachates and Gases', *Ground Water*. Blackwell Publishing Ltd, 34(5), pp. 827–836. doi:10.1111/j.1745-6584.1996.tb02077.x.
Hinrichs, K.-U., Hayes, J. M., Bach, W., Spivack, A. J., Hmelo, L. R., Holm, N. G., Johnson, C. G. and Sylva, S. P. (2006) 'Biological formation of ethane and propane in the deep marine subsurface', *Proceedings of the National Academy of Sciences* , 103(40), pp. 14684–14689.
Hitchman, S. P., Darling, W. G. and Williams, G. M. (1989) *STABLE ISOTOPE RATIOS IN METHANE*

CONTAINING GASES IN THE UNITED KINGDOM, *Technical Report WE/89/30*. Nottingham: British Geological Survey. Available at: http://nora.nerc.ac.uk/id/eprint/502528/1/WE89030.pdf.

de Hoffman, E. and Stroobant, V. (2007) *Mass spectrometry: principles and applications*. Wiley. ISBN: 978-0-470-03310-4.

Joseph, C., Campbell, K. A., Torres, M. E., Martin, R. A., Pohlman, J. W., Riedel, M. and Rose, K. (2013) 'Methane-derived authigenic carbonates from modern and paleoseeps on the Cascadia margin: Mechanisms of formation and diagenetic signals', *Palaeogeography, Palaeoclimatology, Palaeoecology*, 390, pp. 52–67. doi:10.1016/j.palaeo.2013.01.012.

Judd, A. G., Sim, R., Kingston, P. and McNally, J. (2002) 'Gas seepage on an intertidal site: Torry Bay, Firth of Forth, Scotland', *Continental Shelf Research*, 22(16), pp. 2317–2331. doi:10.1016/S0278-4343(02)00058-4.

Kampbell, D. H. and Vandegrift, S. A. (1998) 'Analysis of Dissolved Methane, Ethane, and Ethylene in Ground Water by a Standard Gas Chromatographic Technique', *Journal of Chromatographic Science*, 36(5), pp. 253–256. doi:10.1093/chromsci/36.5.253.

Mace, E. K., Aalseth, C. E., Day, A. R., Hoppe, E. W., Keillor, M. E., Moran, J. J., Panisko, M. E., Seifert, A., Tatishvili, G. and Williams, R. M. (2016) 'First results of a simultaneous measurement of tritium and14C in an ultra-low-background proportional counter for environmental sources of methane', *Journal of Environmental Radioactivity*, 155–156, pp. 122–129. doi:10.1016/j.jenvrad.2016.02.001.

Mackintosh, S. J. and Ballentine, C. J. (2012) 'Using 3He/4He isotope ratios to identify the source of deep reservoir contributions to shallow fluids and soil gas', *Chemical Geology*. Elsevier B.V., 304–305(0), pp. 142–150. doi:10.1016/j.chemgeo.2012.02.006.

Mackintosh, S. J., Ballentine, C. J. and Gawthorpe, R. (2006) 'The use of noble gases as a tracer in carbon dioxide sequestration', *Geochimica et Cosmochimica Acta*, 70, p. A381. doi:10.1016/j.gca.2006.06.770.

Mamyrin, B. W., Annufriev, G., Kamenskiy, G. S. and Tolstikhin, I. L. (1970) 'Determination of the isotopic composition of atmospheric helium', *Geochem. Int.*, 7, pp. 498–505.

Mark, D. F., Stuart, F. M. and de Podesta, M. (2011) 'New high-precision measurements of the isotopic composition of atmospheric argon', *Geochimica et Cosmochimica Acta*. Elsevier Ltd, 75(23), pp. 7494–7501. doi:10.1016/j.gca.2011.09.042.

Molofsky, L. J., Richardson, S. D., Gorody, A. W., Baldassare, F., Black, J. A., Mchugh, T. E. and Connor, J. A. (2016) 'Effect of Different Sampling Methodologies Groundwater Samples', 54(5), pp. 669–680. doi:10.1111/gwat.12415.

Niemann, M. and Whiticar, M. (2017) 'Stable Isotope Systematics of Coalbed Gas during Desorption and Production', *Geosciences*, 7(2), p. 43. doi:10.3390/geosciences7020043.

Ó Dochartaigh, B. E., Smedley, P. L., MacDonald, A. M., Darling, W. G. and Homoncik, S. (2012) *Baseline Scotland: groundwater chemistry of the Carboniferous sedimentary aquifers of the Midland Valley*, *Open Report OR/11/021*. Nottingham: British Geological Survey.

Oremland, R. S., Whiticar, M. J., Strohmaier, F. E. and Kiene, R. P. (1988) 'Bacterial ethane formation from reduced, ethylated sulfur compounds in anoxic sediments', *Geochimica et Cosmochimica Acta*, 52(7), pp. 1895–1904. doi:10.1016/0016-7037(88)90013-0.

Oxburgh, E. R., O'Nions, R. K. and Hill, R. I. (1986) 'Helium isotopes in sedimentary basins', *Nature*, 324(6098), pp. 632–635. doi:10.1038/324632a0.

Picarro Inc. (2017) *Picarro G2201-i Analyzer - δ13C for methane (CH4) and carbon dioxide (CO2)*.

Reeves, J. W. (1948) 'Surface problems in the search for oil in Sussex', *Proceedings of the Geologists' Association*, 59, pp. 234-IN8. doi:10.1016/S0016-7878(48)80003-9.

Schloemer, S., Elbracht, J., Blumenberg, M. and Illing, C. J. (2016) 'Distribution and origin of dissolved methane, ethane and propane in shallow groundwater of Lower Saxony, Germany', *Applied Geochemistry*, 67, pp. 118–132. doi:http://dx.doi.org/10.1016/j.apgeochem.2016.02.005.

Schoell, M. (1980) 'The hydrogen and carbon isotopic composition of methane from natural gases of various origins', *Geochimica et Cosmochimica Acta*, 44(5), pp. 649–661. doi:10.1016/0016-7037(80)90155-6.

Schoell, M. (1983) 'Genetic Characterization of Natural Gases', *AAPG Bulletin*, 67(12), pp. 2225–2238.

Schowalter, S. J., Connolly, C. B. and Doyle, J. M. (2010) 'Permeability of noble gases through Kapton, butyl, nylon, and "Silver Shield"', *Nuclear Instruments and Methods in Physics Research Section A: Accelerators, Spectrometers, Detectors and Associated Equipment*. Elsevier, 615(3), pp. 267–271. doi:10.1016/j.nima.2010.01.041.

Stolper, D. A., Sessions, A. L., Ferreira, A. a., Santos Neto, E. V., Schimmelmann, A., Shusta, S. S., Valentine, D. L. and Eiler, J. M. (2014) 'Combined 13C–D and D–D clumping in methane: Methods and preliminary results', *Geochimica et Cosmochimica Acta*. Elsevier Ltd, 126, pp. 169–191. doi:10.1016/j.gca.2013.10.045.

Stolper, D. A., Lawson, M., Davis, C. L., Ferreira, a a, Neto, E. V. S., Ellis, G. S., Lewan, M. D., Martini, a M.,

Tang, Y., Schoell, M., Sessions, a L. and Eiler, J. M. (2014) 'Formation temperatures of thermogenic and biogenic methane', *Science*, 344(6191), pp. 1500–1503. doi:10.1126/science.1254509.

Stolper, D. A., Martini, A. M., Clog, M., Douglas, P. M., Shusta, S. S., Valentine, D. L., Sessions, A. L. and Eiler, J. M. (2015) 'Distinguishing and understanding thermogenic and biogenic sources of methane using multiply substituted isotopologues', *Geochimica et Cosmochimica Acta*, 161(0), pp. 219–247. doi:10.1016/j.gca.2015.04.015.

Strąpoć, D., Mastalerz, M., Dawson, K., Macalady, J., Callaghan, A. V., Wawrik, B., Turich, C. and Ashby, M. (2011) 'Biogeochemistry of Microbial Coal-Bed Methane', *Annual Review of Earth and Planetary Sciences*. Annual Reviews, 39(1), pp. 617–656. doi:10.1146/annurev-earth-040610-133343.

Underhill, J. R., Monaghan, A. A. and Browne, M. A. E. (2008) 'Controls on structural styles, basin development and petroleum prospectivity in the Midland Valley of Scotland', *Marine and Petroleum Geology*, 25(10), pp. 1000–1022. doi:10.1016/j.marpetgeo.2007.12.002.

Vinson, D. S., Blair, N. E., Martini, A. M., Larter, S., Orem, W. H. and McIntosh, J. C. (2017) 'Microbial methane from in situ biodegradation of coal and shale: A review and reevaluation of hydrogen and carbon isotope signatures', *Chemical Geology*, 453, pp. 128–145. doi:10.1016/j.chemgeo.2017.01.027.

Wen, T., Castro, M. C., Nicot, J.-P., Hall, C. M., Larson, T., Mickler, P. and Darvari, R. (2016) 'Methane Sources and Migration Mechanisms in Shallow Groundwaters in Parker and Hood Counties, Texas—A Heavy Noble Gas Analysis', *Environmental Science & Technology*. American Chemical Society, 50(21), pp. 12012–12021. doi:10.1021/acs.est.6b01494.

Whiticar, M. J. (1994) 'Correlation of natural gases with their sources', in *The Petroleum System - from Source to Trap*. AAPG Special Edition, pp. 261–283.

Whiticar, M. J. (1996) 'Stable isotope geochemistry of coals, humic kerogens and related natural gases', *International Journal of Coal Geology*, 32(1–4), pp. 191–215. doi:10.1016/S0166-5162(96)00042-0.

Whiticar, M. J. (1999) 'Carbon and hydrogen isotope systematics of bacterial formation and oxidation of methane', *Chemical Geology*, 161(1–3), pp. 291–314. doi:10.1016/S0009-2541(99)00092-3.

Zare, R. N., Kuramoto, D. S., Haase, C., Tan, S. M., Crosson, E. R. and Saad, N. M. R. (2009) 'High-precision optical measurements of 13C/12C isotope ratios in organic compounds at natural abundance', *Proceedings of the National Academy of Sciences* , 106(27), pp. 10928–10932.

Zhou, Z., Ballentine, C. J., Kipfer, R., Schoell, M. and Thibodeaux, S. (2005) 'Noble gas tracing of groundwater/coalbed methane interaction in the San Juan Basin, USA', *Geochimica et Cosmochimica Acta*, 69(23), pp. 5413–5428. doi:10.1016/j.gca.2005.06.027.

6 Conclusions

A combination of unconventional gas samples in the UK including Coal Bed Methane (CBM), Abandoned Mine Methane (AMM), shale-oil associated gas, shale gas, and natural surface seeps were analysed for their bulk gas compositions, stable carbon and hydrogen isotopes, radiocarbon, and noble gas inventories. The data is reported and analysed with reference to gas sources, and key geochemical parameters which may be used to develop geochemical 'fingerprints' to identify gases, and their trace their migration through the surface and subsurface.

6.1 Key Findings

6.1.1 Noble Gases

All of the deep-sourced gases sampled have elevated ^{4}He concentrations ranging from 250 ppm to 2984 ppm, which is the largest concentration of ^{4}He found in a Palaeozoic aquifer. These concentrations are ~×48 to ~×569 the concentration found in air (5.24 ppm; (Ozima and Podosek, 2001)). Moreover, due to the low solubility of helium in water, these are ×5413 to ×25339 the concentration expected from shallow groundwater equilibrated with the atmosphere, *i.e.* Air Saturated Water (ASW).

The quantities of helium measured cannot have been generated within the units themselves from U and Th decay chains (Györe *et al.*, 2018). The helium is likely sourced both from surrounding formations with higher detrital mineral contents, and from steady-state degassing of the crust (Torgersen *et al.*, 1989). High ^{4}He concentrations are in-line with other Paleozoic-aged gas reservoirs, and seem to be independent of gas type (conventional, unconventional, CBM, *etc.*), and therefore high ^{4}He concentrations can be expected in other Paleozoic-aged UK unconventional gases (Györe *et al.*, 2018). Furthermore, all gases in this study, once adjusted for atmospheric dilution, contain greater ^{4}He concentrations than a sample of typical gas from the UK gas network.

All samples measured show a radiogenically-dominated $^{3}He/^{4}He$ ratio, with East Pennine coal gases $<0.05_{(Ra)}$, Scottish CBM at $\sim0.18_{(Ra)}$, and other gases between $0.02\text{-}0.10_{(Ra)}$ which are typical of the average crust (Ballentine and Burnard, 2002). This is contrasted with the atmospheric value (defined as $1_{(RA)}$) and the ASW value of

~0.97$_{(Ra)}$, which is what would be observed in groundwater that had equilibrated with the atmosphere. The combination of high helium concentrations and radiogenically dominated $^3He/^4He$ ratios shows that helium is an excellent tracer for migrating deep gases. (see Figure 6-1).

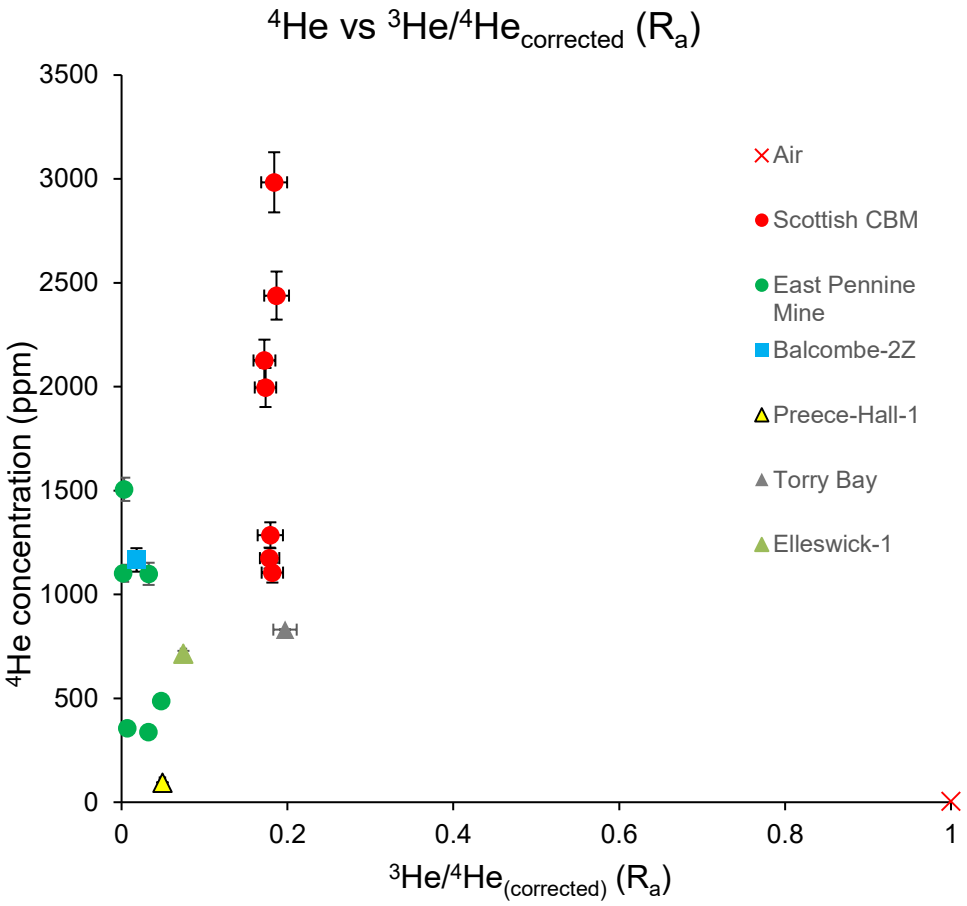

Figure 6-1 – Plot of ^4He vs. $^3He/^4He_{((Ra\text{-}corrected)}$.All samples show elevations of ^4He relative to the air value (red cross).

The Scottish CBM gases at the Airth Field had a small, but clearly resolvable mantle contribution to the helium and neon inventories. This is unexpected in continental Scotland due to the lack of recent magmatic activity, and is the first recorded example of mantle input in UK hydrocarbons (Oxburgh *et al.*, 1986). It is hypothesised to be related to the proto-Iceland plume under the N. Atlantic causing magmatism in W. Scotland around 58-61 Ma (Saunders *et al.*, 1997). The nearby deep-seated Ochil fault to the north has a ~4 km throw and is a plausible conduit for deep fluid migration for mantle volatiles. This mantle signature in gas demonstrates the ability of coals to store and preserve volatile noble gases for tens of millions of years.

In samples that contain less atmospheric component there is resolvable crustally-derived $^{21}Ne^*$ and $^{40}Ar^*$, shown by elevated $^{21}Ne/^{22}Ne$ and $^{40}Ar/^{36}Ar$ ratios, which could be used as tracers for deep-sourced gases in the subsurface.

In the Scottish CBM Airth Field, a range of noble gas isotopic ratios and compositional trends was observed that cannot be explained by common processes (*e.g.* simple single-step degassing of water, or mass-fractionation). A model was proposed where formation waters and coals contained different noble gas inventories: formation waters, containing a greater degree of atmospherically-derived noble gases, and coals, containing a smaller volume of older, crustal and mantle-rich noble gases. Dewatering the strata as part of the production process strips the noble gases from the formation waters in the permeable cleat/fracture network. Continued production of gas and further dewatering of coals preferentially remove this water-sourced component. Coals begin to desorb gas when the pressure is lowered further by the dewatering process, and this results in a contribution of a more crustally-rich component to the produced gases from the coals. An evolution from formation-water derived gases at 'unpumped' wells to a lower concentration of crustally-rich components at the most developed wells can be observed in the Airth Field.

6.1.2 Gas Composition, and Carbon and Hydrogen Stable Isotopes:

The carbon and hydrogen stable isotope ratios found in Scottish CBM (Airth Field) occupy a narrow isotopic range ($\delta^{13}C_{CH4}$ = -39.5‰ to -41.8‰; δD_{CH4} = -211 to -238‰) which can be considered characteristic of these gases, and indicate a thermogenic source. AMM gases have a lighter isotopic composition of a similarly narrow characteristic range ($\delta^{13}C_{CH4}$ = --46.5‰ to -51.1‰; δD_{CH4} = -163 to -220‰), which shows a predominantly thermogenic gas, but up to one third could be lighter biogenic methane. No relationship between isotopic and compositional parameters could be found in either set of coal gases. The gases from the shale-oil well Balcombe-2 plot within the ranges of English AMM gases, while Lancashire shale gas and tight gas are noticeably isotopically heavier.

Importantly, these isotopic ranges overlap those of coals, North Sea gases, and landfill sites previously measured in the UK (Hitchman *et al.*, 1989), which makes carbon and hydrogen stable isotopes ambiguous tracers for determining gas origins (see Figure 6-2).

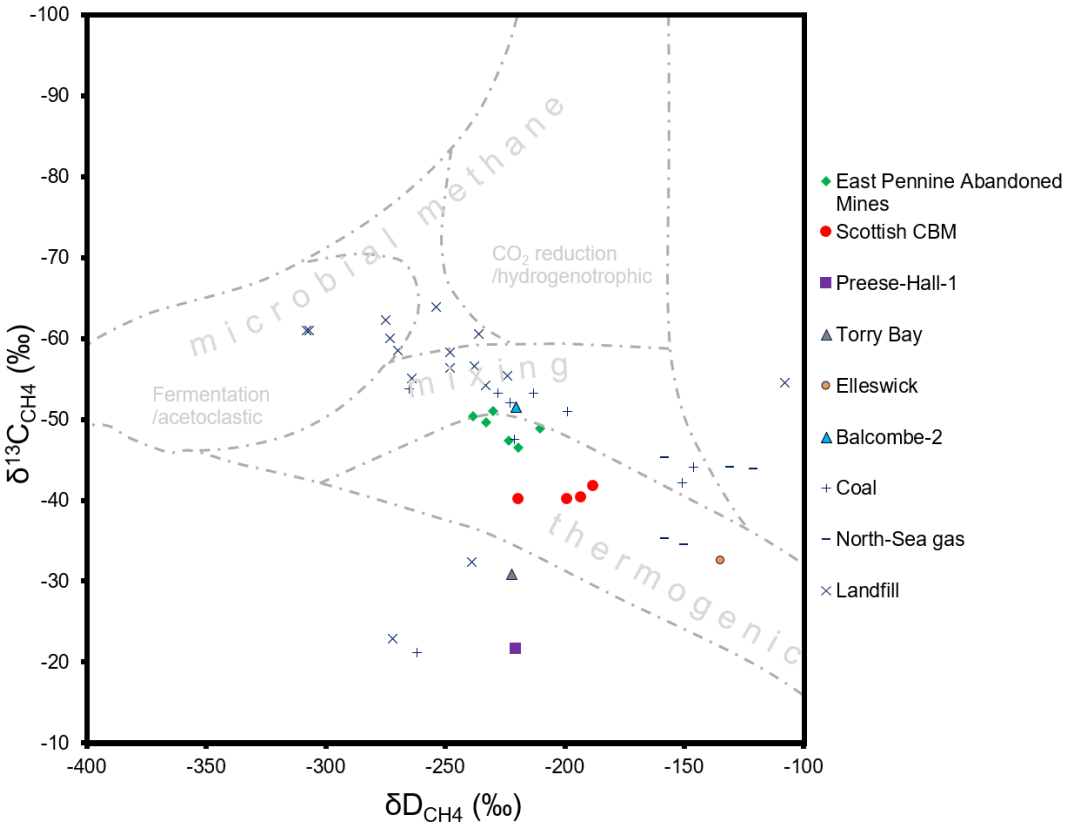

Figure 6-2 - 'Whiticar' style $\delta^{13}C_{CH4}$ vs. δD_{CH4} plot of sampled gases (this study), and Coal/North-Sea gas/Landfill samples measured by Hitchman et al., (1989).

Scottish CBM gases are principally methane, with low carbon dioxide (<0.1%), and are relatively 'dry', showing trace ethane and propane components: $(C_1/(C_2+C_3)) = 75 - 121$. English AMM gases are slightly wetter $(C_1/(C_2+C_3)) = 20 - 69$, which is probably related to both lower thermal maturity and localised oil-association. All deep gas samples showed a 'wetter' character than biogenic gases which are typically very dry, which makes the presence of C_{2+} hydrocarbons a reliable discriminant between thermogenic and biogenic gases (see Figure 6-3)

Methane contents in English AMM samples from 35% to 79%, variably diluted with nitrogen, carbon dioxide, and trace noble gases. The nitrogen is sourced from the atmosphere, with O_2 having been consumed in the mine workings. The source of CO_2 is mix between coal oxidation processes, and chemical carbonate dissolution from the acidic mine environment.

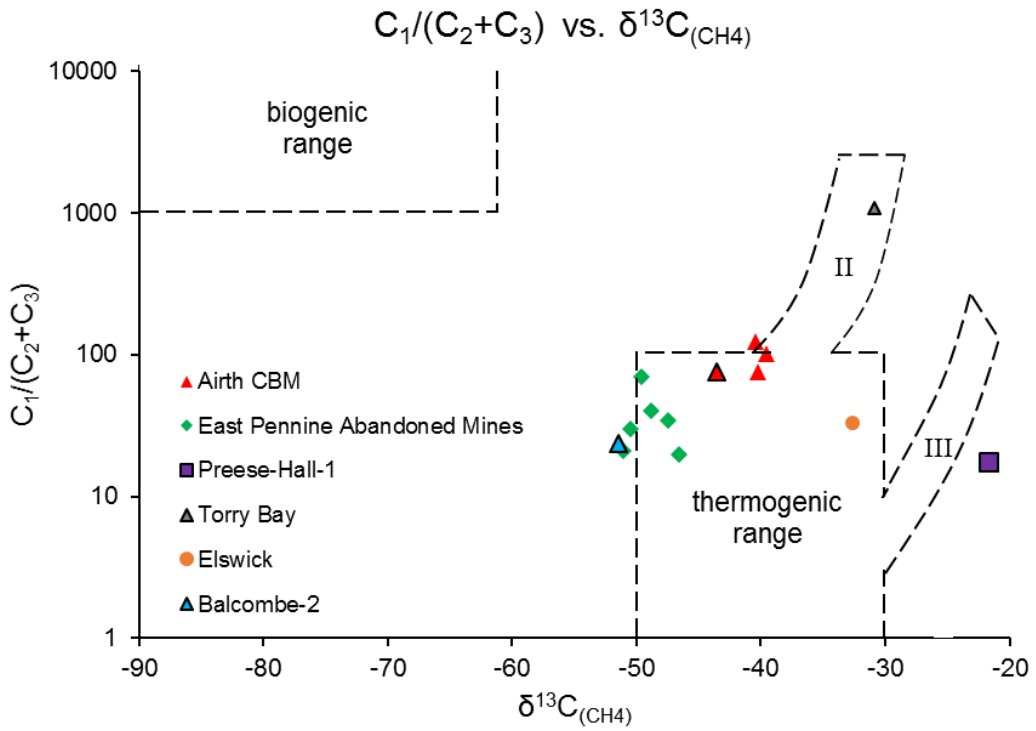

Figure 6-3 – 'Bernard' plot of $C_1/(C_2+C_3)$ vs. $\delta^{13}C_{CH4}$. II refers to the maturation trend for type II kerogen, III refers to the maturation trend for type III kerogen.

6.2 Further work

There are other unconventional and conventional oil and gas wells in the UK, and sampling these for noble gases would add to the baseline measurements. As well as source characterisations, receptor aquifers in the UK are poorly categorised. While work is ongoing to define baseline methane and water chemistries. (e.g. Bell *et al.*, 2016), there is little work on noble gas inventories of these systems. For typical mixing between deep-gas and shallow waters, an ASW composition is assumed to be the shallow end-member. This may not be the case, and regional sampling of the baseline noble gas inventory of aquifer waters would be a logical next step, as they represent the most vulnerable systems to methane contamination. Regional measurements could also help to constrain the geographic area of the mantle helium input in Scotland.

6.3 Bibliography

Ballentine, C. J. and Burnard, P. G. (2002) 'Production, Release and Transport of Noble Gases in the Continental Crust', *Reviews in Mineralogy and Geochemistry*, 47(1), pp. 481–538. doi:10.2138/rmg.2002.47.12.

Bell, R. A., Darling, W. G., Manamsa, K. and Ó Dochartaigh, B. E. (2016) *The Baseline Concentrations of*

Methane in Great British Groundwater - the National Methane Baseline Survey, *British Geological Survey Open Report OR/15/071*. Nottingham, U.K.: British Geological Survey. Available at: http://nora.nerc.ac.uk/id/eprint/514557/1/National Methane Baseline Survey OR15071.pdf.

Györe, D., McKavney, R., Gilfillan, S. M. V. and Stuart, F. M. (2018) 'Fingerprinting coal-derived gases from the UK', *Chemical Geology*, 480, pp. 75–85. doi:10.1016/j.chemgeo.2017.09.016.

Hitchman, S. P., Darling, W. G. and Williams, G. M. (1989) *STABLE ISOTOPE RATIOS IN METHANE CONTAINING GASES IN THE UNITED KINGDOM*, *Technical Report WE/89/30*. Nottingham: British Geological Survey. Available at: http://nora.nerc.ac.uk/id/eprint/502528/1/WE89030.pdf.

Oxburgh, E. R., O'Nions, R. K. and Hill, R. I. (1986) 'Helium isotopes in sedimentary basins', *Nature*, 324(6098), pp. 632–635. doi:10.1038/324632a0.

Ozima, M. and Podosek, F. A. (2001) *Noble Gas Geochemistry*. 2nd edn. Cambridge: Cambridge University Press. doi:10.1017/CBO9780511545986 ISBN: 9780511545986.

Saunders, A. D., Fitton, J. G., Kerr, A. C., Norry, M. J. and Kent, R. W. (1997) 'The North Atlantic Igneous Province', in Mahoney, J. J. and Coffin, M. F. (eds) *Large Igneous Provinces: Continental, Oceanic, and Planetary Flood Volcanism, Volume 100*. American Geophysical Union, pp. 45–93. doi:10.1029/GM100p0045.

Torgersen, T., Kennedy, B. M., Hiyagon, H., Chiou, K. Y., Reynolds, J. H. and Clarke, W. B. (1989) 'Argon accumulation and the crustal degassing flux of 40Ar in the Great Artesian Basin, Australia', *Earth and Planetary Science Letters*, 92(1), pp. 43–56. doi:10.1016/0012-821X(89)90019-8.

7 Appendices

This chapter contains additional reference material and calculations.

7.1 Sample Collection and Storage Issues Affecting Noble Gas Abundances

For the Airth Field samples (Chapter 3, this volume) the clamp system utilised for sample collection (see Methodology, this volume) was observed to have leaked helium out of the tube over a 300 day period. For reasons of lab availability, there can often be a large time gap between sample collection and analysis in the lab. The samples however were not observed to have had an obvious ingress of atmospheric neon or argon into the tube, suggesting that the leakage was on a small scale and only affecting helium. The large volumes of helium present in samples (both ^{3}He and ^{4}He) relative to the atmosphere meant that no change in helium isotopic ratios was observed from atmospheric ingress of ^{3}He. The leakage rates are hard to quantify, as they are specific to each tube (which can only be analysed once), or were derived from tubes that had been split into two sections using similar clamps in the lab. This is investigated further.

Airth-1 was sampled in August 2014 with four copper tubes (denoted "Airth-1 2014") and four stainless steel sampling cells (denoted "sample cell"), to evaluate a new system for capturing and storing samples over time. The copper tube clamps used for the 2014 sampling trip were similar in design, but manufactured at a different time to the clamps used for the samples taken in 2013.

Copper tubes were analysed 2, 161, 274, and 303 days after sampling. Where available, data is also given for Airth-1 (2013) and Airth-10, reanalysed at a later date. Helium concentrations were found to have decreased from 2901±108 ppm to 1285±62 ppm (Figure 7-1). The same pattern is seen in ^{3}He (Figure 7-2), which suggests leakage of helium from the tubes.

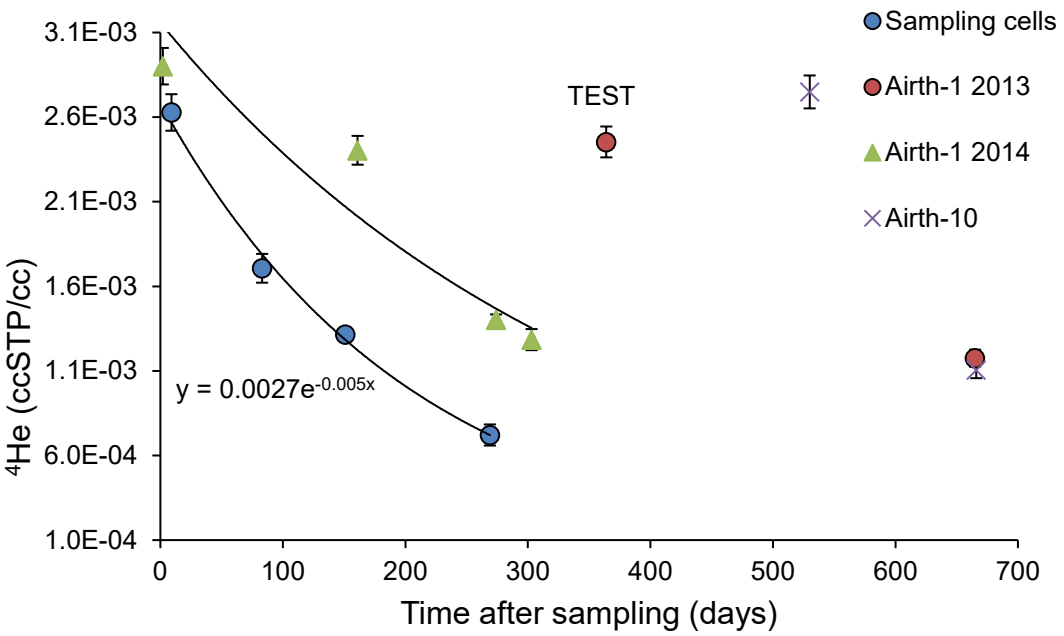

Figure 7-1 – Plot of ^4He concentrations (cc/ccSTP = ppm ×10^{-6}) versus the time from sampling to analysis. A clear trend in every sample shows a decrease in ^4He concentration over a period of time. Lines represents best-fit exponential curves.

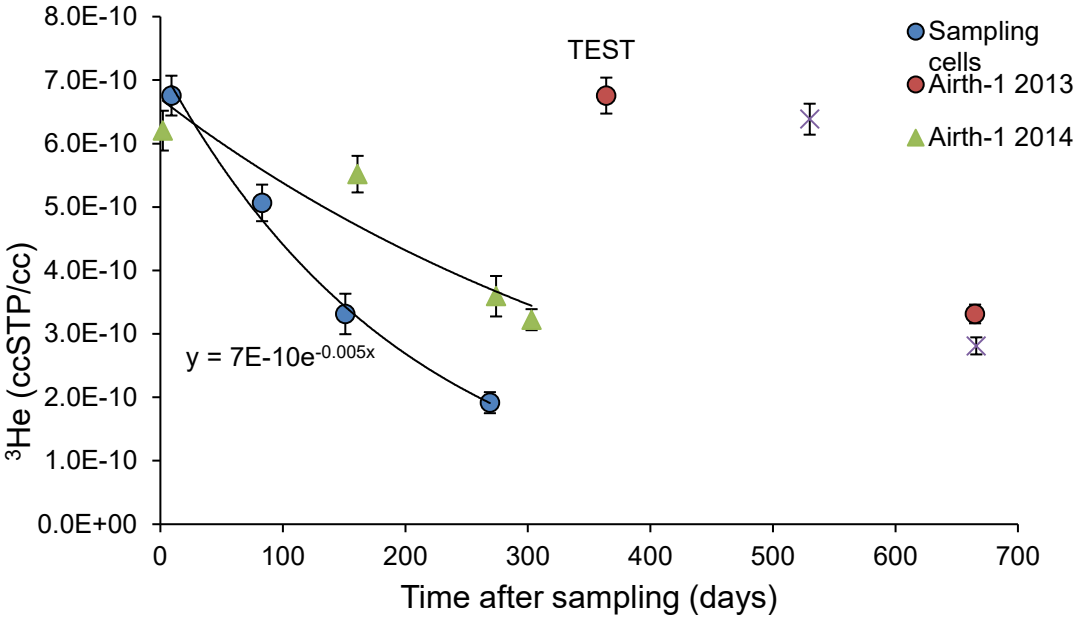

Figure 7-2 - Plot of ^3He concentrations (cc/ccSTP = ppm ×10^{-6}) versus the time from sampling to analysis. A clear trend in every sample shows a decrease in ^3He over a period of time. Line represents best-fit exponential curve.

Air ingress in "typical samples" (*i.e.* lower helium concentrations and radiogenic $^{3}He/^{4}He_{(Ra)} < 0.05$) would result in a net input of ^{3}He from the atmosphere. Both ^{3}He and ^{4}He concentrations in the sample tubes were 2-3 orders of magnitude above the atmospheric concentrations, and tubes were stored at 1 bar above atmospheric pressure. Therefore, the concentration gradient for all helium species would result in migration out of the tube and no atmospheric ingress for helium would be expected. Clearly, even with leakage, the tubes have maintained a significant concentration gradient for helium *versus* the atmosphere, suggesting a slow leakage rate. The larger ^{4}He concentrations in samples *versus* atmospheric ^{4}He result in a stronger concentration gradient than sample ^{3}He *versus* the atmospheric values, which may suggest a greater loss of ^{4}He *versus* ^{3}He, resulting in an increase of the $^{3}He/^{4}He_{(Ra)}$ ratio. However, the diffusivity of ^{3}He is greater than ^{4}He, so assuming a slow diffusive leak one may expect a preferential loss of ^{3}He, and the $^{3}He/^{4}He_{(Ra)}$ to decrease over time. What is observed is an inconsistent but small increase in the $^{3}He/^{4}He_{(Ra)}$ ratios (Figure 7-3), possibly related to differential leakage with different tubes. It should be noted that in the samples analysed within days, the concentrations of ^{3}He and ^{4}He in both the sampling cell and copper tube are similar, but the resultant $^{3}He/^{4}He_{(Ra)}$ are different. This is unexpected as no significant leakage could have occurred during this period.

^{3}He and ^{4}He are typically analysed in the same sequence, with ^{4}He measured on a Faraday cup detector and ^{3}He measured on an electron multiplier detector, both calibrated to the same standard (HESJ helium standard (Matsuda *et al.*, 2002). Therefore, the isotopic ratio is independent of separately analysed ratios (unlike *e.g.* $^{4}He/^{20}Ne$, where helium and neon are analysed separately), but may be subject to non-linear effects arising from the use of separate detectors. $^{3}He/^{4}He_{(Ra)}$ for the copper tube sample analysed 303 days after sampling shows the same $^{3}He/^{4}He_{(Ra)}$ within error to the sample cell analysed 9 days after sampling, although the helium concentration for the latter is over double.

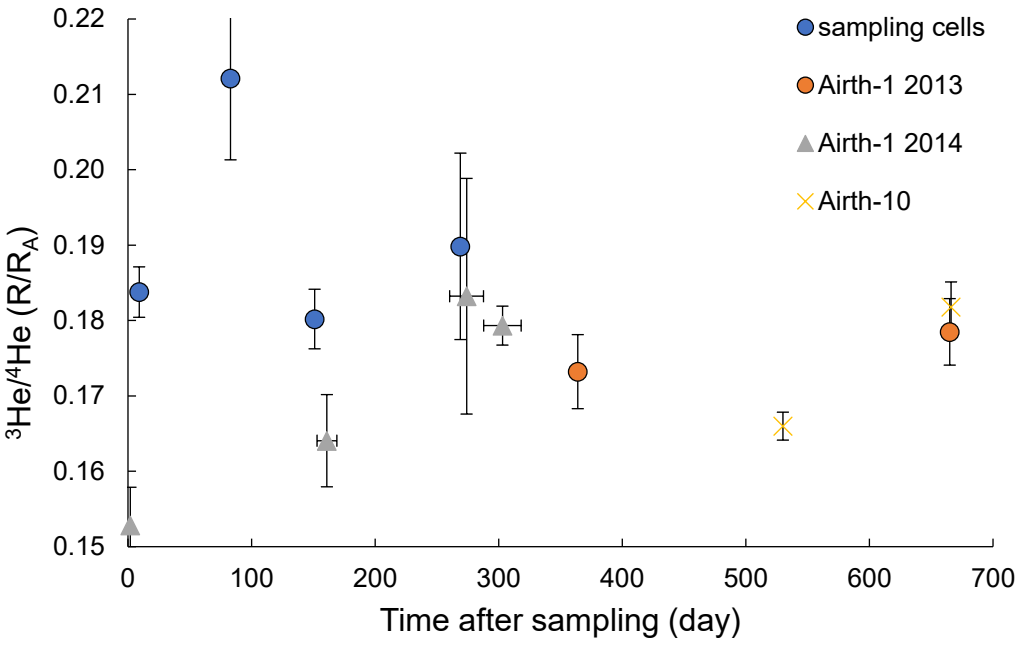

Figure 7-3 – Plot of $^3He/^4He_{(Ra)}$ vs. time from sampling until analysis. $^3He/^4He_{(Ra)}$ ratios generally increase, but this is sporadic.

If helium is leaking out of samples, it might be reasonable to expect variations in neon content due to its small ionic radius. The atmosphere has a huge inventory of ^{20}Ne (16.5 ppm) (Ozima and Podosek, 2002) relative to samples (max ^{20}Ne = 0.19 ppm), so the concentration gradient of neon would result in neon ingress into tubes, and a rise in sample neon concentrations if leakage occurred.

The stainless sample cells can clearly be seen to experience atmospheric ingress with an increase in ^{20}Ne (see Figure 7-4). The copper tubes however do not show an obvious pattern (Figure 7-5), with initial neon contents being higher than in later samples which does not fit the trend of air leakage.

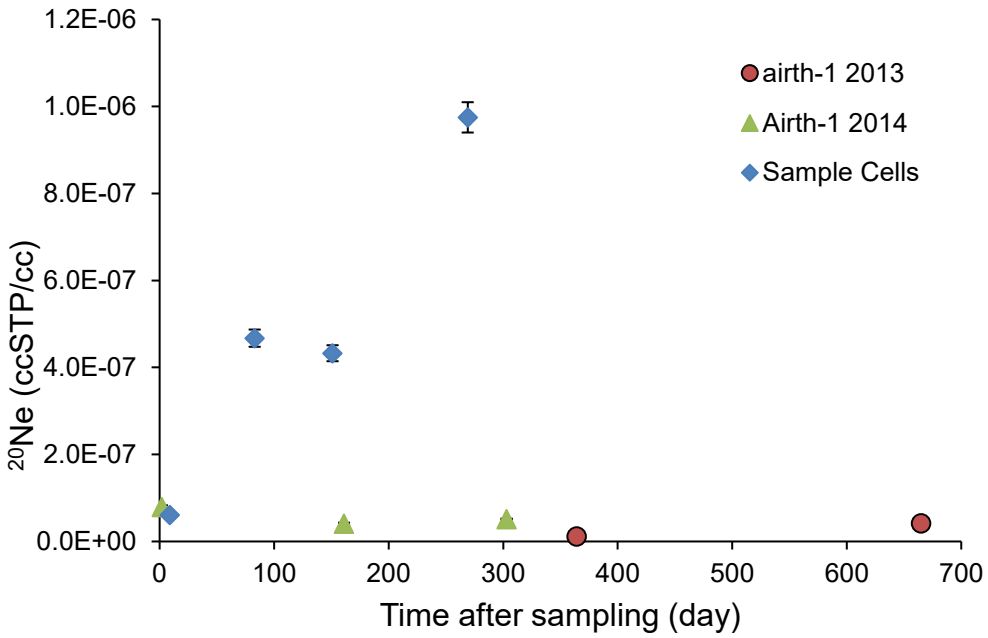

Figure 7-4 – Plot of ^{20}Ne (cc/ccSTP) vs. time after sampling until analysis. Note that the stainless sample cells have clearly experienced atmospheric ^{20}Ne, while the copper tubes (all other samples) seem less affected (see Figure 7-5).

The neon isotopes (Figure 7-6) appear to show a trend from a crustal-mantle mix towards the air-value with time, which suggests air ingress, however this cannot be correlated with measured ^{20}Ne concentrations which is counter-intuitive to air-leakage. The Airth-1 (2014) copper tube analysed at 303 days shows isotopic overlap with the sample cell analysed after 9 days, and both samples show similar ^{20}Ne concentrations (^{20}Ne = 0.080±0.0034 ppm (copper tube) vs. 0.061±0.0026 ppm (sample cell), showing that atmospheric neon ingress over time is not observed, at least in that sample. It should be noted that the generated data over time involved two different operators of the mass spectrometer, as well as different computer sequences for neon isotopes. For the data used in this text, the computer controlled analytical cycle for neon measured the background interferences every cycle (x10), rather than only at the first three cycles, which ensured greater reproducibility but took almost an hour longer per run.

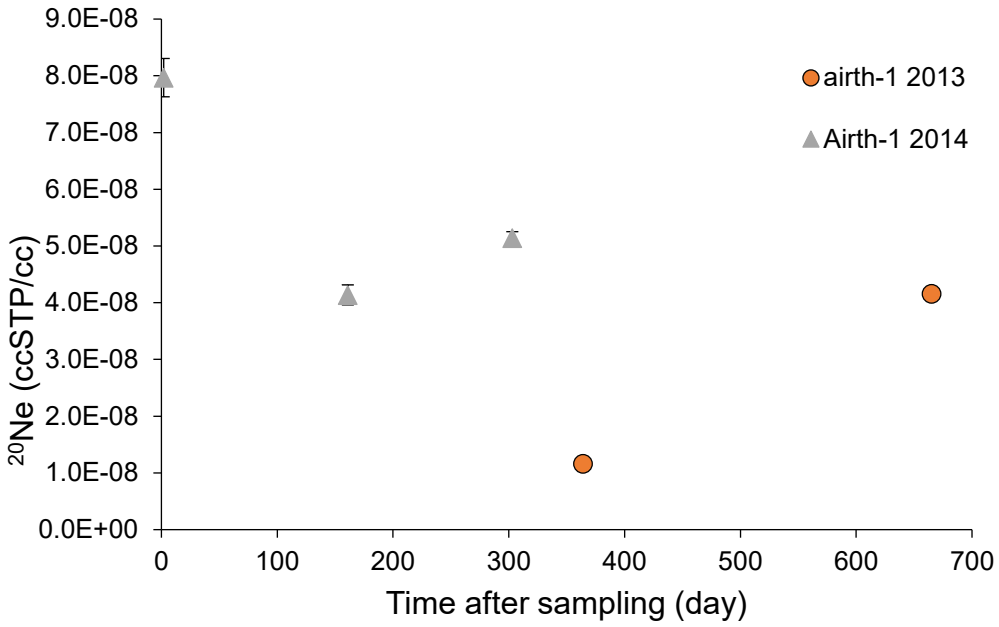

Figure 7-5– Identical to Figure 7-4, minus sample cell data. Note that concentrations can vary by ~50%, but there is no obvious increase in concentration with time of analysis after sampling.

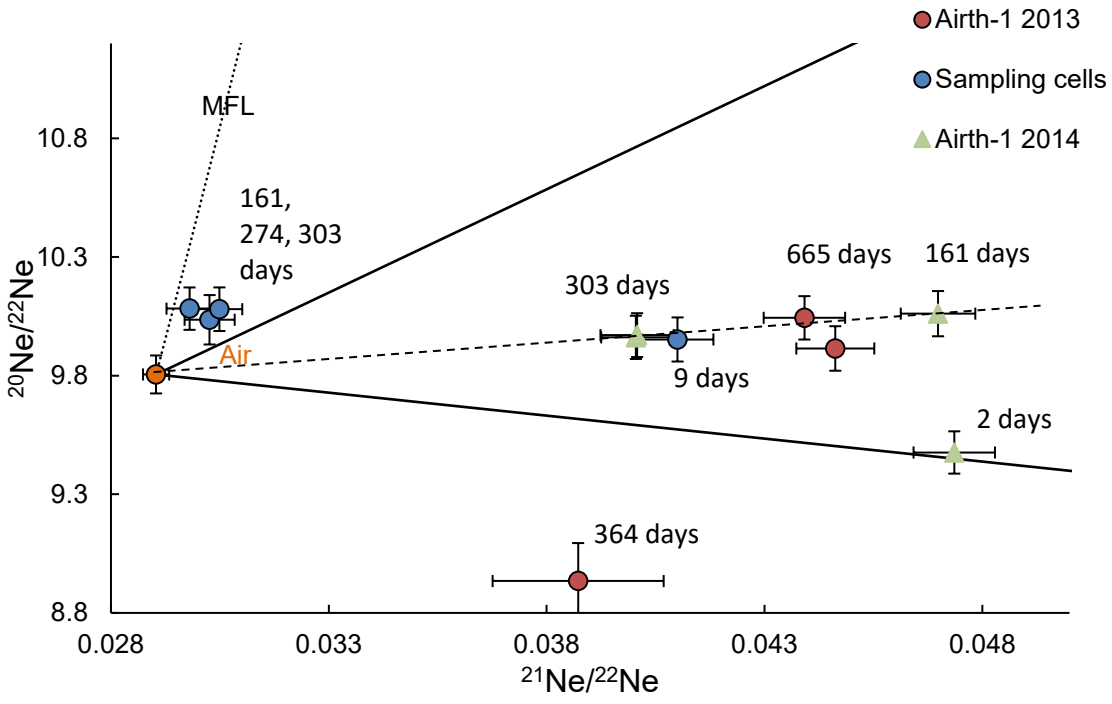

Figure 7-6 – Plot of $^{20}Ne/^{22}Ne$ vs. $^{21}Ne/^{22}Ne$ for samples analysed at different periods in time. There is an apparent general trend towards the air value (dashed line). Error bars include the air value in their calculation.

In the event of sample tube leakage, the $^{4}He/^{20}Ne$ ratio would be expected to drop as helium left the tube and neon entered. In the event of an infinitesimally small leak

that allowed only helium exchange and not neon, a drop in $^{4}He/^{20}Ne$ would still be expected. The sample cells show a clear increase in ^{20}Ne and drop in ^{4}He over time, with the resultant $^{4}He/^{20}Ne$ trending towards the air ratio. The copper tubes show an apparent drop in ^{4}He, but no obvious ^{20}Ne ingress, and no clear pattern in the reduction of $^{4}He/^{20}Ne$ (Figure 7-7).

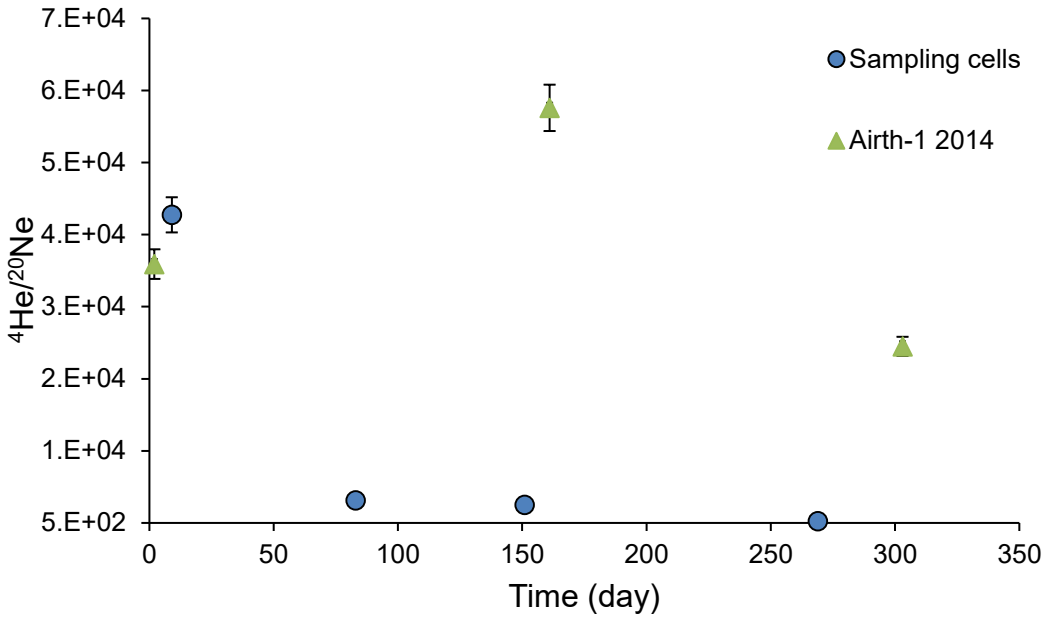

Figure 7-7 – Plot of $^{4}He/^{20}Ne$ vs. time between sampling and analysis. While sample cells show a clear trend in the reduction of $^{4}He/^{20}Ne$ due to tube leakage, this effect is not obvious in the copper tube samples.

A plot of $^{4}He/^{36}Ar$ vs. time after sampling shows a very similar pattern to $^{4}He/^{20}Ne$ for copper tubes (not shown). Both ^{20}Ne and ^{36}Ar in subsurface systems are ultimately derived from the atmosphere, and the same covariation within samples suggest the same atmospherically derived component within each sample. Sample cells show a systematic increase in $^{20}Ne/^{36}Ar$ vs. time to values > 2 (~4 times the atmospheric value), highlighting the preferential diffusion of ^{20}Ne into the sample over the less diffusive ^{36}Ar. Copper tubes show no increase over time (see Figure 7-8), and thus no additional ^{20}Ne entering via diffusion.

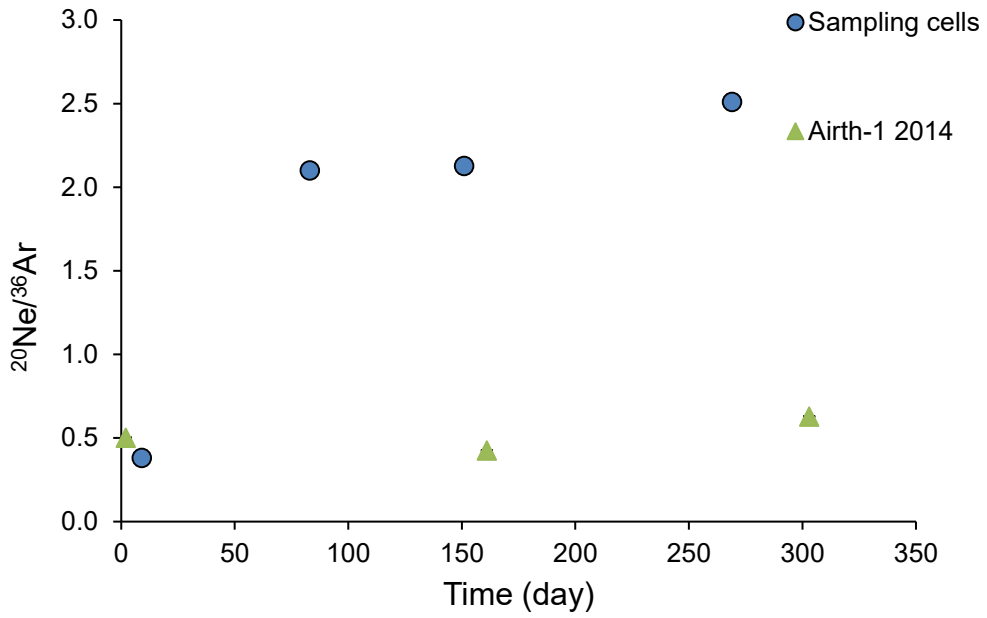

Figure 7-8 – Plot of $^{20}Ne/^{36}Ar$ vs. time after sampling before analysis. Sample cells show clear atmospheric ^{20}Ne ingress relative to ^{36}Ar, but copper tubes do not.

Comparing temporal measurements is also problematic as the measurements are referenced back to the calibration standards. Helium is calibrated with a bottle of HESJ helium standard (Matsuda et al., 2002), and all other noble gases with a bottle of air.

The concentration measurements for a noble gas are tied to their standard, and within any 'analytical run' the depletion (1 cc per calibration shot) in the calibration bottle (5 litres) is assumed to be negligible. However, the calibration bottles are periodically re-analysed to account for depletion, so technically the concentration data for He and Ne are not internally consistent when comparing samples measured over long periods of time. However, isotopic ratio data should remain consistent providing correct reference to the calibration. Different conditions in the setup and running of the mass spectrometer over time and with different operators may produce unquantifiable effects. Another problem with comparing raw data is sample bottle depletion; data used in this text has been corrected for depletion, while the temporal data presented has not. In most cases sample bottle depletion is negligible, but in some samples where repeat analysis was necessary the corrections made a several percent difference to the final concentrations.

In conclusion, apparent helium depletions from samples over time are not correlated with ^{20}Ne ingress from the atmosphere. The lack of increase in ^{20}Ne concentrations and lack of consistent change in both Ne isotopes and $^{4}He/^{20}Ne$ ratios

implies that interaction of the samples with the atmosphere cannot explain the variation. This strongly implies that simple loss of helium cannot account for the variations within the Airth-1 2014 sample sets, so the measurements are valid. The data selected for this text is part of a series analysed in an uninterrupted several week block by the same operator to ensure internal consistency and calibrations, and so the lower helium concentration associated with that Airth-1 (2014) analytical run was chosen.

In order to reduce the risk of helium loss reoccurring in the future, suggestions of modifications to the clamp system and sampling method are outlined in the Methodology section (this volume).

7.2 AMM Stable Isotopes

This section details calculations relating to the predicted stable isotope evolution of 'pure' coal gas, using experimental pyrolysis data from various studies. It was performed to quantify possible biogenic gas inputs into English AMM gases.

Hydrocarbons derived from coals (type III humic kerogens (Van Krevelen, 1961)) are characteristically heavy, closely related to source kerogen $\delta^{13}C$ which ranges from -21‰ to -28‰ (Whiticar, 1996; Rimmer *et al.*, 2006; Hamilton *et al.*, 2014; Warwick and Ruppert, 2016). It changes little with rank until very high rank is reached, where anthracites show heavier carbon isotopes likely a result of methane generation and other volatile loss (Rimmer *et al.*, 2006). Modern C_3-type terrestrial plant matter shows a similar range (-23‰ to -34‰, average: -27‰) (Gröcke, 1998), while type II kerogens range from: -32‰ to -27‰ (Whiticar, 1996). Variations in $\delta^{13}C$ are also seen between coal macerals. Generated hydrocarbons and CO_2 increase in $\delta^{13}C$ and δD with increasing thermal maturity (Schoell, 1980; Burruss and Laughrey, 2010). The carbon isotope values of generated gases generally become more positive with increasing carbon number (Chung *et al.*, 1988; Whiticar, 1994; Rooney *et al.*, 1995; Golding *et al.*, 2013).

7.2.1 Thermogenic Carbon and Hydrogen Isotopes in Coal

The carbon and hydrogen stable isotopes of methane and higher hydrocarbons have been measured from the artificial hydrous pyrolysis of coal, simulating the coalification process at different thermal maturities (Stahl, 1977; Sackett, 1978; Schoell, 1980;

Berner, 1989; Strąpoć *et al.*, 2007; Duan *et al.*, 2012; Bao *et al.*, 2013). Observations that the isotopic weight of hydrocarbons increases with thermal maturity is both empirical and also derived from these laboratory experiments. These are well defined for higher maturity (R_o = >0.7%) coals, but are less clear for low maturity coals. Lower maturity coals have produced less gas and have lower seam gas contents than higher maturity coals (*e.g.* anthracites) (Rice, 1993; Clayton, 1998; Thomas, 2013), and so are less likely to be source rocks for migrated commercial hydrocarbon accumulations, and thus the focus on gas geochemistry has been on higher rank coals. The interest in lower maturity coals is growing due to the increasing development of biogenic and mixed biogenic-thermogenic CBM, and "low-mature"/"early-mature" coal gases capable of producing large economic reserves in China (Dai *et al.*, 2005; Xiao *et al.*, 2008; Xu *et al.*, 2008; Ni *et al.*, 2013).

Bao et al., (2013) performed a series of peat pyrolysis experiments at stepped temperatures, and related the thermal maturity in terms of vitrinite reflectance (R_o) of the synthetic coals to the stable isotope measurements of produced gases. $\delta^{13}C_{CH4}$ values were spread around a relatively narrow range from -25‰ to -33‰ (R_o = 0.5% – 2.5%), with most values at lower maturities ranging from -30‰ to -33‰, and $\delta^{13}C_{CO2}$ values ranging from -22‰ to -24.5‰ ((R_o = 0.5% – 2.5%).

The relationships can be used to predict the stable isotope values of a purely thermogenic gas from a given vitrinite reflectance (R_o) using the equations:

$\delta^{13}C_{CH4}$ = -26.20 log R_o – 34.12 (for R_o < 1.3%)

δD_{CH4} = 95.00 log R_o – 303.9

$\delta^{13}C_{CO2}$ = 3.26 log R_o – 22.86

Using mean vitrinite reflectance data from the Barnsley seam (aka Top Hard) from the Markham Main colliery (S.Yorks) of R_o = 0.50%, the Parkgate seam at Thoresby colliery (S. Yorks) at 0.71%, to a maximum of 1.03% recorded in the Silkstone seam at Cortonwood colliery (S.Yorks) (BCURA, 2002), the thermogenic end-member $\delta^{13}C_{CH4}$ for AMM gases can be predicted:

Seam:	Barnsley	Parkgate	Silkstone
R_o	0.50%	0.71%	1.03%
$\delta^{13}C_{CH4}$	-26.2	-30.2	-34.5
δD_{CH4}	-332.5	-318.0	-302.7
$\delta^{13}C_{CO2}$	-23.8	-23.3	-22.8

Table 24 – Table of predicted isotopic compositions of gases produced by peat hydrous pyrolysis via the model equations of Bao et al., (2013)

Other data (Figure 7-9) from assorted models assembled by Whiticar (1996, and references therein), place the $\delta^{13}C_{CH4}$ at R_o = 0.5% at -30‰ to -32‰, and at R_o = 1%, $\delta^{13}C_{CH4}$ = -27 to -29, though the reliability of these data at lower maturities (R_o < 0.7%) is not certain. Interestingly the pyrolysis data show a decrease in $\delta^{13}C_{CH4}$ with increasing maturity for low values of R_o, before increasing at greater maturities (R_o > 1.3%), while the data from models compiled by Whiticar (1996) (see Figure 7-9) show an increase in $\delta^{13}C_{CH4}$ with increased maturity. Further data from Xu and Shen (1996) fall outside of this range. This highlights the relative lack of research into low maturity coal gases compared to more oil-prone source rocks, and the complexity of unravelling biogenic from thermogenic gases from sources which are prone to generate both types, on the boundary where transition into the different generation mechanisms occurs.

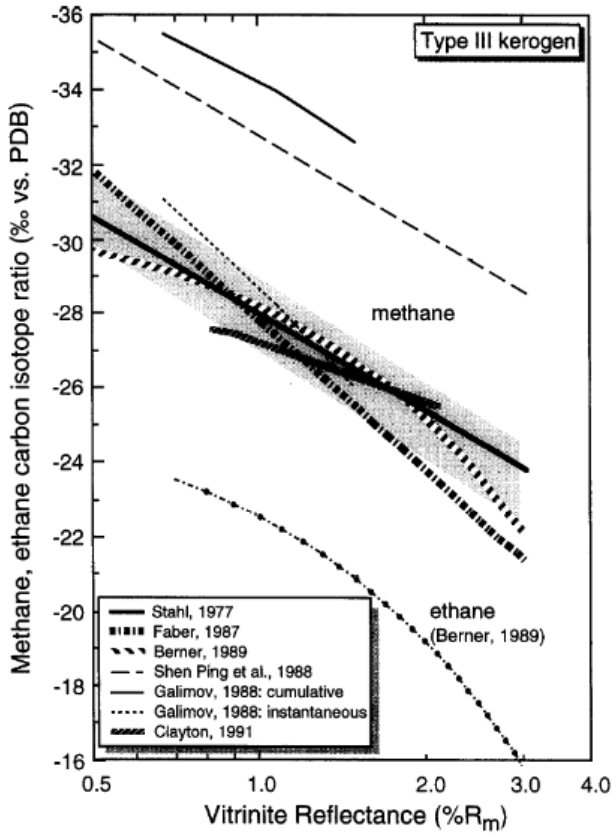

Figure 7-9 – Plot of $\delta^{13}C$ ratios vs. maturity (vitrinite reflectance) from various models, from Whiticar (1996). Plot shows several experimentally derived $\delta^{13}C_{CH4}$ and $\delta^{13}C_{C2H6}$ values for coals at different thermal maturity. These can be used to predict the isotopic ratios of purely thermogenic gas.

It can be seen that using any maturity value characteristic of sub-bituminous coals and with any predictive model, the predicted $\delta^{13}C_{CH4}$ values of thermogenic methane are more positive than the measured gases. This shows that there must be a secondary isotopically lighter CH_4 input to AMM gases, which is likely to be biogenic gas. Laboratory hydrous pyrolysis experiments of coals and peat are known to be fundamentally affected by the δD signature of the water added to the reaction chamber (Strąpoć *et al.*, 2007; Dias *et al.*, 2014), so δD_{CH4} predictions are disregarded as non-representative and are not used in any interpretation.

The predicted $\delta^{13}C_{CH4}$ from pyrolysis experiments can then be used to estimate the non-thermogenic component in a gas. Biogenic $\delta^{13}C_{CH4}$ in CBM can range from -90‰ to -50‰ (Rice, 1993), but is on average -70‰ (Tao *et al.*, 2007, 2014). If -70‰ is assumed as the biogenic $\delta^{13}C_{CH4}$ end-member, and the thermogenic end-members chosen to be -26.2‰ and -34.5‰ (the most extreme values calculated from min and max observed R_o using the equations of Bao et al., (2013)), then simple binary mixing

can be performed to estimate the minimum biogenic CH_4 content in the AMM gases. Table 13 shows the calculated minimum and maximum values of biogenic gas input to Crown-Farm-1 (maximum, lightest $\delta^{13}C_{CH4}$) and Bevercotes (minimum, heaviest $\delta^{13}C_{CH4}$). It is therefore estimated that over a third to over half of the CH_4 in the mine gas is biogenic in origin. This component would have to be ancient microbial CH_4 related to primary biogenic gas, or produced more recently.

7.3 Bibliography

Bao, Y., Wei, C., Wang, C., Li, L. and Sun, Y. (2013) 'Geochemical characteristics and identification of thermogenic CBM generated during the low and middle coalification stages', *Geochemical Journal*, 47(4), pp. 451–458.

BCURA (2002) *BCURA Database*. Cheltenham: British Coal Utilisation Research Association. Available at: http://www.bcura.org/coalbank.html.

Berner, U. (1989) *Entwicklung und Anwendung empirischer Modelle für die Kohlenstoffisotopenvariationen in Mischungen thermogener Erdgase*. T.U. Clausthal.

Burruss, R. C. and Laughrey, C. D. (2010) 'Carbon and hydrogen isotopic reversals in deep basin gas: Evidence for limits to the stability of hydrocarbons', *Organic Geochemistry*. Elsevier Ltd, 41(12), pp. 1285–1296. doi:10.1016/j.orggeochem.2010.09.008.

Chung, H. M., Gormly, J. R. and Squires, R. M. (1988) 'Origin of gaseous hydrocarbons in subsurface environments: Theoretical considerations of carbon isotope distribution', *Chemical Geology*, 71(1–3), pp. 97–104. doi:10.1016/0009-2541(88)90108-8.

Clayton, J. . (1998) 'Geochemistry of coalbed gas – A review', *International Journal of Coal Geology*, 35(1–4), pp. 159–173. doi:10.1016/S0166-5162(97)00017-7.

Dai, J., Qin, S., Tao, S., Zhu, G. and Mi, J. (2005) 'Developing trends of natural gas industry and the significant progress on natural gas geological theories in China', *Natural Gas Geoscience*, 2.

Dias, R. F., Lewan, M. D., Birdwell, J. E. and Kotarba, M. J. (2014) 'Differentiation of pre-existing trapped methane from thermogenic methane in an igneous-intruded coal by hydrous pyrolysis', *Organic Geochemistry*. Elsevier Ltd, 67, pp. 1–7. doi:10.1016/j.orggeochem.2013.11.010.

Duan, Y., Sun, T., Qian, Y., He, J., Zhang, X., Xu, L. and Wu, B. (2012) 'Pyrolysis experiments of forest marsh peat samples with different maturities: An attempt to understand the isotopic fractionation of coalbed methane during staged accumulation', *Fuel*, 94(0), pp. 480–485. doi:10.1016/j.fuel.2011.09.003.

Golding, S. D., Boreham, C. J. and Esterle, J. S. (2013) 'Stable isotope geochemistry of coal bed and shale gas and related production waters: A review', *International Journal of Coal Geology*, 120, pp. 24–40. doi:10.1016/j.coal.2013.09.001.

Gröcke, D. R. (1998) 'Carbon-isotope analyses of fossil plants as a chemostratigraphic and palaeoenvironmental tool', *Lethaia*, 31(1), pp. 1–13. doi:10.1111/j.1502-3931.1998.tb00482.x.

Hamilton, S. K., Golding, S. D., Baublys, K. A. and Esterle, J. S. (2014) 'Stable isotopic and molecular composition of desorbed coal seam gases from the Walloon Subgroup, eastern Surat Basin, Australia', *International Journal of Coal Geology*. Elsevier B.V., 122(0), pp. 21–36. doi:10.1016/j.coal.2013.12.003.

Van Krevelen, D. W. (1961) *Coal*. Amsterdam: Elsevier Scientific Publishing Company. ISBN: 0444895868.

Matsuda, J., Matsumoto, T., Sumino, H., Nagao, K., Yamamoto, J., Miura, Y., Kaneoka, I., Takahata, N. and Sano, Y. (2002) 'The 3He/4He ratio of the new internal He Standard of Japan (HESJ).', *Geochemical Journal*, 36(2), pp. 191–195. doi:10.2343/geochemj.36.191.

Ni, Y., Dai, J., Zhu, G., Zhang, S., Zhang, D., Su, J., Tao, X., Liao, F., Wu, W., Gong, D. and Liu, Q. (2013) 'Stable hydrogen and carbon isotopic ratios of coal-derived and oil-derived gases: A case study in the Tarim basin, NW China', *International Journal of Coal Geology*. Elsevier B.V., 116–117, pp. 302–313. doi:10.1016/j.coal.2013.06.006.

Rice, D. D. (1993) 'Composition and Origins of Coalbed Gas', *AAPG Bulletin*, 77(1), pp. 159–184. doi:10.1306/D9CB61EB-1715-11D7-8645000102C1865D.

Rimmer, S. M., Rowe, H. D., Taulbee, D. N. and Hower, J. C. (2006) 'Influence of maceral content on ??13C and ??15N in a Middle Pennsylvanian coal', *Chemical Geology*, 225(1–2), pp. 77–90.

doi:10.1016/j.chemgeo.2005.08.012.
Rooney, M. A., Claypool, G. E. and Moses Chung, H. (1995) 'Modeling thermogenic gas generation using carbon isotope ratios of natural gas hydrocarbons', *Chemical Geology*, 126(3–4), pp. 219–232. doi:10.1016/0009-2541(95)00119-0.
Sackett, W. M. (1978) 'Carbon and hydrogen isotope effects during the thermocatalytic production of hydrocarbons in laboratory simulation experiments', *Geochimica et Cosmochimica Acta*, 42(6), pp. 571–580. doi:10.1016/0016-7037(78)90002-9.
Schoell, M. (1980) 'The hydrogen and carbon isotopic composition of methane from natural gases of various origins', *Geochimica et Cosmochimica Acta*, 44(5), pp. 649–661. doi:10.1016/0016-7037(80)90155-6.
Stahl, W. J. (1977) 'Carbon and nitrogen isotopes in hydrocarbon research and exploration', *Chemical Geology*, 20, pp. 121–149. doi:10.1016/0009-2541(77)90041-9.
Strąpoć, D., Mastalerz, M., Eble, C. and Schimmelmann, A. (2007) 'Characterization of the origin of coalbed gases in southeastern Illinois Basin by compound-specific carbon and hydrogen stable isotope ratios', *Organic Geochemistry*, 38(2), pp. 267–287. doi:10.1016/j.orggeochem.2006.09.005.
Tao, M., Shi, B., Li, J., Wang, W., Li, X. and Gao, B. (2007) 'Secondary biological coalbed gas in the Xinji area, Anhui province, China: Evidence from the geochemical features and secondary changes', *International Journal of Coal Geology*, 71(2–3), pp. 358–370. doi:10.1016/j.coal.2006.12.002.
Tao, M., Wang, W., Li, Z., Ma, Y., Li, J. and Li, X. (2014) 'Comprehensive study on genetic pathways and parent materials of secondary biogenic gas in coalbeds', *Chinese Science Bulletin*. Science China Press, 59(10), pp. 992–1001. doi:10.1007/s11434-014-0151-7.
Thomas, L. (2013) *Coal Geology*. II. Oxford, UK: Wiley-Blackwell. ISBN: 9781119990444.
Warwick, P. D. and Ruppert, L. F. (2016) 'Carbon and oxygen isotopic composition of coal and carbon dioxide derived from laboratory coal combustion: A preliminary study', *International Journal of Coal Geology*. Elsevier B.V., 166, pp. 128–135. doi:10.1016/j.coal.2016.06.009.
Whiticar, M. J. (1994) 'Correlation of natural gases with their sources', in *The Petroleum System - from Source to Trap*. AAPG Special Edition, pp. 261–283.
Whiticar, M. J. (1996) 'Stable isotope geochemistry of coals, humic kerogens and related natural gases', *International Journal of Coal Geology*, 32(1–4), pp. 191–215. doi:10.1016/S0166-5162(96)00042-0.
Xiao, Z., Xie, Z., Li, Z., Ma, C. and Sun, Q. W. (2008) 'Isotopic characteristics of natural gas of Xujiahe Formation in southern and middle of Sichuan Basin', *Geochimica*, 37(3), pp. 245–250.
Xu, Y. C., Wang ZhiYong, Z. Y., Wang, X. F., Zheng, J. J. and Du, H. Y. (2008) 'Low-mature gases and typical low-mature gas fields in China', *Science in China, Series D: Earth Sciences*, 51(2), pp. 312–320. doi:10.1007/s11430-008-0011-x.
Xu, Y. and Shen, P. (1996) 'A study of natural gas origins in China', *AAPG Bulletin*, 80(10), pp. 1604–1614.